Arthritis & Rheumatology

An Official Journal of the American College of Rheumatology
www.arthritisrheum.org and wileyonlinelibrary.com

Cover design: Todd Machen

♾This journal is printed on acid-free paper.

Arthritis & Rheumatology

An Official Journal of the American College of Rheumatology
www.arthritisrheum.org and wileyonlinelibrary.com

VOLUME 77 • January 2025 • NO. 1

Cover image: The image on the cover (Amudalapalli et al; page 118) shows clusters of histiocytes with emperipolesis on hematoxylin and eosinstaining. Emperipolesis is a unique cellular process in which the engulfed cell remains viable within another cell. It is characteristic of Rosai–Dorfman disease and is also rarely observed in hematologic malignancies, including lymphoma and leukemia.

In this Issue

Highlights from this issue of *A&R* | By Lara C. Pullen, PhD

Epitope Spreading in Systemic Sclerosis May Serve as Biomarker

Previous studies have found that immunologic abnormalities, especially B cell abnormalities, are pivotal in patients with systemic sclerosis (SSc). Investigating this association requires accurate and reproducible antibody assays, however. In this issue, Kotani et al (p. 67) report a correlation between epitope spreading (ES) levels and the severity of skin sclerosis or the risk of other complications in SSc. Their findings suggest that measures of ES in SSc may serve as a novel biomarker for disease activity.

p. 67

In their retrospective study of patients with SSc, the researchers measured autoantibodies against various subunits of the RNA polymerase III (RNAP III) complex using an approach that allowed for enhanced sensitivity in detecting anti-RNAP III antibodies (ARA). They found that ARA-positive patients with SSc had autoantibodies against different RNAP III complex subunits. Intermolecular ES occurred with RNAP III complex subunits, and intramolecular ES occurred within RNA polymerase III subunit A (RPC1).

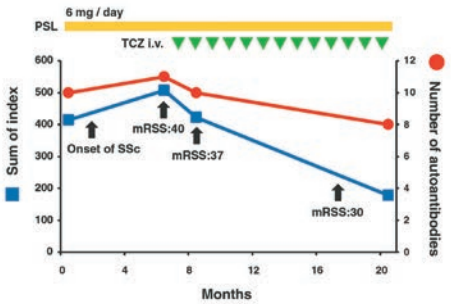

Figure 1. Serial measurements of the intermolecular ES levels and skin thickness score in a 68-year-old woman with SSc, myositis, RA, and SLE.

The investigators reported that ES levels correlated with complication severity. The intermolecular ES indicators significantly correlated with the modified Rodnan skin thickness score (mRSS) and surfactant protein-D, a biomarker of interstitial lung disease. Intermolecular ES indicators did not correlate with the extent of disease on high-resolution computed tomography or pulmonary function tests. Intramolecular ES indicators against RPC1 significantly correlated with mRSS and renal crisis. Moreover, longitudinal assessment of ES in RNAP III complex subunits correlated with mRSS, thereby exhibiting potential as a disease activity biomarker.

Targeting CD13/Aminopeptidase N as a Novel Therapeutic Approach for Scleroderma

Previous studies demonstrated that matrix metalloproteinase 14 (MMP14) generates the soluble form of CD13 (sCD13) in synoviocytes and that sCD13 can then induce the phosphorylation of extracellular signal-regulated kinases (ERK1/2) in various cell types. In this issue, Muraoka et al (p. 80) extend their research with the first report that sCD13 plays a critical role in systemic sclerosis (SSc) skin fibrosis. Their data suggest that targeting the sCD13-bradykinin receptor B1 (B1R) signaling axis may be a promising novel therapeutic approach for SSc.

p. 80

The investigators designed their study to determine the expression and role of the widely expressed aminopeptidase CD13 in patients with SSc and focused their experiments on skin fibrosis. They first analyzed a transcriptome data set generated from skin biopsies of patients with SSc to characterize the sCD13 signaling axis. Quantitative polymerase chain reaction and immunoblotting of fibroblasts isolated from skin biopsies of healthy controls and patients with dcSSc revealed high levels of expression of *ANPEP*, *MMP14*, and *BDKRB1* in SSc skin and isolated dermal fibroblasts. Immunolabelling of skin biopsies confirmed that B1R was abundant in dcSSc skin, specifically in myofibroblasts. In performing a single-cell analysis on skin biopsies from 22 patients with SSc and 18 healthy adults, the team found the highest *BDKRB1* expression in COL8A1-positive myofibroblasts, a population exclusively seen in SSc.

Recognizing that transforming growth factor beta (TGFβ) plays a crucial role in SSc fibrosis, the team next treated dcSSc skin fibroblasts with TGFβ and found that it induced the expression of *BDKRB1* and the production of sCD13. Moreover, SSc fibroblasts treated with sCD13 exhibited characteristic myofibroblast features, including fibrotic gene expression, signaling, cell proliferation, migration, and gel contraction. The researchers then tested whether the sCD13 and the B1R inhibitor SSR240612 affected fibrotic genes and found that it suppressed myofibroblast transition by sCD13 and TGFβ.

Turning to animal models, the researchers found that intracutaneous injection of bleomycin or PBS into *Cd13*$^{-/-}$, *Bdkrb1*$^{-/-}$ and sex- and age-matched wild-type mice revealed that mice lacking *Cd13* or *Bdkrb1* were resistant to bleomycin-induced skin fibrosis and inflammation. Moreover, pharmacological B1R inhibition had a comparable anti-fibrotic effect on wild-type mice. The authors conclude that since sCD13 activates the ERK signaling pathway via B1R, the pro-fibrotic effect of the sCD13-B1R axis may also be mediated via the ERK pathway.

Relationship Between Ultrasound and Physical Examination in Assessing Enthesitis

Rheumatologists lack a gold standard for evaluating enthesitis in patients with spondyloarthritis (SpA). While ultrasound has an advantage over clinical examination in that it can assess the extent of active inflammation and structural damage in the affected enthesis, previous studies have yielded conflicting findings about the agreement between ultrasound and physical examination in evaluating enthesitis. In this issue, Di Matteo et al (p. 22) report results from a multicenter study that underscore the need for a comprehensive tool that integrates ultrasound and physical examination in assessing enthesitis in patients with SpA. They write that combining clinical and imaging modalities would allow clinicians to evaluate enthesitis and better tailor treatment strategies.

p. 22

The investigators examined the agreement between ultrasound and physical examination in assessing enthesitis and explored the prevalence of subclinical enthesitis in patients with SpA. The study included 413 patients with SpA from 20 rheumatology centers in 11 countries. Across all ultrasound lesions, the highest levels of agreement between ultrasound and physical examination occurred in the presence of a negative finding. Moreover, they found that approximately 20% of patients with normal clinical and serological findings exhibited active inflammation on ultrasound. Such entheseal inflammation was often associated with local structural damage.

The researchers found that the variability in the agreement between ultrasound and physical examination depended on the specific ultrasound finding and the entheseal site being evaluated. The Achilles tendon enthesis, for example, exhibited the lowest agreement values for all ultrasound lesions and clinical signs of enthesitis. The fact that the demographic, serological, and clinical profiles of the patients with SpA with subclinical enthesitis did not significantly differ from those without SpA led the researchers to conclude that ultrasound subclinical enthesitis predominantly reflects localized changes at the entheseal level rather than systemic ones.

Journal Club

A monthly feature designed to facilitate discussion on research methods in rheumatology.

Efficacy Versus Effectiveness: The HORIZON Pivotal Fracture Trial and its Emulation in Claims Data

D'Andrea et al. *Arthritis Rheumatol.* 2025;77:12–21

The HORIZON–Pivotal Fracture Trial (PFT) is a randomized, double-blind, placebo-controlled trial assessing the efficacy of zoledronic acid in reducing hip fractures over 3 years among postmenopausal women with osteoporosis. The results indicated a 41% reduction in hip fracture risk in the zoledronic acid group compared to placebo. Adherence to the treatment schedule exceeded 80% by the end of the study; however, adherence in clinical practice is substantially lower. D'Andrea et al emulated the HORIZON–PFT using claims-based databases to evaluate the effectiveness of zoledronic acid in preventing hip fractures in clinical settings, where poor adherence is common.

An active comparator, new initiator cohort study was conducted using two large U.S. claims databases. Raloxifene served as a placebo proxy, with eligibility criteria mirroring HORIZON–PFT. This approach reduced the risk of major biases that could invalidate the study findings, such as immortal time bias, selection bias, and confounding by indication. Propensity score matching was used to reduce confounding. Zoledronic acid initiators were 1:1 matched to raloxifene initiators, emulating randomization trial groups. Over 1.5 years, most of them failed to receive a second infusion. Women initiating once-yearly infusions of zoledronic acid had a 28% lower risk of hip fractures vs. raloxifene recipients. Although the preventive benefits were consistent, the effectiveness was attenuated compared to the efficacy shown in HORIZON–PFT. This diminished effect could be explained by the shorter duration of therapy in clinical practice, coupled with the increasing beneficial effect seen with longer treatment in the trial.

Questions

1. **What is currently known about the adherence in clinical practice to osteoporosis therapies and its impact on the effectiveness of treatments for osteoporosis, such as zoledronic acid?**
2. **Why did the effectiveness of zoledronic acid in reducing hip fractures in the database study differ from the efficacy results observed in HORIZON–PFT?**
3. **How did use of an active comparator (raloxifene as a placebo proxy) and inclusion of new treatment initiators only (incident users) increase the validity of the study results?**
4. **What other statistical methods beside propensity score matching could be used to minimize confounding?**
5. **What implications do the differences in adherence rates and treatment duration between clinical trials and real-world settings have for future research and clinical practice?**

Clinical Connections

Enhanced Type 1 IFN Signature in AxSpA Patients Unresponsive to Secukinumab Treatment

Pacheco et al, *Arthritis Rheumatol.* 2025;77:34–46

CORRESPONDENCE
Robert Inman, MD: robert.inman@uhn.ca

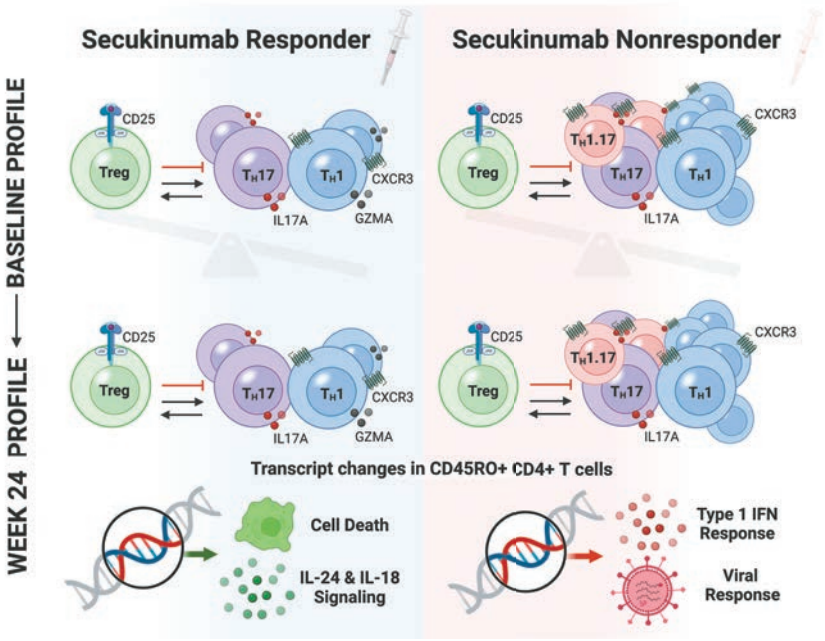

KEY POINTS

- AxSpA patients unresponsive to secukinumab treatment have a distinctive immune profile in peripheral blood before treatment.
- At baseline, secukinumab nonresponders have an increased frequency of T_H1, $T_H1.17$ and IL17A+ CD4+ T cells compared to secukinumab responders.
- Secukinumab nonresponders demonstrate enhancement of genes associated with type 1 IFN after treatment.
- Type 1 IFN may contribute to the inflammatory burden in some axSpA patients, raising the possibility of new targeted therapeutics.

SUMMARY

Type 3 immunity, specifically interleukin-17A (IL-17A), contributes to the joint inflammation that underlies both pain and spinal ankylosis in axial spondyloarthritis (axSpA). Biologic treatments that target IL-17A, such as secukinumab, are effective for ~60% of patients, but it is currently unknown why the remaining 40% of patients do not respond to secukinumab. Pacheco et al demonstrated that previous biologic usage was associated with suboptimal secukinumab response, whereas biologic-naive patients were significantly more likely to respond to secukinumab. A higher frequency of T helper 1 (T_H1) and T helper 1.17 ($T_H1.17$) cells in peripheral blood at baseline was associated with nonresponse to secukinumab treatment. Secukinumab nonresponders were also observed to have higher frequencies of IL-17A+ CD4+ T cells at baseline that remained unchanged with secukinumab treatment.

The peripheral blood transcriptome of nonresponders demonstrated elevated transcripts associated with type 1 interferon (IFN) after treatment. This signature was most pronounced in secukinumab nonresponders who had failed previous biologics. These data demonstrate that type 1 IFN signaling may contribute to the inflammatory burden in some axSpA patients. Targeted therapy incorporating these novel findings merits further study in axSpA.

Muscle Tissue Transcriptome of Idiopathic Inflammatory Myopathy Reflects Muscle Damage Process and Presence of Skin Lesions

Izuka et al, *Arthritis Rheumatol*. 2025;77:99–106

CORRESPONDENCE
Shinji Izuka, MD: izukas-int@h.u-tokyo.ac.jp
Toshihiko Komai, MD, PhD: komait-int@h.u-tokyo.ac.jp
Keishi Fujio, MD, PhD: fujiok-int@h.u-tokyo.ac.jp

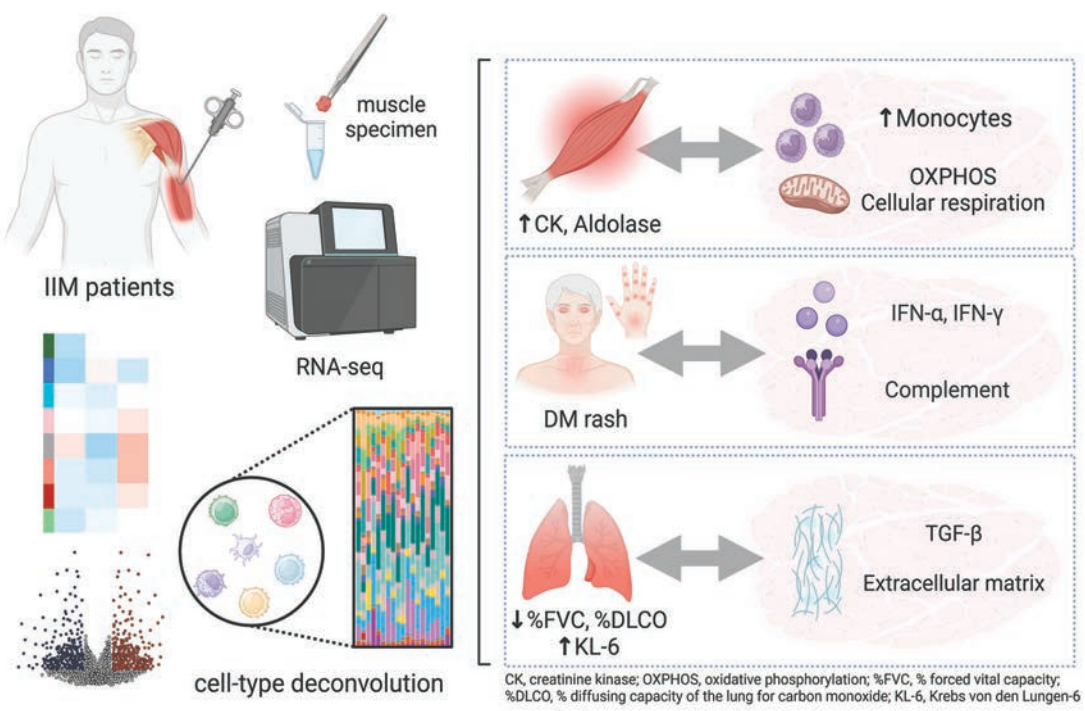

CK, creatinine kinase; OXPHOS, oxidative phosphorylation; %FVC, % forced vital capacity; %DLCO, % diffusing capacity of the lung for carbon monoxide; KL-6, Krebs von den Lungen-6

KEY POINTS

- Muscle tissue transcriptome reflects clinical manifestations in IIM.
- Tissue-infiltrating monocytes appear to play a crucial role in muscle damage and delineate pathological processes in IIM.
- Dermatomyositis is characterized by complement systems and interferon signaling, while antisynthetase syndrome is associated with oxidative phosphorylation.

SUMMARY

Idiopathic inflammatory myopathy (IIM) encompasses several clinical phenotypes, such as polymyositis, dermatomyositis, and antisynthetase syndrome. The underlying mechanisms that define clinical phenotypes remain poorly understood.

Izuka et al demonstrated transcriptomic and immunophenotypic alterations associated with clinical phenotypes of IIM using muscle tissue bulk RNA-sequencing. A deconvolution approach to estimate cell proportions enabled identification of immune cell subsets infiltrating muscle tissues in IIM, which showed that monocytes and myeloid dendritic cells were associated with muscle damage. Differentially expressed gene analysis revealed enrichment of complement and interferon pathway genes in muscle from patients with dermatomyositis, and oxidative phosphorylation pathway involvement in patients with antisynthetase syndrome. Uniquely, the data also showed a positive correlation between the expression of genes related to the extracellular matrix as well as transforming growth factor-β signaling pathway and clinical parameters associated with interstitial lung disease. These findings suggest that distinctive gene expression profiles in muscle specimens underlie each clinical phenotype in IIM.

Arthritis & Rheumatology
Vol. 77, No. 1, January 2025, pp 1–11
DOI 10.1002/art.42983

American College of Rheumatology
Empowering Rheumatology Professionals

REVIEW

Understanding the Role of Type I Interferons in Cutaneous Lupus and Dermatomyositis: Toward Better Therapeutics

Grace A. Hile[1] and Victoria P. Werth[2]

A 29-year-old female presented to a rheumatology-dermatology clinic with a pruritic rash that began 6 months prior, after a viral illness. She had previously been diagnosed with eczema and treated with antihistamines and topical steroids without improvement. She also noted fatigue, hair loss, and severe scalp pruritus. Physical examination was notable for violaceous periorbital edema, scaly erythematous papules on the metacarpophalangeal joints of bilateral hands, dilated capillaries of the proximal nail folds, scaly plaques on bilateral elbows, and excoriated erythematous plaques on upper chest, back and hips. The patient reported no muscle weakness, and strength testing and creatinine phosphokinase were normal. Magnetic resonance imaging of the thigh showed no evidence of inflammation or edema. Antibody testing was negative. A diagnosis of clinically amyopathic dermatomyositis was made. Computed tomography scans of the chest, abdomen and pelvis, colonoscopy, and mammogram showed no evidence of cancer. The patient was initiated on methotrexate. Her cutaneous manifestations persisted with debilitating intractable pruritus, and thus, she was transitioned to mycophenolate mofetil, again with minimal improvement. Intravenous immunoglobulin was not approved by insurance given the lack of muscle involvement in her disease. This patient's case highlights a common clinical scenario in rheumatology and dermatology and raises several important issues related to the immunologic underpinnings of cutaneous lupus erythematosus (CLE) and dermatomyositis (DM): What is the role of type I interferon (IFN) in triggering skin disease in CLE and DM? What is the role of IFN in the pathogenesis of skin inflammation in CLE and DM? Can we apply what we know about IFN-targeted therapeutics in CLE and DM to develop better treatments for skin disease?

Introduction

Dermatomyositis (DM) is a chronic autoimmune disease with characteristic skin findings and often affects the muscles, heart, gastrointestinal, joints, and lungs but can also occur only or predominantly on the skin. Patients with amyopathic or hypomyopathic DM demonstrate absent or clinically insignificant muscle findings. In the absence of myopathy, the diagnosis of DM is often delayed. Studies suggest that the clinically amyopathic DM subphenotype is more common than previously thought, and such patients comprise up to 60% of patients with DM in dermatology clinics.[1] Skin disease in DM is often relapsing and recalcitrant to therapy, even when systemic disease is well controlled. Importantly, DM skin activity correlates with a poorer quality of life, even compared with other chronic diseases.[2]

Lack of knowledge regarding the pathogenesis of DM and drivers that instigate skin disease has delayed effective therapy development. To date, there are no US Food and Drug Administration (FDA)–approved therapies for the treatment of cutaneous lupus erythematosus (CLE) or skin disease in DM. As in our case, many patients have refractory skin lesions and pruritus. Additionally, a lack of inclusion criteria for skin disease activity and damage in ongoing clinical trials limit therapeutic options. Current therapies are broadly immunosuppressive, often ineffective, and cause significant morbidity.

DM rashes appear similar clinically and histologically to those seen in CLE and can be challenging to differentiate, particularly if disease is limited to the skin (Figure 1). Like in CLE, type I interferons (IFNs) are highly up-regulated in DM blood, muscle, and skin and correlate with disease activity.[3] Additionally, both CLE and DM skin are thought to be induced or "triggered" by

Supported by the United States Department of Veterans Affairs Office of Research and Development (grants 1-I01-BX-005921 and R01-AR-R076766 to Dr Werth).

[1]Grace A. Hile, MD: University of Michigan, Ann Arbor; [2]Victoria P. Werth, MD: Corporal Michael J. Crescenz Department of Veterans Affairs Medical Center and the University of Pennsylvania, Philadelphia.

Author disclosures are available at https://onlinelibrary.wiley.com/doi/10.1002/art.42983.

Address correspondence via email to Victoria P. Werth, MD, at werth@pennmedicine.upenn.edu.

Submitted for publication July 31, 2023; accepted in revised form September 4, 2024.

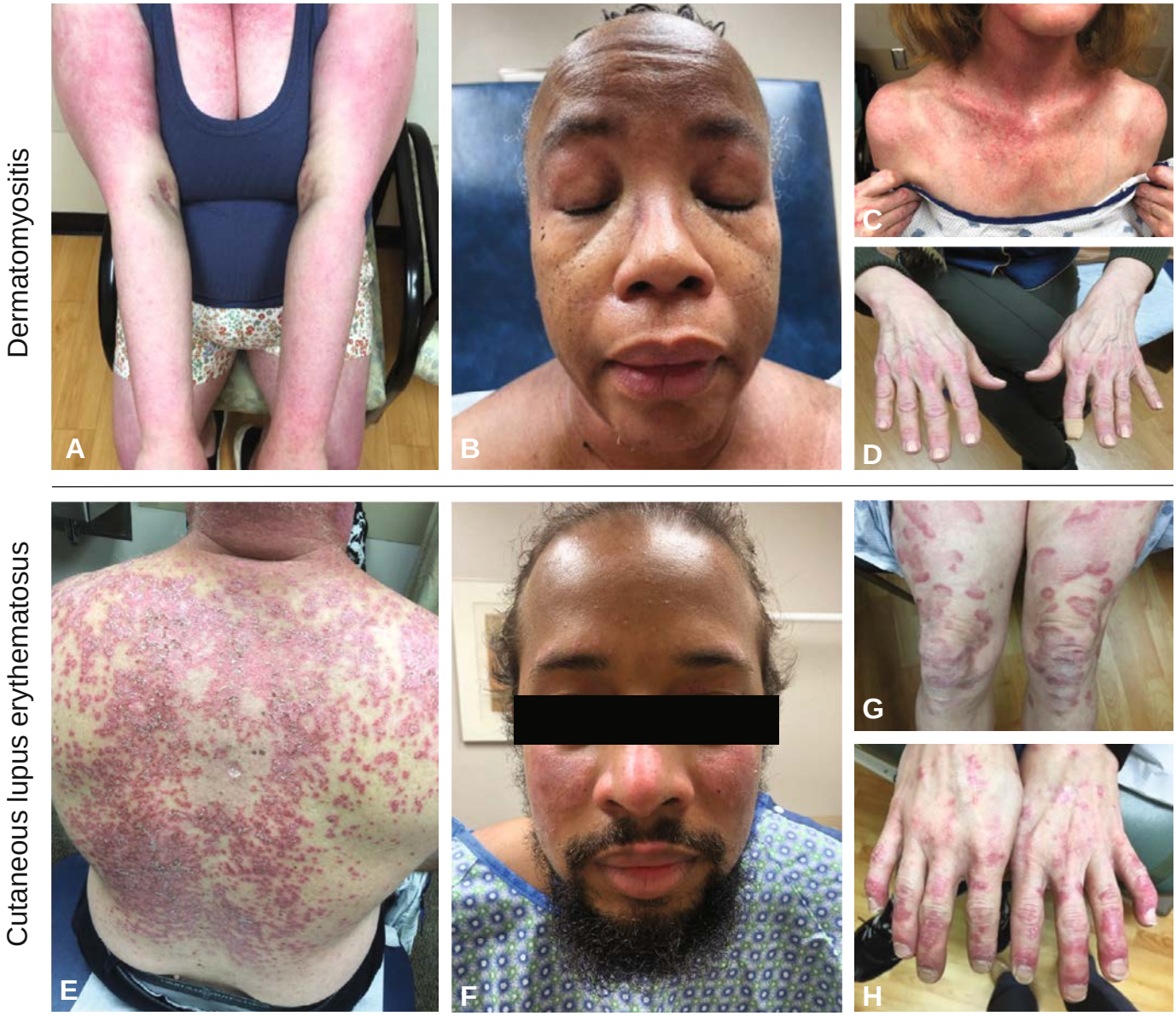

Figure 1. IFN-driven cutaneous manifestations of dermatomyositis (A–D) and cutaneous lupus erythematosus (E–H) are pictured: (A) widespread erythematous to violaceous papules and plaques on extensor surfaces; (B) heliotrope sign; (C) poikilodermatous erythema on anterior neck in "V" distribution; (D) Gottron's papules overlying joints; (E) psoriasiform SCLE; (F) malar erythema of acute LE; (G) annular erythematous plaques of SCLE; (H) dorsal hand erythema sparing joints of LE. IFN, interferon; LE, lupus erythematosus; SCLE, subacute cutaneous lupus erythematosus.

heightened IFN exposure, such as after sunlight, medications such as hydroxyurea and immune checkpoint inhibitors, and immune-stimulating supplements or infections such as COVID-19 in genetically predisposed individuals (Figure 2A). Although DM and CLE share common triggers, the type I IFN subtype and efficacy of current therapeutics differ and may indicate key differences in disease pathogenesis, such as CLE being IFNα driven, whereas IFNβ may play a dominant role in DM (Figure 2B). A number of novel therapeutics are emerging that act on the IFN system and the type I IFN receptor–associated JAK/STAT signaling pathway (Figure 2A). In this review, we will discuss our current understanding of the role of type I IFN in the immunopathogenesis of CLE and DM skin inflammation. Furthermore, we will discuss emerging IFN-targeted therapies used in ongoing trials in systemic lupus erythematosus (SLE) and how they may be applicable and efficacious in the treatment of DM skin disease.

Type I IFNs

Type I IFNs are an immunomodulatory class of cytokines that are involved in the innate and adaptive immune system and serve to protect against viral infection and provide cancer

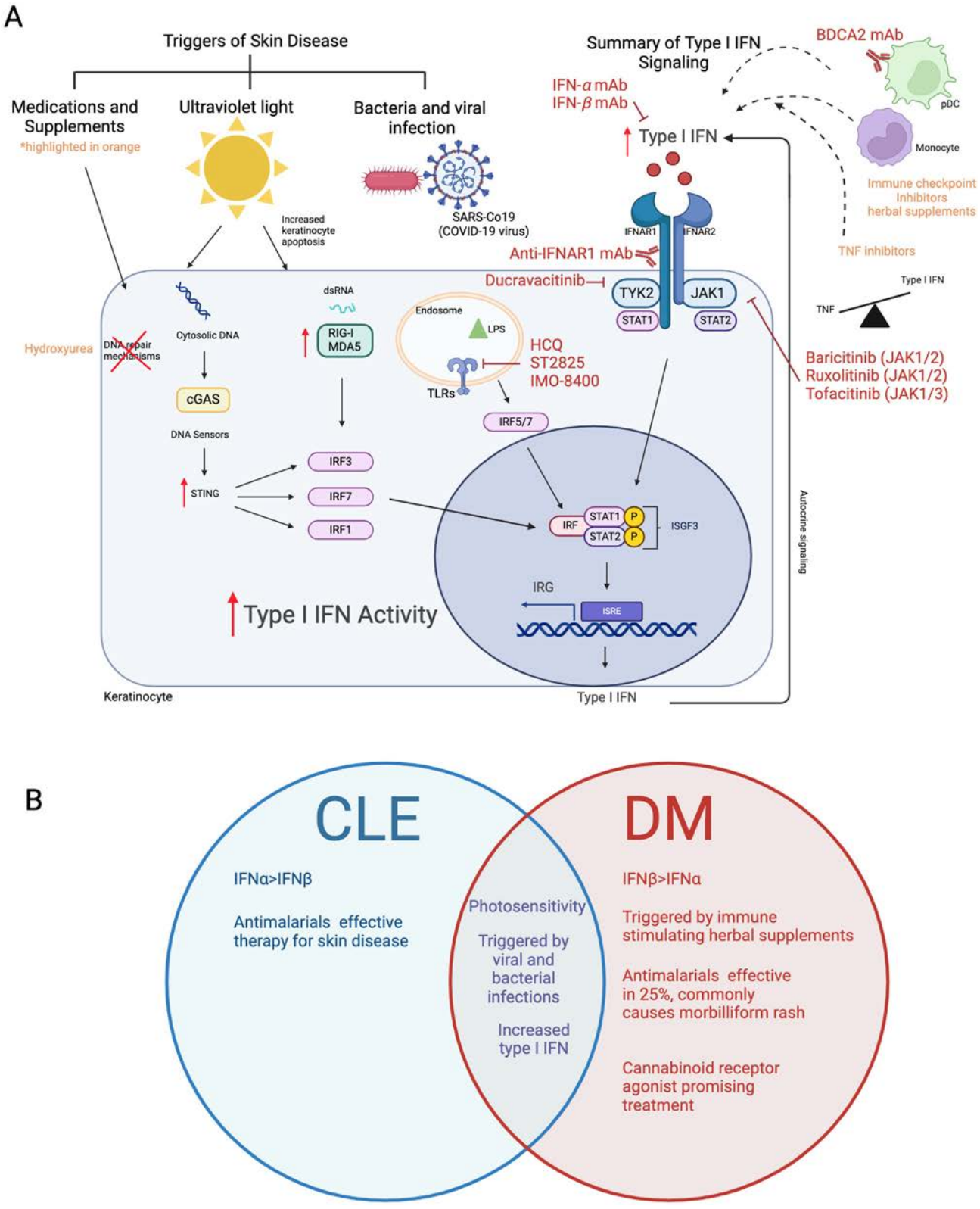

Figure 2. (A) Summary of the type I IFN pathway, potential disease triggers, and mechanisms of new therapeutics is given. (B) Similarities and differences between CLE and DM are shown. BDCA2, blood DC antigen 2; cGAS, Cyclic GMP-AMP synthase; CLE, cutaneous lupus erythematosus; DM, dermatomyositis; dsRNA, double-stranded RNA; HCQ, hydroxychloroquine; IFN, interferon; IFNAR, IFNα receptor; IMO, Isomalto-oligosaccharide; IRF, IFN response factor; IRG, IFN response gene; ISGF3, IFN-stimulated gene factor 3; ISRE, IFN-stimulated response element; LPS, Lipopolysaccharide; mAb, monoclonal antibody; MDA5, melanoma differentation-associated protein 5; pDC, plasmacytoid dendritic cell; RIG-I, retinoic acid–iducible gene I; ST2825, small molecule inhibitor of MyD88; STING, stimulator of IFN genes; TLR, Toll-like receptor; TNF, tumor necrosis factor; TYK2, Tyrosine Kinase 2.

immunosurveillance.[4] Mounting evidence suggests that type I IFNs are important to the initiation and maintenance of autoimmune and inflammatory skin diseases, such as CLE and DM (Figure 2A). IFNs promote antigen presentation and natural killer cell function, regulate inflammatory pathways, and activate the adaptive immune system to form immunologic memory.[5] The type I IFN family of cytokines is composed of 17 members: 13 subtypes of IFNα, IFNβ, IFNε, IFNκ, and IFNω.[6,7] All type I IFNs signal through the same heterodimeric transmembrane receptor, the IFNα receptor (IFNAR), which is composed of two subunits: IFNAR1 and IFNAR2. The IFNAR is expressed in nearly all cell types. Activation of JAK1 and Tyrosine Kinase 2 (TYK2) result in the tyrosine phosphorylation and activation of several STAT family members. Activation of STAT1 and STAT2 lead to the recruitment of IFN response factor 9 (IRF9) and the formation of the STAT1–STAT2–IRF9 complex, which is known as the IFN-stimulated gene factor (ISGF3) complex. This complex then migrates to the nucleus and binds to IFN-stimulated response elements in the promoters of ISGs to initiate gene transcription. Activated genes include up-regulation of IFN signaling components, IFN genes themselves, and effector genes for antiviral responses. A number of therapies that target type I IFN and downstream signaling are emerging and are exciting avenues of interest in the treatment of autoimmune skin disease, as discussed below.

Most cell types can produce type I IFNs (leukocytes, fibroblasts, endothelial cells, keratinocytes), but the primary producers of IFNs may be context and disease dependent. The dominant cytokine profile and inflammatory cell populations of CLE lesions are heterogeneous and have been shown to reflect different responsiveness to antimalarials.[8] Hydroxychloroquine (HCQ)–responsive patients had significantly higher type I IFN–regulated transcripts and lower tumor necrosis factor α (TNFα) levels than HCQ-refractory patients.[8] In contrast, patients who were refractory to HCQ, thus needing addition of quinacrine, had significantly up-regulated TNFα expression produced by myeloid dendritic cells.[8]

Triggers of skin disease

UV light. Photosensitivity, a sensitivity to UV light whereby even ambient light can result in inflammatory skin lesions, is a hallmark of CLE and SLE and occurs in 60% to 80% of patients.[9] The exact mechanism of photosensitivity is still unfolding, but type I IFNs likely play an important role (Figure 2A and B). SLE keratinocytes (KCs) exhibit a more robust type I IFN response after UV exposure when compared with healthy controls.[10] This proinflammatory effect of ultraviolet B (UVB) in patients with SLE with photosensitivity likely stems from the IFN-rich environment.[11]

UV stimulation likely up-regulates IFN production through endogenous nucleic acid triggering cyclic GMP-AMP synthase (cGAS) and the stimulator of IFN genes (STING) pathway. This is supported by a study showing that UV stimulation of murine skin results in rapid up-regulation of *Ifnb* that is blocked by absence of cGAS.[12] UVB has also been noted to induce activation of human endogenous retroviruses, which leads to production of double-stranded RNA and activation of retinoic acid–inducible gene I (RIG-1)/melanoma differentiation-associated protein 5 (MDA5)-mediated type I IFN induction.[12] Interestingly, the presence of enhanced IFN genes in the skin has been translated to systemic increases in IFN-regulated genes, suggesting that systemic IFN responses can result from skin exposure.[12] UVB can also increase the IFN-stimulating capacity of nucleic acids because cells exposed to UV-treated DNA have increased IFN production compared with cells not exposed to UVB-treated DNA.[12,13] Injection of DNA treated with UV light into lupus-prone mice can induce CLE-like lesions, and deletion of the enzyme that removes degradation of UV-treated DNA leads to CLE-like lesions with enhanced IFN production in a STING-dependent manner.[14] Together, these data suggest that UV modulation of nucleic acids and nucleic acid sensing is critical for UV-mediated IFN responses.

Similar to CLE, cutaneous signs of DM are frequently present on sun-exposed areas such as the upper neck and back and/or shoulders. Photosensitivity may be an initial presenting sign of DM and should prompt consideration of the diagnosis. Photoprovocation testing in patients with DM resulted in increased photosensitivity and inducement of new lesions in ∼25% of patients.[15] Formal UVB testing of these patients demonstrated a reduced minimal erythema dose. Certain myositis-specific antibodies have been correlated with increased incidence of photosensitivity in DM, including anti-Mi2 and anti–transcription intermediary factor 1γ.[16] The role of type I IFNs in the photosensitive response of DM has not been studied.

Medications. Drug-induced lupus erythematosus is a lupus-like autoimmune disorder that occurs with exposure to certain medications. Terbinafine (an allylamine derivative) is one of the most widely prescribed medications associated with drug-induced subacute CLE, with all studied patients exhibiting resolution after drug cessation. Although the mechanism of the terbinafine-induced autoimmune reaction is not entirely clear, it may be related to the lipophilic and keratinophilic properties that contribute to altered nuclear antigen configuration, antinuclear and antihistone antibodies, and enhanced IFN production.[17]

Several medications have been linked to DM onset or flare, including hydroxyurea, TNFα inhibitors, immune checkpoint inhibitors (ICIs), penicillamine, and statins.[18] Hydroxyurea is a cytotoxic agent used to treat myeloproliferative disorders and has been reported as the most common culprit for drug-induced DM, accounting for 51% of patients (n = 36/70).[19] The mechanism of hydroxyurea-induced DM is not entirely clear but may be due to the synergistic effects of hydroxyurea blocking DNA site repair and UV irradiation, causing DNA strand breaks and likely up-

regulating KC production of type I IFNs.[20] TNFα inhibitors have also been implicated in DM onset or flare.[21] This may be explained by TNF inhibition paradoxically increasing the production of type I IFN, which activates antigen-presenting cells and stimulates autoantigen production.[22] Supporting this, in an open pilot study of infliximab in patients with refractory inflammatory myopathies, several patients experienced acute worsening, and these flares were associated with increased type I IFN activity in both blood and muscle.[23]

ICIs, which target programmed cell death 1 (PD-1), programmed cell death ligand (PDL-1) mDC and CTLA-4, are increasingly being used to treat both solid and hematologic malignancies by harnessing the immune system's ability to recognize and destroy malignant cells. ICIs result in a wide range of autoimmune skin manifestations, including LE and DM, as a consequence of unleashing immune system regulation.[24] The mechanism underlying ICI induction of autoimmune skin disease is complex but likely in part due to enhanced CD4+ and CD8+ T cell activation with subsequent release of cytokines such as type I IFNs.[25]

Supplements. Treatment with a number of herbal supplements, including *Spirulina plantensis*, *Aphanizomenon flos-aquae*, *Chlorella*, *Echinacea*, and alfalfa, stimulates the immune system, and treatment with them has been associated with autoimmune skin disease onset and exacerbations.[26–30] Patients with DM have been reported to have a higher rate of herbal supplement treatment compared with patients with CLE or autoimmune blistering diseases and healthy controls. In vitro testing showed that IsaLean weight loss powder dose-dependently stimulates peripheral blood mononuclear cell secretion of inflammatory cytokines, including TNFα, IFNα, and IFNβ, primarily via Toll-like receptor 4 activation.[29] Practitioners should be aware of the potential immunostimulatory effects of herbal supplements on DM and specifically ask their patients about possible consumption.

Viral illness. In genetically susceptible individuals, viral infections have been suspected to induce or exacerbate autoimmune skin disease, including LE and DM, through up-regulation of type I IFN. Recent reports have shown an increased incidence of disease flares in patients with autoimmune skin disease after COVID-19 vaccination, with an increased proportion of patients with DM compared with patients with lupus erythematosus.[31] Of the patients who had autoimmune exacerbations after vaccination, 20% had symptoms after the first dose, 82% after the second dose, and 4% after the third dose.[31] The underlying mechanisms of immune stimulation are believed to be in part be driven by type I IFN production, which the COVID-19 vaccines have been shown to up-regulate.[32] It is unclear why DM appears to be disproportionally affected; however, differences in cells and type of IFN or an increased propensity to flare at any given time may be contributing factors.[31]

Role of IFN in the immunopathogenesis of skin disease

CLE. It has been well-documented that CLE has a strong type I IFN signature.[33–36] Histologically normal skin in patients with SLE produces type I IFN[10,37] with a marked concentration of type I IFN response in the absence of infiltrating leukocytes.[37] In a recent study using single-cell RNA sequencing of paired lesional and nonlesional skin samples from patients with SLE, an IFN-rich signature was seen in both lesional and nonlesional KCs as well as other cell populations, such as fibroblasts and T cells.[38] In addition, a proinflammatory cellular communication network between stromal and inflammatory cells was seen in lesional and nonlesional skin that supports the role of KCs priming myeloid recruitment and inflammatory responses.[38] Further investigation into the transcriptional IFN dominant phenotypes and communication networks may provide targeted therapeutic strategies.

Other cell populations besides KCs likely contribute to enhanced IFN production in the skin. Most research on type I IFN production has focused on plasmacytoid dendritic cells (pDCs). In otherwise healthy individuals, pDCs produce large amounts of IFN upon recognition of viral antigens via endosomal Toll-like receptors TLR7 and TLR9.[39,40] However, the role of pDCs in type I IFN production in autoimmune diseases such as SLE is less clear. Psarras et al show that, in preclinical autoimmunity and in SLE, pDCs are not effector cells, but rather have lost their capacity for TLR-mediated IFNα and TNFα production and fail to induce T cell activation, independently of disease activity and blood IFN signature.[37] pDCs in lesional CLE were not major type I IFN producers.[41] This may be in part due to inflammatory environments with high TNFα production,[42] such as can be found in the skin of patients with SLE.[43] Additionally, monocytes exhibit STING-dependent type I IFN production after UVB stimulation.[44] How the inflammatory environment modulates the functional status of pDCs and other IFN-producing cells in lupus is still being uncovered.

DM. Overexpression of type I IFN also has been linked to the immunopathogenesis of DM. IFN-inducible transcripts and activated type I IFN signatures are observed in patients with DM.[3] Increased expression of IFNα/β-inducible genes and proteins induced by type I IFNs such as myxovirus resistance protein are seen in peripheral blood mononuclear cells and affected muscle and skin of patients with DM.[45–47] Elevated blood IFNβ protein is seen in DM muscle and blood and correlates with high blood type I IFN–inducible genes.[48] In the skin, IFNβ protein is highly up-regulated in the T cell, macrophage, dendritic cell, and endothelial cell populations.[41] Additionally, IFN signatures, in particular IFNβ, closely correlate with cutaneous disease

activity.[49] IFNβ expression is abundant in all cells present in the epidermis and dermis of DM skin.[41] TLR3 has been shown to be elevated in vascular endothelial cells, myeloid dendritic cells, and regenerating myofibers in patients with juvenile DM (JDM). Type I IFN signatures are increased in B cells of patients with JDM, and the activation of TLR7 and IFNα may lead to expansion of immature B cell populations.[50] In vivo and in vitro studies show that myogenic precursor cells are a source of type I IFNs.[50]

Emerging therapies targeting type I IFNs

With mounting evidence suggesting a role of type I IFN signaling in the pathogenesis of autoimmune diseases, an increasing number of monoclonal antibodies (mAb) and small molecule inhibitors are being developed to target the type I IFN signaling pathway (summarized in Figure 2A and Table 1). Therapies targeting IFNα or IFNβ, the IFNAR chain, pDCs, TLRs, and their downstream IFN signaling pathways, including JAK inhibitors and TYK2 inhibitors, will be discussed below. We also will discuss cannabinoid receptor type 2 agonist lenabasum.

Anti-IFNα. A phase Ib clinical trial study (NCT00533091) observed that the anti-IFNα mAb sifalimumab inhibited type I IFN signatures in patients with DM.[51] Sifalimumab has specificity only for IFNα, leaving other type I IFNs unaffected and able to bind to the IFNAR. Given that current data suggest that DM seems to be predominantly driven by IFNβ compared with IFNα, it is unclear whether further investigations into IFNα inhibition will yield efficacy in treating DM skin disease.

Anti-IFNβ. A phase II trial (NCT03181893, Ddzukibart) tested anti-IFNβ, an immunoglobin G1 neutralizing antibody, in adults with DM and showed efficacy in skin.[52] Clinical end point Cutaneous Dermatomyositis Disease Area and Severity Index (CDASI) reduction of <5 points was achieved in 100% and 96% for the 150-mg and 600-mg doses, respectively. The placebo response was 35.7%. For the Cutaneous Dermatomyositis Disease Area and Severity Index CDASI reduction of >40%, the rates were 80%, 82.1%, and 7.1% for the 150 mg, 600 mg, and placebo arms, respectively.[52]

Anti-IFNAR1 mAb. An anti-IFNAR1 mAb, anifrolumab, showed significant effects in decreasing the disease activity of SLE in phase II trials, and another phase IIb study in patients with moderate to severe SLE was considered very successful.[53,54] Two phase III trials (known as TULIP-1 and TULIP-2) in patients with SLE were completed in 2019 and showed promise in treatment of skin disease in lupus erythematosus with a >50% reduction in CLASI was noted at week 12 in patients with a baseline CLASI-A >10.[55,56] Several recent case series have shown promise of anifrolumab for the treatment of refractory CLE[57,58]; further studies are needed for skin limited disease.

IFNAR blockade blunts the effects of both IFNα and IFNβ and has been shown to reverse many of the proteomic and cellular changes of enhanced type I IFN seen in SLE. Given similar IFN-driven changes in DM, further studies are warranted to determine if IFNAR blockade may provide clinical benefit.

Inhibition of pDCs. Litifilimab is an mAb that binds to blood DC antigen 2, an inhibitory receptor on pDCs, and induces rapid internalization to inhibit the production of type I IFNs.[56] Litifilimab was beneficial to patients with CLE.[59]

pDCs have also been implicated in DM, with increased numbers noted in DM skin,[41,60,61] although there were more pDCs in CLE than DM.[62] Single-cell analysis using mass cytometry of DM skin supports this, showing increased pDC numbers in DM skin. However, this study suggests that pDCs may not be the main drivers of type I IFN production. Monocyte and/or macrophages, monocytoid dendritic cells (mDCs), and T cells were shown to be main contributors, with mDCs being the main drivers of IFNβ production. In DM, pDCs were shown to produce high IFNγ, which activates a receptor complex distinct from that of the type I interferons. Whether inhibition of pDCs through down-regulation of IFNγ will result in clinical improvement in DM is not known.

TLR inhibition. HCQ is a TLR7, TLR8, and TLR9 antagonist and a conventional antimalarial drug for autoimmune skin diseases, particularly CLE.[63] A significant proportion (20%–30%) of patients with DM develop a cutaneous reaction, most commonly a morbilliform rash,[64] limiting treatment with HCQ in DM. Additionally, studies suggest that only 25% of patients with DM respond to HCQ.[65] This may be explained by elevated numbers of CD11c+ mDCs, which are important producers of IFNβ, in HCQ nonresponders compared with HCQ responders in DM.[62] Interestingly, IFNα was lower in HCQ nonresponders, and there was no difference in IFNβ expression between the two groups.[62] This suggests that HCQ may have effects on high IFNα–expressing responders, whereas HCQ nonresponders may not respond due to differences in cell sources such as mDCs that alter the type I IFN composition.[62] It is unknown whether additional mechanisms of TLR inhibition will be more efficacious in DM or result in cutaneous adverse events such as occur with HCQ.

Downstream interferon signaling. JAK inhibitors target inhibition of cytokine-mediated signaling via the JAK/STAT pathway, which is important for signaling of inflammatory cytokines, immunoregulation, and different cell growth factors.[66,67] Baricitinib is a selective inhibitor of Janus kinase inhibitor JAK1/JAK2 that has shown significant efficacy in patients with SLE in a phase II trial but failed in two phase II trials.[68] Tofacitinib, an inhibitor of JAK1/3, is approved by the FDA for the treatment of rheumatoid arthritis, psoriatic arthritis, and ulcerative colitis.[69] Limited reports have shown that tofacitinib improves recalcitrant cutaneous

Table 1. Emerging therapies in CLE and DM*

		CLE				DM			
Therapy	Mechanism of action	Level of evidence	Clinical endpoints for skin	Comments	Ref	Level of evidence	Clinical endpoints for skin	Comments	Ref
Targeting IFN									
Sifalimumab	Anti-IFNα mAb	Phase IIb, randomized, double-masked, placebo-controlled study	≥4-point reduction in CLASI	Slight reduction in CLASI subset of patients with CLASI activity score ≥10, after week 28	82	Phase Ib, randomized, double-masked placebo-controlled trial	15% reduction in MMT8, no skin-specific endpoints	Inhibited ISG in skin (and muscle)	52
F-06823859 (dazukibart)	Anti-IFNβ IgG1 neutralizing Ab					Phase II, double-masked, placebo-controlled trial	>5-point reduction in CDASI score or >40% CDASI improvement from baseline at 12 weeks	>5-point reduction in 100% and 95% of 150 mg and 600 mg doses vs. placebo of 35.7% R>40% reduction in CDASI shown in 80%, 82.1% and 7.1% for the 150 mg, 600 mg and placebo groups	83
Anifrolumab	Anti-IFNAR1 mAb	Phase IIb (moderate to severe SLE); phase III trial (TULIP-I and TULIP-II)	≥50% improvement in CLASI; reduction of 50% or more in CLASI	Phase IIb and TULIP-II met primary endpoint; 50% reduction in CLASI was noted at week 12 in patients with baseline CLASI-A>10	53, 55, 56				
Inhibition of pDCs									
Litifilimab		Randomized, double-blind, placebo-controlled trial	CLASI-A	The difference from placebo in the change from baseline in CLASI-A score at week 16 was −33.4 percentage points in the 150-mg group, and −28.0 percentage points in the 450-mg group.	59				
Downstream IFN signaling									
Deucravacitinib	TYK2 inhibitor	Phase II, Randomized, Double-masked, placebo-controlled trial	CLASI-50 at 52 weeks	CLASI-50 was significant in patients with baseline CLASI-A score ≥10	78				

(Continued)

Table 1. (*Cont'd*)

Therapy	Mechanism of action	CLE				DM			
		Level of evidence	Clinical endpoints for skin	Comments	Ref	Level of evidence	Clinical endpoints for skin	Comments	Ref
Cannabinoid receptor type 2 agonist									
Lenabasum	Selective CB2 agonist					Phase 2 randomized, placebo-controlled	CDASI	Reduced *IFNβ* gene expression and IL-31 protein expression	81

*: Ab, antibody; CDASI, Cutaneous Dermatomyositis Disease Area and Severity Index; CLASI; Cutaneous lupus erythematosus Disease Area and Severity Index; CLASI-50, decrease of ≥50% from baseline CLASI activity score; CLE, cutaneous lupus erythematosus; DM; dermatomyositis; HCQ, hydroxychloroquine; IFN, interferon; IFNAR, IFNα receptor; IL, interleukin; ISG, interferon-stimulated gene; mAb, monoclonal antibody; MMT8I, Manual Muscle Testing; pDC, plasmacytoid dendritic cell; SLE, systemic lupus erythematosus; TYK2, Tyrosine Kinase 2.

lupus.[70] In a recent phase I double-masked randomized safety trial of tofacitinib, authors suggest that inhibition of aberrant IFN signaling results in improvement of cardiometabolic and immunologic parameters associated with the premature atherosclerosis in SLE,[71] the results of which will need to be followed up with long-term studies. Clinical trials of tofacitinib for SLE and CLE are still in progress.[69] Filgotinib, a highly selective JAK1 inhibitor, failed in a phase II clinical trial.[69,72]

A few studies have reported a positive response to JAK inhibitors in DM[73,74] as well as in a subset of patients with refractory JDM.[74] In a recent systematic review, 38 female patients and 15 male patients with DM had been treated with JAK inhibition without serious side effects.[75] Tofacitinib was the most frequently prescribed, followed by ruxolitinib (inhibitor of JAK1/2).[75] Improvement of CDASI was reported in most of the studies; however, the duration of follow-up was limited to 1 to 15 months.[75] The first prospective, open-label clinical trial of tofacitinib in 10 patients with DM was recently published and showed promising efficacy and decreased STAT1 signaling and IFN gene expression in the skin.[73] Further studies are warranted to determine the long-term safety and efficacy of JAK inhibitors to treat DM skin disease.

TYK2 inhibition. Ducravacitinib is an oral, selective, allosteric inhibitor of TYK2 that binds the regulatory domain and locks the enzyme in an inactive state, distinguishing it from inhibitors of JAK1, JAK2, and/or JAK3 that bind the highly conserved active domains.[76] Ducravacitinib is FDA approved for the treatment of adults with moderate to severe plaque psoriasis.[77] A recent phase II randomized, double-masked, placebo-controlled trial suggests higher response, including for CLASI-50, in patients with SLE compared with placebo, with acceptable safety profile.[78]

Cannabinoid receptor type 2 agonist. The endocannabinoid system can modulate inflammatory and fibrotic responses.[79] Cannabinoid receptor type 2 (CB2) is mainly expressed on immune cells and plays a role in returning an activated immune response to homeostasis through modulation of inflammation,[80] leading to reductions in type I IFNs. Lenabasum is a selective CB2 agonist. A recent phase II randomized, placebo-controlled clinical trial study showed that lenabasum treatment was well tolerated and associated with improvement of CDASI and multiple efficacy outcomes in patients with moderate to severe skin involvement.[81] Additionally, lenabasum had a significant effect on *IFNβ* gene expression in the skin and reduced interleukin-31 protein, a cytokine associated with itching of the skin.[81] The degree and consistency of clinical benefit, combined with a favorable safety profile, warrant further evaluation of lenabasum for skin predominant DM.

Conclusion

There is a critical need for better treatments for dermatomyositis, particularly skin disease. Understanding the pathogenesis of skin diseases and drivers that instigate disease, in particular the role of type I IFNs, is key to propel effective therapy development. Skin only, skin predominant, and postmyopathic skin disease are more common than previously reported. As for our patient, skin disease is often refractory to current systemic directed therapies and results in debilitating pruritus and increased morbidity. Current and ongoing trial data mostly require active myositis, excluding patients with predominantly skin disease, and this often limits clinicians' ability to get medications covered by insurance companies for skin disease. Novel therapeutics are emerging that act on the IFN system and associated signaling and are promising new avenues for treatment (Table 1). To expand use of this armamentarium for refractory skin disease in DM, validated disease severity scores need to be accepted by the FDA and used as primary outcomes. Given the effectiveness of intravenous immunoglobulin (IVIg) and the likelihood of success with IVIg in this case, it is essential that DM trials include patients with amyopathic DM so that they can access appropriate therapies.

ACKNOWLEDGMENT

The University of Pennsylvania owns the copyright for the CLASI and CDASI.

AUTHOR CONTRIBUTIONS

All authors were involved in drafting the article or revising it critically for important intellectual content, and all authors approved the final version to be published.

REFERENCES

1. Klein RQ, Teal V, Taylor L, et al. Number, characteristics, and classification of patients with dermatomyositis seen by dermatology and rheumatology departments at a large tertiary medical center. J Am Acad Dermatol 2007;57(6):937–943.
2. Goreshi R, Chock M, Foering K, et al. Quality of life in dermatomyositis. J Am Acad Dermatol 2011;65(6):1107–1116.
3. Wong D, Kea B, Pesich R, et al. Interferon and biologic signatures in dermatomyositis skin: specificity and heterogeneity across diseases. PLoS One 2012;7(1):e29161.
4. Lazear HM, Schoggins JW, Diamond MS. Shared and distinct functions of type I and type III interferons. Immunity 2019;50(4):907–923.
5. Ivashkiv LB, Donlin LT. Regulation of type I interferon responses. Nat Rev Immunol 2014;14(1):36–49.
6. Gad HH, Dellgren C, Hamming OJ, et al. Interferon-lambda is functionally an interferon but structurally related to the interleukin-10 family. J Biol Chem 2009;284(31):20869–20875.
7. Gibbert K, Schlaak JF, Yang D, et al. IFN-α subtypes: distinct biological activities in anti-viral therapy. Br J Pharmacol 2013;168(5):1048–1058.
8. Zeidi M, Kim HJ, Werth VP. Increased myeloid dendritic cells and TNF-α expression predicts poor response to hydroxychloroquine in cutaneous lupus erythematosus. J Invest Dermatol 2019;139(2):324–332.
9. Foering K, Chang AY, Piette EW, et al. Characterization of clinical photosensitivity in cutaneous lupus erythematosus. J Am Acad Dermatol 2013;69(2):205–213.
10. Sarkar MK, Hile GA, Tsoi LC, et al. Photosensitivity and type I IFN responses in cutaneous lupus are driven by epidermal-derived interferon kappa. Ann Rheum Dis 2018;77(11):1653–1664.
11. Billi AC, Ma F, Plazyo O, et al. Nonlesional lupus skin contributes to inflammatory education of myeloid cells and primes for cutaneous inflammation. Sci Transl Med 2022;14(642):eabn2263.
12. Skopelja-Gardner S, An J, Tai J, et al. The early local and systemic type I interferon responses to ultraviolet B light exposure are cGAS dependent. Sci Rep 2020;10(1):7908.
13. Scholtissek B, Zahn S, Maier J, et al. Immunostimulatory endogenous nucleic acids drive the lesional inflammation in cutaneous lupus erythematosus. J Invest Dermatol 2017;137(7):1484–1492.
14. Sontheimer C, Liggitt D, Elkon KB. Ultraviolet B irradiation causes stimulator of interferon genes-dependent production of protective type I interferon in mouse skin by recruited inflammatory monocytes. Arthritis Rheumatol 2017;69(4):826–836.
15. Dourmishev L, Meffert H, Piazena H. Dermatomyositis: comparative studies of cutaneous photosensitivity in lupus erythematosus and normal subjects. Photodermatol Photoimmunol Photomed 2004;20(5):230–234.
16. Parkes JE, Rothwell S, Oldroyd A, et al; Myositis Genetics Consortium (MYOGEN). Genetic background may contribute to the latitude-dependent prevalence of dermatomyositis and anti-TIF1-γ autoantibodies in adult patients with myositis. Arthritis Res Ther 2018;20(1):117.
17. Bonsmann G, Schiller M, Luger TA, et al. Terbinafine-induced subacute cutaneous lupus erythematosus. J Am Acad Dermatol 2001;44(6):925–931.
18. Bax CE, Chakka S, Concha JSS, et al. The effects of immunostimulatory herbal supplements on autoimmune skin diseases. J Am Acad Dermatol 2021;84(4):1051–1058.
19. Seidler AM, Gottlieb AB. Dermatomyositis induced by drug therapy: a review of case reports. J Am Acad Dermatol 2008;59(5):872–880.
20. Kalajian AH, Cely SJ, Malone JC, et al. Hydroxyurea-associated dermatomyositis-like eruption demonstrating abnormal epidermal p53 expression: a potential premalignant manifestation of chronic hydroxyurea and UV radiation exposure. Arch Dermatol 2010;146(3):305–310.
21. Klein R, Rosenbach M, Kim EJ, et al. Tumor necrosis factor inhibitor-associated dermatomyositis. Arch Dermatol 2010;146(7):780–784.
22. Singh VK, Mehrotra S, Agarwal SS. The paradigm of Th1 and Th2 cytokines: its relevance to autoimmunity and allergy. Immunol Res 1999;20(2):147–161.
23. Dastmalchi M, Grundtman C, Alexanderson H, et al. A high incidence of disease flares in an open pilot study of infliximab in patients with refractory inflammatory myopathies. Ann Rheum Dis 2008;67(12):1670–1677.
24. Bhardwaj M, Chiu MN, Pilkhwal Sah S. Adverse cutaneous toxicities by PD-1/PD-L1 immune checkpoint inhibitors: pathogenesis, treatment, and surveillance. Cutan Ocul Toxicol 2022;41(1):73–90.
25. Ramos-Casals M, Brahmer JR, Callahan MK, et al. Immune-related adverse events of checkpoint inhibitors. Nat Rev Dis Primers 2020;6(1):38.
26. Lee AN, Werth VP. Activation of autoimmunity following use of immunostimulatory herbal supplements. Arch Dermatol 2004;140(6):723–727.

27. Konno T, Umeda Y, Umeda M, et al. [A case of inflammatory myopathy with widely skin rash following use of supplements containing Spirulina]. Rinsho Shinkeigaku 2011;51(5):330–333.
28. Ravishankar A, Bax CE, Grinnell M, et al. Frequency of immunostimulatory herbal supplement use among patients with autoimmune skin disease. J Am Acad Dermatol 2022;87(5):1093–1095.
29. Zeidi M, Chansky PB, Werth VP. Acute onset/flares of dermatomyositis following ingestion of IsaLean herbal supplement: clinical and immunostimulatory findings. J Am Acad Dermatol 2019;80(3):801–804.
30. Bax CE, Diaz D, Li Y, et al. Herbal supplement Spirulina stimulates inflammatory cytokine production in patients with dermatomyositis *in vitro*. iScience 2023;26(11):108355.
31. Sprow G, Afarideh M, Dan J, et al. Autoimmune skin disease exacerbations following COVID-19 vaccination. Front Immunol 2022;13:899526.
32. Sadarangani M, Marchant A, Kollmann TR. Immunological mechanisms of vaccine-induced protection against COVID-19 in humans. Nat Rev Immunol 2021;21(8):475–484.
33. Fäh J, Pavlovic J, Burg G. Expression of MxA protein in inflammatory dermatoses. J Histochem Cytochem 1995;43(1):47–52.
34. Blomberg S, Eloranta ML, Magnusson M, et al. Expression of the markers BDCA-2 and BDCA-4 and production of interferon-alpha by plasmacytoid dendritic cells in systemic lupus erythematosus. Arthritis Rheum 2003;48(9):2524–2532.
35. Wenzel J, Uerlich M, Wörrenkämper E, et al. Scarring skin lesions of discoid lupus erythematosus are characterized by high numbers of skin-homing cytotoxic lymphocytes associated with strong expression of the type I interferon-induced protein MxA. Br J Dermatol 2005;153(5):1011–1015.
36. Berthier CC, Tsoi LC, Reed TJ, et al. Molecular profiling of cutaneous lupus lesions identifies subgroups distinct from clinical phenotypes. J Clin Med 2019;8(8):1244.
37. Psarras A, Alase A, Antanaviciute A, et al. Functionally impaired plasmacytoid dendritic cells and non-haematopoietic sources of type I interferon characterize human autoimmunity. Nat Commun 2020;11(1):6149.
38. Billi AC, Ma F, Plazyo O, et al. Non-lesional and lesional lupus skin share inflammatory phenotypes that drive activation of CD16+ dendritic cells. bioRxiv Preprint posted online September 20, 2021. https://doi.org/10.1101/2021.09.17.460124
39. Siegal FP, Kadowaki N, Shodell M, et al. The nature of the principal type 1 interferon-producing cells in human blood. Science 1999;284(5421):1835–1837.
40. Swiecki M, Colonna M. The multifaceted biology of plasmacytoid dendritic cells. Nat Rev Immunol 2015;15(8):471–485.
41. Patel J, Maddukuri S, Li Y, et al. Highly multiplexed mass cytometry identifies the immunophenotype in the skin of dermatomyositis. J Invest Dermatol 2021;141(9):2151–2160.
42. Psarras A, Antanaviciute A, Alase A, et al. TNF-α regulates human plasmacytoid dendritic cells by suppressing IFN-α production and enhancing T cell activation. J Immunol 2021;206(4):785–796.
43. Billi AC, Gharaee-Kermani M, Fullmer J, et al. The female-biased factor VGLL3 drives cutaneous and systemic autoimmunity. JCI Insight 2019;4(8):e127291.
44. Farkas A, Kemény L. Monocyte-derived interferon-alpha primed dendritic cells in the pathogenesis of psoriasis: new pieces in the puzzle. Int Immunopharmacol 2012;13(2):215–218.
45. Baechler EC, Bilgic H, Reed AM. Type I interferon pathway in adult and juvenile dermatomyositis. Arthritis Res Ther 2011;13(6):249.
46. O'Connor KA, Abbott KA, Sabin B, et al. MxA gene expression in juvenile dermatomyositis peripheral blood mononuclear cells: association with muscle involvement. Clin Immunol 2006;120(3):319–325.
47. Moneta GM, Pires Marafon D, Marasco E, et al. Muscle expression of type I and type II interferons is increased in juvenile dermatomyositis and related to clinical and histologic features. Arthritis Rheumatol 2019;71(6):1011–1021.
48. Liao AP, Salajegheh M, Nazareno R, et al. Interferon β is associated with type 1 interferon-inducible gene expression in dermatomyositis. Ann Rheum Dis 2011;70(5):831–836.
49. Huard C, Gullà SV, Bennett DV, et al. Correlation of cutaneous disease activity with type 1 interferon gene signature and interferon β in dermatomyositis. Br J Dermatol 2017;176(5):1224–1230.
50. Gitiaux C, Latroche C, Weiss-Gayet M, et al. Myogenic progenitor cells exhibit type I interferon-driven proangiogenic properties and molecular signature during juvenile dermatomyositis. Arthritis Rheumatol 2018;70(1):134–145.
51. Higgs BW, Liu Z, White B, et al. Patients with systemic lupus erythematosus, myositis, rheumatoid arthritis and scleroderma share activation of a common type I interferon pathway. Ann Rheum Dis 2011;70(11):2029–2036.
52. Higgs BW, Zhu W, Morehouse C, et al. A phase 1b clinical trial evaluating sifalimumab, an anti-IFN-α monoclonal antibody, shows target neutralisation of a type I IFN signature in blood of dermatomyositis and polymyositis patients. Ann Rheum Dis. 2014 Jan;73(1):256–262.
53. Furie R, Khamashta M, Merrill JT, et al; CD1013 Study Investigators. Anifrolumab, an anti-interferon-alpha receptor monoclonal antibody, in moderate-to-severe systemic lupus erythematosus. Arthritis Rheumatol 2017;69(2):376–386.
54. Houssiau FA, Thanou A, Mazur M, et al. IFN-α kinoid in systemic lupus erythematosus: results from a phase IIb, randomised, placebo-controlled study. Ann Rheum Dis 2020;79(3):347–355.
55. Morand EF, Furie R, Tanaka Y, et al; TULIP-2 Trial Investigators. Trial of anifrolumab in active systemic lupus erythematosus. N Engl J Med 2020;382(3):211–221.
56. Bruce IN, Furie RA, Morand EF, et al. Concordance and discordance in SLE clinical trial outcome measures: analysis of three anifrolumab phase 2/3 trials. Ann Rheum Dis 2022;81(7):962–969.
57. Blum FR, Sampath AJ, Foulke GT. Anifrolumab for treatment of refractory cutaneous lupus erythematosus. Clin Exp Dermatol 2022;47(11):1998–2001.
58. Chasset F, Jaume L, Mathian A, et al; EMSED (Etude des maladies systémiques en dermatologie) study group. Rapid efficacy of anifrolumab in refractory cutaneous lupus erythematosus. J Am Acad Dermatol 2023;89(1):171–173.
59. Werth VP, Furie RA, Romero-Diaz J, et al. LILAC Trial Investigators. Trial of Anti-BDCA2 Antibody Litifilimab for Cutaneous Lupus Erythematosus. The New England Journal of Medicine. 2022;387(4):321–331.
60. McNiff JM, Kaplan DH. Plasmacytoid dendritic cells are present in cutaneous dermatomyositis lesions in a pattern distinct from lupus erythematosus. J Cutan Pathol 2008;35(5):452–456.
61. Wenzel J, Schmidt R, Proelss J, et al. Type I interferon-associated skin recruitment of CXCR3+ lymphocytes in dermatomyositis. Clin Exp Dermatol 2006;31:576–582.
62. Chen KL, Patel J, Zeidi M, et al. Myeloid dendritic cells are major producers of IFN-β in dermatomyositis and may contribute to hydroxychloroquine refractoriness. J Invest Dermatol 2021;141(8):1906–1914.e2.
63. Davis LS, Reimold AM. Research and therapeutics-traditional and emerging therapies in systemic lupus erythematosus. Rheumatology (Oxford) 2017;56(suppl_1):i100–i113.
64. Pelle MT, Callen JP. Adverse cutaneous reactions to hydroxychloroquine are more common in patients with dermatomyositis than in patients with cutaneous lupus erythematosus. Arch Dermatol 2002;138(9):1231–1233.

65. Anyanwu CO, Chansky PB, Feng R, et al. The systemic management of cutaneous dermatomyositis: results of a stepwise strategy. Int J Womens Dermatol 2017;3(4):189–194.
66. Cinats A, Heck E, Robertson L. Janus kinase inhibitors: a review of their emerging applications in dermatology. Skin Therapy Lett 2018; 23(3):5–9.
67. Kisseleva T, Bhattacharya S, Braunstein J, et al. Signaling through the JAK/STAT pathway, recent advances and future challenges. Gene 2002;285(1–2):1–24.
68. Kubo S, Nakayamada S, Tanaka Y. Baricitinib for the treatment of rheumatoid arthritis and systemic lupus erythematosus: a 2019 update. Expert Rev Clin Immunol 2019;15(7):693–700.
69. Klavdianou K, Lazarini A, Fanouriakis A. Targeted biologic therapy for systemic lupus erythematosus: emerging pathways and drug pipeline. BioDrugs 2020;34(2):133–147.
70. Bonnardeaux E, Dutz JP. Oral tofacitinib citrate for recalcitrant cutaneous lupus. JAAD Case Rep 2022;20:61–64.
71. Hasni SA, Gupta S, Davis M, et al. Phase 1 double-blind randomized safety trial of the Janus kinase inhibitor tofacitinib in systemic lupus erythematosus. Nat Commun 2021;12(1):3391.
72. Werth VP, Fleischmann R, Robern M, et al. Filgotinib or lanraplenib in moderate to severe cutaneous lupus erythematosus: a phase 2, randomized, double-blind, placebo-controlled study. Rheumatology (Oxford) 2022;61(6):2413–2423.
73. Paik JJ, Casciola-Rosen L, Shin JY, et al. Study of tofacitinib in refractory dermatomyositis: an open-label pilot study of ten patients. Arthritis Rheumatol 2021;73(5):858–865.
74. Le Voyer T, Gitiaux C, Authier FJ, et al. JAK inhibitors are effective in a subset of patients with juvenile dermatomyositis: a monocentric retrospective study. Rheumatology (Oxford) 2021;60(12):5801–5808.
75. Paudyal A, Zheng M, Lyu L, et al. JAK-inhibitors for dermatomyositis: a concise literature review. Dermatol Ther 2021;34(3):e14939.
76. Burke JR, Cheng L, Gillooly KM, et al. Autoimmune pathways in mice and humans are blocked by pharmacological stabilization of the TYK2 pseudokinase domain. Sci Transl Med 2019;11(502):eaaw1736.
77. Hoy SM. Deucravacitinib: first approval. Drugs 2022;82(17):1671–1679.
78. Morand E, Pike M, Merrill JT, et al. Deucravacitinib, a tyrosine kinase 2 inhibitor, in systemic lupus erythematosus: a phase II, randomized, double-blind, placebo-controlled trial. Arthritis Rheumatol 2023; 75(2):242–252.
79. Rom S, Persidsky Y. Cannabinoid receptor 2: potential role in immunomodulation and neuroinflammation. J Neuroimmune Pharmacol 2013;8(3):608–620.
80. Serhan CN, Chiang N, Van Dyke TE. Resolving inflammation: dual anti-inflammatory and pro-resolution lipid mediators. Nat Rev Immunol 2008;8(5):349–361.
81. Werth VP, Hejazi E, Pena SM, et al. Safety and efficacy of lenabasum, a cannabinoid receptor type 2 agonist, in patients with dermatomyositis with refractory skin disease: a randomized clinical trial. J Invest Dermatol 2022;142(10):2651–2659.e1.
82. khamashta M, Merrill JT, Werth VP, et al. CD1067 study investigators. Sifalimumab, an anti-interferon-α monoclonal antibody, in moderate to severe systemic lupus erythematosus: a randomised, double-blind, placebo-controlled study. Ann Rheum Dis 2016;75(11):1909–1916.
83. Fiorentino D, Mangold AR, Werth VP, et al. Efficacy, safety, and target engagement of dazukibart, an interferon-β specific monoclonal antibody, in adults with dermatomyositis: a double-blind, randomised, placebo-controlled phase 2 study. Lancet, in press.

American College of Rheumatology
Empowering Rheumatology Professionals

Arthritis & Rheumatology
Vol. 77, No. 1, January 2025, pp 12–21
DOI 10.1002/art.42968

Efficacy Versus Effectiveness: The HORIZON-Pivotal Fracture Trial and Its Emulation in Claims Data

Elvira D'Andrea, Sebastian Schneeweiss, Jessica M. Franklin, Seoyoung C. Kim, Robert J. Glynn, Su Been Lee, and Shirley V. Wang

Objective. The objective of this study is to evaluate the concordance of results between the Health Outcomes and Reduced Incidence with Zoledronic Acid Once Yearly (HORIZON)–Pivotal Fracture Trial (PFT) and a nonrandomized database study designed to emulate the trial.

Methods. HORIZON-PFT evaluated the efficacy of zoledronic acid versus placebo in reducing the risk of hip fractures and found a 41% risk reduction over a three-year treatment period (hazard ratio [HR] = 0.59; 95% confidence interval [95% CI] 0.42–0.83). Using two US claims databases from August 2007 to December 2020 or June 2021, we applied eligibility criteria from HORIZON-PFT and identified women with osteoporosis who initiated zoledronic acid or raloxifene as a proxy for placebo. The study protocol was registered on ClinicalTrials.gov (NCT04736693) before inferential analyses. We compared HORIZON-PFT and database study results using prespecified metrics.

Results. Because of low adherence in clinical practice, on-treatment follow-up was truncated at 18 months in the database study. The hip fracture risk after 18 months was 9.3 in 1,000 in the trial and 8.3 in 1,000 in the database analysis. In the database study, zoledronic acid was associated with a 28% reduction in hip fractures risk compared with raloxifene (HR = 0.72; 95% CI 0.51–0.92). The attenuated effect of zoledronic acid in the database study may be explained by its shorter follow-up, because the interpolated estimate of the effect in HORIZON-PFT at 18 months was HR_{RCT} (randomized controlled trial), 0.74, nearly identical to the observational estimate $HR_{database}$ 0.72.

Conclusion. Real-world emulation of the HORIZON-PFT found that zoledronic acid reduced hip fractures risk over an 18-month follow-up period. Limited adherence in clinical practice diminished the magnitude of its preventive effect and precluded long-term estimation of effectiveness in this setting.

INTRODUCTION

The Health Outcomes and Reduced Incidence with Zoledronic Acid Once Yearly (HORIZON)–Pivotal Fracture Trial (PFT) was a randomized double-blinded, placebo-controlled trial conducted in postmenopausal women with osteoporosis to investigate the efficacy of zoledronic acid in reducing the risk of hip and vertebral fractures.[1] Participants were randomly assigned to receive either a once-yearly intravenous administration of zoledronic acid (5 mg) or placebo for three years and were monitored periodically with telephone interviews and clinic visits for 36 months. HORIZON-PFT found that zoledronic acid reduced the risk of hip fractures by 41% compared with placebo over a three-year study period.[1]

Over 80% of participants were adherent to the annual infusion schedule over the three-year follow-up for HORIZON-PFT.[1] However, in clinical practice, adherence to pharmacotherapies for osteoporosis is less than ideal.[2–5] Only about half of patients continue oral bisphosphonate treatment after one year.[2–4] Although the availability of parenteral preparations, which circumvented the gastrointestinal effects of early oral formulations, and the introduction of agents with extended intervals of

ClinicalTrials.gov identifier: NCT04736693.

Neither the FDA nor the NIH had any role in the design and conduct of the study; collection, management, analysis, and interpretation of the data; preparation, review, or approval of the manuscript; and decision to submit the manuscript for publication.

Supported by the US Food and Drug Administration to the Brigham and Women's Hospital (HHSF223201710186C and HHSF223201810146C).

Elvira D'Andrea, MD, MPH, PhD, Sebastian Schneeweiss, MD, ScD, Jessica M. Franklin, PhD, Seoyoung C. Kim, MD, ScD, Robert J. Glynn, PhD, ScD, Su Been Lee, BA, Shirley V. Wang, PhD: Brigham and Women's Hospital and Harvard Medical School, Boston, Massachusetts.

Additional supplementary information cited in this article can be found online in the Supporting Information section (https://acrjournals.onlinelibrary.wiley.com/doi/10.1002/art.42968).

Author disclosures are available at https://onlinelibrary.wiley.com/doi/10.1002/art.42968.

Address correspondence via email to Elvira D'Andrea, MD, MPH, PhD, at elvira.dandrea@mail.harvard.edu.

Submitted for publication January 4, 2024; accepted in revised form July 16, 2024.

administration, such as once-yearly infusions of zoledronic acid, improved adherence rates, those rates are still suboptimal. Among US Medicare beneficiaries, 32% of zoledronic acid initiators did not receive their second annual doses.[5] Poor adherence limits the effectiveness of the treatment against fractures.[6–8]

We emulated the design of the HORIZON-PFT using observational analogs in claims-based databases to define key study parameters, including the population, intervention, comparator, and outcome. Our goal was to compare the results between the trial and the database study and to understand how differences in adherence affect concordance in results. The study methodology has been described and discussed as part of the RCT-DUPLICATE initiative.[9–14]

MATERIALS AND METHODS

Study design and data source. To emulate HORIZON-PFT, we performed an active comparator, incident user cohort study using real-world data from two US claims databases (Optum's de-identified Clinformatics Data Mart Database and Merative MarketScan Research Database) derived from databases of administrative health claims for members of large commercial and Medicare Advantage health plans. The data sets contain demographic information, health plan enrollment status, longitudinal patient-level information on all reimbursed medical services, inpatient and outpatient diagnoses and procedures, and pharmacy dispensing records. The Mass General Brigham Institutional Review Board provided ethics approval, and data use agreements were in place. The protocol was registered before the inferential analysis of study outcomes was started (NCT04736693).

Study patients and treatment. Within the two US real-world data sources, we identified a cohort of women with osteoporosis, between 65 and 89 years of age, who had their first annual infusion of zoledronic acid or started daily oral raloxifene from August 21, 2007 (when the US Food and Drug Administration approved zoledronic acid for the treatment of osteoporosis in postmenopausal women) to the end of available data (through 2020 for MarketScan and through March 2022 for CDM). To mimic the placebo arm of HORIZON-PFT, we selected women initiating raloxifene as a placebo-proxy comparator group. Raloxifene is similarly indicated for the treatment of postmenopausal osteoporosis; however, high-quality evidence has found that it is not effective at preventing hip fractures.[15] The advantages of such a new-user active-comparator cohort design are well described.[16–18] The cohort entry date was the day of the first infusion of zoledronic acid or the first filled prescription of raloxifene after at least 15 months of continuous enrollment within the database. To this cohort, we applied eligibility criteria analogs to the HORIZON-PFT using claims data (Supplementary Table 1). Like HORIZON-PFT, we allowed patients who initiated zoledronic acid to be exposed to raloxifene before cohort entry.

Study eligibility was limited to women with a recorded diagnosis of osteoporosis before drug initiation or a previous prescription for oral bisphosphonates with a required washout period of two years before cohort entry. Patients were excluded if they had a life expectancy shorter than six months; lower extremity amputations; use of parathyroid hormone, bisphosphonates, denosumab, or romosozumab; or a recorded diagnosis of glucocorticoid-induced osteoporosis or Paget syndrome within two years before cohort entry. We also excluded patients with a diagnosis of malignancy, bone metabolism diseases, end-stage renal disease, end-stage liver disease, blindness, noncompliance with medical treatment, substance use disorder within 12 months before cohort entry, or with a recent use of anabolic steroids or growth hormone or systemic glucocorticoids (Supplementary Table 1 and Supplementary Figure 1).

Outcome and follow-up. The primary outcome was hip fracture, which was defined using a validated claims-based algorithm with a positive predictive value (PPV) of 95%.[19] Contrary to HORIZON-PFT, we did not pursue the evaluation of vertebral fractures over concerns of the substantial misclassification of incident vertebral fractures in claims data.[20] However, we did evaluate nonvertebral fractures as a secondary outcome, as reported in the HORIZON-PFT (see Supplementary Table 2 for outcome definitions and PPVs).[1,19]

Follow-up started one day after cohort entry and continued for up to 18 months, censoring at the occurrence of an outcome event, nursing home admission, disenrollment from the insurance plan, death, or end of the study period, whichever came first. Because HORIZON-PFT participants were largely adherent to treatment during follow-up, ie, received an infusion at 12 and 24 months, the trial's intention-to-treat estimates were closely reflective of a "on-treatment" estimand. However, only ~30% of patients in our clinical practice cohort received a second annual infusion of zoledronic acid within 18 months after the first infusion, prompting the need for a shorter follow-up period in our study to estimate an analog of the intention-to-treat effect over a time frame for which we could emulate the high adherence to treatment observed in HORIZON-PFT. Given the demonstrated preventive effects of zoledronic acid against osteoporotic fractures for at least 18 months after the initial infusion,[21] we limited the study period to 18 months. This included a 12-month treatment duration and a 6-month grace period to account for the lingering effects of zoledronic acid among patients who discontinued treatment and the ongoing effects in those who continued. By observing patients for 18 months, we maintained statistical power to detect meaningful differences in hip fracture events and sample size consistency until the end of follow-up, similar to the HORIZON trial. As a result, the 18-month analog of the intention-

to-treat analysis was also reflective of an "on-treatment" estimand because it censored patients after the hypothesized window for biologic effect of therapy had passed.

We also conducted analogs of the intention-to-treat analyses for follow-up periods of 12, 15, and 21 months, as well as an analysis for up to 3 years (36 months) after treatment initiation, similar to the HORIZON trial. These analyses evaluated the effect of starting therapy, regardless of whether patients continued to receive it.

Statistical analysis. Separately within each database, propensity score (PS) matching was used to balance 85 prespecified covariates between treatment arms, in which zoledronic acid initiators were 1:1 matched to raloxifene initiators without replacement on their estimated PS using a nearest-neighbor approach with a caliper width of 0.01 on the PS scale. Covariates were measured within 15 months before cohort entry and included demographics (age, sex, geographic region, metropolitan area), calendar time of drug initiation, indexes of the overall health state such as combined comorbidity score and claims-based frailty index,[22,23] conditions that may alter bone metabolism (disorders of the digestive system, premature menopause, vitamin D deficiency, oophorectomy, osteopenia, previous fractures), other comorbidities, use of medications, and indicators of health care use as a proxy for overall disease state, care intensity, and surveillance (Supplementary Tables 3 and 4).

Before registering the protocol, we conducted several feasibility and validity checks. First, we estimated the expected power for detecting superiority of the primary endpoint at an α level of 0.05 using outcome counts unstratified by exposure. Second, we assessed the post-matching covariate balance between treatment groups by calculating standardized differences (values lower than 10% indicating balance), overlap in the PS distributions of the treatment groups, and C-statistics before and after matching, expecting a value close to 0.5 indicating multivariate balance. The primary analysis was conducted first in early 2020 using data available at that time.[9] We conducted the same analysis in late 2022 with updated data that are presented here.

For the primary analysis, we tabulated numbers of events, incidence risks (intention-to-treat estimand, comparable with interpolated incidence of events in the trial at 18 months) and rates (on-treatment estimand), and rate differences (RDs) per 1,000 person-years (PY). Hazard ratios (HRs) and 95% confidence intervals (95% CIs) were estimated by Cox regression models. Using Kaplan–Meier methods, we plotted the cumulative incidence of hip fractures and estimated the number needed to treat by inverting the difference in cumulative incidence between the two groups at 18 months of follow-up.[24,25] We also performed log-rank tests to compare hazard rates between the two drugs over the same period. We conducted a sensitivity analysis to account for the competing risk of death by using Fine and Gray's proportional subhazards model.[26–28] Analyses were conducted in each data source separately and results pooled using a fixed-effects meta-analysis. All analyses were performed using Aetion Evidence Platform (Aetion Inc.) and STATA 15.1 statistical software (StataCorp LLC).

Agreement assessment. The concordance of the effect estimates between HORIZON-PFT and the database study emulating the trial was measured using three prespecified binary agreement metrics: the "statistical significance agreement," which is met when statistical significance at an alpha level of 0.05 agrees; the "estimate agreement," which is reached when the database study effect estimate is within the 95% CI of the primary trial effect estimate of 0.42 to 0.83[1]; and the "standardized difference agreement," which is met when the absolute standardized difference between the treatment effect estimates between the trial and emulation are less than 1.96.

Given the different lengths of follow-up between the HORIZON-PFT and database study, we also estimated the concordance of the effect estimates over an aligned follow-up window of 18 months. To estimate the HR of HORIZON-PFT at 18 months, we extracted the cumulative incidence of hip fracture at 18 months for both zoledronic acid and placebo from the Kaplan–Meier curves observed in HORIZON-PFT by using the Graph Grabber 2.0.2 data retrieval software (Quintessa Limited).[29]

Data availability. Individual patient-level data cannot be shared with third parties based on the Data Use Agreement in place between the Division of Pharmacoepidemiology and Pharmacoeconomics of Mass General Brigham and Optum and between the Division of Pharmacoepidemiology and Pharmacoeconomics of Mass General Brigham and Merative MarketScan.

RESULTS

We identified 52,631 eligible postmenopausal women with osteoporosis, of whom 38,107 initiated zoledronic acid and 14,524 initiated raloxifene (Figure 1). Compared with those who initiated raloxifene, those who initiated zoledronic acid were older, had a greater burden of comorbidities (including coronary artery diseases, atrial fibrillation, chronic obstructive pulmonary disease, obstructive sleep apnea, and osteoarthrosis), were frailer, and had a higher number of recorded falls, gait abnormalities, history of hospitalizations and emergency department admissions, outpatient visits, flu and pneumococcal vaccines, and screening tests such as regular blood tests and bone density examinations. Women initiating zoledronic acid were more likely to receive multiple drug prescriptions and to contribute with a smaller copay to the overall medication costs than women initiating raloxifene (Table 1 and Supplementary Table 3). A small number of patients

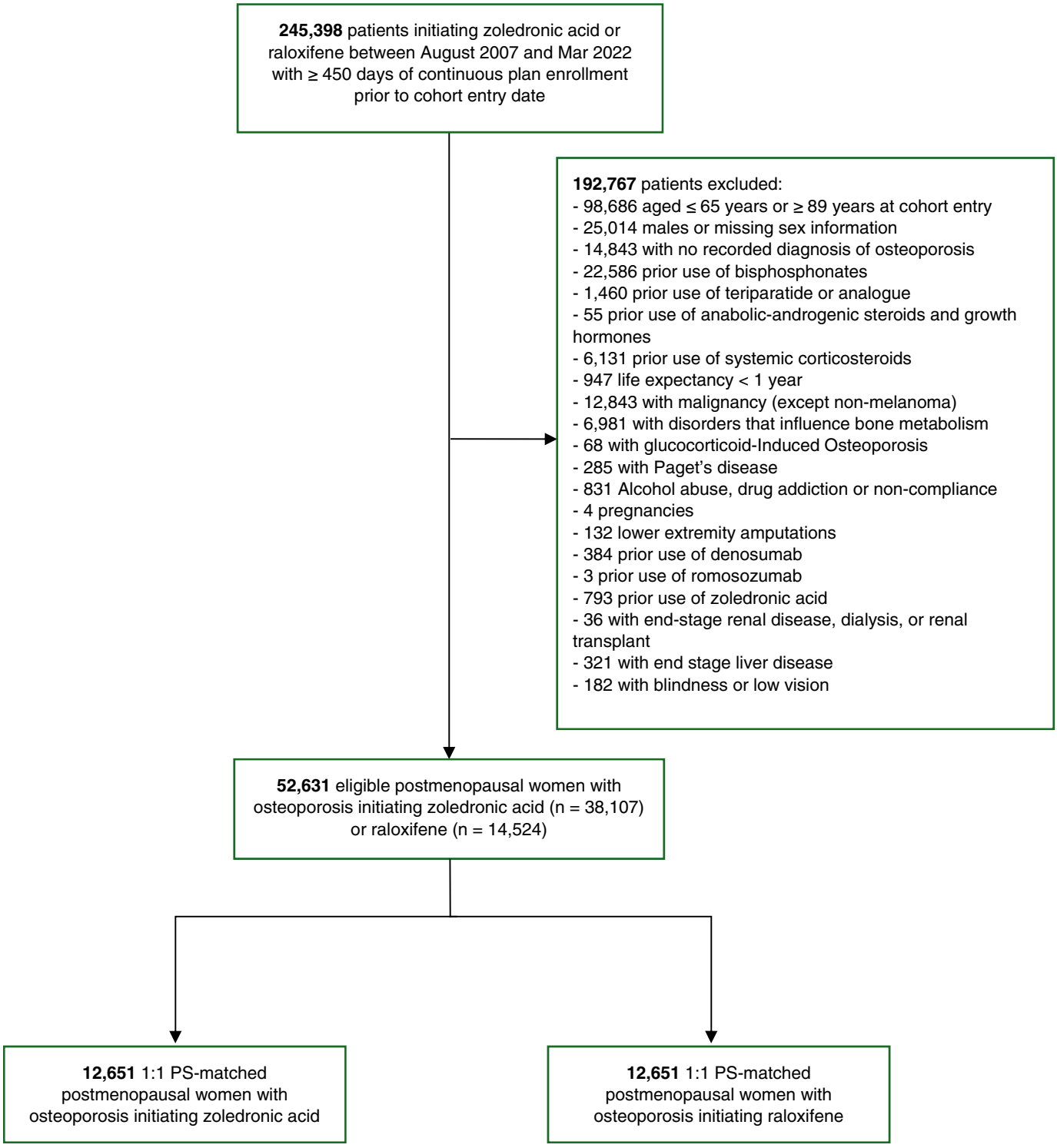

Figure 1. Study flowchart: Eligible population included in the study cohort initiating zoledronic acid or raloxifene between August 2007 and March 2022 before and after matching. PS, propensity score. Color figure can be viewed in the online issue, which is available at http://onlinelibrary.wiley.com/doi/10.1002/art.42968/abstract.

initiating zoledronic acid also received a prescription for raloxifene at baseline (264 patients, 2.1%) because of the new-user design.

After PS matching, we retained 25,302 eligible women initiating zoledronic acid or raloxifene (12,651 in each cohort) with well-balanced baseline characteristics (Table 1, Supplementary Table 4, and Figure 2) and identical PS distributions (Supplementary Figure 2). Compared with the HORIZON-PFT, patients included in the database analysis were slightly older (mean age of 73.1 versus 73.9).[1] The estimated power for the primary analysis exceeded 99% for superiority, and the post-

Table 1. Selected baseline characteristics of patients initiating treatment with zoledronic acid versus raloxifene after 1:1 PS matching*

Baseline characteristics	Before 1:1 PS matching			After 1:1 PS matching		
	Raloxifene, n = 14,524	Zoledronic acid, n = 38,107	Standardized difference	Raloxifene, n = 12,651	Zoledronic acid, n = 12,651	Standardized difference
Demographics						
Age of patients, mean ± SD, y	73.67 ± 6.46	74.78 ± 6.46	−0.17	73.89 ± 6.49	73.86 ± 6.39	0.00
Age categories, n (%)						
<70	4,779 (32.9)	9,852 (25.9)	0.15	3,958 (31.3)	3,998 (31.6)	−0.01
70–74	3,704 (25.5)	9,674 (25.4)	0.00	3,244 (25.6)	3,326 (26.3)	−0.02
≥75	6,041 (41.6)	18,581 (48.8)	−0.15	5,449 (43.1)	5,327 (42.1)	0.02
Calendar time, n (%)						
August 2007–December 2010	4,315 (29.7)	6,471 (17.0)	0.30	3,280 (25.9)	3,338 (26.4)	−0.01
January 2011–December 2013	3,536 (24.3)	9,333 (24.5)	0.00	3,320 (26.2)	3,342 (26.4)	0.00
January 2014–December 2016	2,902 (20.0)	6,594 (17.3)	0.07	2,553 (20.2)	2,565 (20.3)	0.00
January 2017–June 2021	3,771 (26.0)	15,709 (41.2)	−0.33	3,498 (27.6)	3,406 (26.9)	0.02
Lifestyle factors, n (%)						
Smoking	944 (6.5)	4,474 (11.7)	−0.18	895 (7.1)	915 (7.2)	0.00
Obesity or overweight	1,372 (9.4)	4,668 (12.2)	−0.09	1,259 (10.0)	1,261 (10.0)	0.00
Burden of comorbidities						
Combined comorbidity index, mean ± SD	0.54 ± 1.60	0.89 ± 1.83	−0.20	0.59 ± 1.62	0.61 ± 1.63	−0.01
Frailty score, n (%)						
Robust	11,289 (77.7)	27,401 (71.9)	0.13	9,606 (75.9)	9,567 (75.6)	0.01
Prefrail	2,932 (20.2)	9,238 (24.2)	−0.10	2,761 (21.8)	2,765 (21.9)	0.00
Mildly to severely frail	303 (2.1)	1,468 (3.9)	−0.11	284 (2.2)	319 (2.5)	−0.02
Cardiovascular and metabolic conditions, n (%)						
Hypertension	8,221 (56.6)	23,025 (60.4)	−0.08	7,290 (57.6)	7,313 (57.8)	0.00
Hyperlipidemia	8,476 (58.4)	22,917 (60.1)	−0.03	7,504 (59.3)	7,527 (59.5)	0.00
Atherosclerotic cardiovascular disease[a]	1,755 (12.1)	6,149 (16.1)	−0.12	1,613 (12.7)	1,646 (13.0)	−0.01
Cerebrovascular disease[b]	534 (3.7)	2,132 (5.6)	−0.09	493 (3.9)	492 (3.9)	0.00
Heart failure	394 (2.7)	1,181 (3.1)	−0.02	351 (2.8)	361 (2.9)	−0.01
PVD or PVD surgery	913 (6.3)	2,735 (7.2)	−0.04	830 (6.6)	820 (6.5)	0.00
Atrial fibrillation or other cardiac dysrhythmia	1,647 (11.3)	6,336 (16.6)	−0.15	1,520 (12.0)	1,583 (12.5)	−0.02
Diabetes with or without complications	2,518 (17.3)	6,599 (17.3)	0.00	2,232 (17.6)	2,270 (17.9)	−0.01
Gastrointestinal conditions, n (%)						
Malabsorption disorders[c]	1,307 (9.0)	4,295 (11.3)	−0.08	1,191 (9.4)	1,214 (9.6)	−0.01
Disorders of esophagus, stomach, and duodenum	819 (5.6)	2,638 (6.9)	−0.05	753 (6.0)	741 (5.9)	0.00
Gastrointestinal bleeding	537 (3.7)	1,654 (4.3)	−0.03	485 (3.8)	504 (4.0)	−0.01
Disorders of gallbladder, biliary tract, and pancreas	414 (2.9)	1,384 (3.6)	−0.04	374 (3.0)	370 (2.9)	0.01
Other conditions, n (%)						
Osteoarthrosis	4,096 (28.2)	14,754 (38.7)	−0.22	3,823 (30.2)	3,772 (29.8)	0.01
Alzheimer disease and other forms of dementia	681 (4.7)	2,588 (6.8)	−0.09	623 (4.9)	620 (4.9)	0.00
Hypothyroidism	3,422 (23.6)	10,513 (27.6)	−0.09	3,106 (24.6)	3,109 (24.6)	0.00
Liver disease	591 (4.1)	1,646 (4.3)	−0.01	514 (4.1)	483 (3.8)	0.02
Chronic kidney disease stages I–III	1,150 (7.9)	2,769 (7.3)	0.02	992 (7.8)	968 (7.7)	0.00
Chronic kidney disease stages IV or V	303 (2.1)	421 (1.1)	0.08	257 (2.0)	164 (1.3)	0.05
Premature menopause	14 (0.1)	94 (0.2)	−0.03	13 (0.1)	18 (0.1)	0.00
Oophorectomy	14 (0.1)	51 (0.1)	0.00	11 (0.1)	9 (0.1)	0.00
COPD	1,372 (9.4)	5,027 (13.2)	−0.12	1,261 (10.0)	1,306 (10.3)	−0.01
Asthma	1,157 (8.0)	3,834 (10.1)	−0.07	1,060 (8.4)	1,073 (8.5)	0.00
Obstructive sleep apnea	475 (3.3)	2,471 (6.5)	−0.15	454 (3.6)	455 (3.6)	0.00
Syncope	517 (3.6)	1,918 (5.0)	−0.07	478 (3.8)	477 (3.8)	0.00

(Continued)

Table 1. (*Cont'd*)

Baseline characteristics	Before 1:1 PS matching			After 1:1 PS matching		
	Raloxifene, n = 14,524	Zoledronic acid, n = 38,107	Standardized difference	Raloxifene, n = 12,651	Zoledronic acid, n = 12,651	Standardized difference
Falls	825 (5.7)	3,665 (9.6)	−0.15	770 (6.1)	755 (6.0)	0.00
VTE	183 (1.3)	1,023 (2.7)	−0.10	179 (1.4)	236 (1.9)	−0.04
Gait abnormality	1,080 (7.4)	4,617 (12.1)	−0.16	1,002 (7.9)	1,011 (8.0)	0.00
Osteopenia	4,797 (33.0)	13,153 (34.5)	−0.03	4,229 (33.4)	4,134 (32.7)	0.01
Hip and femur fractures	286 (2.0)	1,295 (3.4)	−0.09	266 (2.1)	287 (2.3)	−0.01
Vertebral fractures	1,037 (7.1)	4,201 (11.0)	−0.14	976 (7.7)	965 (7.6)	0.00
Other fractures	522 (3.6)	2,141 (5.6)	−0.10	482 (3.8)	509 (4.0)	−0.01
Medication use, n (%)						
Calcitonin	257 (1.8)	487 (1.3)	0.00	238 (1.9)	217 (1.7)	0.00
Oral glucocorticoids	3,443 (23.7)	10,203 (26.8)	−0.07	3,189 (25.2)	3,196 (25.3)	0.00
Antidepressants	3,409 (23.5)	11,364 (29.8)	−0.14	3,232 (25.5)	3,194 (25.2)	0.01
Anticonvulsants	1,490 (10.3)	5,579 (14.6)	−0.13	1,408 (11.1)	1,483 (11.7)	−0.02
Beta blocker or calcium channel blockers	4,209 (29.0)	10,574 (27.7)	0.03	3,761 (29.7)	3,748 (29.6)	0.00
PPIs	3,973 (27.4)	11,972 (31.4)	−0.09	3,705 (29.3)	3,632 (28.7)	0.01
Opioids	4,160 (28.6)	12,718 (33.4)	−0.10	3,932 (31.1)	3,919 (31.0)	0.00
Antipsychotics	233 (1.6)	708 (1.9)	−0.02	214 (1.7)	210 (1.7)	0.00
Anxiolytics/hypnotics	1,279 (8.8)	3,265 (8.6)	0.01	1,158 (9.2)	1,206 (9.5)	−0.01
Dementia medications	425 (2.9)	1,375 (3.6)	−0.04	400 (3.2)	393 (3.1)	0.01
Antiparkinsonian medications	350 (2.4)	1,304 (3.4)	−0.06	333 (2.6)	343 (2.7)	−0.01
Benzodiazepine	2,283 (15.7)	6,249 (16.4)	−0.02	2,116 (16.7)	2,155 (17.0)	−0.01
Glucose-lowering medications	1,499 (10.3)	3,561 (9.3)	0.03	1,329 (10.5)	1,331 (10.5)	0.00
ACEi/ARBs	5,493 (37.8)	12,859 (33.7)	0.09	4,840 (38.3)	4,818 (38.1)	0.00
Anticoagulants	629 (4.3)	2,800 (7.3)	−0.13	598 (4.7)	647 (5.1)	−0.02
Diuretics	4,198 (28.9)	10,120 (26.6)	0.05	3,729 (29.5)	3,711 (29.3)	0.00
NSAIDs	2,884 (19.9)	7,334 (19.2)	0.02	2,661 (21.0)	2,459 (19.4)	0.04
Hormone replacement therapy	1,456 (10.0)	3,446 (9.0)	0.03	1,305 (10.3)	1,343 (10.6)	−0.01
Statins	6,430 (44.3)	16,170 (42.4)	0.04	5,804 (45.9)	5,817 (46.0)	0.00
Previous use of bisphosphonates[d]	4,198 (28.9)	10,467 (27.5)	0.03	3,697 (29.2)	3,986 (31.5)	−0.05
Measures of health care use						
No. of prescribed medications, mean ± SD	18.84 ± 16.04	21.39 ± 18.67	−0.15	20.01 ± 16.32	20.22 ± 15.25	−0.01
No. of hospitalizations, mean ± SD	0.38 ± 1.85	0.53 ± 2.19	−0.07	0.40 ± 1.94	0.41 ± 1.94	−0.01
No. of ED visits, mean ± SD	0.32 ± 0.80	0.47 ± 1.02	−0.16	0.34 ± 0.82	0.35 ± 0.82	−0.01
No. of office visits, mean ± SD	10.53 ± 8.09	13.64 ± 9.51	−0.35	11.08 ± 8.24	11.18 ± 7.56	−0.01
No. of bone density test, mean ± SD	0.60 ± 0.56	0.69 ± 0.58	−0.16	0.62 ± 0.56	0.62 ± 0.54	0.00
Metabolic blood chemistry test, n (%)	8,244 (56.8)	27,974 (73.4)	−0.35	7,698 (60.8)	7,661 (60.6)	0.00
Flexible sigmoidoscopy, colonoscopy or CT virtual colonoscopy, n (%)	1,752 (12.1)	4,917 (12.9)	−0.02	1,569 (12.4)	1,556 (12.3)	0.00
Mammograms, n (%)	8,840 (60.9)	22,873 (60.0)	0.02	7,656 (60.5)	7,769 (61.4)	−0.02
Pap smear, n (%)	3,327 (22.9)	5,793 (15.2)	0.20	2,652 (21.0)	2,772 (21.9)	−0.02
Flu vaccine, n (%)	4,648 (32.0)	14,345 (37.6)	−0.12	4,182 (33.1)	4,143 (32.7)	0.01
Pneumococcal vaccine, n (%)	3,009 (20.7)	11,378 (29.9)	−0.21	2,767 (21.9)	2,734 (21.6)	0.01
Copay for pharmacy cost (USD)	28.05 (33.64)	22.63 (26.67)	0.18	25.43 (26.75)	25.44 (33.07)	0.00

* ACEi, angiotensin-converting enzyme; ARB, angiotensin receptor blocker; COPD, chronic obstructive pulmonary disease; CT, computerized tomography; ED, emergency department; NSAID, nonsteroidal anti-inflammatory drugs; PPIs, proton-pump inhibitors; PS, propensity score; PVD, peripheral vascular disease; TIA, transient ischemic attack; VTE, venous thromboembolism.

[a] Myocardial infarction, stable or unstable angina, coronary atherosclerosis, history of cardiovascular procedures.

[b] Ischemic or hemorrhagic stroke, TIA, late effects of cerebrovascular disease.

[c] Noninfective enteritis and colitis, other intestinal malabsorption, intraoperative and postprocedural complications and disorders of lower digestive system.

[d] Measured from the time of insurance enrollment to 730 days (2 years) before the day of treatment initiation.

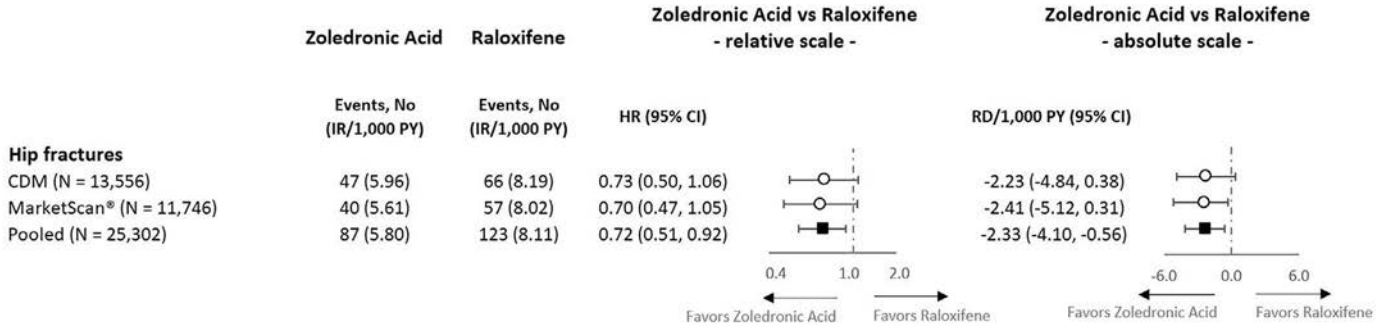

Figure 2. Number of events, person-time, and incidence rates for the outcome hip fractures in 1:1 propensity score–matched initiators of zoledronic acid versus raloxifene: Number of events and incidence rates by treatment group and point estimates of the effect sizes are presented overall (pooled) and for individual databases. Estimates of the effect sizes were pooled using a fixed-effects meta-analysis. HRs and RDs for individual databases are indicated by circles, whereas pooled estimates are indicated by squares; 95% CIs are indicated by horizontal lines. 95% CI, 95% confidence interval; CDM, Clinformatics® Data Mart Database; HR, hazard ratio; IR, incidence rate; PY, person-years; RD, rate difference.

matching C-statistic was about 0.53 (Supplementary Figure 3). The mean and median follow-up time were 435 and 540 days (Supplementary Table 5).

Overall, the hip fracture risk after 18 months was 8.3 in 1,000 (zoledronic acid: 6.9 in 1,000 events, raloxifene: 9.7 in 1,000 events), which was similar to the interpolated incidence at 18 months of 9.3 in 1,000 (zoledronic acid: 7.9 in 1,000 events, placebo: 10.6 in 1,000 events) found in the HORIZON-PFT. The incidence rate was 5.8 in 1,000 (87 events) among those who initiated zoledronic acid and 8.1 in 1,000 (123 events) among those who initiated raloxifene. This resulted in a 28% decreased risk (HR = 0.72; 95% CI 0.51–0.92) or two fewer events (RD –2.3; 95% CI –4.10 to –0.56) per 1,000 PY of zoledronic acid use versus raloxifene (Figures 2 and 3). Findings were consistent across the individual databases; specifically, the risk reduction of hip fracture varied little between the two databases: HR = 0.73 (95% CI 0.50–1.06) and HR = 0.70 (95% CI 0.47–1.05) (Figure 2). The cumulative incidence of hip fracture among those who initiated zoledronic acid versus raloxifene began to diverge after about five months (Figure 3). The number needed to treat with zoledronic acid to prevent hip fractures in one patient was 286 at 18 months. Results remained consistent when we performed the competing risk regression analysis (HR = 0.71; 95% CI 0.54–0.94).

All three prespecified binary agreement metrics were met. The "statistical significance agreement" was satisfied because the upper limit of the 95% CI in the database analysis did not cross the null, which was consistent with the results from the trial. The "estimate agreement" was satisfied because the effect

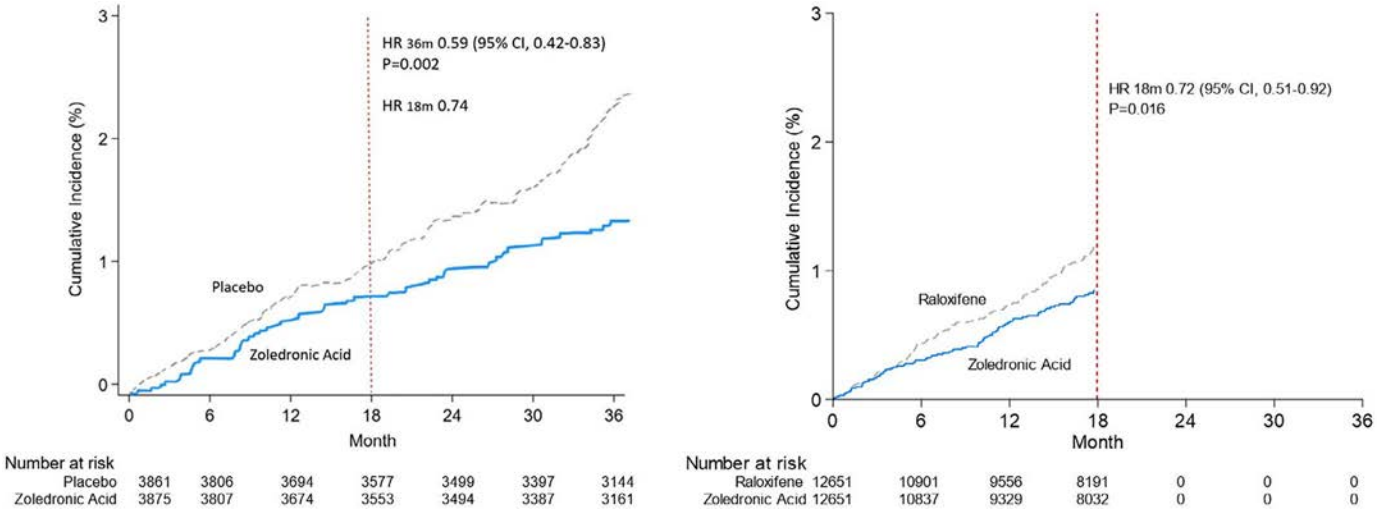

Figure 3. Cumulative incidence for hip fracture comparing zoledronic acid versus placebo in the HORIZON-PFT and PS-matched zoledronic acid versus raloxifene initiators in the RWE emulation trial: Cumulative incidence for hip fracture during 18 and 36 months in the HORIZON-PFT (A) and cumulative incidence for hip fracture during 18 months in the RWE emulation of the HORIZON-PFT (B). To estimate the hazard ratio of HORIZON-PFT at 18 months, we extracted the cumulative incidence of hip fracture for both zoledronic acid and placebo from the Kaplan–Meier curves observed in HORIZON-PFT, using by the Graph Grabber 2.0.2 data retrieval software (Quintessa Limited).[27] 95% CI, 95% confidence interval; HORIZON-PFT, Health Outcomes and Reduced Incidence with Zoledronic Acid Once Yearly–Pivotal Fracture Trial; HR, hazard ratio; PS, propensity score; RWE, real-world evidence. Color figure can be viewed in the online issue, which is available at http://onlinelibrary.wiley.com/doi/10.1002/art.42968/abstract.

estimate from the database study (ie, 0.72) was within the 95% CI of the HORIZON-PFT effect estimate (ie, 95% CI 0.42–0.83). The "standardized difference agreement" was also met (standardized difference = –0.90).

Although the comparison of estimates for HORIZON-PFT at 36 months to the database study emulation at 18 months met the three binary agreement metrics, the results were more closely aligned when follow-up time for the HORIZON-PFT trial was truncated to 18 months. If the trial had evaluated the efficacy of zoledronic acid versus placebo at 18 months, the effect estimate would have been almost identical to the one calculated in our database study ($HR_{database}$ = 0.72 versus HR_{RCT} [randomized control trial] = 0.74).

The sensitivity analyses conducted over different follow-up windows showed a gradually increasing effect of zoledronic acid in preventing hip fractures from 12 to 18 months of follow-up, along with a stable effect between 18 and 21 months (Supplementary Table 6). In the analog of the intention-to-treat analysis that observed patients for up to three years, only 40% of patients completed three years of follow-up due to disenrollment from the insurance plan, death, and end of data availability. The estimated effect from the three-year analysis was consistent with the primary "on-treatment" database study analysis up to 18 months (HR = 0.74; 95% CI 0.58–0.91) (Supplementary Table 6). The stable effect observed in clinical practice at 18 months and 3 years is in line with some evidence that the beneficial effect of zoledronic may increase with cumulative dosing over multiple years.[1] Unlike the HORIZON trial, there was low adherence to annual infusions in clinical practice, and about 30% had a second infusion within 18 months.

A similar pattern was observed for nonvertebral fractures, with the preventive effect of zoledronic acid increasing up to 18 months and subsequently reaching a plateau or even declining (Supplementary Table 6). The analysis conducted over 18 months of follow-up showed an attenuated effect of zoledronic acid in preventing nonvertebral fractures (HR = 0.92, 95% CI 0.74 to 1.06) compared with the effect shown in the HORIZON-PFT over a three-year follow-up (HR = 0.75, 95% CI 0.64 to 0.87), which is consistent with the attenuated database study results for hip fractures.

DISCUSSION

We emulated the randomized placebo-controlled trial HORIZON-PFT using claims-based databases to evaluate the effectiveness of zoledronic acid in preventing hip fracture in a clinical setting in which poor adherence to pharmacotherapies for osteoporosis after one year is the norm. We identified a large population-based cohort of 25,302 postmenopausal women with osteoporosis, about 6.5 times the size of the sample recruited by the HORIZON-PFT, and observed them for a year and a half when most women failed to receive a second infusion. In contrast, the strict trial protocol and procedures that were part of HORIZON-PFT resulted in over 80% adherence over three years of follow-up. We observed that women initiating once-yearly infusions of zoledronic acid in clinical practice had a 28% lower risk of hip fractures than those receiving raloxifene, a drug that is also indicated for osteoporosis but that has been shown not to affect risk of hip fracture. In contrast, HORIZON-PFT showed a 41% reduced risk over three years.

Although the prespecified binary concordance metrics were met, the effectiveness of zoledronic acid on preventing hip fractures was attenuated in the clinical practice setting compared with the efficacy shown in the trial. The trial results suggested that the beneficial effect of zoledronic acid on reducing risk of hip fractures increased with subsequent infusions over the three years of follow-up.[1,30,31] The diminished effect found in the database study may be explained by shorter time on therapy in clinical practice coupled with the increasing beneficial effect with longer treatment in the trial.[1]

The findings also indicate that the preventive effect of zoledronic acid on hip fractures may extend beyond the recommended annual administration interval, persisting for at least 18 months after the initial infusion. These results align with the results from other studies and contribute to evaluating the appropriate dosing interval of zoledronic acid.[21,32] Additionally, given the association between nonadherence and frailty and history of fragility fractures, it is crucial not to overlook the long-lasting effectiveness of a single dose, particularly for individuals at a high risk of fractures.[32,33]

Randomized controlled trials (RCTs) often evaluate the efficacy of medications for osteoporosis or other diseases with historically suboptimal or poor adherence rates in clinical practice. Our results highlight the importance of generating evidence that is complementary to trials, which can inform key stakeholders about the anticipated benefits of a considered therapy under clinical practice conditions. Real-world data can be used in different ways to support the evaluation of drug effectiveness. First, such data can provide evidence of utilization patterns and adherence in clinical practice. This data can be used to inform secondary analyses of trials that truncate follow-up at intermediate time intervals that are reflective of the anticipated duration of treatment in practice. Alternatively, real-world data can be used to emulate a target trial's design and directly generate estimates of effectiveness in populations analogous to the trial population, as well as in different populations in which, for various reasons, a trial cannot be conducted. Such estimates of effectiveness would supply clinicians with evidence that can be more precisely translated into a clinical setting. They could also be highly informative for regulatory and coverage decisions. Such evidence may also be useful to inform identification of effective interventions to improve adherence to antiosteoporosis medications, which remains a major goal in clinical practice.[34]

The likelihood of claims-based database studies closely replicating the results of RCTs increases when the study design and measurements can be emulated well. This includes having a

real-world patient population similar to the trial population; accurately measuring exposure, outcomes, and population defining characteristics; emulating a placebo control arm with an active-comparator proxy for placebo; and addressing confounding factors.[9,35] Another challenge in replicating trial results, as highlighted by the HORIZON-PFT real-world evidence (RWE) emulation, is the potential for a delayed effect of medication over a long follow-up period. Differences in results may stem from divergence in follow-up time and adherence between RCTs and database studies. These design differences reflect differences in the research questions that can be asked with a trial versus a database study, also described as the efficacy-effectiveness gap.[36]

This study includes several limitations. In the database study, we could not use placebo as a comparator group; however, the placebo comparator was emulated by raloxifene, which is an alternative medication very unlikely to have a direct effect on the endpoint of interest (hip fractures) and used in patients with similar characteristics, as shown in the baseline covariate balance of zoledronic acid versus raloxifene.

Second, there are differences in measurement and ascertainment of key study parameters between the primary data collection for the trial versus the definitions applied in the database study. For example, unlike the HORIZON-PFT, which required eligible participants to have evidence of osteoporosis based on bone mineral density T scores of –2.5 or less at the femoral neck or –1.5 or less with radiologic evidence of at least two mild or one moderate vertebral fractures, the database emulation selected patients solely based on international classification for diseases codes of osteoporosis (70%) and/or previous use of bisphosphonates (30%). Moreover, less than half of the clinical practice patients had evidence of a bone density test at baseline in their claims, potentially limiting the accuracy of their osteoporosis diagnosis and selecting those at a lower risk for fractures than the trial participants. This could have contributed to the smaller risk reduction of hip fractures observed in the database study compared with the HORIZON trial. However, patients included in the database analysis were of similar age, and the different proportion of vertebral fractures at baseline (4% of the database study patients had a claim for history of vertebral fractures in contrast to 63% of the HORIZON trial participants with a radiographic diagnosis of vertebral fracture) does not necessarily indicate a lower fracture risk among clinical practice patients than trial participants because 65% to 75% of vertebral fractures in real-world settings among postmenopausal women with osteoporosis are clinically silent and do not come to medical attention.[37] Furthermore, underdiagnosis of vertebral fractures limits our ability to accurately stratify patients into subgroups of higher versus lower risk of fractures using claims data, preventing exploration of whether patients at higher risk have greater benefits from treatment with zoledronic acid than those at lower risk over a short period of time.[32]

Third, because residual confounding for unmeasured characteristics, such as bone mineral density score or body mass index, cannot be entirely ruled out, we balanced 85 baseline covariates between treatment groups through PS matching to minimize any potential imbalances in such factors. Including a large number of covariates ascertained from patients' health care claims data improves control of confounding, as those variables may collectively be proxy for unobserved factors.[27,38]

Fourth, this study was not designed to evaluate whether the beneficial effect of zoledronic acid on preventing hip fractures increases with cumulative dosing over time. Although 30% of the zoledronic acid cohort received a second infusion, the short time of observation from the second infusion to the end of the study, the consequent limited number of outcome events, and the lingering effect of zoledronic acid for at least 18 months (end of study period) after the initial infusion prevented us from assessing the difference in hip fracture risk between patients who received one infusion versus two infusions. Further investigation, with more data and appropriate design, is needed to determine whether a cumulative dosing effect of zoledronic acid on preventing the risk of hip fractures could be observed in claims-database studies.[32]

To our knowledge, this study is the first to directly compare an existing RCT with a corresponding database study designed to emulate it in postmenopausal women with osteoporosis. Our study shows how differences in adherence influences the magnitude of effects observed in a clinical setting versus a trial setting. It follows a rigorous methodology with a prespecified protocol, including validity checks, and was publicly registered before implementing inferential analyses. Like the HORIZON-PFT trial, we observed that zoledronic acid reduced the risk of hip fracture compared with raloxifene. However, given low adherence in clinical practice, the anticipated effectiveness of zoledronic acid in clinical practice was attenuated compared with the efficacy estimated in HORIZON-PFT. RWE provides important complementary evidence to inform clinicians about the effect of drugs in their practice.

AUTHOR CONTRIBUTIONS

All authors were involved in drafting the article or revising it critically for important intellectual content, and all authors approved the final version to be published. Dr D'Andrea had full access to all of the data in the study and takes responsibility for the integrity of the data and the accuracy of the data analysis.

Study conception and design. D'Andrea, Schneeweiss, Franklin, Kim, Glynn, Wang.

Acquisition of data. D'Andrea, Schneeweiss, Franklin, Glynn, Lee, Wang.

Analysis and interpretation of data. D'Andrea, Schneeweiss, Franklin, Kim, Glynn, Wang.

REFERENCES

1. Black DM, Delmas PD, Eastell R, et al; HORIZON Pivotal Fracture Trial. Once-yearly zoledronic acid for treatment of postmenopausal osteoporosis. N Engl J Med 2007;356(18):1809–1822.
2. Curtis JR, Westfall AO, Allison JJ, et al. Channeling and adherence with alendronate and risedronate among chronic glucocorticoid users. Osteoporos Int 2006;17(8):1268–1274.

3. Kothawala P, Badamgarav E, Ryu S, et al. Systematic review and meta-analysis of real-world adherence to drug therapy for osteoporosis. Mayo Clin Proc 2007;82(12):1493–1501.
4. Fatoye F, Smith P, Gebrye T, et al. Real-world persistence and adherence with oral bisphosphonates for osteoporosis: a systematic review. BMJ Open 2019;9(4):e027049.
5. Curtis JR, Yun H, Matthews R, Saag KG, et al. Adherence with intravenous zoledronate and intravenous ibandronate in the United States Medicare population. Arthritis Care Res (Hoboken) 2012;64(7):1054–1060.
6. Cotté FE, Mercier F, De Pouvourville G. Relationship between compliance and persistence with osteoporosis medications and fracture risk in primary health care in France: a retrospective case-control analysis. Clin Ther 2008;30(12):2410–2422.
7. Siris ES, Harris ST, Rosen CJ, et al. Adherence to bisphosphonate therapy and fracture rates in osteoporotic women: relationship to vertebral and nonvertebral fractures from 2 US claims databases. Mayo Clin Proc 2006;81(8):1013–1022.
8. Ross S, Samuels E, Gairy K, et al. A meta-analysis of osteoporotic fracture risk with medication nonadherence. Value Health 2011; 14(4):571–581.
9. Wang SV, Schneeweiss S, Franklin JM, et al; RCT-DUPLICATE Initiative. Emulation of randomized clinical trials with nonrandomized database analyses: results of 32 clinical trials. JAMA 2023;329(16): 1376–1385.
10. Franklin JM, Glynn RJ, Martin D, et al. Evaluating the use of nonrandomized real-world data analyses for regulatory decision making. Clin Pharmacol Ther 2019;105(4):867–877.
11. Patorno E, Schneeweiss S, Gopalakrishnan C, et al. Using real-world data to predict findings of an ongoing phase IV cardiovascular outcome trial: cardiovascular safety of linagliptin versus glimepiride. Diabetes Care 2019;42(12):2204–2210.
12. Franklin JM, Pawar A, Martin D, et al. Nonrandomized real-world evidence to support regulatory decision making: process for a randomized trial replication project. Clin Pharmacol Ther 2020;107(4): 817–826.
13. Franklin JM, Glynn RJ, Suissa S, et al. Emulation differences vs. biases when calibrating real-world evidence findings against randomized controlled trials. Clin Pharmacol Ther 2020;107(4):735–737.
14. Franklin JM, Patorno E, Desai RJ, et al. Emulating randomized clinical trials with nonrandomized real-world evidence studies: first results from the RCT DUPLICATE initiative. Circulation 2021;143(10):1002–1013.
15. Qaseem A, Forciea MA, McLean RM, et al; Clinical Guidelines Committee of the American College of Physicians. Treatment of low bone density or osteoporosis to prevent fractures in men and women: a clinical practice guideline update from the American College of Physicians. Ann Intern Med 2017;166(11):818–839.
16. Johnson ES, Bartman BA, Briesacher BA, et al. The incident user design in comparative effectiveness research. Pharmacoepidemiol Drug Saf 2013;22(1):1–6.
17. Schneeweiss S, Patorno E. Conducting real-world evidence studies on the clinical outcomes of diabetes treatments. Endocr Rev 2021; 42(5):658–690.
18. D'Andrea E, Wexler DJ, Kim SC, et al. Comparing effectiveness and safety of SGLT2 inhibitors vs DPP-4 inhibitors in patients with type 2 diabetes and varying baseline HbA1c levels. JAMA Intern Med 2023;183(3):242–254.
19. Wright NC, Daigle SG, Melton ME, et al. The design and validation of a new algorithm to identify incident fractures in administrative claims data. J Bone Miner Res 2019;34(10):1798–1807.
20. Curtis JR, Mudano AS, Solomon DH, et al. Identification and validation of vertebral compression fractures using administrative claims data. Med Care 2009;47(1):69–72.
21. Reid IR, Horne AM, Mihov B, et al. Fracture prevention with zoledronate in older women with osteopenia. N Engl J Med 2018;379(25): 2407–2416.
22. Kim DH, Schneeweiss S, Glynn RJ, et al. Measuring frailty in Medicare data: development and validation of a claims-based frailty index. J Gerontol A Biol Sci Med Sci 2018;73(7):980–987.
23. Gagne JJ, Glynn RJ, Avorn J, et al. A combined comorbidity score predicted mortality in elderly patients better than existing scores. J Clin Epidemiol 2011;64(7):749–759.
24. Altman DG, Andersen PK. Calculating the number needed to treat for trials where the outcome is time to an event. BMJ 1999;319(7223): 1492–1495.
25. Suissa S. The number needed to treat: 25 years of trials and tribulations in clinical research. Rambam Maimonides Med J 2015;6(3): e0033.
26. Berry SD, Ngo L, Samelson EJ, Kiel DP. Competing risk of death: an important consideration in studies of older adults. J Am Geriatr Soc 2010;58(4):783–787.
27. Austin PC, Lee DS, Fine JP. Introduction to the analysis of survival data in the presence of competing risks. Circulation 2016;133(6): 601–609.
28. Fine JP, Gray RJ. A proportional hazards model for the subdistributions of a competing risk. J Am Stat Assoc 1999;94(446):496–509.
29. Benbow S. Graph Grabber 2.0.2. July 2021. Accessed June 3, 2023. https://www.quintessa.org/software/downloads-and-demos/graph-grabber-2.0.2
30. Boonen S, Eastell R, Su G, et al. Time to onset of antifracture efficacy and year-by-year persistence of effect of zoledronic acid in women with osteoporosis. J Bone Miner Res 2012;27(7):1487–1493.
31. Shalev V, Sharman Moser S, Goldshtein I, et al. Adherence with bisphosphonates and long-term risk of hip fractures: a nested case-control study using real-world data. Ann Pharmacother 2017;51(9): 757–767.
32. Reid IR, Black DM, Eastell R, et al; HORIZON Pivotal Fracture Trial and HORIZON Recurrent Fracture Trial Steering Committees. Reduction in the risk of clinical fractures after a single dose of zoledronic acid 5 milligrams. J Clin Endocrinol Metab 2013;98(2):557–563.
33. Tasci I, Cintosun U, Safer U, et al. Assessment of geriatric predictors of adherence to zoledronic acid treatment for osteoporosis: a prospective follow-up study. Acta Clin Belg 2018;73(4):237–243.
34. Cornelissen D, de Kunder S, Si L, et al; European Society for Clinical and Economic Aspect of Osteoporosis, Osteoarthritis and Musculoskeletal Diseases (ESCEO). Interventions to improve adherence to anti-osteoporosis medications: an updated systematic review. Osteoporos Int 2020;31(9):1645–1669.
35. Wang SV, Sreedhara SK, Schneeweiss S, et al; REPEAT Initiative. Reproducibility of real-world evidence studies using clinical practice data to inform regulatory and coverage decisions. Nat Commun 2022;13(1):5126.
36. Eichler HG, Abadie E, Breckenridge A, et al. Bridging the efficacy-effectiveness gap: a regulator's perspective on addressing variability of drug response. Nat Rev Drug Discov 2011;10(7):495–506.
37. Lems WF, Paccou J, Zhang J, et al; International Osteoporosis Foundation Fracture Working Group. Vertebral fracture: epidemiology, impact and use of DXA vertebral fracture assessment in fracture liaison services. Osteoporos Int 2021;32(3):399–411.
38. Greenland S. Invited commentary: variable selection versus shrinkage in the control of multiple confounders. Am J Epidemiol 2008;167(5): 523–529.

American College of Rheumatology
Empowering Rheumatology Professionals

Arthritis & Rheumatology
Vol. 77, No. 1, January 2025, pp 22–33
DOI 10.1002/art.42971

Relationship Between Ultrasound and Physical Examination in the Assessment of Enthesitis in Patients With Spondyloarthritis: Results From the DEUS Multicenter Study

Andrea Di Matteo,[1] Stefano Di Donato,[2] Gianluca Smerilli,[3] Andrea Becciolini,[4] Federica Camarda,[5] Alberto Cauli,[6] Tomás Cazenave,[7] Edoardo Cipolletta,[3] Davide Corradini,[6] Juan Jose de Agustin,[8] Giulia M. Destro Castaniti,[5] Eleonora Di Donato,[4] Emine Duran,[9] Bayram Farisogullari,[9] Marco Fornaro,[10] Francesca Francioso,[3] Pamela Giorgis,[7] Raquel Granados,[11] Amelia Granel,[12] Cristina Hernandez-Diaz,[13] Rudolf Horvath,[14] Jana Hurnakova,[14] Diogo Jesus,[15] Omer Karadag,[9] Ling Li,[16] Yang Li,[16] Maria G. Lommano,[3] Josefina Marin,[17] María V. Martire,[12] Xabier Michelena,[8] Laura Muntean,[18] Matteo Piga,[6] Marcos Rosemffet,[7] João Rovisco,[19] Fausto Salaffi,[3] Liliana Saraiva,[19] Crescenzio Scioscia,[10] Maria-Magdalena Tamas,[18] Shun Tanimura,[20] Aliki Venetsanopoulou,[21] Lucio Ventura Rios,[22] Orlando Villota,[23] Catalina Villota-Eraso,[23] Paraskevi V. Voulgari,[21] Gentiana Vukatana,[24] Johana Zacariaz Hereter,[17] Walter Grassi,[3] and Emilio Filippucci[3]

Objective. The study objectives were (i) to explore the agreement between the Outcome Measures in Rheumatology (OMERACT) ultrasound lesions of enthesitis and physical examination in assessing enthesitis in patients with spondyloarthritis (SpA) and (ii) to investigate the prevalence and clinical relevance of subclinical enthesitis in this population.

Methods. Twenty rheumatology centers participated in this cross-sectional study. Patients with SpA, including axial spondyloarthritis (axSpA) and psoriatic arthritis (PsA), underwent both ultrasound scan and physical examination of large lower limb entheses. The OMERACT ultrasound lesions of enthesitis were considered, along with a recently proposed definition for "active enthesitis" by our group. Subclinical enthesitis was defined as the presence of "active enthesitis" in ≥1 enthesis in patients with SpA without clinical enthesitis (ie, number of positive entheses on physical examination and Leeds Enthesitis Index score = 0).

Results. A total of 4,130 entheses in 413 patients with SpA (224 with axSpA and 189 with PsA) were evaluated through ultrasound and physical examination. Agreement between ultrasound and physical examination ranged from moderate (ie, enthesophytes) to almost perfect (ie, power Doppler and "active enthesitis"). Patellar tendon entheses demonstrated the highest agreement, whereas Achilles tendon insertion showed the lowest. Among 158 (38.3%) of 413 patients with SpA with clinical enthesitis, 108 (68.4%) exhibited no "active enthesitis" on ultrasound. Conversely, of those 255 without clinical enthesitis, 39 (15.3%) showed subclinical enthesitis. Subclinical enthesitis was strongly associated with local structural damage. However, no differences were observed regarding the demographic and clinical profiles of patients with SpA with and without subclinical enthesitis.

Conclusion. Our study underscores the need for a comprehensive tool integrating ultrasound and physical examination for assessing enthesitis in patients with SpA.

INTRODUCTION

Enthesitis, inflammation at the sites where tendons, ligaments, and joint capsules insert into bone, is regarded as the hallmark feature of spondyloarthritis (SpA).[1] Enthesitis plays a key role in the diagnosis and management of patients with SpA. It is part of the Classification Criteria for Psoriatic Arthritis and the Assessment of Spondyloarthritis International Society

The views expressed herein are those of the authors and do not necessarily represent those of the UK NHS, the NIHR, or the UK Department of Health.

Drs Di Matteo and Di Donato's work was supported by the Leeds Institute of Rheumatic and Musculoskeletal Medicine and the Leeds Biomedical Research Centre. Drs Horvath and Hurnakova's work was supported by the Ministry of Health, Czech Republic and the Conceptual Development of Research Organization, Motol University Hospital, Prague, Czech Republic (grant 00064203).

[1]Andrea Di Matteo, MD, PhD: "Carlo Urbani" Hospital and Polytechnic University of Marche, Ancona, Italy, and University of Leeds, Leeds, United Kingdom; [2]Stefano Di Donato, MD: University of Leeds, NIHR Leeds BRC, Leeds, United Kingdom; [3]Gianluca Smerilli, MD, Edoardo Cipolletta, MD, Francesca Francioso, MD, Maria G. Lommano, MD, Fausto Salaffi,

classification criteria for axial spondyloarthritis (axSpA).[2–4] In addition, according to EULAR, patients with psoriatic arthritis (PsA) who show unequivocal signs of enthesitis and insufficient response to nonsteroidal anti-inflammatory drugs (NSAIDs) (or local glucocorticoid injections) should be considered for treatment escalation to a biologic disease-modifying antirheumatic drug (DMARD).[5]

Physical examination is the reference method for assessing enthesitis, relying on tenderness, swelling, warmth, and restricted movement at entheseal sites. However, this approach may show low sensitivity due to the often absence of objective findings of inflammation at the entheseal level, such as specificity (ie, chronic pain, mechanical enthesitis) and swelling.[6] Various clinical scoring systems have been developed to evaluate enthesitis in SpA.[7] These include the Leeds Enthesitis Index (LEI), the Spondyloarthritis Research Consortium of Canada (SPARCC) Enthesitis Index, the Maastricht Ankylosing Spondylitis Enthesitis Score (MASES), the University of California, San Francisco (UCSF) index, and the Berlin index. These scores are commonly employed in both clinical practice and research trials to assess enthesis disease activity and response to treatment.[8–12]

Ultrasound has emerged as a valuable tool for detecting enthesitis, offering real-time imaging assessment of entheseal pathologic abnormalities indicative of inflammation and structural damage.[13–15] Recently, the Outcome Measures in Rheumatology (OMERACT) ultrasound task force has defined six elementary lesions of enthesitis, categorizing them into "inflammatory" lesions (ie, entheseal thickening, hypoechoic areas, and power Doppler [PD] signal at the enthesis) and "structural damage" lesions (ie, calcifications, enthesophytes, and bone erosions).[16,17]

Some studies have demonstrated the ability of imaging, particularly ultrasound, to identify subclinical enthesitis, which refers to the presence of inflammatory findings at the enthesis not apparent during physical examination.[18,19] However, there are instances in which painful entheses during physical examination do not show signs of inflammation on ultrasound, especially in patients with diffuse pain or fibromyalgia (FBM).[20]

In patients with SpA, the relationships between the different ultrasound lesions of enthesitis (ie, inflammatory lesions and structural damage lesions) and physical examination findings in the assessment of enthesitis, and how these relationships vary across individual entheses, remain incompletely understood. Importantly, existing studies on this subject have not adopted the latest OMERACT definitions of enthesitis.[16,17] Furthermore, within the population with SpA, the prevalence, clinical associations, and correlations with local factors (such as structural damage at the enthesis) of ultrasound subclinical enthesitis have been scarcely explored.

Clarifying these aspects is crucial for understanding the reliability and role of ultrasound, as a complementary tool to physical examination, in the assessment of enthesitis in patients with SpA. Therefore, the objectives of this study were three-fold: (1) to examine the agreement between the OMERACT ultrasound lesions of enthesitis and physical examination findings in the assessment of enthesitis in patients with SpA; (2) to explore, in patients with SpA without clinical enthesitis, the prevalence of ultrasound-detected inflammation at the enthesis (ie, subclinical enthesitis); and (3) to investigate, in patients with SpA without clinical enthesitis, the relationships between subclinical enthesitis and patients' demographic factors, clinical characteristics, and local structural damage at the enthesis (ie, bone erosions, calcifications, and/or enthesophytes).

MATERIALS AND METHODS

The Defining Enthesitis on Ultrasound in Spondyloarthritis (DEUS) study adopted an observational, cross-sectional, multicentric approach. The details of the DEUS study have been previously reported.[21] Briefly, consecutive patients with SpA, including axSpA and PsA, were recruited from 20 different rheumatology centers across 11 countries based on their respective classification criteria.[2–4] The following exclusion criteria were used: being

MD, PhD, Walter Grassi, MD Emilio Filippucci, MD, PhD: "Carlo Urbani" Hospital and Polytechnic University of Marche, Ancona, Italy; [4]Andrea Becciolini, MD, Eleonora Di Donato, MD: Azienda Ospedaliero-Universitaria di Parma, Parma, Italy; [5]Federica Camarda, MD, Giulia M. Destro Castaniti, MD: University of Palermo, Palermo, Italy; [6]Alberto Cauli, MD, Davide Corradini, MD, Matteo Piga, MD: Azienda Ospedaliera-Universitaria (AOU) and University of Cagliari, Monserrato, Italy; [7]Tomás Cazenave, MD, Pamela Giorgis, MD, Marcos Rosemffet, MD: Institute of Psychophysical Rehabilitation, Buenos Aires, Argentina; [8]Juan Jose de Agustin, MD, PhD, Xabier Michelena, MD, PhD: Vall d'Hebron Barcelona Hospital Campus, Barcelona, Spain; [9]Emine Duran, MD, Bayram Farisogullari, MD, Omer Karadag, MD: Hacettepe University, Ankara, Turkey; [10]Marco Fornaro, MD, Crescenzio Scioscia, MD, PhD: University of Bari, Bari, Italy; [11]Raquel Granados, MD: Reina Sofia University Hospital, Cordoba, Spain; [12]Amelia Granel, MD, María V. Martire, MD: Hospital San Roque de Gonnet, La Plata, Argentina; [13]Cristina Hernandez-Diaz, MD, MSc: Hospital Juárez de México, Mexico City, Mexico; [14]Rudolf Horvath, MD, PhD, Jana Hurnakova, MD, PhD: University Hospital Motol, Prague, Czech Republic; [15]Diogo Jesus, MD: Centro Hospitalar de Leiria, Leiria, Portugal, and University of Beira Interior, Covilhã, Portugal; [16]Ling Li, MD, Yang Li, MD: Guangdong Provincial People's Hospital (Guangdong Academy of Medical Sciences) and Southern Medical University, Guangdong, China; [17]Josefina Marin, MD, Johana Zacariaz Hereter, MD: Hospital Italiano de Buenos Aires, Buenos Aires, Argentina; [18]Laura Muntean, MD, Maria-Magdalena Tamas, MD: "Iuliu Hatieganu" University of Medicine and Pharmacy, Cluj-Napoca, Romania; [19]João Rovisco, MD, Liliana Saraiva, MD: Centro Hospitalar e Universitário de Coimbra, University of Coimbra, Coimbra, Portugal; [20]Shun Tanimura, MD, PhD: Hokkaido Medical Center for Rheumatic Diseases, Sapporo, Japan; [21]Aliki Venetsanopoulou, MD, Paraskevi V. Voulgari, MD, PhD: University of Ioannina, Ioannina, Greece; [22]Lucio Ventura Rios, MD, MSc: National Institute of Rehabilitation Luis Guillermo Ibarra Ibarra, Mexico City, Mexico; [23]Orlando Villota, MD, Catalina Villota-Eras, MD: Institución Prestadora de Salud (IPS) Servicio Integral de Reumatología e Inmunología Doctor Orlando Villota and Fundación Hospital San Pedro, Pasto, Colombia; [24]Gentiana Vukatana, MD: IRCCS Azienda Ospedaliero-Universitaria di Bologna, Bologna, Italy.

Additional supplementary information cited in this article can be found online in the Supporting Information section (https://acrjournals.onlinelibrary.wiley.com/doi/10.1002/art.42971).

Author disclosures and graphical abstract are available at https://onlinelibrary.wiley.com/doi/10.1002/art.42971.

Address correspondence via email to Andrea Di Matteo, MD, PhD, at andrea.dimatteo@hotmail.com.

Submitted for publication April 1, 2024; accepted in revised form August 5, 2024.

aged less than 18 years, having a history of major knee or ankle surgery or trauma, performing intense physical activity in the 2 weeks preceding the clinical evaluation, and having a concomitant diagnosis of FBM. The following clinical data were collected in patients with SpA: age, sex, weight, height, body mass index (BMI), physical activity, presence of cardiovascular disease, erythrocyte sedimentation rate, C-reactive protein, current use of DMARD therapy, and use of NSAIDs or steroidal anti-inflammatory drugs. Additional information collected included disease duration, previous enthesitis episodes, presence of psoriasis or inflammatory bowel disease, and HLA-B27 status (when clinically indicated).

The following disease activity indices were also recorded: the LEI score in both patients with axSpA and patients with PsA[8]; tender joint count (0–68) and swollen joint count (0–66) in both patients with axSpA and patients with PsA; the Disease Activity in Psoriatic Arthritis score in patients with PsA[22]; the Ankylosing Spondylitis Disease Activity Score, Bath Ankylosing Spondylitis Disease Activity Index, Bath Ankylosing Spondylitis Functional Index, and Bath Ankylosing Spondylitis Metrology Index in patients with axSpA[23–26]; 26; and the Health Assessment Questionnaire Disability Index in both patients with axSpA and patients with PsA.[27]

A rheumatologist conducted a physical examination, diagnosing enthesitis in the presence of tenderness upon pressure, mobilization or contraction against resistance, with or without swelling at the enthesis.[28] Both the physical evaluation and ultrasound were conducted on the same day, with a specific focus on the following lower limb entheses: patellar insertion of the quadriceps tendon, patellar (proximal) insertion of the patellar tendon, tibial (distal) insertion of the patellar tendon, calcaneal insertions of the Achilles tendon, and calcaneal insertion of the plantar fascia.

The ultrasound scan, conducted by a blinded rheumatologist, assessed the elementary lesions of enthesitis as recently defined by the OMERACT ultrasound task force, including entheseal thickening, hypoechoic areas, PD signal, enthesophytes, calcifications, and bone erosions,[16,17] as follows:

- Entheseal thickening increased thickness of the tendon insertion into the bone (<2 mm from the cortical bone) as compared with the body of the tendon, with or without blurring of the tendon margins
- Hypoechogenicity at the enthesis: lack of the homogeneous fibrillar pattern in the enthesis (<2 mm from the cortical bone) with loss of the tightly packed echogenic lines after correcting for anisotropy
- Doppler signal at enthesis: Doppler signal seen at bone insertion (<2 mm from the cortical bone), different from reflecting surface artifact or nutrition vessel signal, with or without cortical irregularities, erosions, or enthesophytes
- Enthesophytes: step-up of bony prominence, seen in two perpendicular planes at the end of the bone contour of the enthesis
- Calcifications: hyperechoic foci, with or without acoustic shadow, detected at the enthesis (<2 mm from the cortical bone)
- Bone erosions: cortical break with a step-down contour defect, seen in two perpendicular planes, at the insertion of the enthesis

According to the OMERACT ultrasound task force, entheseal thickening, hypoechoic areas, and PD signal at the enthesis were considered inflammatory lesions. On the other hand, bone erosions, enthesophytes, and calcifications were considered structural damage lesions.[16,17]

The ultrasound assessment of each enthesis was conducted according to the EULAR guidelines on the use of musculoskeletal ultrasound in rheumatology.[29] As previously defined by our group, active enthesitis was considered as having either PD at the enthesis Grade ≥1 plus entheseal thickening and/or hypoechoic areas or PD at the enthesis Grade >1 (independent of the presence of entheseal thickening or hypoechoic areas).[21,30,31]

PD signal was scored semiquantitatively from 0 to 3, where Grade 0 = absent (ie, no PD signal); Grade 1 = mild (ie, separate dot signals or short linear signals); Grade 2 = moderate (ie, PD signal occupying less than half of the enthesis); and Grade 3 = severe (ie, PD signal occupying more than half of the enthesis).[32–34] Prior to the current study, a web-based inter- and intrareliability exercise was performed by the current authors to evaluate the agreement on the OMERACT ultrasound elementary lesions of enthesitis.[35]

In the current study, subclinical enthesitis was defined as the presence of ultrasound "active enthesitis" in ≥1 enthesis in patients with SpA without signs of clinical enthesitis on physical examination (ie, number of positive entheses on physical examination = 0, including the quadriceps tendon, proximal and distal patellar tendon, Achilles tendon, and plantar fascia, and LEI score = 0). Details regarding the ultrasound machines and settings utilized in the study, as well as information about the PD settings employed and the level of experience of the sonographers in conducting ultrasound examinations, have been reported in Supplementary Table 1.

Categorical variables were reported as count and percentage, and continuous variables were reported as mean and SD for normally distributed data or median and interquartile range for non-normally distributed data. Two-group comparisons of continuous variables were conducted with unpaired Student's *t*-test or Mann-Whitney-Wilcoxon's test. Comparisons among categorical variables were performed using chi-square test or Fisher's exact test. Data normality was tested with Kolmogorov-Smirnov's test and graphically assessed using QQ plots.

To evaluate agreement between the ultrasound OMERACT elementary lesions of enthesitis (as well as "active enthesitis" as proposed by our group) and clinical enthesitis findings on physical examination, we used the prevalence-adjusted bias-adjusted kappa (PABAK) alongside its 95% confidence interval (CI) for each

confusion matrix. To estimate the 95% CI for PABAK, we utilized a bootstrapping approach across each matrix dataset, conducting 1,000 iterations to generate a distribution of PABAK scores; the distribution was then used to derive the 95% CI, providing a robust statistical framework to assess the precision of the PABAK estimates. Kappa coefficients were interpreted according to Landis and Koch.[36]

Univariate logistic regressions examined the associations between the OMERACT ultrasound enthesitis lesions, as well as "active enthesitis" proposed by our group, and the OMERACT structural damage lesions (ie, enthesophytes, calcifications, and bone erosions). Multivariate logistic regressions were built including all the ultrasound lesions that showed statistical significance at univariate analysis. When "active enthesitis" was considered, the individual ultrasound inflammatory lesions according to OMERACT (ie, entheseal thickening, hypoechoic areas, and PD at the enthesis) were excluded to avoid collinearity. The multivariate analyses were adjusted for age and sex.

Data analysis was conducted using R core team software (https://www.R-project.org) and RStudio (PBC, Boston, MA). This study was approved by the ethics committees of the participating centers (leading center Polytechnic University of Marche, Comitato Etico Regionale delle Marche [CERM n: 50/2021]). All patients provided written informed consent.

RESULTS

Overall, 413 patients with SpA, of whom 224 had axSpA and 189 had PsA, were included in the current study. The demographic features, clinical characteristics, and treatment of the included patients have been reported in Supplementary Table 2.

Agreement between ultrasound and physical examination for the assessment of enthesitis. A total of 4,130 entheses were assessed by both ultrasound and physical examination in patients with SpA, of which 2,240 were in patients with axSpA and 1,890 were in patients with PsA. The prevalence and distribution of the ultrasound lesions in patients with SpA, including patients with axSpA and those with PsA, have been reported in Supplementary Table 3.

As shown in Table 1, the overall agreement between ultrasound and physical examination in the assessment of enthesitis ranged from being moderate for enthesophytes to substantial for entheseal thickening, hypoechoic areas, calcifications, and bone

Table 1. Relationships and agreement between ultrasound and physical evaluation in the assessment of enthesitis in patients with SpA (n = 413 patients)*

	Negative	Positive	Total
Clinical enthesitis status: thickening			
Negative	3,250	559	3,809
Positive	173	148	321
PABAK		0.65 (0.63–0.67)	
Clinical enthesitis status: enthesophytes			
Negative	2,758	1,051	3,809
Positive	161	160	321
PABAK		0.41 (0.39–0.44)	
Clinical enthesitis status: hypoechoic areas			
Negative	3,201	608	3,809
Positive	163	158	321
PABAK		0.63 (0.60–0.65)	
Clinical enthesitis status: calcifications			
Negative	3,466	343	3,809
Positive	291	30	321
PABAK		0.69 (0.67–0.72)	
Clinical enthesitis status: PD at the enthesis			
Negative	3,671	138	3,809
Positive	254	67	321
PABAK		0.81 (0.79–0.83)	
Clinical enthesitis status: bone erosions			
Negative	3,673	136	3,809
Positive	279	42	321
PABAK		0.79 (0.77–0.81)	
Clinical enthesitis status: "active enthesitis"			
Negative	3,703	106	3,809
Positive	257	64	321
PABAK		0.83 (0.81–0.85)	

* "Active enthesitis" was considered as either PD at the enthesis Grade ≥1 + entheseal thickening and/or hypoechoic areas or PD at the enthesis Grade >1 (independent of the presence of entheseal thickening or hypoechoic areas).[21] PABAK, prevalence-adjusted bias-adjusted kappa; PD, power Doppler; SpA, spondyloarthritis. PABAK values are expressed as point estimate with 95% confidence interval.

Table 2. Agreement between ultrasound and physical evaluation divided by single entheses in patients with SpA (n = 413)*

Ultrasound findings	Agreement (PABAK)				
	Quadriceps tendon	Patellar proximal	Patellar distal	Achilles tendon	Plantar fascia
Thickening	0.73 (0.68 to 0.77)	0.71 (0.66 to 0.75)	0.68 (0.62 to 0.72)	0.56 (0.50 to 0.61)	0.54 (0.48 to 0.59)
Hypoechoic areas	0.58 (0.52 to 0.63)	0.72 (0.67 to 0.77)	0.68 (0.63 to 0.73)	0.52 (0.46 to 0.58)	0.60 (0.54 to 0.65)
PD at the enthesis	0.81 (0.77 to 0.85)	0.85 (0.82 to 0.89)	0.85 (0.82 to 0.88)	0.68 (0.63 to 0.73)	0.83 (0.79 to 0.87)
Enthesophytes	0.20 (0.13 to 0.27)	0.60 (0.54 to 0.65)	0.71 (0.66 to 0.75)	0.01 (−0.05 to 0.08)	0.52 (0.46 to 0.58)
Calcifications	0.70 (0.67 to 0.73)	0.79 (0.75 to 0.83)	0.73 (0.67 to 0.77)	0.52 (0.46 to 0.58)	0.72 (0.67 to 0.76)
Bone erosions	0.82 (0.77 to 0.85)	0.86 (0.83 to 0.89)	0.89 (0.86 to 0.92)	0.62 (0.56 to 0.67)	0.79 (0.74 to 0.83)
"Active enthesitis"	0.83 (0.80 to 0.87)	0.86 (0.82 to 0.89)	0.87 (0.84 to 0.91)	0.70 (0.65 to 0.75)	0.84 (0.80 to 0.88)

* "Active enthesitis" was considered as either PD at the enthesis Grade ≥1 + entheseal thickening and/or hypoechoic areas or PD at the enthesis Grade >1 (independent of the presence of entheseal thickening or hypoechoic areas).[21] PABAK, prevalence-adjusted bias-adjusted kappa; PD, power Doppler; SpA, spondyloarthritis. PABAK values are expressed as point estimate with 95% confidence interval.

erosions, and to almost perfect for PD at the enthesis and "active enthesitis." Similar results were observed when patients with SpA were divided between those taking biologic DMARDs and those not taking biologic DMARDs (Supplementary Table 4). When considering the agreement between ultrasound and physical examination in the single enthesis, the patellar tendon entheses (both proximal and distal) resulted in the sites with the highest PABAK values of agreement for all ultrasound lesions of enthesitis, except for entheseal thickening (Table 2). On the other hand, the Achilles tendon insertion resulted in the entheseal site with the lowest PABAK values for all ultrasound lesions of enthesitis. Further details regarding the agreement between ultrasound and physical examination in the assessment of enthesitis in the individual entheses have been reported in Supplementary Tables 5 through 9.

Similar agreement results were observed when axSpA and PsA were considered independently, with axSpA showing a slightly higher agreement compared to PsA for all ultrasound lesions of enthesitis, except for bone erosions (Table 3; Supplementary Tables 10–11).

Table 3. Agreement between ultrasound and physical examination in enthesitis assessment in patients with axSpA and patients with PsA*

Ultrasound findings	Agreement (PABAK)	
	axSpA (n = 224)	PsA (n = 119)
Thickening	0.65 (0.62–0.69)	0.64 (0.60–0.67)
Hypoechoic areas	0.67 (0.64–0.70)	0.58 (0.54–0.61)
PD at the enthesis	0.82 (0.80–0.84)	0.80 (0.77–0.83)
Enthesophytes	0.47 (0.43–0.50)	0.34 (0.31–0.39)
Calcifications	0.70 (0.67–0.73)	0.68 (0.65–0.71)
Bone erosions	0.79 (0.76–0.81)	0.81 (0.79–0.84)
"Active enthesitis"	0.83 (0.81–0.86)	0.82 (0.80–0.85)

* "Active enthesitis" was considered as either PD at the enthesis Grade ≥1 + entheseal thickening and/or hypoechoic areas or PD at the enthesis Grade >1 (independent of the presence of entheseal thickening or hypoechoic areas).[21] axSpA, axial spondyloarthritis; PABAK, prevalence-adjusted bias-adjusted kappa; PD, power Doppler; PsA, psoriatic arthritis; SpA, spondyloarthritis. PABAK values are expressed as point estimate with 95% confidence interval.

Ultrasound subclinical enthesitis: prevalence, association with patient demographic factors, clinical characteristics, and local structural damage at the enthesis. Among the 413 included patients, 255 (61.7%) were classified as not having clinical enthesitis, which was defined as having zero positive entheses on physical examination and an LEI score = 0. Of these 255 patients with SpA (140 with axSpA and 115 with PsA) without clinical enthesitis, 39 (15.3%) showed subclinical enthesitis in ≥1 enthesis. Conversely, of the 158 (38.3%) of 413 patients with SpA with clinical enthesitis, 108 (68.4%) had no evidence of active enthesitis in any of the entheses evaluated.

The prevalence and distribution of the ultrasound findings in the 255 patients with SpA without clinical enthesitis (including patients with axSpA and those with SpA) have been reported in Table 4 and Supplementary Table 12. As showed in Table 5, the demographics and clinical and serological characteristics of patients with subclinical enthesitis did not differ from those without subclinical synovitis. A significant association was found in the univariate and multivariate analysis between the ultrasound inflammation lesions (ie, entheseal thickening, hypoechoic areas, PD at the enthesis and "active enthesitis") and local structural damage at the enthesis (ie, enthesophytes, calcifications, and bone erosions), which has been illustrated in Table 6.

DISCUSSION

In this multicenter study, we examined the agreement between ultrasound and physical examination in the assessment of enthesitis in a large cohort of patients with SpA. While previous research has reported on this topic,[18,19] our study stands out for encompassing the largest cohort of patients with SpA to date, including both patients with axSpA and patients with PsA, and for providing a detailed analysis based on individual ultrasound findings and entheses evaluated. In addition, to our knowledge, this was the first study that used the recently developed

Table 4. Prevalence and distribution of the ultrasound findings in patients with SpA, axSpA, and PsA without clinical enthesitis*

	Quadriceps			Patellar proximal			Patellar distal			Achilles tendon			Plantar fascia			Overall		
Ultrasound findings	axSpA n = 140	PsA n = 115	P^a	axSpA n = 140	PsA n = 115	P^a	axSpA n = 140	PsA n = 115	P^a	axSpA n = 140	PsA n = 115	P^a	axSpA n = 140	PsA n = 115	P^a	axSpA n = 140	PsA n = 115	P^a
Thickening	19 (14.0)	14 (12.2)	>0.9	23 (16.4)	17 (14.7)	>0.9	24 (17.1)	24 (20.9)	>0.9	25 (17.8)	25 (21.7)	>0.9	33 (23.6)	29 (25.3)	>0.9	56 (40.0)	59 (51.3)	0.14
Hypoechoic area	26 (18.6)	31 (26.9)	0.6	15 (10.7)	21 (18.3)	0.7	18 (12.9)	27 (23.5)	0.2	31 (22.1)	30 (26.1)	>0.9	18 (12.9)	29 (25.3)	0.068	47 (33.8)	63 (54.8)	0.003
PD at the enthesis	6 (4.3)	6 (5.2)	>0.9	6 (4.3)	7 (6.1)	>0.9	9 (6.4)	10 (8.7)	>0.9	10 (7.1)	10 (8.7)	>0.9	0 (0)	1 (0.9)	>0.9	25 (17.8)	25 (21.7)	0.6
Enthesophytes	54 (38.6)	60 (52.4)	0.2	35 (25.0)	27 (23.5)	>0.9	21 (14.3)	17 (15.8)	>0.9	71 (50.7)	76 (66.1)	0.11	25 (17.8)	41 (36.6)	0.007	91 (65.0)	94 (81.4)	0.012
Calcifications	19 (14.0)	26 (22.6)	0.5	13 (9.3)	7 (6.1)	>0.9	27 (19.3)	16 (13.9)	>0.9	23 (16.4)	16 (13.9)	>0.9	8 (5.7)	19 (16.5)	0.032	55 (39.3)	49 (42.6)	0.7
Bone erosions	6 (4.3)	3 (2.6)	>0.9	4 (2.9)	4 (3.5)	>0.9	4 (2.9)	1 (0.9)	>0.9	19 (13.5)	14 (12.2)	>0.9	10 (7.1)	1 (0.9)	0.084	34 (24.3)	18 (15.6)	0.14
"Active enthesitis"	6 (4.3)	6 (5.2)	>0.9	5 (3.6)	6 (5.2)	>0.9	7 (5.0)	7 (6.1)	>0.9	10 (7.1)	6 (5.2)	>0.9	0 (0)	0 (0)	NA	20 (14.3)	19 (16.5)	0.8

* "Active enthesitis" was considered as either PD at the enthesis Grade ≥1 + entheseal thickening and/or hypoechoic areas or PD at the enthesis Grade >1 (independent of the presence of entheseal thickening or hypoechoic areas).[21] axSpA, axial spondyloarthritis; NA, not available; PD, power Doppler; PsA, psoriatic arthritis; SpA, spondyloarthritis. Values are the number (%) unless otherwise indicated.

[a] Pearson's chi-square test; Fisher's exact test with Bonferroni correction for multiple testing.

Table 5. Demographic features and clinical characteristics of patients with SpA without clinical enthesitis (N = 255) with or without subclinical enthesitis*

	Overall N = 255	Subclinical enthesitis n = 39	No subclinical enthesitis n = 216	P[a]
Age (y), mean (SD)	47.0 (14.3)	48.0 (14.7)	46.8 (14.2)	0.9
Female gender, n (%)	69 (27.1)	7 (17.9)	62 (28.7)	0.7
BMI (kg/m^2), median (IQR)	26.4 (23.6–29.2)	27.0 (24.6–29.3)	26.4 (23.5–29.1)	0.9
Physical activity (times/wk), median (IQR)	2 (0–3)	1 (0–3)	2 (0–3)	0.7
Disease duration (mo), median (IQR)	89 (36–180)	120 (54–245)	84 (28–166)	0.7
CRP (mg/L), mean (SD)	1.3 (2.7)	1.9 (4.0)	1.2 (2.4)	0.9
ESR (mm/h), mean (SD)	17.8 (17.9)	26.9 (32.0)	16.2 (13.6)	0.9
Metabolic syndrome, n (%)	42 (16.5)	9 (23.1)	33 (15.3)	0.7
Diabetes, n (%)	17 (6.7)	1 (2.6)	16 (7.4)	0.9
Dyslipidemia, n (%)	61 (23.9)	11 (28.2)	50 (23.1)	0.9
Hypertension, n (%)	62 (24.3)	10 (25.6)	52 (24.1)	>0.9
Psoriasis (previous/current), n (%)	104 (40.8)	17 (43.6)	87 (40.2)	0.9
IBD, n (%)	4 (1.6)	2 (5.1)	2 (0.9)	0.7
Previous enthesitis, n (%)	67 (26.3)	15 (38.5)	52 (24.1)	0.7
HLA-B27[b], n (%)	109 (73.6)	16 (72.7)	93 (73.8)	>0.9
Nonradiographic axSpA, n (%)	36 (24.5)	3 (14.3)	33 (26.2)	0.7
Disease activity indices in patients with SpA				
TJC, median (IQR)	0 (0–1)	0 (0–1)	0 (0–1)	NA
TJC, mean (SD)	1.0 (2.5)	0.7 (1.3)	1.1 (2.7)	>0.9
SJC, median (IQR)	0 (0–1)	0 (0–1)	0 (0–0)	NA
SJC, mean (SD)	0.8 (2.1)	0.7 (1.5)	0.8 (2.2)	0.9
DAPSA, median (IQR) (patients with PsA)	8 (2–16)	6 (2–15)	8 (3–16)	0.9
ASDAS, median (IQR) (patients with axSpA)	1.4 (1.0–2.2)	1.8 (1.3–2.2)	1.4 (1.0–2.2)	0.4
BASMI, median (IQR) (patients with axSpA)	1.8 (0.8–3.0)	1.6 (1.0–2.9)	1.8 (0.7–3.0)	>0.9
BASFI, median (IQR) (patients with axSpA)	0.6 (0.0–3.7)	1.4 (0.0–5.6)	0.5 (0.0–3.2)	0.8
BASDAI, median (IQR) (patients with axSpA)	1.4 (0.4–3.6)	2.1 (0.7–4.7)	1.3 (0.4–3.5)	0.7
HAQ, median (IQR)	0.1 (0.0–0.5)	0.0 (0.0–0.5)	0.1 (0.0–0.5)	>0.9
Treatment of patients with SpA				
NSAIDs, n (%)	63 (24.7)	8 (20.5)	55 (25.4)	>0.9
GCs (≥5 mg prednisolone), n (%)	26 (10.2)	4 (10.3)	22 (10.2)	>0.9
cs-DMARDs, n (%)	95 (37.3)	18 (46.2)	77 (35.7)	0.7
b-DMARDs, n (%)	142 (55.7)	21 (53.8)	121 (56.0)	0.7
TNFi, (%)	113 (79.6)	15 (71.4)	98 (81.0)	
Anti-IL12/23, n (%)	4 (2.8)	2 (9.5)	2 (1.7)	
Anti-IL17, n (%)	23 (16.2)	4 (19.0)	19 (15.7)	
JAKi, n (%)	0	0	0	
Others (apremilast), n (%)	2 (0.7)	0 (0.0)	2 (0.9)	

* ASDAS, Ankylosing Spondylitis Disease Activity Score; axSpA, axial spondyloarthritis; b-DMARD, biologic disease-modifying antirheumatic drug; BASDAI, Bath Ankylosing Spondylitis Disease Activity Index; BASFI, Bath Ankylosing Spondylitis Functional Index; BASMI, Bath Ankylosing Spondylitis Metrology Index; BMI, body mass index; CRP, C-reactive protein; cs-DMARD, conventional synthetic disease-modifying antirheumatic drug; DAPSA, Disease Activity in Psoriatic Arthritis; ESR, erythrocyte sedimentation rate; GC, glucocorticoid; HAQ, Health Assessment Questionnaire Disability Index; IBD, inflammatory bowel disease; IL, interleukin; IQR, interquartile range; JAKi, Janus kinase inhibitor; NA, not available; NSAID, nonsteroidal anti-inflammatory drug; PsA, psoriatic arthritis; SJC, swollen joint count; SpA, spondyloarthritis; TJC, tender joint count; TNFi, tumor necrosis factor-α inhibitor.
[a] Between patients with and without subclinical enthesitis, false discovery rate correction for multiple testing.
[b] Available in 148 patients with SpA (22 subclinical enthesitis, 126 no subclinical enthesitis).

OMERACT ultrasound definitions of enthesitis.[16,17] Following the publication of the OMERACT elementary lesions of enthesitis in SpA,[16,17] several studies have demonstrated that some of these lesions can also be detected in non-inflammatory conditions, including metabolic or mechanical enthesopathy, as well as in healthy individuals. This finding raises questions about the specificity and clinical relevance of these ultrasound features.[14,15] Therefore, clarifying the agreement between different ultrasound lesions of enthesitis and physical examination findings in patients with SpA, along with assessing whether this agreement varies based on the entheseal site being evaluated, is crucial for a better understanding of their accuracy for detecting enthesitis and their potential implications for the diagnosis and management of patients with SpA.

Our results revealed variability in the agreement between ultrasound and physical examination in the assessment of enthesitis, depending on the specific ultrasound finding considered and, to a lesser extent, the entheseal site being evaluated. PD at the enthesis and "active enthesitis" resulted in the ultrasound findings showing the highest agreement with the physical examination across all entheseal sites included in the study. This observation could arguably be explained by considering PD at the enthesis (which represents the main component of "active enthesitis") as the "most inflammatory" lesion among those defined by

Table 6. Association between ultrasound inflammatory lesions (entheseal thickening, hypoechoic areas, PD at the enthesis, active enthesitis) and structural lesions (bone erosions, enthesophytes, and calcifications) in patients with SpA without clinical enthesitis (n = 255)*

	Univariate regression				Multivariate regression			Multivariate regression with "active enthesitis"		
	Overall N = 2,550	Yes n = 658	No n = 1,892	*P*[a]	OR	95% CI	*P*	OR	95% CI	*P*
Enthesophytes										
Thickening	314 (12.3%)	161 (24.5%)	153 (8.9%)	<0.001	1.74	1.29–2.35	<0.001			
Hypoechoic area	341 (13.7%)	188 (28.6%)	153 (8.9%)	<0.001	2.65	1.98–3.55	<0.001			
PD at the enthesis	79 (3.1%)	46 (7.0%)	33 (1.7%)	<0.001	1.97	1.18–3.28	0.009			
Calcifications	210 (8.2%)	108 (16.4)	102 (5.4%)	<0.001	2.41	1.77–3.28	<0.001	3.04	2.26–4.08	<0.001
Bone erosions	83 (3.6%)	47 (7.1)	36 (1.9)	<0.001	2.15	1.33–3.50	0.002	3.16	1.99–5.05	<0.001
"Active enthesitis"	56 (2.2%)	35 (6.0%)	21 (1.3%)	<0.001				3.68	2.09–6.61	<0.001
	Univariate regression				Multivariate regression			Multivariate regression with "active enthesitis"		
	Overall N = 2,550	Yes n = 210	No n = 2,340	*P*[a]	OR	95% CI	*P*	OR	95% CI	*P*
Calcifications										
Thickening	314 (12.3%)	61 (29.0%)	253 (10.8%)	<0.001	1.36	0.89–2.04	0.2			
Hypoechoic area	341 (13.7%)	76 (36.2%)	265 (11.3%)	<0.001	2.42	1.62–3.60	<0.001			
PD at the enthesis	79 (3.1%)	21 (10.0%)	58 (2.5%)	<0.001	1.85	1.02–3.24	0.037			
Enthesophytes	658 (25.8%)	108 (51.4%)	550 (23.5%)	<0.001	2.44	1.79–3.32	0.038	2.45	1.38–4.19	0.002
Bone erosions	83 (3.6%)	20 (9.5%)	63 (2.7%)	<0.001	1.82	1.01–3.17	<0.001	3.05	2.27–4.10	<0.001
"Active enthesitis"	56 (2.2%)	17 (8.1%)	39 (1.8%)	<0.001				3.20	1.68–5.85	<0.001
	Univariate regression				Multivariate regression			Multivariate regression with "active enthesitis"		
	Overall n = 2,550	Yes n = 83	No n = 2,467	*P*[a]	OR	95% CI	*P*	OR	95% CI	*P*
Bone erosions										
Thickening	314 (12.3%)	33 (39.8%)	281 (11.4%)	<0.001	1.63	0.91–2.91	0.10			
Hypoechoic area	341 (13.7%)	42 (50.6%)	299 (12.2%)	<0.001	3.80	2.12–6.75	<0.001			
PD at the enthesis	79 (3.1%)	9 (10.8%)	70 (2.8%)	0.005	1.17	0.49–2.51	0.7			
Enthesophytes	658 (25.8%)	47 (56.6%)	611 (24.8%)	<0.001	2.25	1.39–3.66	0.001	2.41	1.34–4.14	0.002
Calcifications	210 (8.2%)	20 (24.1%)	190 (7.7%)	<0.001	1.81	1.00–3.16	0.043	3.19	2.01–5.09	<0.001
"Active enthesitis"	56 (2.2%)	9 (10.8%)	47 (1.9%)	<0.001				3.28	1.39–7.0	0.004

* "Active enthesitis" was considered as either PD at the enthesis Grade ≥1 + entheseal thickening and/or hypoechoic areas or PD at the enthesis Grade >1 (independent of the presence of entheseal thickening or hypoechoic areas).[21] CI, confidence interval; OR, odds ratio; PD, power Doppler; SpA, spondyloarthritis.
[a] Bonferroni correction for multiple testing.

OMERACT (ie, entheseal thickening, hypoechoic areas, and PD signal), making it potentially more closely linked to signs or symptoms of entheseal inflammation, especially pain. It is important to note, however, that our study examines the agreement between ultrasound and physical examination findings rather than implying causation.

In the present study, we observed that, across all ultrasound lesions, the highest levels of agreement between ultrasound and physical examination occurred in the presence of a negative finding. However, discrepancies between the two methods emerged when either ultrasound or physical examination detected enthesitis. Due to the notable discrepancy between the positive and negative detections of enthesitis through ultrasound and physical examination, with the latter significantly outnumbering the former, we employed PABAK. This approach adjusts for bias arising from differences in prevalence when calculating kappa values.

Interestingly, among the included entheses, the Achilles tendon enthesis exhibited the lowest agreement values for all ultrasound lesions and clinical signs of enthesitis. The Achilles tendon is traditionally regarded as a key site for the evaluation of enthesitis in patients with SpA.[37,38] However, it is recognized that an accurate assessment of this area through physical examination can pose challenges.[39] These often arise from the frequent absence of obvious signs of inflammation, such as pain, redness, warmth, or swelling. Additionally, distinguishing genuine enthesitis from tendinitis or tendinopathy presents further difficulty. In a recent study of our group, the Achilles tendon enthesis emerged as a key site for differentiating SpA-related "inflammatory enthesitis" from "mechanical enthesitis."[21] Therefore, these findings underscore the importance of employing ultrasound alongside physical examination to improve assessment of this area.

Prior studies have explored the relationship between ultrasound and physical examination in the assessment of enthesitis, yielding conflicting findings. Fiorenza et al compared clinical and ultrasound enthesitis in patients with PsA and patients with FBM using MASES, the LEI, and the Glasgow Ultrasound Enthesitis Scoring System (GUESS).[40] The authors found a lack of correlation between GUESS and MASES, and a weak correlation with LEI score in patients with PsA and patients with FBM. Aydin et al studied ultrasound and physical examination of enthesitis in PsA and psoriasis, noting a strong correlation between the two methods at Achilles tendon and proximal patellar tendon levels but not at other sites.[41] Sapsford et al found a moderate association between ultrasound-detected enthesitis and clinical indices in patients with PsA, while cautioning interpretation in patients with FBM patients.[42] Michelsen et al detected no association between clinical and ultrasound findings of enthesitis at the level of the Achilles tendon in patients with PsA.[43] In this study, an association between ultrasound lesions indicative of structural damage and age, BMI, exercise, and biologic DMARD use was found.[43]

Another important objective of the current study was to explore the prevalence of subclinical enthesitis in patients with SpA. Despite employing stringent criteria for defining absence of clinical enthesitis, which included having no clinical enthesitis on physical examination (using the entheses that were also evaluated through ultrasound) and a LEI score of 0, we observed a relatively high proportion of patients with SpA exhibiting PD signal at the enthesis and "active enthesitis" at the patient level (19.6% and 15.3%, respectively). When considering axSpA and PsA groups separately, hypoechoic areas and enthesophytes were generally more common in patients with PsA compared to those with axSpA, although variations were observed at the level of the individual entheses.

The demographic, serological, and clinical profiles (including disease activity indices) of the patients with SpA with subclinical enthesitis did not significantly differ from those without SpA, suggesting that ultrasound subclinical enthesitis predominantly reflects localized changes at the entheseal level rather than systemic ones. In support of this hypothesis, we found a significant association between the OMERACT ultrasound inflammatory lesions (ie, entheseal thickening, hypoechoic areas, and PD signal), particularly "active enthesitis," and local structural damage (ie, enthesophytes, calcifications, and bone erosions). However, an important aspect to consider in interpreting these findings is the significant asymmetry between the subclinical enthesitis group (39 patients) and the group without subclinical enthesitis (216 patients). In addition, the cross-sectional design of the current study does not allow us to establish whether the presence of subclinical inflammation had a causative role in the development of structural damage or whether entheseal damage, combined with mechanical factors, could perpetuate inflammation at the enthesis. Longitudinal research is needed to investigate this aspect further. Interestingly, in patients with rheumatoid arthritis, subclinical synovitis on ultrasound has been observed to precede the development of radiographic bone erosions, even in those in clinical remission.[44]

The results of the current study indicate that, in patients with SpA with normal clinical and serological findings, evidence of entheseal inflammation detected through imaging persists, albeit in a minority of patients. This underscores a limitation to relying solely on physical examination for the assessment of entheseal involvement in patients with SpA, as it may not fully capture clinically relevant levels of inflammation. Conversely, more than two-thirds of patients with SpA with clinical enthesitis showed no "active enthesitis" on ultrasound, indicating the potential risk of overestimating enthesitis through physical examination alone.

These discrepancies underscore the importance of integrating clinical and imaging approaches for a comprehensive evaluation of enthesitis in clinical practice. In addition, by combining clinical and imaging modalities, clinicians can better evaluate enthesitis and tailor treatment strategies accordingly, leading to a clearer understanding of the disease process and identification of subtle manifestations missed by either ultrasound or physical examination alone. Most trials assessing the effectiveness of drugs targeting the enthesis

have primarily relied on clinical physical evaluation,[45] focusing on outcomes such as pain reduction as the primary measure. On the other hand, only a minority of studies have incorporated ultrasound assessment to evaluate treatment response.[46–48]

One of the advantages of ultrasound over clinical examination is its ability to assess the extent of both active inflammation and structural damage in the affected enthesis, an aspect that would not be achievable through clinical examination alone. On the other hand, physical examination is relatively quick and can be conducted bedside without the necessity for specialized equipment. Compared to other imaging techniques, such as magnetic resonance imaging (MRI), ultrasound presents superior feasibility, availability, costs, and scanning time.[49,50] However, operator dependency, time, and variability among the different ultrasound machines represent limitations to the routine use of this imaging tool in routine clinical practice.

A strength of our study is the participation of a large number of rheumatology centers, with ultrasound experts participating from multiple countries worldwide. All investigators were involved in a web-based reliability exercise on the OMERACT ultrasound lesions of enthesitis in SpA aimed to calibrate the different operators and in the standardization of ultrasound assessments before study recruitment.[35]

The lack of a gold standard for the evaluation of enthesitis, such as MRI or histology, represents the main limitation of the current study. The sensitivity of MRI for detecting bone marrow edema below the enthesis could potentially explain why some clinically active entheses might appear negative on ultrasound. However, a previous study showed good agreement between ultrasound and MRI in the detection of findings of enthesopathy in patients with SpA at the level of the Achilles tendon.[51] Another important limitation is the absence of evaluation for ultrasound synovitis adjacent to the entheses under investigation. Previous research has suggested that entheseal pain in the heel region could derive from subtalar synovitis (or tenosynovitis of the posterior tibialis tendon) rather than enthesitis. This could explain at least in part the lack of agreement between ultrasound and physical examination, which was observed in the current study.[52] Additionally, we did not assess the correlation between ultrasound findings and radiographic damage at the entheseal level, which could have further supported the clinical relevance of our results, particularly concerning subclinical enthesitis.[53,54] The decision to exclude tendinitis (ie, PD signal >2 mm from the bone) and bursitis was made to align with the recent OMERACT definitions of enthesitis, which do not include these findings as part of the enthesitis definition.[16,17] Instead, OMERACT defines enthesitis more narrowly, excluding these separate pathologic findings, even though they could also represent sources of pain. Furthermore, our study's "real world" approach spanning various countries and incorporating broad inclusion criteria aimed to replicate typical clinical settings. As a result, the included populations exhibited considerable heterogeneity from a clinical perspective, particularly among patients with SpA who presented with varying disease durations, activity status, and treatment regimens. Finally, although a web-based reliability test was conducted initially, no further reliability assessments, including central reading, were implemented during the study period, which we acknowledge as a limitation of the study.

Future research should aim to investigate the link between clinical versus subclinical/ultrasound-detected enthesitis and their respective impacts on long-term outcomes. Longitudinal studies comparing both methods can provide insights into the progression of enthesitis in SpA. Ultrasound might detect early changes that physical examination cannot, allowing for earlier diagnosis and potentially intervention. This remains an essential next step for a comprehensive understanding of this important SpA domain.

Our study revealed varying agreement between ultrasound and physical examination in the assessment of enthesitis, depending on individual ultrasound lesions and the entheseal site evaluated. PD signal at the enthesis and "active enthesitis" showed the highest agreement values with physical examination across all ultrasound findings, reflecting the inflammatory nature of these ultrasound lesions. On the other hand, the Achilles tendon insertion, which is traditionally regarded as a key area in the assessment of enthesitis in patients with SpA, showed the lowest agreement among the entheseal sites evaluated, regardless of the ultrasound finding being considered.

Up to 20% of patients with SpA without clinical enthesitis exhibited active inflammation on ultrasound, often accompanied by local structural damage. Conversely, more than two-thirds of patients with SpA with clinical enthesitis had no evidence of ultrasound inflammation at the enthesis, suggesting potential overestimation via physical examination. Our results underscore the importance of developing a comprehensive tool that integrates both methods to ensure a more precise evaluation of this crucial aspect of SpA, applicable in both clinical practice and research settings.

AUTHOR CONTRIBUTIONS

All authors contributed to at least one of the following manuscript preparation roles: conceptualization AND/OR methodology, software, investigation, formal analysis, data curation, visualization, and validation AND drafting or reviewing/editing the final draft. As corresponding author, Dr Di Matteo confirms that all authors have provided the final approval of the version to be published, and takes responsibility for the affirmations regarding article submission (eg, not under consideration by another journal), the integrity of the data presented, and the statements regarding compliance with institutional review board/Helsinki Declaration requirements.

REFERENCES

1. Kehl AS, Corr M, Weisman MH. Review: enthesitis: new insights into pathogenesis, diagnostic modalities, and treatment. Arthritis Rheumatol 2016;68:312–322.

2. Gossec L, Baraliakos X, Kerschbaumer A, et al. EULAR recommendations for the management of psoriatic arthritis with pharmacological therapies: 2019 update. Ann Rheum Dis 2020;79:700–712.
3. Rudwaleit M, Landewé R, van der Heijde D, et al. The development of Assessment of SpondyloArthritis international Society classification criteria for axial spondyloarthritis (part I): classification of paper patients by expert opinion including uncertainty appraisal. Ann Rheum Dis 2009;68:770–776.
4. Rudwaleit M, van der Heijde D, Landewé R, et al. The development of Assessment of SpondyloArthritis international Society classification criteria for axial spondyloarthritis (part II): validation and final selection. Ann Rheum Dis 2009;68:777–783.
5. Gossec L, Kerschbaumer A, Ferreira RJO, et al. EULAR recommendations for the management of psoriatic arthritis with pharmacological therapies: 2023 update. Ann Rheum Dis 2024;83:706–719.
6. McGonagle DG, Helliwell P, Veale D. Enthesitis in psoriatic disease. Dermatology 2012;225:100–109.
7. Wu X, Liu D, Li Y, et al. A clinical practice guideline for the screening and assessment of enthesitis in patients with spondyloarthritis. Front Immunol 2022;13:978504.
8. Healy PJ, Helliwell PS. Measuring clinical enthesitis in psoriatic arthritis: assessment of existing measures and development of an instrument specific to psoriatic arthritis. Arthritis Rheum 2008;59:686–691.
9. Maksymowych WP, Mallon C, Morrow S, et al. Development and validation of the Spondyloarthritis Research Consortium of Canada (SPARCC) Enthesitis Index. Ann Rheum Dis 2009;68:948–953.
10. Heuft-Dorenbosch L, Spoorenberg A, van Tubergen A, et al. Assessment of enthesitis in ankylosing spondylitis. Ann Rheum Dis 2003;62:127–132.
11. Braun J, Brandt J, Listing J, et al. Treatment of active ankylosing spondylitis with infliximab: a randomised controlled multicentre trial. Lancet 2002;359:1187–1193.
12. Gorman JD, Sack KE, Davis JC Jr. Treatment of ankylosing spondylitis by inhibition of tumor necrosis factor alpha. N Engl J Med 2002;346:1349–1356.
13. Kaeley GS. Visualization of enthesitis by ultrasound: a key diagnostic tool in spondyloarthropathy diagnosis and management. Curr Rheumatol Rep 2020;22:48.
14. Filippucci E, Smerilli G, Di Matteo A, et al. Ultrasound definition of enthesitis in spondyloarthritis and psoriatic arthritis: arrival or starting point? Ann Rheum Dis 2021;80:1373–1375.
15. Smerilli G, Di Matteo A, Cipolletta E, et al. Enthesitis in psoriatic arthritis, the sonographic perspective. Curr Rheumatol Rep 2021;23:75.
16. Terslev L, Naredo E, Iagnocco A, et al. Defining enthesitis in spondyloarthritis by ultrasound: results of a delphi process and of a reliability reading exercise. Arthritis Care Res (Hoboken) 2014;66:741–748.
17. Balint PV, Terslev L, Aegerter P, et al. Reliability of a consensus-based ultrasound definition and scoring for enthesitis in spondyloarthritis and psoriatic arthritis: an OMERACT US initiative. Ann Rheum Dis 2018;77:1730–1735.
18. Zabotti A, Bandinelli F, Batticciotto A, et al.; Musculoskeletal Ultrasound Study Group of the Italian Society of Rheumatology. Musculoskeletal ultrasonography for psoriatic arthritis and psoriasis patients: a systematic literature review. Rheumatology (Oxford) 2017;56:1518–1532.
19. Gouze H, Backhaus M, Balint P, et al. Ultrasound in the management of patients with psoriatic arthritis: systematic literature review and novel algorithms for pragmatic use. J Rheumatol Published online September 15, 2023. https://doi.org/10.3899/jrheum.2023-0091
20. Macchioni P, Salvarani C, Possemato N, et al. Ultrasonographic and clinical assessment of peripheral enthesitis in patients with psoriatic arthritis, psoriasis, and fibromyalgia syndrome: the ULISSE study. J Rheumatol 2019;46:904–911.
21. Di Matteo A, Smerilli G, Di Donato S, et al. Power Doppler signal at the enthesis and bone erosions are the most discriminative OMERACT ultrasound lesions for SpA: results from the DEUS (Defining Enthesitis on Ultrasound in Spondyloarthritis) multicentre study. Ann Rheum Dis Published online June 12, 2024. https://doi.org/10.1136/ard-2023-225443
22. Schoels M, Aletaha D, Funovits J, et al. Application of the DAREA/DAPSA score for assessment of disease activity in psoriatic arthritis. Ann Rheum Dis 2010;69:1441–1447.
23. Lukas C, Landewé R, Sieper J, et al. Development of an ASAS-endorsed disease activity score (ASDAS) in patients with ankylosing spondylitis. Ann Rheum Dis 2009;68:18–24.
24. Gossec L, Portier A, Landewé R, et al. Preliminary definitions of "flare" in axial spondyloarthritis, based on pain, BASDAI and ASDAS-CRP: an ASAS initiative. Ann Rheum Dis 2016;75:991–996.
25. Calin A, Garrett S, Whitelock H, et al. A new approach to defining functional ability in ankylosing spondylitis: the development of the Bath Ankylosing Spondylitis Functional Index. J Rheumatol 1994;21:2281–2285.
26. Jenkinson TR, Mallorie PA, Whitelock H, et al. Defining spinal mobility in ankylosing spondylitis: the Bath Ankylosing Spondylitis Metrology Index. J Rheumatol 1994;21:1694–1698.
27. Fries JF, Spitz P, Kraines G, et al. Measurement of patient outcome in arthritis. Arthritis Rheum 1980;23:137–145.
28. Di Matteo A, Filippucci E, Cipolletta E, et al. Entheseal involvement in patients with systemic lupus erythematosus: an ultrasound study. Rheumatology (Oxford) 2018;1;57:1822–1829.
29. Möller I, Janta I, Backhaus M, et al. The 2017 EULAR standardised procedures for ultrasound imaging in rheumatology. Ann Rheum Dis 2017;76:1974–1979.
30. Di Matteo A, Filippucci E, Cipolletta E, et al. How normal is the enthesis by ultrasound in healthy subjects? Clin Exp Rheumatol 2020;38:472–478.
31. Di Matteo A, Filippucci E, Cipolletta E, et.al Reply to: High prevalence of ultrasound-defined enthesitis in patients with metabolic syndrome. Clin Exp Rheumatol 2021;39:437.
32. de Miguel E, Cobo T, Munoz-Fernandez S, et al. Validity of enthesis ultrasound assessment in spondyloarthropathy. Ann Rheum Dis 2009;68:169–174.
33. Kiris A, Kaya A, Ozgocmen S, et al. Assessment of enthesitis in ankylosing spondylitis by power Doppler ultrasonography. Skeletal Radiol 2006;35:522–528.
34. Freeston JE, Coates LC, Helliwell PS, et al. Is there subclinical enthesitis in early psoriatic arthritis? A clinical comparison with power Doppler ultrasound. Arthritis Care Res (Hoboken) 2012;64:1617–1621.
35. Di Matteo A, Cipolletta E, Destro Castaniti GM, et al. Reliability assessment of the definition of ultrasound enthesitis in SpA: results of a large, multicentre, international, web-based study. Rheumatology (Oxford) 2022;28;61:4863–4874.
36. Landis JR, Koch GG. An application of hierarchical kappa-type statistics in the assessment of majority agreement among multiple observers. Biometrics 1977;33:363–374.
37. Zabotti A, Piga M, Canzoni M, et al; UPSTREAM study group. Ultrasonography in psoriatic arthritis: which sites should we scan? Ann Rheum Dis 2018;77:1537–1538.
38. McGonagle D, Aydin SZ, Marzo-Ortega H, et al Hidden in plain sight: is there a crucial role for enthesitis assessment in the treatment and monitoring of axial spondyloarthritis? Semin Arthritis Rheum 2021;51:1147–1161.
39. Helliwell PS. Assessment of enthesitis in psoriatic arthritis. J Rheumatol 2019;46:869–870.

40. Fiorenza A, Bonitta G, Gerratana E, et al. Assessment of enthesis in patients with psoriatic arthritis and fibromyalgia using clinical examination and ultrasound. Clin Exp Rheumatol 2020;38 Suppl 123:31–39.
41. Aydin SZ, Bakirci S, Kasapoglu E, et al. The relationship between physical examination and ultrasonography of large entheses of the Achilles tendon and patellar tendon origin. J Rheumatol 2020;47: 1026–1030.
42. Sapsford M, Evans J, Clunie G, et al. A comparison of clinical examination and ultrasound enthesitis indices in patients with psoriatic arthritis, adjusted for concomitant fibromyalgia. Ther Adv Musculoskelet Dis 2021;13:1759720X211003812.
43. Michelsen B, Diamantopoulos AP, Soldal DM, et al. Achilles enthesitis defined by ultrasound is not associated with clinical enthesitis in patients with psoriatic arthritis. RMD Open 2017;16;3:e000486.
44. Di Matteo A, Mankia K, Azukizawa M, et al. The role of musculoskeletal ultrasound in the rheumatoid arthritis continuum. Curr Rheumatol Rep 2020;22:41.
45. Eder L, Mathew AJ, Carron P, et al. Management of enthesitis in patients with psoriatic arthritis: an updated literature review informing the 2021 GRAPPA treatment recommendations. J Rheumatol 2023; 50:258–264.
46. D'Agostino MA, Carron P, Gaillez C, et al. Effects of secukinumab on synovitis and enthesitis in patients with psoriatic arthritis: 52-week clinical and ultrasound results from the randomised, double-blind ULTIMATE trial with open label extension. Semin Arthritis Rheum 2023;63:152259.
47. Elliott A, Wright G, Pendleton A, et al. Effects of TNF-α inhibition versus secukinumab on active ultrasound-confirmed enthesitis in psoriatic arthritis. Ther Adv Musculoskelet Dis 2023;15: 1759720X231179524.
48. Smerilli G, Cipolletta E, Di Matteo A, et al. 'Double target' ultrasound monitoring of biologic therapy in psoriatic arthritis. Clin Exp Rheumatol 2024;42:626–632.
49. Aydin SZ, Mathew AJ, Koppikar S, et al. Imaging in the diagnosis and management of peripheral psoriatic arthritis. Best Pract Res Clin Rheumatol 2020;34:101594.
50. D'Agostino MA, Terslev L. Imaging evaluation of the entheses: ultrasonography, MRI, and scoring of evaluation. Rheum Dis Clin North Am 2016;42:679–693.
51. Maldonado RA, Ruta S, Valuntas ML, et al. Ultrasonography assessment of heel entheses in patients with spondyloarthritis: a comparative study with magnetic resonance imaging and conventional radiography. Clin Rheumatol 2017;36:1811–1817.
52. Felbo SK, Østergaard M, Sørensen IJ, et al. Ultrasound of the heel improves diagnosis-tender entheses in the heel region rarely corresponds to inflammatory enthesitis in patients with peripheral spondyloarthritis. J Clin Med 2022;11:2325.
53. Polachek A, Cook R, Chandran V, et al. The association between sonographic enthesitis and radiographic damage in psoriatic arthritis. Arthritis Res Ther 2017;19:189.
54. Smerilli G, Cipolletta E, Destro Castaniti GM, et al. Doppler signal and bone erosions at the enthesis are independently associated with ultrasound joint erosive damage in psoriatic arthritis. J Rheumatol 2023; 50:70–75.

American College of Rheumatology
Empowering Rheumatology Professionals

Arthritis & Rheumatology
Vol. 77, No. 1, January 2025, pp 34–46
DOI 10.1002/art.42974

Enhanced Type 1 Interferon Signature in Axial Spondyloarthritis Patients Unresponsive to Secukinumab Treatment

Addison Pacheco,[1] Sinead Maguire,[2] Zoya Qaiyum,[3] Michael Tang,[3] Adam Bridger,[3] Melissa Lim,[3] Fataneh Tavasolian,[3] Enoch Yau,[3] Sarah Q. Crome,[4] Nigil Haroon,[5] and Robert D. Inman[6]

Objective. Axial spondyloarthritis (axSpA) is an inflammatory disease in which overactive interleukin (IL)-17A–producing cells are implicated in a central role. Therapeutically, biologics that target IL-17A, such as secukinumab, have demonstrated improved clinical outcomes. Despite this translational success, there is a gap in understanding why some patients with axSpA do not respond to IL-17A–blocking therapy. Our study aims to discriminate immune profiles between secukinumab responders (SEC-R) and nonresponders (SEC-NR).

Methods. Peripheral blood mononuclear cells were collected from 30 patients with axSpA before and 24 weeks after secukinumab treatment. Frequency of CD4+ subsets were compared between SEC-R and SEC-NR using flow cytometry. Mature CD45RO+CD45RA-CD4+ T cells were fluorescent-activated cell sorting sorted, and RNA was measured using NanoString analysis.

Results. SEC-NR had an increased frequency of IL-17A–producing RORγt+CD4+ T cells compared to healthy controls before secukinumab treatment ($P < 0.01$). SEC-NR had a significant increase of CXCR3+ CD4+ T cells before secukinumab treatment compared to SEC-R ($P < 0.01$). Differentially expressed gene analysis revealed up-regulation of type 1 interferon (IFN)-regulated genes in SEC-NR patients compared to SEC-R patients after receiving the biologic. SEC-R patients had an up-regulated cytotoxic CD4+ T cell gene signature before receiving secukinumab treatment compared to SEC-NR patients.

Conclusion. The increased frequency of IL-17A–producing cells in SEC-NR patients suggests a larger inflammatory burden than SEC-R patients. With treatment, SEC-NR patients have a more pronounced type 1 IFN signature than SEC-R patients, suggesting a mechanism contributing to this larger inflammatory burden. The results point toward more immune heterogeneity in axSpA than has been recognized and highlights the need for precision therapeutics in this disease.

INTRODUCTION

Axial spondyloarthritis (axSpA) is a chronic inflammatory disease characterized by back pain, spinal ankylosis, and extra-articular manifestations.[1] The subsets of axSpA include radiographic axSpA (r-axSpA or AS), which is characterized by radiographic structural damage to the sacroiliac joints,[2] and nonradiographic axSpA (nr-axSpA), in which there is an absence of significant sacroiliitis on x-ray.[3] The burden of symptoms for the two forms of axSpA are similar, but patients with nr-axSpA are often younger and have shorter disease duration.[4] Current European and American guidelines recommend similar treatment for r- and nr-axSpA.[5,6]

Supported by an investigator-initiated study funded through Novartis (CAPCR ID#20-5095). Addison Pacheco's PhD stipend was funded through the Arthritis Society Canada's TGP competition (#22-0000000135).

[1]Addison Pacheco, HBSc: Schroeder Arthritis Institute, University Health Network and University of Toronto, Toronto, Ontario, Canada; [2]Sinead Maguire, MD: Schroeder Arthritis Institute, University Health Network and Toronto Western Hospital, University Health Network, Toronto, Ontario, Canada; [3]Zoya Qaiyum, MSc, Michael Tang, PhD, Adam Bridger, BSc, Melissa Lim, MSc, Fataneh Tavasolian, PhD, Enoch Yau, MSc: Schroeder Arthritis Institute, University Health Network, Toronto, Ontario, Canada; [4]Sarah Q. Crome, PhD: University of Toronto, Ajmera Transplant Centre, University Health Network, and Toronto General Hospital Research Institute, University Health Network, Toronto, Ontario, Canada; [5]Nigil Haroon, MD, PhD: University of Toronto and Toronto Western Hospital, University Health Network, Toronto, Ontario, Canada; [6]Robert D. Inman, MD: Schroeder Arthritis Institute, University Health Network, Ajmera Transplant Centre, University Health Network, Toronto Western Hospital, University Health Network, and University of Toronto, Toronto, Ontario, Canada.

Mr. Pacheco and Dr. Maguire contributed equally to this work.

Additional Supplementary information cited in this article can be found online in the Supporting Information section (http://onlinelibrary.wiley.com/doi/10.1002/art.42974).

Author disclosures and graphical abstract are available at https://onlinelibrary.wiley.com/doi/10.1002/art.42974.

Address correspondence via email to Robert D. Inman, MD, at Robert.Inman@uhn.ca.

Submitted for publication February 28, 2024; accepted in revised form August 5, 2024.

Many of the other known single nucleotide polymorphisms associated with axSpA are genes involved in type 3 immunity, specifically the interleukin (IL)-23/IL-17A pathway. This pathway contributes to overactivated cells driving the joint inflammation that underlies both pain and spinal ankylosis in axSpA.[7] The physiological control of type 3 immunity involves the balance between T helper 17 (T_H17) cells, which are proinflammatory, and regulatory T cells (Treg cells), which are anti-inflammatory. T_H17 cells are commonly defined as CD4+ T cells that co-express CCR6 and RORγt and lack CXCR3 expression. It is important to note, however, that CCR6 and CXCR3 are chemokine receptors and that some T_H17 have been documented to express CXCR3.[8,9] The CXCR3 receptor binds to three interferon (IFN)-inducing chemokines: CXCL9 (MIG), CXCL10 (IP-10), and CXCL11 (IP-9).[10] In contrast, CCR6 binds to only one known ligand, CCL20, and directs the cell to the site of inflammation.[11] Previously, it has been demonstrated that T_H17 cells are elevated in male patients with axSpA, but not female patients with axSpA, whereas alterations in the T helper 1 axis was independent of a patient's sex.[12] Other proinflammatory IL-17A producing cells such as mucosal-associated invariant T (MAIT) cells,[13] innate lymphoid cells (ILCs),[14] and γδ T cells[15] have also been shown to be elevated in axSpA peripheral blood.

Treg cells are defined as CD4+ T cells with high expression of IL-2 Receptor (CD25) and stable expression of FOXP3, which are capable of suppressing effector cell proliferation and functionality. Treg cells acquire an effector phenotype similar to the cells they are suppressing, reflected in their acquiring of CCR6, RORγt, and STAT3 expression for the suppression of T_H17.[16] The role of Treg cells in axSpA pathobiology is not well defined to date. The frequency of Treg cells in axSpA peripheral blood is debated and is in part dependent on how the Treg cells are defined.[17] Certain effector Treg populations have been described to be reduced and have greater methylation in the CNS2 region of FOXP3 in axSpA compared to healthy controls (HCs).[18,19] We also have recently demonstrated that exosome-mediated signals in AS could change Treg suppressive ligands and cytokines in vitro, hinting at a possible mechanism of how inflammation remains uncontrolled in axSpA.[20] The role Tregs have in modulating IL-17A in axSpA remains unknown.

Biologics are commonly employed to reduce inflammation and pain in patients with axSpA. Secukinumab is a monoclonal antibody that targets the cytokine IL-17A and is an approved biologic for the treatment of axSpA.[21] Secukinumab is approved to be dosed at 150 mg every four weeks usually after a loading dose of 150 mg weekly for the first five doses.[21] The efficacy and safety of secukinumab has been demonstrated in nine randomized controlled phase III trials: the MEASURE studies,[22–26] MAXIMISE study,[27] PREVENT study,[28] SKIPPAIN study,[29] and the SURPASS study.[30] Approximately 60% of patients met the Assessment of Spondyloarthritis International Society criteria for 20% improvement (ASAS20) and showed significant improvement in secondary endpoints of disease activity such as C-reactive protein (CRP) levels, Ankylosing Spondylitis Disease Activity Score (ASDAS), and Bath Ankylosing Spondylitis Disease Activity Index (BASDAI).[5,22–25] Although this therapeutic advance has led to a significant improvement in the symptoms of axSpA, it is currently unknown why approximately 40% of patients do not respond to secukinumab. Our study aimed to distinguish clinical and immune cellular profiles between secukinumab treatment responders (SEC-R) and nonresponders (SEC-NR). We further aim to determine transcriptional changes that occur in SEC-R and SEC-NR patients.

MATERIALS AND METHODS

Patient and public involvement. A longitudinal axSpA cohort was used for the study with the approval of the University Health Network research ethics board (REB# 20-5095) along with HCs recruited under an ongoing axSpA cohort biobank (REB#21-5565). All patients and HCs provided written consent to participate. Patients with AS fulfilled the modified New York AS criteria and nr-axSpA patients fulfilled ASAS classification criteria for nr-axSpA.[31,32] Patients, aged 18 to 65 years old, were recruited to the study from 2020 to 2023 if unresponsive to prior treatment with nonsteroidal anti-inflammatory drugs and received fewer than two tumor necrosis factor inhibitors (TNFi) previously, with a median biologic washout period of two months (Figure 1A, Supplementary Figure S1A). Inadequate response to previous biologics was determined when a patient's BASDAI exceeded 4 and the shared decision between physician and patient recommended a switch in biologics. Patients who had not used any biologic for more than five years were considered biologic naive. Patient response to secukinumab treatment was defined by a BASDAI reduction >2 or by a reduction >1.1 in BASDAI-based Ankylosing Spondylitis Disease Activity Score (BASDAS), a surrogate score for ASDAS-CRP.[33,34] Supplementary Table S1 provides characteristics of all study participants.

Peripheral blood mononuclear cells isolation. Peripheral blood mononuclear cells (PBMCs) were isolated from venous blood using Ficoll-Paque Plus (GE Healthcare, cat#17-1440-02) and were frozen in 50% DMSO and 50% complete media (RPMI+L-Glu [Gibco, cat#11875-093], 10% fetal bovine serum [FBS, Gibco, cat#12483-020], 10% P/S, 2 μL/500 mL β-mercaptoethanol) in liquid nitrogen. Blood samples were collected between 9:00 AM and 5:00 PM.

Flow cytometry. Isolated frozen PBMCs were thawed and were rested in complete media for four hours before staining for flow cytometry experiment. Cells were first stained with live/dead (BD, cat#564402, lot#2221729) for 20 minutes at 4°C, then were blocked for 10 minutes with human TruStain FcX (Biolegend, cat#422302). After blocking, cells were stained with pretitrated

A

Secukinumab Response Defined by BASDAI 2 OR BASDAS reduced by 1.1		
Characteristic	25 Responders (57%)	19 Non Responder (43%)
Average Age, Years	42.28 (+/- 15.79)	46.16 (+/- 9.73)
Sex, Male	17 (68.0%)	12 (63.2%)
HLA-B27, Positive	22 (88.0%)	15 (78.9%)
Radiographic/nr-axSpA	20/5 (80.0% AS)	15/4 (78.9% AS)
BASDAI at Baseline	6.18 (+/-1.61)	5.72 (+/-1.54)
BASDAS at Baseline	3.65 (+/-0.79)	3.11 (+/-0.70)
Psoriasis, Yes	3 (11.5%)	4 (22.2%)
Uveitis, Yes	4 (15.4%)	4 (22.2%)
Syndesmophytes, Yes	14 (57.7%)	6 (27.8%)
Biologic Naïve, Yes	14 (53.8%)	2 (11.1%)
Enrollment	Inclusion -AxSpA patients unresponsive to prior treatment with NSAIDS or ≤2 TNF inhibitors -Ages 18-65yrs old Exclusion -Patients with alternative source of back pain, active IBD or active infection -Consent not given	

B

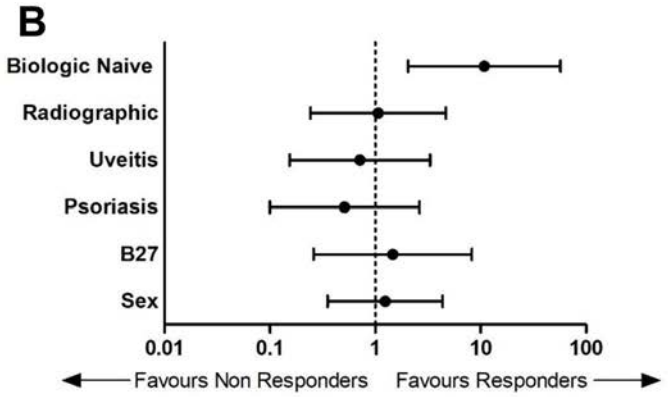

Figure 1. (A) Patient recruitment for the observational one-arm study with secukinumab. All active patients (n = 44) received secukinumab at 150 mg monthly after five weekly loading doses in which biologic response was determined after 24 weeks of treatment. Response was determined by a reduction in BASDAI scoring >2 or by a BASDAS reduction >1.1. Characteristic averages are listed for age, BASDAI pre-secukinumab, and BASDAS pre-secukinumab for secukinumab treatment responders and nonresponders. Characteristic tally and percentages are listed for other characteristics. (B) Forest plot shows odd ratio value with upper and lower 95% confidence intervals. axSpA, axial spondyloarthritis; BASDAI, Bath Ankylosing Spondylitis Disease Activity Index; BASDAS, BASDAI-based Ankylosing Spondylitis Disease Activity Score; IBD, inflammatory bowel disease; nr-axSpA, nonradiographic axial spondyloarthritis; NSAIDs, nonsteroidal anti-inflammatory drugs; TNF, tumor necrosis factor.

surface antibodies for 30 minutes at 4°C. CXCR3 and CCR6 were stained for 30 minutes at 37°C before the staining of other surface staining antibodies. Cells were fixed with FOXP3 Transcription Factor Staining Buffer Set (eBioscience, cat#00-5523-00) for intracellular staining of FOXP3. Cells were fixed for one hour and were permeabilized for one hour before intracellular staining for 30 minutes at room temperature. When RORγt was in the panel, intracellular staining was done overnight at room temperature. In intracellular cytokine analysis, cells were stimulated with phorbol myristate acetate (PMA) and ionomycin (BioLegend, cat#423302, lot#B352056) four hours before staining, and GolgiPlug (BD, cat#51-2301K7, lot#0227731) was supplemented 30 minutes after the addition of PMA and ionomycin. Data were acquired using a BD Canto flow cytometry (BD Biosciences) or BD Symphony A3 (BD Biosciences). Acquired data were analyzed using FlowJo software version 10.8.0. Antibodies used are listed in Supplementary Table S2.

Fluorescent-activated cell sorting. Isolated frozen PBMCs were thawed and were rested overnight in complete media at 37°C. Cells were stained with live/dead, blocked with FcX, and stained for surface markers as described in flow cytometry methods. Cells were sorted into a 2 mL DNA LoBind tube (Eppendorf cat#022431048, lot#L2064210) containing 50% FBS complete media using a BD Aria (BD Biosciences). Antibodies used are listed in Supplementary Table S2.

RNA extraction and NanoString Analysis. Using the PicoPure RNA Isolation Kit (Invitrogen, cat#12204-01, lot#01340972), total RNA was extracted from CD45RO +CD45RA– CD4+ T cells according to the manufacturer's instructions. Two hundred nanograms of RNA was hybridized for 12 to 30 hours at 65°C using an nCounter messenger RNA assay for the nCounter Autoimmune Profiling Panel version 2 (Human) (NanoString Technologies) at the Princess Margaret Genomics Centre. Posthybridization was performed using nCounter Prep Station, and Digital Analyzer was used for data collection. Raw RNA transcript counts were assessed for quality control and normalized using the nSolver version 4 software. Normalized RNA transcripts were converted into $\log_2$ values for statistical analysis.

Functional pathway analysis and statistical assessment. Differentially expressed genes (DEGs) with a fold change ≥ 1 and unadjusted $P < 0.05$ were run on gene ontology (GO) enrichment analysis and visualized using G:Profiler. In the case of categorical variables, data were presented as odds ratio (OR) and 95% confidence interval (CI). Univariate clinical characteristics were analyzed using Fischer's exact test. In the case of continuous variables, data were presented as mean ± SD. The pre-secukinumab flow cytometry analyses were compared using multiple nonparametric Mann-Whitney U tests. Paired analyses were analyzed using two-tailed Wilcoxon signed rank test with $P = 0.05$ used as threshold. A multivariate logistic regression analysis was performed using R version 4.3.1 to calculate the likelihood of responding to secukinumab, expressed as the odds ratio.

RESULTS

Biologic-naive patients more likely to respond to secukinumab. We were first interested if any clinical

characteristic increased the odds of responding to secukinumab. Patient characteristics did not differ significantly between SEC-R and SEC-NR patients, with the exception of previous biologic treatment. Biologic-naive patients were significantly more likely to respond to secukinumab (Figure 1B) (OR = 10.82, 95% CI = 2.05–52.17; $P < 0.01$). The association between clinical variables and secukinumab response were then investigated using a logistic regression model (Table 1). Previous biologic treatment (OR = 0.03, 95% CI = 0.0–0.29; $P < 0.05$) was associated with secukinumab response, whereas other clinical variables had no association with secukinumab response. In summary, we found patients that had inadequate response to previous biologics were more likely to also have inadequate response to secukinumab.

Higher frequency of IL-17A producing CD4+ T cells in SEC-NR patients. To start immune profiling SEC-R and SEC-NR patients, we observed IL-17A production in stimulated CD4+ T cells from patient PBMCs at different secukinumab treatment timepoints (Supplementary Figure S1A and B, Supplementary Figure S2A). IL-17A+ CD4+ T cells frequency was significantly higher in SEC-NR patients (mean 1.63%) compared to SEC-R patients (mean 0.60%, $P < 0.01$) and HCs (mean 0.53%, $P < 0.01$) (Supplementary Figure S2B). Interestingly, the frequency of FOXP3+CD4+ T cells that produce IL-17A was significantly higher in SEC-NR patients (mean 1.68%) compared to HCs (mean 0.98%, $P < 0.05$) (Supplementary Figure S2C). The frequency of IL-17A+ FOXP3+ CD4+ T cells in SEC-NR patients trended higher than in SEC-R patients (mean 0.98%, $P = 0.06$) (Supplementary Figure S2C). This subpopulation was not CD25+ and therefore not reflective of Treg cells nor did the frequency change post-secukinumab treatment (Supplementary Figure S2D). IL-17A+ RORγt+ CD4+ T cell frequency was significantly higher in SEC-NR patients (mean 11.4%) compared to HCs (mean 4.66%, $P < 0.01$) and trended toward a higher frequency compared to SEC-R patients before secukinumab treatment (mean 6.26%, Figure 2A and B). The frequency of this subset did not change after 24 weeks of secukinumab treatment for SEC-R and SEC-NR patients (Figure 2C). To measure the amount of IL-17A being produced by RORγt+ CD4+ T cells, the median fluorescence intensity of IL-17A was multiplied by the proportion of IL17A+RORγt+ CD4+ T cells. This value was consistent between HC, SEC-R, and SEC-NR patients at the pre-secukinumab timepoint (Figure 2D). This value did not decrease significantly for SEC-R patients after secukinumab treatment, but there was a decreasing trend in the SEC-NR patients after 24 weeks of treatment ($P = 0.06$) (Figure 2E). Taken together, we found SEC-NR patients have significantly more IL-17A producing cells, and response to secukinumab does not require a reduction of IL-17A production from CD4+ T cells.

Table 1. Logistic regression model of response to secukinumab treatment*

Patient characteristic	Odds ratio (95% CI)	*P* value
Age	0.99 (0.92–1.05)	0.7
Sex		
Female	(Reference)	
Male	0.86 (0.16–4.26)	0.9
Previous Biologic		
No	(Reference)	
Yes	0.03 (0.0–0.29)	**0.015**
B27 Status		
Negative	(Reference)	
Positive	7.20 (0.30–391)	0.3
Radiographic		
No	(Reference)	
Yes	1.33 (0.16–11.9)	0.8
Psoriasis		
No	(Reference)	
Yes	0.10 (0.0–1.23)	0.11
Uveitis		
No	(Reference)	
Yes	0.84 (0.14–5.00)	0.8
Inflammatory[a]		
CXCR3+CCR6+	0.36 (0.06–0.72)	0.052
CXCR3+CCR6−	0.52 (0.24–0.82)	**0.028**

* Bolded *P* values are considered statistically significant differences. CI, confidence interval.
[a] Adjusted for age, sex, previous biologic, B27 status, radiographic, psoriasis, and uveitis.

Increased CXCR3 expressing cells pre-secukinumab treatment in SEC-NR patients. Because SEC-NR patients demonstrate a decrease in IL-17A production in CD4+ T cells, we investigated whether the frequency of different CD4+ T cell subsets change at the different treatment time points, without in vitro stimulation (Supplementary Figure S3A). The frequency of Treg cells (CD25+CD127−FOXP3+CD4+ T cells) and T_H17 (CCR6+CXCR3−RORγt+CD4+ T cells) did not differ significantly between HCs and patients with axSpA pre-secukinumab, regardless of secukinumab response (Supplementary Figure S3B and D). The frequency of these subsets did not change with secukinumab treatment (Supplementary Figure S3C and E). The frequency of RORγt+ Treg cells relative to total Treg cells was significantly reduced in patients with axSpA pre-secukinumab (mean 6.38%) compared to HCs (mean 9.87%, $P < 0.05$) (Figure 3A). There was no significant difference between SEC-R and SEC-NR patients pre-secukinumab (Figure 3B) nor did the frequency significantly change post-secukinumab treatment (data not shown). However, CXCR3+ cell frequency was higher in SEC-NR patients pre-secukinumab compared to SEC-R patients and HCs (Figure 3C). T_H17 (CXCR3−CCR6+ CD4+ T cells) (16.58% vs 12.84%, $P = 0.0575$) trend toward a higher frequency in SEC-NR patients compared to SEC-R patients (Figure 3D). T_H1 (CXCR3+CCR6− CD4+ T cells) (14.21% vs 9.85%) and $T_H1.17$ cells (CXCR3+CCR6+ CD4+ T cells) showed significantly elevated frequencies in SEC-NR patients compared to SEC-R patients (Figure 3F and H). These subset frequencies did not change for SEC-NR patients after treatment (Figure 3E, G, and I) but SEC-R patients did trend toward an increase of T_H1 cell

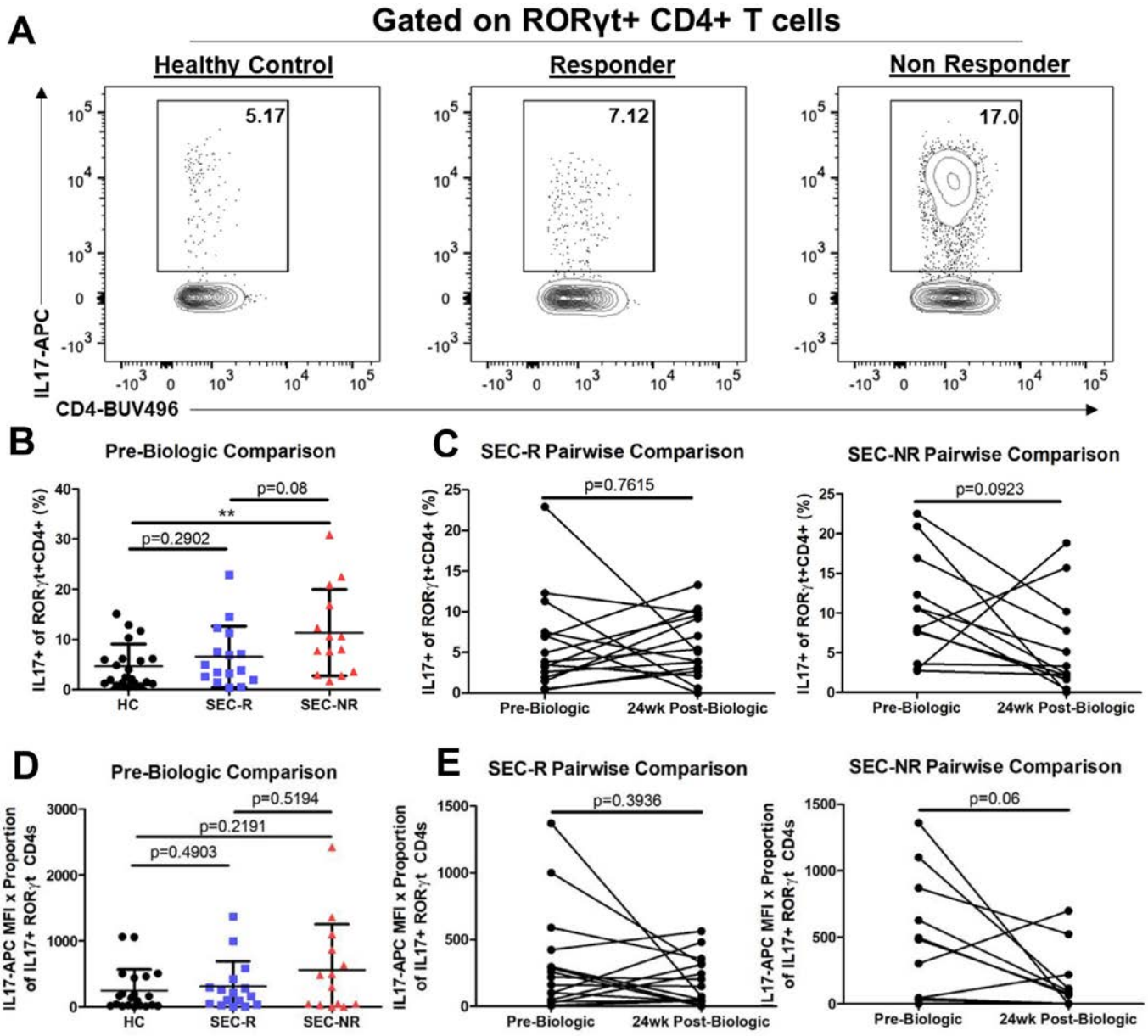

Figure 2. (A) Representative frequency of IL-17A producing RORγt+ CD4s T cells from HC and SEC-R and SEC-NR. (B) Dot plot represent frequencies of IL-17A producing RORγt+ CD4 T cells from PBMCs of HCs and patients with axSpA before secukinumab treatment. (C) Paired analysis of IL17-producing RORγt+ CD4 T cells frequency in responders and nonresponders. (D) Dot plot represent median of IL-17 APC MFI from IL17+ producing RORγt+ CD4 T cells (multiplied by proportion of IL17+ RORγt+ CD4+ T cells) collected from the PBMCs of HCs and patients with axSpA before secukinumab treatment. (E) Paired analysis of IL-17 APC MFI × proportion of IL17+ RORγt+ CD4+ T cells in responders and nonresponders. Data represent 21 HCs, 16 secukinumab responders (blue squares), and 14 nonresponders (red triangles). $^{**}P < 0.01$ significant by Mann-Whitney U test for dot plot analysis and two-tailed Wilcoxon signed rank test for paired analysis. APC, allophycocyanin; axSpA, axial spondyloarthritis; HC, healthy control; IL, interleukin; MFI, mean fluorescence intensity; PBMC, peripheral blood mononuclear cell; SEC-NR, secukinumab treatment nonresponders; SEC-R, secukinumab treatment responders.

frequency post-treatment (from 9.69% to 12.35%, Figure 3G). Interestingly Tbet+ CD4+ T cells and Tbet-BV605 median fluorescence intensity (MFI) of these positive cells did not differ significantly among all groups (Supplementary Figure S3F and G). When adjusted for the clinical variables listed in Table 1, the frequency of $T_H1.17$ cells (OR 0.36, 95%CI 0.06–0.72; $P = 0.052$) trended toward associating with secukinumab response, whereas T_H1 cell frequency (OR 0.52, 95% CI 0.24–0.82; $P = 0.028$) was significantly associated with secukinumab response. Both subsets appeared to decrease the odds of a patient responding to secukinumab treatment. In summary, we observed increased CXCR3+ CD4+ T cell frequency in SEC-NR patients, and this frequency appeared to decrease the odds of responding to secukinumab treatment.

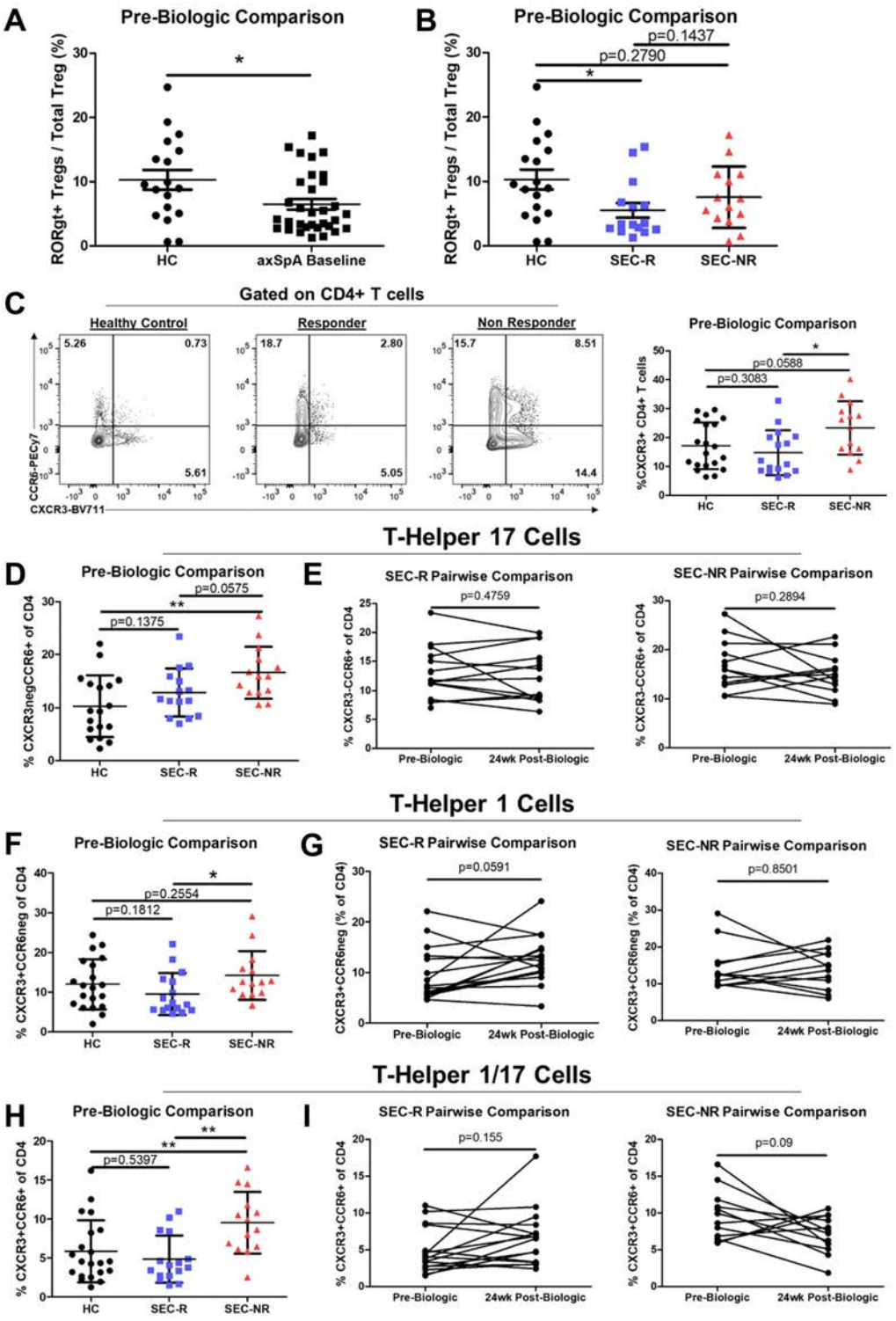

Figure 3. (A) Dot plot representing frequency of RORγt+ Treg frequency relative to total Treg from HCs (n = 21) and patients with axSpA pre-secukinumab (n = 30). (B) Dot plot representing frequency of RORγt+ Treg frequency relative to total Treg between SEC-R (n = 16) and SEC-NR (n = 14) before secukinumab is taken. (C) Representative plot of CXCR3 and CCR6 of CD4+ T cells from HCs (n = 21) and SEC-R (n = 16) and SEC-NR (n = 14). Dot plot represents frequency of CXCR3+ CD4+ T cells in SEC-R and SEC-NR before secukinumab is taken. Dot plot represents frequencies of (D) CCR6+CXCR3– CD4+ T cells, (F) CCR6–CXCR3+ CD4+ T cells, and (H) CCR6+CXCR3+ CD4+ T cells from PBMCs of HCs and patients with axSpA before secukinumab treatment. Paired analysis of frequency in (E) CCR6+CXCR3– CD4+ T cells, (G) CCR6–CXCR3+ CD4+ T cells, and (I) CCR6+CXCR3+ CD4+ T cells in responders and nonresponders. $^{*}P < 0.05$, $^{**}P < 0.01$ significant by Mann-Whitney U test for dot plot analysis and two-tailed Wilcoxon signed rank test for paired analysis. axSpA, axial spondyloarthritis; HC, healthy control; PBMC, peripheral blood mononuclear cell; SEC-NR, secukinumab treatment nonresponders; SEC-R, secukinumab treatment responders; Treg, regulatory T cell.

Transcripts associated with type 1 IFN pathways reflect SEC-NR. Resting mature CD45RO+CD45RA-CD4+ T cells were fluorescent-activated cell sorting (FACS)–sorted to determine transcriptional differences between SEC-R patients (n = 11) and SEC-NR patients (n = 11) before and after treatment (Figure 4A, Supplementary Figure S1A,C, Supplementary Table S3). DEGs are displayed for SEC-R and SEC-NR patients pre-secukinumab (Figure 4B, Supplementary Table S4) and at 24-week post-treatment (Figure 4C, Supplementary Table S5). DEGs before and after secukinumab treatment are also shown for SEC-R patients (Figure 4D, Supplementary Table S6) and SEC-NR patients (Figure 4E, Supplementary Table S7). At the pre-secukinumab timepoint, *CD83* and *TP53INP2* were significantly down-regulated in SEC-R patients compared to SEC-NR patients. Interestingly, *CD83* was a transcript that significantly increased in SEC-R patients post-secukinumab. Genes involved in positive regulation of programmed cell death (*PRF1, CCL5, GZMA*) and granzyme-mediated programmed cell death (*PRF1*, *GZMA*) were elevated in SEC-R compared to SEC-NR patients (Figure 4F, Supplementary Figure S4C, Supplementary Table S8). Secukinumab treatment did not significantly alter the transcriptome of SEC-NR patients; however, some patients demonstrated elevated *IFIT1*, *IFI44L*, *OAS1*, and *RSAD2* transcript expression (Supplementary Figure S4A, Figure 4E). These genes were also found down-regulated when comparing SEC-R patients to SEC-NR patients post-treatment (Figure 4C). GO enrichment determined these genes were associated with type 1 IFN response pathways and response to virus (Figure 4G, Supplementary Table S9). SEC-R patients displayed an altered transcriptome post-treatment (Supplementary Figure S4B, Figure 4D, Supplementary Table S6). Significantly up-regulated transcripts in SEC-R patients post-treatment associated with IL-18 signaling pathway (*CD83, ICAM1, JUN, TNFAIP3, NFKBIA*), IL-24 signaling (*CD83, CDKNIA, ICAM1, JUN, NFKBIA*), and tumor necrosis factor (TNF) signaling (*ICAM1, JUN, TNFAIP3, NFKBIA*) (Figure 4H, Supplementary Table S10). Together, our data indicate the down-regulation of type 1 IFN response genes is important for patients to respond to secukinumab.

Patients switching biologics and respond have a cytotoxic CD4+ T cell signature. Because previous biologic treatment was more common in SEC-NR patients, we assessed whether the frequencies of the different immune subsets studied were different between biologic-naive and biologic-switching patients at the pre-secukinumab treatment timepoint. We found no significant difference in the frequency or MFI of IL17A+ RORγt + CD4 T cells (Supplementary Figure S5A), in the frequency of RORγt+ Treg cells (Supplementary Figure S5B), or in the frequency of the different T helper subsets (Supplementary Figure S5C). We also found that biologic-naive and biologic-switching patients were transcriptionally similar before secukinumab treatment (Supplementary Figure S5D).

We therefore reanalyzed transcriptional differences only in patients switching biologics to investigate why some patients improved after secukinumab administration after inadequate response with previous biologics (Figure 5). SEC-R patients were transcriptionally different compared to SEC-NR patients at the pre-secukinumab timepoint (Figure 5A, Supplementary Table S11). Interestingly, *ICOSLG* and *ALOX5* were transcripts up-regulated in SEC-R biologic-naive patients compared to SEC-R biologic-switching patients at the pre-secukinumab timepoint (Supplementary Figure S5E, Supplementary Tables S12–13). At the post-secukinumab timepoint, cytotoxic transcripts *PRF1* and *GZMA* remain up-regulated. Biologic-switching SEC-R patients transcriptionally differed to SEC-NR patients at the post-secukinumab timepoint (Figure 5B, Supplementary Table S14). Important Treg genes *FOXP3* and *IL2RA* were also down-regulated post-secukinumab in SEC-R patients compared to SEC-NR patients (Figure 5B). Up-regulated genes in SEC-R patients compared to SEC-NR patients post-secukinumab treatment associated with granzyme-mediated programmed cell death signaling (*NKG7, PRF1, GZMA*) and cell killing (*NKG7, PRF1, GZMA, HLA-DPB1, HLA-DRA*) (Figure 5C, Supplementary Table S15). Down-regulated genes associated with response to type 1 IFN (*ISG15, MX1, OAS1, IFIT1, IFIH1*) and IFN alpha/beta signaling (*SOCS3, ISG15, MX1, OAS1, RSAD2, IFIT1*) (Figure 5D, Supplementary Table S16). To confirm if cytotoxic enzymes were increased pre-secukinumab in SEC-R patients who switched biologics, we measured intracellular GZMA and PRF1 in CD45RO +CD45RA- CD4+ T cells using flow cytometry. SEC-R patients demonstrate an increased frequency of GZMA+ CD45RO +CD45RA- CD4+ T cells before secukinumab treatment compared to SEC-NR patients (mean 4.48%, Figure 5E–G). The frequency of PRF1+ CD45RO+CD45RA- CD4+ T cells in SEC-R patients did not significantly differ from SEC-NR patients at pre-secukinumab timepoint (Supplementary Figure S5F and G). There also was no significant difference in the frequency of GZMA+ and PRF1+ CD45RO+CD45RA- CD8 T cells (Supplementary Figure S5H–K).

To investigate the role patient sex has on secukinumab treatment response, transcriptome data was also stratified based on sex (Supplementary Figure S6A and B, Supplementary Tables S17–22). Male patients pre-secukinumab had no significant transcripts discriminating SEC-R from SEC-NR (Supplementary Figure S6C, Supplementary Table S23). After secukinumab, male SEC-R and SEC-NR patients' transcriptome differed (Supplementary Figure S6D, Supplementary Table S24), in which increased transcripts associated with IL-24 signaling (*CD83, CDKN1A, JUN, NFKBIA, NFKB1, TGFB1, ICAM1*), IL-18 signaling (*CD83, JUN, TNFAIP3, NFKBIA, NFKB1, ICAM1*), and Th17 cell differentiation (*JUN, NFKBIA, NFKB1, TGFB1, HLA-DMA, HLA-DRA*) (Supplementary Figure S6E and C, Supplementary Table S25). Transcripts with decreased expression associated with response to type 1 IFN

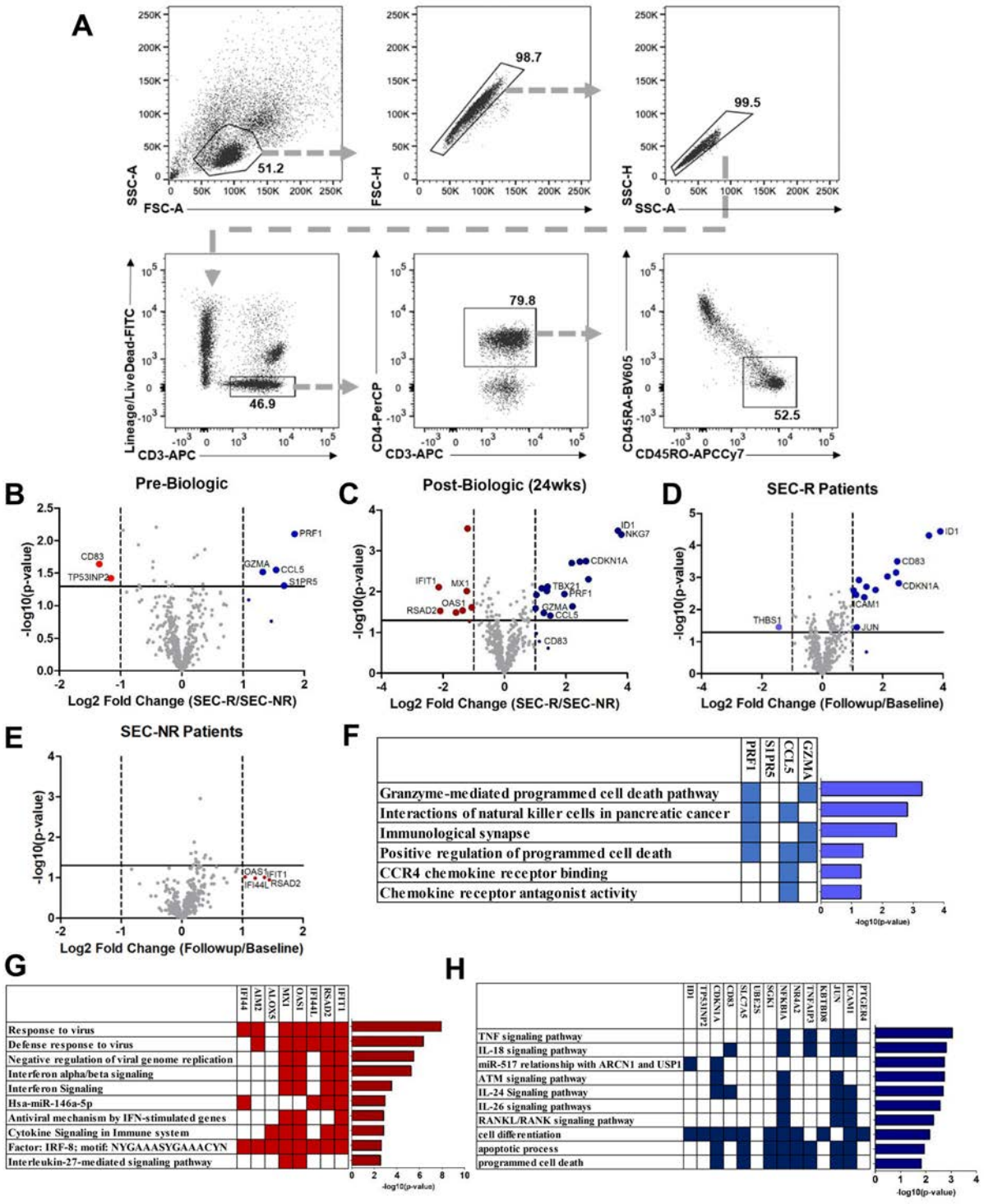

Figure 4. (A) Gating strategy for sorting mature CD45RO+CD45RA- CD4+ T cells from secukinumab responders' and nonresponders' PBMCs pre-secukinumab treatment and week 24 post-treatment. Volcano plot represents differentially regulated genes quantified by NanoString analysis that are unique to secukinumab responder/nonresponder at (B) pre-treatment and (C) 24 weeks post-treatment bleed. Volcano plot also represents differentially regulated genes that are unique to 24-week post-treatment/pre-treatment for (D) SEC-R and (E) SEC-NR. Large-colored dots represent genes with a $\log_2$ fold change above 1 and a $-\log_{10}$(unadjusted *P* value) of 1.3. Small-colored dots represent genes with a $\log_2$ fold change above 1. Pathway analysis is displayed for top 10 relevant pathways for (F) SEC-R/SEC-NR patients at baseline, (G) SEC-NR patients follow-up/pre-treatment, and (H) SEC-R patients follow-up/pre-treatment. APC, allophycocyanin; ATM, ataxia telangiectasia mutated protein; FSC-A, forward scatter area; FSC-H, forward scatter height; FITC, fluorescein isothiocyanate; IFN, interferon; IL, interleukin; miR, microRNA; PBMC, peripheral blood mononuclear cell; SSC-A, side scatter area; SSC-H, side scatter height; SEC-NR, secukinumab treatment nonresponders; SEC-R, secukinumab treatment responders; TNF, tumor necrosis factor.

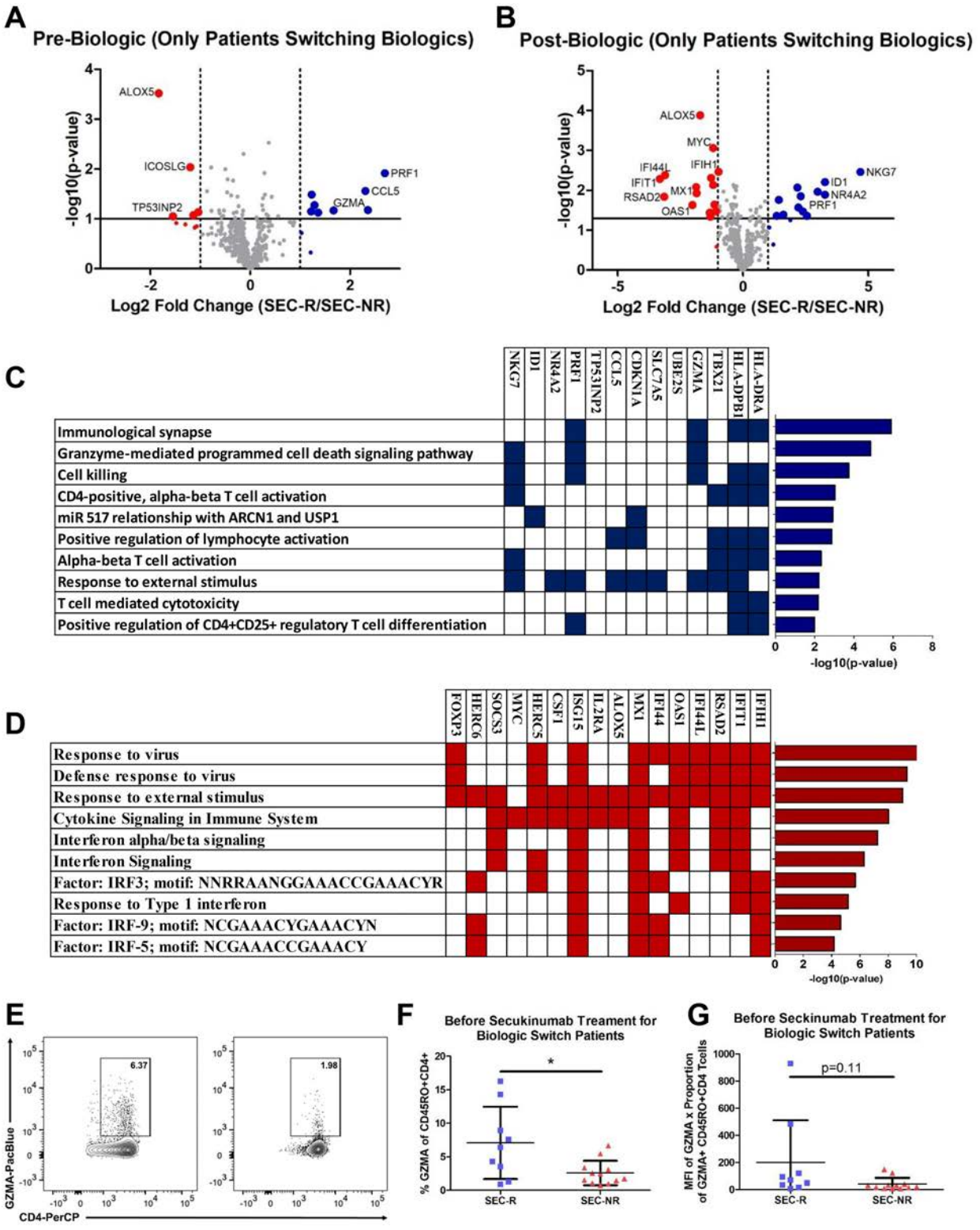

Figure 5. Volcano plot represents differentially regulated genes quantified by NanoString analysis that are unique to patients switching biologics classified as secukinumab responder/nonresponder at (A) pre-secukinumab bleed and (B) 24-week post-secukinumab bleed. Top 10 (C) up-regulated and (D) down-regulated pathways for SEC-R patients post-secukinumab displayed. (E) Representative plot of measured intracellular GZMA in CD4+CD45RO+CD45RA- T cells. Dot plot represents (F) the frequency of GZMA+ relative to CD45RO+ CD4+ T cells and (G) the median fluorescence intensity of GZMA-Pacific Blue multiplied by the proportion of GZMA+ CD45RO+CD4+ T cells in SEC-R (n = 9) and SEC-NR (n = 12) before treatment. *$P < 0.05$ significant by Mann-Whitney U test for dot plot analysis. GZMA, granzyme A; miR, microRNA; SEC-NR, secukinumab treatment nonresponders; SEC-R, secukinumab treatment responders.

(*ISG15*, *OAS1, MX1, OAS2, IFIT1*) and IFN alpha/beta signaling (*IFI35, ISG15, OAS2, MX1, OAS1, IFIT1*) (Supplementary Figure S6F, Supplementary Table S26). SEC-R female patients had a different transcriptome than SEC-NR female patients at the pre-secukinumab timepoint (Supplementary Figure S6G, Supplementary Table S27) that remained post-secukinumab treatment (Supplementary Figure S6H, Supplementary Table S28). Transcripts increased in SEC-R female patients compared to SEC-NR female patients associated with granzyme-mediated programmed cell death (*NKG7, PRF1, GZMA*) (Supplementary Figure S6I, Supplementary Table S29). In all, a cytotoxic CD4+ T cell signature at the pre-secukinumab timepoint can distinguish patients who will respond to secukinumab when switching biologics.

DISCUSSION

Current biologics approved for management of axSpA target IL-17A/F, tumor necrosis factor alpha (TNFα) and JAK1. Although these treatments have improved pain management for majority of patients with axSpA, it is currently unknown why approximately 40% of patients do not respond to available biologic treatments. A better understanding of immune signatures in these nonresponders could provide new therapeutic targets or provide predictors to inadequate treatment response.

Our study of patients with axSpA receiving IL-17A blocking therapy demonstrates that nonresponders have higher CXCR3+ CD4+ T cells pre-secukinumab and an up-regulation of type 1 IFN response genes in mature CD4+ T cells following treatment. This up-regulation of type 1 IFN response genes was found predominantly in male SEC-NR patients and patients who remained unresponsive after switching biologics. These patients also had increased IL-17A+ CD4 T cells pre-secukinumab compared to responders, which did not decrease in frequency after treatment. The CXCR3 receptor binds to CXCL9, IP-10, and IP-9 to induce IFNγ signaling[10] but can also be up-regulated when a cell is stimulated with type 1 IFNs.[35] It has been demonstrated that serum levels of IP-10 and CXCL9 are elevated in axSpA compared to HCs,[36] whereas the decrease of CXCL9 occurs with TNFα inhibitor treatment.[37] This chemokine therefore likely plays a role in both TNFi and secukinumab response through the reduction of type 1 IFN signaling and therefore the reduction of IFNγ production.

Serum levels of IFNα and IFNγ also demonstrate a reduction in TNFi treatment responders but not in nonresponders, highlighting a potential indicator for unresponsiveness to TNFi.[38] IFN response genes were also found to discriminate patients with axSpA at pre-biologic and associate with response to TNFi,[39] similar to what we find in our cohort following treatment with secukinumab. These findings therefore raise important questions about the role of type 1 IFNs and CXCR3 with respect to currently approved biologics for axSpA and its implication in inadequate treatment response. During unfolded protein response, macrophages increase production of type 1 IFNs in response to microbial products such as lipopolysaccharide.[40] Both types of IFNs have been found to activate HLA-B27 at the promoter site, whereas IFNγ was found to increase the expression of proteins related to the unfolded protein response in HLA-B27 expression.[41] In the HLA-B27 transgenic rat model, HLA-B27 misfolding augments the induction of IL-23p19 in bone marrow macrophages, leading to the increase of both T_H1 and T_H17 responses demonstrated through the increase of proinflammatory IL-17, IL-1, TNFα, and IL-6 transcripts.[42] Overproduction of type 1 IFN may therefore increase inflammation by activating this unfolded protein response to a degree unmanageable by available biologics and must be reduced for a patient to respond. Alternatively, the unfolded protein response may activate type 1 IFNs and provide a feedback loop to exacerbate the release of inflammatory cytokines that are not targeted by currently approved biologic therapies for the management of axSpA. Whether the increased CXCR3+ CD4+ T cell frequency found in this study is a response to increased type 1 IFN signaling or causes increased IFNγ signaling remains unanswered at present.

The cytotoxic genes up-regulated in SEC-R patients at the pre-secukinumab timepoint, predominantly in female and biologic-switching patients (*CCL5, PRF1, GZMA, NKG7, FASLG, TBX21*), has recently been a signature identified for a Treg subset that lost suppressive capabilities (exTregs).[43] This is of interest because we identified that an effector Treg subset, RORγt+ Treg, has a reduced frequency in axSpA compared to HCs. We also found transcripts *FOXP3* and *IL2RA* to be down-regulated in SEC-R patients post-secukinumab. It is possible that these Treg cells are losing their suppressive capabilities leading to the conversion of cytotoxic CD4+ T cells and the aberrant control of IL-17A signaling found in patients with axSpA. Because our sorting strategy encompasses all mature CD4+ T cells, future studies should investigate the role of Treg cells in axSpA and validate if this exTreg profile, CD56+CD16+ cytotoxic CD4+ T cells, is indeed expanded in a larger cohort of patients with axSpA. Interestingly, this signature is persistent in SEC-R patients at the post-secukinumab timepoint. Cytotoxic CD4+ T cells have been described in many autoimmune diseases, including axSpA[44] and is a subset that dampens Treg suppressive capabilities and shifts T helper cells toward a T_H17 phenotype *in vitro*.[45] CD4+ T cells in the intestine demonstrate plasticity between a cytotoxic profile and IL-17 production (T_H17 phenotype) dependent on RUNX3 and ThPOK expression. ThPOK expression drives CD4+ T cells to a cytotoxic profile that are still able to secrete IL-17 while RUNX3 at increased expression limits the production of IL-17 while maintaining the cytotoxic phenotype that induces less tissue damage and inflammation.[46] Whether a similar mechanism is occurring in patients with axSpA, particularly those that benefit from biologics that target IL-17, remains unknown.

Clinically, SEC-R patients were more likely to be biologic naive. Another prospective observational study on an Italian

cohort found biologic-naive patients displayed better physical functioning and lower disease activity when taking secukinumab compared to biologic inadequate responder patients.[47] Interestingly, their cohort showed no difference in drug retention between r-axSpA and nr-axSpA. HLA-B27 positivity also did not appear to be a predictive variable for secukinumab withdrawal but other studies have suggested that HLA-B27 positive patients were significantly more likely to respond to secukinumab.[48,49] Our study indicates HLA-B27 positivity is not associated with secukinumab response. HLA-B27 negativity was found to be related to poorer response to TNFi, but its relation to secukinumab response requires further investigation.[50] Our prospective study allowed for the tracking of clinical and immune profiles of patients during secukinumab treatment. A larger prospective cohort would be necessary to confirm if any of the immune differences found in our study could serve as a biomarker to predict secukinumab response. The role that the CXCR3-IFN pathway plays in persistent joint inflammation for SEC-NR patients remains unknown. Ideally, this would be studied using synovial fluid samples, but these are rarely accessible in patients with axSpA. Another limitation was the number of peripheral blood samples on the biologic-naive patients. Additional recruitment would be required for confirmatory analyses pre-secukinumab treatment. Other IL-17A-producing cells and cells that respond to IL-17A require further study and would provide a comprehensive understanding of what is occurring immunologically during secukinumab treatment in SEC-R patients. Although IL-17A–producing CD4+ T cells did not decrease in frequency or in MFI for SEC-R patients, it is possible that secukinumab neutralized IL-17A from circulation before reaching target cells and therefore changing the phenotype of the target cell. Alternatively, other IL-17A-producing cells such as MAIT or ILCs may be the cells targeted during secukinumab treatment.

In conclusion, patients with axSpA have a dysregulated IL-17A response, which is reflected in a reduction of RORγt+ Treg cells frequency. Secukinumab targeting IL-17A can effectively improve symptoms for approximately 60% of patients. Female SEC-R patients and SEC-R patients who switch biologics have a cytotoxic CD4+ T cell profile pre-secukinumab that remains high after secukinumab treatment. Male SEC-NR patients appear to have a greater type 1 IFN gene signature accompanied by increased CXCR3+ CD4+ T cells. This phenotype likely exacerbates the inflammatory response through IFN signaling, which is not modifiable by IL-17A blockade. These findings require validation with a larger cohort to create a predictive algorithm for patient stratification during the prediction of secukinumab response.

ACKNOWLEDGMENTS

The authors would like to thank Edwin Speck at Krembil Flow Cytometry Facility by whom FACS was made possible.

AUTHOR CONTRIBUTIONS

All authors contributed to at least one of the following manuscript preparation roles: conceptualization AND/OR methodology, software, investigation, formal analysis, data curation, visualization, and validation AND drafting or reviewing/editing the final draft. As corresponding author, Dr. Inman confirms that all authors have provided the final approval of the version to be published, and takes responsibility for the affirmations regarding article submission (eg, not under consideration by another journal), the integrity of the data presented, and the statements regarding compliance with institutional review board/Helsinki Declaration requirements.

ROLE OF THE STUDY SPONSOR

Novartis had no role in the study design or in the collection, analysis, or interpretation of the data, the writing of the manuscript, or the decision to submit the manuscript for publication. Publication of this article was not contingent upon approval by Novartis.

REFERENCES

1. Dougados M, Baeten D. Spondyloarthritis. Lancet 2011;377:2127–2137.
2. Wallman JK, Kapetanovic MC, Petersson IF, et al. Comparison of non-radiographic axial spondyloarthritis and ankylosing spondylitis patients–baseline characteristics, treatment adherence, and development of clinical variables during three years of anti-TNF therapy in clinical practice. Arthritis Res Ther 2015;17:378.
3. van der Heijde D, Ramiro S, Landewé R, et al. 2016 update of the ASAS-EULAR management recommendations for axial spondyloarthritis. Ann Rheum Dis 2017;76:978–991.
4. Mease PJ, Heijde DV, Karki C, et al. Characterization of patients with ankylosing spondylitis and nonradiographic axial spondyloarthritis in the US-Based Corrona Registry. Arthritis Care Res (Hoboken) 2018;70:1661–1670.
5. Aparicio M, Guillén-Astete CA, López-Medina C, et al. Evidence for the use of secukinumab in patients with radiographic and non-radiographic axial spondyloarthritis in the last 5 years. Rheumatol Ther 2022;9:73–94.
6. Ward MM, Deodhar A, Gensler LS, et al. 2019 Update of the American College of Rheumatology/Spondylitis Association of America/Spondyloarthritis Research and Treatment Network Recommendations for the Treatment of Ankylosing Spondylitis and Nonradiographic Axial Spondyloarthritis. Arthritis Care Res (Hoboken) 2019;71:1285–1299.
7. Lubberts E. The IL-23-IL-17 axis in inflammatory arthritis. Nat Rev Rheumatol 2015;11:415–429.
8. Drevinge C, Scheffler JM, Koro-Arvidsson C, et al. Intermediate monocytes correlate with CXCR3+ Th17 cells but not with bone characteristics in untreated early rheumatoid arthritis. PLoS One 2021;16:e0249205.
9. Tsiogkas SG, Mavropoulos A, Dardiotis E, et al. A sharp decrease of Th17, CXCR3+-Th17, and Th17.1 in peripheral blood is associated with an early anti-IL-17-mediated clinical remission in psoriasis. Clin Exp Immunol 2022;210:79–89.
10. Kuo PT, Zeng Z, Salim N, et al. The role of CXCR3 and its chemokine ligands in skin disease and cancer. Front Med (Lausanne) 2018;5:1–10.
11. Reboldi A, Coisne C, Baumjohann D, et al. C-C chemokine receptor 6-regulated entry of TH-17 cells into the CNS through the choroid plexus is required for the initiation of EAE. Nat Immunol 2009;10:514–523.
12. Gracey E, Yao Y, Green B, et al. Sexual dimorphism in the Th17 signature of ankylosing spondylitis. Arthritis Rheumatol 2016;68:679–689.

13. Gracey E, Qaiyum Z, Almaghlouth I, et al. IL-7 primes IL-17 in mucosal-associated invariant T (MAIT) cells, which contribute to the Th17-axis in ankylosing spondylitis. Ann Rheum Dis 2016;75:2124–2132.
14. Ciccia F, Guggino G, Rizzo A, et al. Type 3 innate lymphoid cells producing IL-17 and IL-22 are expanded in the gut, in the peripheral blood, synovial fluid and bone marrow of patients with ankylosing spondylitis. Ann Rheum Dis 2015;74:1739–1747.
15. Kenna TJ, Davidson SI, Duan R, et al. Enrichment of circulating interleukin-17-secreting interleukin-23 receptor-positive γ/δ T cells in patients with active ankylosing spondylitis. Arthritis Rheum 2012;64:1420–1429.
16. Chaudhry A, Rudra D, Treuting P, et al. CD4+ regulatory T cells control TH17 responses in a Stat3-dependent manner. Science 2009;326:986–991.
17. Lai N, Zhang S-X, Wang J, et al. The proportion of regulatory t cells in patients with ankylosing spondylitis : a meta-analysis. J Immol Res 2019;2019:1058738.
18. Wang M, Liu C, Bond A, et al. Dysfunction of regulatory T cells in patients with ankylosing spondylitis is associated with a loss of Tim-3. Int. Immunopharmacol. 2018;59:53–60.
19. Guo H, Zheng M, Zhang K, et al. Functional defects in CD4+ CD25high FoxP3+ regulatory cells in ankylosing spondylitis. Sci Rep 2016;6:37559.
20. Tavasolian F, Lively S, Pastrello C, et al. Proteomic and genomic profiling of plasma exosomes from patients with ankylosing spondylitis. Ann Rheum Dis 2023;82:1429–1443.
21. Blair HA. Secukinumab: a review in ankylosing spondylitis. Drugs 2019;79:433–443.
22. Baeten D, Sieper J, Braun J, et al; MEASURE 1 Study Group; MEASURE 2 Study Group. Secukinumab, an interleukin-17a inhibitor, in ankylosing spondylitis. N Engl J Med 2015;373:2534–2548.
23. Huang F, Sun F, Wan WG, et al. Secukinumab provided significant and sustained improvement in the signs and symptoms of ankylosing spondylitis: results from the 52-week, Phase III China-centric study, MEASURE 5. Chin Med J (Engl) 2020;133:2521–2531.
24. Kivitz AJ, Wagner U, Dokoupilova E, et al. Efficacy and safety of secukinumab 150 mg with and without loading regimen in ankylosing spondylitis: 104-week results from MEASURE 4 Study. Rheumatol Ther 2018;5:447–462.
25. Pavelka K, Kivitz A, Dokoupilova E, et al. Efficacy, safety, and tolerability of secukinumab in patients with active ankylosing spondylitis: a randomized, double-blind phase 3 study, MEASURE 3. Arthritis Res Ther 2017;19:285.
26. Kishimoto M, Tanihuchi A, Fujishige A, et al. Efficacy and safety of secukinumab in Japanese patients with active ankylosing spondylitis: 24-week results from an open-label phase 3 study (MEASURE 2-J). Mod Rheumatol 2020;30:132–140.
27. Baraliakos X. Gossec L, Pournara E, et al. Secukinumab in patients with psoriatic arthritis and axial manifestations: results from the double-blind, randomised, phase 3 MAXIMISE trial. Ann Rheum Dis 2021;80:582–590.
28. Deodhar A, Blanco R, Dokoupilová E, et al. Improvement of signs and symptoms of nonradiographic axial spondyloarthritis in patients treated with secukinumab: primary results of a randomized, placebo-controlled phase III study. Arthritis Rheumatol (Hoboken) 2021;73:110–120.
29. Marzo-Ortega H, Perella C, Podubnyy D, et al. P188 Secukinumab provides significant improvement of spinal pain and lowers disease activity in patients with axial spondyloarthritis: 24-week results from a randomised controlled Phase 3b trial. Rheumatology 2021;60:keab247.183.
30. Baraliakos X, Østergaard M, Gensler LS, et al; SURPASS Study Group. Comparison of the Effects of Secukinumab and Adalimumab Biosimilar on Radiographic Progression in Patients with Ankylosing Spondylitis: Design of a Randomized, Phase IIIb Study (SURPASS). Clin Drug Investig 2020;40:269–278.
31. Raychaudhuri SP, Deodhar A. The classification and diagnostic criteria of ankylosing spondylitis. J Autoimmun 2014;48–49:128–133.
32. van der Linden S, Valkenburg HA, Cats A. Evaluation of diagnostic criteria for ankylosing spondylitis. A proposal for modification of the New York criteria. Arthritis Rheum 1984;27:361–368.
33. Aranda-Valera IC, Garrido-Castro JL, Ladehesa-Pineda L, et al. How to calculate the ASDAS based on C-reactive protein without individual questions from the BASDAI: the BASDAI-based ASDAS formula. Rheumatology (Oxford) 2020;59:1545–1549.
34. Ramiro S, Nikiphorou E, Sepriano A, et al. ASAS-EULAR recommendations for the management of axial spondyloarthritis: 2022 update. Ann Rheum Dis 2022;82:19–34.
35. Wenzel J, Tüting T. Identification of type I interferon-associated inflammation in the pathogenesis of cutaneous lupus erythematosus opens up options for novel therapeutic approaches. Exp Dermatol 2007;16:454–463.
36. Wang J, Zhao Q, Wang G, et al. Circulating levels of Th1 and Th2 chemokines in patients with ankylosing spondylitis. Cytokine 2016;81:10–14.
37. Duftner C, Dejaco C, Kullich W, et al. Preferential type 1 chemokine receptors and cytokine production of CD28- T cells in ankylosing spondylitis. Ann Rheum Dis 2006;65:647–653.
38. Hu Y, Lou B, Jiang Z, et al. Predictive values of blood type I and type II interferon production for disease activity and clinical response to TNF-α blocking therapy in patients with ankylosing spondylitis. Tohoku J Exp Med 2023;260:263–271.
39. Harrison SR, Burska AN, Emery P, et al. Interferon-related gene expression in response to TNF inhibitor treatment in ankylosing spondylitis patients: a pilot study. Rheumatology (Oxford) 2021;60:3607–3616.
40. Zeng L, Liu YP, Sha H, et al. XBP-1 couples endoplasmic reticulum stress to augmented IFN-β induction via a cis-acting enhancer in macrophages. J Immunol 2010;185:2324–2330.
41. Feng Y, Ding J, Fan CM, et al. Interferon-γ contributes to HLA-B27-associated unfolded protein response in spondyloarthropathies. J Rheumatol 2012;39:574–582.
42. DeLay ML, Turner MJ, Klenk EI, et al. HLA-B27 misfolding and the unfolded protein response augment interleukin-23 production and are associated with Th17 activation in transgenic rats. Arthritis Rheum 2009;60:2633–2643.
43. Freuchet A, Roy P, Armstrong SS, et al. Identification of human exT(reg) cells as CD16(+)CD56(+) cytotoxic CD4(+) T cells. Nat Immunol 2023;24:1748–1761.
44. Duftner C, Goldberger C, Falkenbach A, et al. Prevalence, clinical relevance and characterization of circulating cytotoxic CD4+CD28- T cells in ankylosing spondylitis. Arthritis Res Ther 2003;5:R292–R300.
45. Hoeks C, Vanheusden M, Peeters LM, et al. Treg-resistant cytotoxic CD4(+) T cells dictate T helper cells in their vicinity: TH17 skewing and modulation of proliferation. Int J Mol Sci 2021;22:5660.
46. Reis BS, Rogoz A, Costa-Pinto FA, et al. Mutual expression of the transcription factors Runx3 and ThPOK regulates intestinal CD4+ T cell immunity. Nat Immunol 2013;14:271–280.
47. Ramonda R, Lorenzin M, Sole Chimenti M, et al. Effectiveness and safety of secukinumab in axial spondyloarthritis: a 24-month

prospective, multicenter real-life study. Ther Adv Musculoskelet Dis 2022;14:X221090310.

48. Braun J, Blanco R, Marzo-Ortega H, et al. Secukinumab in non-radiographic axial spondyloarthritis: subgroup analysis based on key baseline characteristics from a randomized phase III study, PREVENT. Arthritis Res Ther 2021;23:231.
49. Deodhar A, Mease PJ, Poddubnyy D, et al. FRI0271 Impact of HLA-B27 status on clinical outcomes among patients with ankylosing spondylitis treated with secukinumab. Ann Rheum Dis 2020;79:721.
50. Alazmi M, Sari I, Krishnan B, et al. Profiling response to tumor necrosis factor inhibitor treatment in axial spondyloarthritis. Arthritis Care Res (Hoboken) 2018;70:1393–1399.

Arthritis & Rheumatology
Vol. 77, No. 1, January 2025, pp 47–58
DOI 10.1002/art.42967

American College of Rheumatology
Empowering Rheumatology Professionals

Features of Axial Spondyloarthritis in Two Multicenter Cohorts of Patients with Psoriasis, Uveitis, and Colitis Presenting with Undiagnosed Back Pain

Walter P. Maksymowych,[1] Raj Carmona,[2] Ulrich Weber,[3] Sibel Zehra Aydin,[4] James Yeung,[5] Jodie Reis,[6] Ariel Masetto,[7] Sherry Rohekar,[8] Dianne Mosher,[9] Olga Zouzina,[9] Liam Martin,[9] Stephanie O. Keeling,[10] Joel Paschke,[11] Rana Dadashova,[11] Amanda Carapellucci,[11] Stephanie Wichuk,[10] Robert G. Lambert,[10] and Jonathan Chan[12]

Objective. We aimed to assess the following: (1) the frequency of axial spondyloarthritis (axSpA) according to extra-articular presentation and HLA-B27 status, (2) clinical and imaging features that distinguish axSpA from non-axSpA, and (3) the impact of magnetic resonance imaging (MRI) on diagnosis and classification of axSpA.

Methods. The Screening for Axial Spondyloarthritis in Psoriasis, Iritis, and Colitis (SASPIC) study enrolled patients in two multicenter cohorts. Consecutive patients with undiagnosed chronic back pain attending dermatology, ophthalmology, and gastroenterology clinics with psoriasis (PsO), acute anterior uveitis (AAU), or inflammatory bowel disease (IBD) were referred to a local rheumatologist with special expertise in axSpA for a structured diagnostic evaluation. The primary outcome was the proportion of patients diagnosed with axSpA by the final global evaluation.

Results. Frequency of axSpA was 46.7%, 61.6%, and 46.8% in patients in SASPIC-1 (n = 212) and 23.5%, 57.9%, and 23.3% in patients in SASPIC-2 (n = 151) with PsO, AAU, or IBD, respectively. Among those who were B27 positive, axSpA was diagnosed in 70%, 74.5%, and 66.7% of patients in SASPIC-1 and in 71.4%, 87.8%, and 55.6% of patients in SASPIC-2 with PsO, AAU, or IBD, respectively. All musculoskeletal clinical features were nondiscriminatory. MRI was indicative of axSpA in 60% to 80% of patients and MRI in all patients (SASPIC-2) versus on-demand (SASPIC-1) led to 25% fewer diagnoses of axSpA in patients who were HLA-B27 negative with PsO or IBD. Performance of the Assessment of SpondyloArthritis International Society classification criteria was greater with routine MRI (SASPIC-2), though sensitivity was lower than previously reported.

Conclusion. Optimal management of patients presenting with PsO, AAU, IBD, and undiagnosed chronic back pain should include referral to a rheumatologist. Conducting MRI in all patients enhances diagnostic accuracy.

INTRODUCTION

Diagnosis of axial spondyloarthritis (axSpA) is delayed for almost a decade, leading to a substantial burden of illness and a risk of irreversible spinal damage.[1] Patients with back pain who concomitantly have psoriasis (PsO), acute anterior uveitis (AAU), or inflammatory bowel disease (IBD) may initially present to dermatology, ophthalmology, or gastroenterology clinics, respectively,

Screening for Axial Spondyloarthritis in Psoriasis, Iritis, and Colitis (cohort 1) was supported as an investigator-initiated study by grants to CARE Arthritis from AbbVie Canada and Janssen Canada. Screening for Axial Spondyloarthritis in Psoriasis, Iritis, and Colitis (cohort 2) was supported as an investigator-initiated study by a grant to CARE Arthritis from AbbVie Canada. CARE Arthritis is the academic research organization that provided project management for the execution of the study.

[1]Walter P. Maksymowych, MB ChB, FRCPC: University of Alberta and CARE Arthritis, Edmonton, Alberta, Canada; [2]Raj Carmona, MBBS, FRCPC: McMaster University, Hamilton, Ontario, Canada; [3]Ulrich Weber, MD: Practice Buchsbaum, Schaffhausen, Switzerland; [4]Sibel Zehra Aydin, MD: University of Ottawa, the Ottawa Hospital Research Institute, Ottawa, Ontario, Canada; [5]James Yeung, MD, FRCPC: Richmond Health Sciences Centre, Richmond, British Columbia, Canada; [6]Jodie Reis, MD, FRCPC: University of Saskatchewan, Saskatoon, Saskatchewan, Canada; [7]Ariel Masetto, MD, FRCPC: Université de Sherbrooke, Quebec, Canada; [8]Sherry Rohekar, MD, FRCPC: Western University, London, Ontario, Canada; [9]Dianne Mosher, MD, FRCPC, Olga Zouzina, MD, FRCPC, Liam Martin, MD, FRCPC: University of Calgary, Calgary, Alberta, Canada; [10]Stephanie O. Keeling, MD, MSc, FRCPC, Stephanie Wichuk, BSc, Robert G. Lambert, MB BCh, FRCPC: University of Alberta, Edmonton, Alberta, Canada; [11]Joel Paschke, BSc, Rana Dadashova, MD, Amanda Carapellucci, BA: CARE Arthritis, Edmonton, Alberta, Canada; [12]Jonathan Chan, MD, FRCPC: University of British Columbia, Vancouver, British Columbia, Canada.

Additional supplementary information cited in this article can be found online in the Supporting Information section (http://onlinelibrary.wiley.com/doi/10.1002/art.42967).

Author disclosures are available at https://onlinelibrary.wiley.com/doi/10.1002/art.42967.

Address correspondence via email to Walter P. Maksymowych, MB ChB, FRCPC, at walter.maksymowych@ualberta.ca.

Submitted for publication March 12, 2024; accepted in revised form July 23, 2024.

when there may be an opportunity to diagnose the condition much sooner. Earlier diagnosis and treatment might not only alleviate spinal symptoms earlier in the disease course but also help to make more informed decisions aimed at therapeutics that are effective for both axSpA and the comorbid condition. Recent referral recommendations advocate referral to a rheumatologist of patients with chronic back pain, symptom onset at less than 45 years of age, and extra-articular features related to axSpA.[2] However, nonspecific back disorders are common, and access to a rheumatologist is limited in many parts of the world. Moreover, features indicating inflammatory back pain (IBP) are relatively nonspecific, and HLA-B27 appears to be less strongly associated with axSpA in patients with PsO and IBD.[3–5] Previous reports evaluating the prevalence of axSpA, distinguishing clinical features, and associations with HLA-B27 have been largely retrospective case studies of selected populations.[6–14] There are limited prospective studies in which the Assessment of Spondyloarthritis International Society (ASAS) classification criteria[15] have been used to identify patients with axSpA, but magnetic resonance imaging (MRI) evaluation of the sacroiliac joints (SIJs) was only conducted when considered clinically indicated as opposed to being done routinely for all patients.[16,17] However, the performance of the ASAS criteria has not been assessed in these disease subgroups and may be adversely impacted by the lack of association with HLA-B27. Moreover, MRI findings in the SIJs that are indicative of axSpA do not correlate well with clinical features of IBP and may be present even in asymptomatic patients with AAU, PsO, or IBD.[18,19]

We conducted two multicenter studies (Screening for Axial Spondyloarthritis in Psoriasis, Iritis, and Colitis [SASPIC] cohorts 1 and 2) in which consecutive patients with undiagnosed chronic back pain attending dermatology, ophthalmology, and gastroenterology clinics with PsO, AAU, and IBD, respectively, were referred to a local rheumatologist with special expertise in axSpA for a structured clinical evaluation and imaging. Our aims were threefold: (1) to establish the frequency of axSpA according to extra-articular presentation and HLA-B27 status; (2) to identify the clinical, laboratory, and imaging features that distinguish patients with axSpA from those with nonspecific back pain; and (3) to assess the impact of MRI evaluation on diagnosis and classification of axSpA. In SASPIC cohort 1 (SASPIC-1), MRI evaluation was conducted only if deemed necessary by the local rheumatologist and the findings used to inform the diagnosis, as routinely performed in a real-world setting. In SASPIC cohort 2 (SASPIC-2), all patients had MRI of the SIJs, and scans were evaluated first by local radiologists and then by central readers. The reports were provided to local rheumatologists to aid in establishing the final diagnosis.

PATIENTS AND METHODS

Study design and patient eligibility. The SASPIC study enrolled patients in two cohorts, first SASPIC-1 and then SASPIC-2. The two multicenter studies were conducted in Canada at 10 sites in SASPIC-1 and at 8 sites in SASPIC-2, with 7 sites contributing patients to both cohorts. Consecutive adult patients ≤45 years of age diagnosed with PsO, AAU, or IBD attending dermatology, ophthalmology, or gastroenterology practices, respectively, were recruited if they presented with chronic undiagnosed back and/or buttock pain of three months' duration or longer and signed consent forms. Exclusion criteria were absence of chronic back pain, rheumatologist-established diagnosis of axSpA, history of recent spinal trauma, contraindication to or inability to have MRI evaluation, and treatment with any biologic or targeted synthetic disease-modifying antirheumatic drug (DMARD) within 12 weeks before screening.

Eligible patients were assessed by local rheumatologists with special expertise in spondyloarthritis (SpA). This consisted of a history, physical examination, C-reactive protein (CRP), HLA-B27, and an anteroposterior pelvic radiograph done within the last six months. MRI of the SIJs (oblique coronal STIR and T1-weighted spine echo [T1W SE]) and spine (sagittal STIR and T1W SE of thoracolumbar and cervicothoracic halves) was ordered as deemed appropriate by the rheumatologist in SASPIC-1, whereas all patients in SASPIC-2 had MRI evaluation of the SIJs within four weeks of the clinical evaluation of the patient. After clinical assessment, the rheumatologist determined whether the patient's back and/or buttock pain was consistent with IBP (yes/no and numerical rating scale [NRS; 0–10] with anchors: 0 being no probability of IBP and 10 being definite IBP). The rheumatologist also completed an electronic case report form that included all the clinical axSpA variables in the 2009 ASAS classification criteria.[15] The diagnostic conclusion and level of confidence in the diagnosis was assessed at each stage of the diagnostic process by the following question: this patient's clinical presentation indicates a diagnosis of axSpA (yes/no and the degree of confidence on a −10 to +10 NRS, with −10 being definitely not axSpA, 0 being I cannot decide if the patient has axSpA or not, and +10 being definitely has axSpA). In SASPIC-1, this question was addressed after the following evaluations: stage 1 after completion of the history and physical examination; stage 2 after review of the CRP, HLA-B27, and pelvic radiograph; and Stage 3 after review of the MRI and local radiologist report in those patients who had this evaluation (Supplementary Figure 1). In SASPIC-2, the diagnostic global question was addressed after the same three sequential steps as in SASPIC-1 but also included a fourth stage in which the rheumatologist completed the question after receiving central reader evaluations of the pelvic radiograph and MRI scan. All patients provided informed consent. The study was approved by an institutional review board or ethics committee at each study site and conducted according to the Declaration of Helsinki and the International Council for Harmonisation guidelines.

Central reader imaging evaluation. Images were independently evaluated by two experienced readers (rheumatologist

[WPM] and a musculoskeletal radiologist [RGL]) for the presence or absence of radiographic sacroiliitis according to the modified New York (mNY) criteria.[20] Once radiographs had been assessed, readers could evaluate the presence or absence of active inflammatory and structural changes on MRI indicative of axSpA. Discrepancies in these assessments were independently evaluated by an experienced adjudicator (rheumatologist [UW]). Readers also provided a standard narrative report to local rheumatologists for patients recruited to SASPIC-2. Patients and/or public were not involved in any steps of the design, conduct, analysis, and results dissemination of this study.

Outcomes. The primary outcome of the study was the proportion of patients diagnosed with axSpA among the three groups of patients after final global evaluation. Secondary outcomes included proportions of patients with a diagnosis of axSpA stratified by the presence/absence of HLA-B27, clinical and imaging variables that distinguished axSpA from non-axSpA among the three groups, impact of on-demand versus systematic MRI evaluation on diagnosis and classification of axSpA, and the proportion of patients fulfilling the ASAS 2009 classification criteria for axSpA.

Statistical analysis. The proportion of patients diagnosed and classified with axSpA was calculated out of the total number of patients evaluated at each of the rheumatology sites. Descriptive analysis of demographic variables, clinical features of axSpA, and imaging and laboratory variables were tabulated and summarized by means, SD, medians, interquartile ranges, and by numbers and percentages for categorical variables. Statistically significant differences between patients diagnosed with and without axSpA were determined by using Mann–Whitney U test for continuous variables and χ^2 test for categorical variables. Significance tests were conducted at significance level $\alpha = 0.05$. All statistical analyses were conducted in SAS Studio version 9.4 (SAS Institute).

RESULTS

A total of 212 patients (10 sites) were recruited to SASPIC-1 between February 22, 2013, and March 5, 2018, of whom 45 (21.2%) had PsO, 73 (34.4%) had AAU, and 94 (44.3%) had IBD. For SASPIC-2, 151 patients (eight sites, seven sites participated in SASPIC-2) were recruited between May 28, 2018, and September 27, 2022, of whom 51 (33.8%) had PsO, 57 (37.7%) had AAU, and 43 (28.5%) had IBD. The percentage per site diagnosed with axSpA varied from 15.8% to 100% in SASPIC-1 and from 20% to 71.4% in SASPIC-2 (Supplementary Table 1).

Demographic and clinical characteristics. The proportions of patients diagnosed with axSpA were 46.7%, 61.6%, and 46.8% for those with PsO, AAU, and IBD, respectively, in SASPIC-1, whereas the respective proportions were 23.5%, 57.9%, and 23.3% for SASPIC-2 (Tables 1 and 2; Supplementary Tables 2 and 3). A higher proportion of male patients was evident among all groups in patients diagnosed with axSpA, and this was particularly notable in SASPIC-2. In both cohorts, having PsO and IBD preceded back symptoms (76.2% and 68.2%, respectively, of patients with axSpA in SASPIC-1, and 91.7% and 70%, respectively, of patients with axSpA in SASPIC-2), whereas the opposite was evident for having AAU (35.6% and 18.2% of patients with axSpA in SASPIC-1 and -2, respectively). Mean duration of back symptoms before a diagnosis of axSpA was similar in both cohorts and varied from six to nine years among the subgroups. This delay in diagnosis was shortest in patients with IBD in both cohorts and was longest in those with PsO in SASPIC-1 and in those with AAU in SASPIC-2. The majority of patients diagnosed with axSpA in all groups and in both cohorts reported back pain severity >5 on a 0 to 10 scale. The mean percentage of patients receiving nonsteroidal anti-inflammatory drugs (NSAIDs) and reporting back pain severity >5 was 76.6% and ranged from 66.7% to 87.5% of the three subgroups in SASPIC-1 and -2.

More patients with axSpA in the groups with AAU and IBD were deemed to have IBP with a probability >5 on a 0 to 10 scale, and this was particularly evident in SASPIC-1 (Supplementary Data). This was not consistently evident in those with PsO, and the proportion with high probability of IBP was even greater in those diagnosed with non-axSpA in the group with PsO of SASPIC-2. Only a minority of patients reported a complete or very good response to NSAIDs, and this did not differ significantly according to diagnosis. For patients with PsO in both cohorts, a complete or very good NSAID response was even reported more frequently in those diagnosed with non-axSpA.

Physical examination did not reveal any significant differences in frequencies of patients with axSpA on the basis of Spondyloarthritis Research Consortium of Canada entheseal tender points, peripheral arthritis, or hip involvement between those with and without axSpA in any group (Tables 1 and 2). There were numerically more patients with enthesitis on physical examination in patients with non-axSpA than those with axSpA, with the sole exception of the subgroup with PsO in SASPIC-2, in which more patients and a higher mean enthesitis count were evident in those diagnosed with axSpA. Peripheral arthritis was more frequent on physical examination in the group with PsO, especially in SASPIC-2, though without significant differences between those diagnosed with and without axSpA. Dactylitis was more frequent in patients with PsO diagnosed with axSpA in SASPIC-2 but not in SASPIC-1. Overall, musculoskeletal physical examination findings were not helpful in differentiating patients with axSpA versus non-axSpA.

HLA-B27 was present in 33.3%, 84.4%, and 37.2% of patients diagnosed with axSpA who had PsO, AAU, and IBD, respectively, in SASPIC-1, whereas the respective frequencies

Table 1. Demographic and clinical disease characteristics of patients presenting with undiagnosed back pain in an inception cohort of patients with PsO, AAU, and IBD recruited to SASPIC-1 according to final local rheumatologist diagnosis of axSpA versus non-axSpA*

	Patients with PsO			Patients with AAU			Patients with IBD		
Feature	axSpA (n = 21)	Non-axSpA (n = 24)	*P* value	axSpA (n = 45)	Non-axSpA (n = 28)	*P* value	axSpA (n = 44)	Non-axSpA (n = 50)	*P* value
Male, n (%)	15 (71.4)	9 (37.5)	0.04	28 (62.2)	13 (46.4)	0.23	23 (52.3)	20 (40)	0.30
Age, mean (±SD), y	36.3 (±6.2)	36.7 (±5.8)	0.84	33.4 (±5.3)	35.0 (±6.5)	0.24	34.0 (±7.6)	35.9 (±7.0)	0.22
Age at onset of back symptoms, mean (±SD), y	27.2 (±9.2)	30.0 (±8.6)	0.29	25.0 (±7.4)	25.8 (±7.7)	0.67	27.4 (±8.6)	28.9 (±7.3)	0.36
Symptom duration, mean (±SD), y	9.2 (±7.9)	6.7 (±7.5)	0.28	8.4 (±6.1)	9.3 (±7.6)	0.59	6.6 (±5.6)	6.9 (±6.3)	0.80
Age at onset of extra-articular symptoms (PsO, AAU, and IBD), mean (±SD), y	19.7 (±7.4)	20.3 (±7.9)	0.80	28.2 (±6.0)	32.0 (±7.3)	0.021	25.7 (±8.6)	23.4 (±8.8)	0.20
Family history of SpA, n (%)[a]									
AS	1 (4.8)	2 (8.3)	1.00	6 (13.3)	2 (7.1)	0.70	0	1 (2)	1.00
PsO	10 (47.6)	15 (62.5)	0.38	5 (11.1)	8 (28.6)	0.07	9 (20.4)	4 (8)	0.13
IBD	3 (14.3)	2 (8.3)	0.65	5 (11.1)	3 (10.7)	1.00	15 (34.1)	10 (20)	0.16
AAU	0	0	na	9 (20.0)	5 (17.9)	1.00	2 (4.5)	2 (4)	1.00
Back pain characteristics									
Severity of current back pain, (0–10 NRS), mean (±SD)[b]	6.6 (±2.3)	5.2 (±2.4)	0.04	5.1 (±2.9)	4.9 (±2.4)	0.78	6.0 (±2.6)	5.3 (±4.0)	0.11
Current back pain >5 (0–10 NRS), n (%)	15 (71.4)	11 (45.8)	0.13	24 (53.3)	14 (50)	0.81	26 (59.1)	24 (48)	0.31
Inflammatory back pain, n (%)	18 (85.7)	17 (70.8)	0.30	40 (88.9)	17 (60.7)	0.008	40 (90.9)	25 (50)	<0.001
Respond to NSAIDs within 48 hours, n (%)									
Yes	11 (64.7)	15 (75)	0.72	26 (81.3)	15 (78.9)	1.00	17 (58.6)	21 (58.3)	1.00
Mostly complete	0	1 (5)	1.00	3 (9.4)	3 (15.8)	0.66	1 (3.4)	0	0.45
Very good (>50% relief)	4 (23.5)	6 (30)	0.73	11 (34.4)	4 (21.1)	0.36	8 (27.6)	5 (13.9)	0.22
Some benefit (20%–50% relief)	7 (41.2)	6 (30)	0.51	8 (25)	7 (36.8)	0.53	5 (17.2)	12 (33.3)	0.17
Minimal (<20% relief)	0	2 (10)	0.49	4 (12.5)	1 (5.3)	0.64	3 (10.3)	4 (11.1)	1.00
No response	6 (35.3)	5 (25)	0.72	6 (18.8)	4 (21.1)	1.00	12 (41.4)	15 (41.7)	1.00
Treatment, n (%)									
Currently receiving NSAIDs	14 (66.7)	11 (45.8)	0.23	23 (51.1)	5 (17.8)	0.006	9 (20.5)	9 (18)	0.80
Currently receiving csDMARDs[c]	2 (9.5)	2 (8.3)	1.00	0	0 (0)	na	2 (4.5)	5 (10)	0.44
Previously received bioDMARDs[d]	1 (4.8)	3 (12.5)	0.61	0	0 (0)	na	4 (9.1)	9 (18)	0.25
Peripheral and extra-articular symptoms, n (%)									
Heel pain	8 (38.1)	8 (33.3)	0.77	6 (13.3)	5 (17.9)	0.74	7 (15.9)	6 (12)	0.77
History of enthesitis	5 (23.8)	7 (29.2)	0.75	7 (15.6)	5 (17.9)	1.00	3 (6.8)	14 (28)	0.01
History of peripheral arthritis	9 (42.9)	10 (41.7)	1.00	9 (20)	2 (7.1)	0.19	9 (20.5)	8 (16)	0.60
History of extra-articular symptoms									
AAU	2 (9.5)	0	0.21	45 (100)	28 (100)	na	1 (2.3)	0	0.47
Crohn disease colitis	0	0	na	1 (2.2)	0	1.00	25 (56.8)	28 (56)	1.00
Ulcerative colitis	0	0	na	1 (2.2)	0	1.00	19 (43.2)	22 (41)	1.00
PsO	21 (100)	24 (100)	na	0	0	na	3 (6.8)	1 (2)	0.34
Dactylitis	1 (4.8)	0	0.47	1 (2.2)	0	1.00	0	2 (4)	0.50
Physical examination									
Enthesitis, n (%)	6 (28.6)	7 (29.2)	0.23	9 (20)	6 (21.4)	0.26	12 (27.3)	20 (40)	0.28
Number of SPARCC enthesitis points, mean (±SD)	1.2 (±1.7)	0.6 (±1.2)	0.17	0.3 (±1.0)	0.8 (±1.6)	0.22	0.5 (±1.3)	1.0 (±1.6)	0.05
Dactylitis, n (%)	1 (4.8)	2 (8.3)	1.00	2 (4.4)	0	0.52	1 (2.3)	1 (2)	1.00
Hip involvement, n (%)[e]	2 (9.5)	2 (8.3)	1.00	3 (6.7)	1 (3.6)	1.00	7 (15.9)	6 (12)	0.77
PsO, n (%)	21 (100)	24 (100)	na	0	1 (3.6)	0.38	6 (13.6)	1 (2)	0.05
Peripheral arthritis, n (%)	7 (33.3)	6 (25)	1.00	2 (4.4)	0	0.52	3 (6.8)	3 (6)	1.00
Number of swollen joints, mean (±SD)	1.0 (±2.1)	0.9 (±2.0)	0.83	0.6 (±0.9)	0.0 (±0.0)	na	0.05 (±0.2)	0.1 (±0.3)	0.55
BASMI, mean (±SD)	2.7 (±0.8)	2.1 (±0.7)	0.001	2.4 (±1.0)	2.0 (±0.7)	0.05	2.5 (±1.3)	2.2 (±0.8)	0.23
EDASMI, mean (±SD)	2.3 (±1.4)	2.0 (±0.9)	0.34	2.1 (±1.4)	1.8 (±1.0)	0.24	2.0 (±1.5)	1.9 (±0.9)	0.78
Laboratory									
B27 positive, n (%)[f]	7 (33.3)	3 (13.0)	0.16	38 (84.4)	13 (46.4)	0.001	16 (37.2)	8 (16.3)	0.03
CRP abnormal (≥6 mg/L), n (%)	7 (33.3)	7 (29.2)	1.00	16 (35.6)	9 (32.1)	0.81	19 (43.2)	12 (24)	0.05
CRP, mean (±SD)	5.8 (±6.4)	6.7 (±9.6)	0.71	7.1 (±10.7)	3.8 (±3.0)	0.05	11.9 (±20.0)	4.7 (±7.8)	0.03

* AAU, acute anterior uveitis; AS, ankylosing spondylitis; axSpA, axial spondyloarthritis; BASMI, Bath Ankylosing Spondylitis Metrology Index; bioDMARD, biologic disease-modifying antirheumatic drug; CRP, C-reactive protein; csDMARD, conventional synthetic disease-modifying antirheumatic drug; EDASMI, Edmonton Ankylosing Spondylitis Metrology Index; IBD, inflammatory bowel disease; na, not applicable; NRS, numerical rating scale; NSAID, nonsteroidal anti-inflammatory drug; PsO, psoriasis; SASPIC-1, Screening for Axial Spondyloarthritis in Psoriasis, Iritis, and Colitis cohort 1; SpA, spondyloarthritis; SPARCC, Spondyloarthritis Research Consortium of Canada.

[a] AS, PsO, AAU, and IBD are included.

[b] Severity of current back pain is measured as the amount of back and/or hip pain during the last week on a 0 to 10 (most severe) NRS.

[c] csDMARDs include methotrexate and salazopyrin.

[d] bioDMARDs include etanercept, golimumab, adalimumab, infliximab, and certolizumab.

[e] Hip involvement is defined as groin pain and/or restricted range of internal rotation.

[f] One and two patients were missing HLA-B27 data in the cohorts with PsO and IBD, respectively.

Table 2. Demographic and clinical disease characteristics of patients presenting with undiagnosed back pain in an inception cohort of patients with PsO, AAU, and IBD recruited to SASPIC-2 according to final local rheumatologist diagnosis of axSpA versus non-axSpA*

	Patients with PsO			Patients with AAU			Patients with IBD		
Feature	axSpA (n = 12)	Non-axSpA (n = 39)	*P* value	axSpA (n = 33)	Non-axSpA (n = 24)	*P* value	axSpA (n = 10)	Non-axSpA (n = 33)	*P* value
Male, n (%)	8 (67)	18 (46)	0.32	25 (76)	6 (25)	<0.001	6 (60)	12 (36)	0.28
Age, mean (±SD), y	36.3 (±6.5)	35.4 (±7.2)	0.71	34.8 (±6.4)	35.2 (±6.9)	0.84	30.6 (±7.8)	34.0 (±9.0)	0.28
Age at onset of back symptoms, mean (±SD), y	28.7 (±8.1)	28.4 (±7.6)	0.91	25.3 (±8.2)	27.1 (±6.9)	0.40	24.2 (±25.6)	28.1 (±9.9)	0.10
Symptom duration, mean (±SD), y	7.6 (±9.9)	7.0 (±5.8)	0.85	9.5 (±7.3)	8.1 (±7.7)	0.50	6.4 (±38.9)	6.0 (±7.0)	0.86
Age at onset of extra-articular symptoms (PsO, AAU, and IBD), mean (±SD), y	20.5 (±6.8)	20.9 (±9.3)	0.88	32.5 (±7.4)	29.5 (±8.1)	0.16	20.4 (±8.4)	23.4 (±9.6)	0.38
Family history of SpA, n (%)[a]									
AS	1 (8.3)	1 (2.6)	0.42	6 (18.2)	1 (4.2)	0.22	0	4 (12.1)	0.56
PsO	5 (41.7)	21 (53.8)	0.52	5 (15.2)	6 (25.0)	0.50	2 (20.0)	9 (27.3)	1.00
IBD	1 (8.3)	7 (17.9)	0.66	4 (12.1)	2 (8.3)	1.00	4 (12.1)	7 (21.2)	1.00
AAU	3 (25.0)	2 (5.1)	0.08	2 (6.1)	2 (8.3)	1.00	1 (10.0)	0	0.23
Back pain characteristics									
Severity of current back pain, (0–10 NRS), mean (±SD)[b]	6.4 (±2.2)	5.6 (±2.3)	0.30	4.9 (±2.8)	5.0 (±2.3)	0.88	5.8 (±2.8)	5.4 (±1.9)	0.57
Current back pain >5 (0–10 NRS), n (%)	8 (66.7)	22 (56.4)	0.74	16 (48.5)	12 (50.0)	1.00	6 (60)	16 (48.5)	0.72
Inflammatory back pain, n (%)	9 (75)	27 (69.2)	1.00	28 (84.8)	19 (79.2)	0.73	8 (80)	22 (66.7)	0.70
Respond to NSAIDs within 48 hours, n (%)									
Yes	9 (81.8)	21 (75.0)	1.00	20 (87.0)	11 (73.3)	0.40	7 (100)	9 (64.3)	0.12
Mostly complete	1 (9.1)	0 (0)	0.28	4 (17.4)	2 (13.3)	1.00	2 (28.6)	0	0.10
Very good (>50% relief)	1 (9.1)	10 (35.7)	0.13	7 (30.4)	3 (20.0)	0.71	2 (28.6)	4 (28.6)	1.00
Some benefit (20%–50% relief)	3 (27.3)	5 (17.9)	1.00	7 (30.4)	2 (13.3)	0.27	3 (42.9)	4 (28.6)	1.00
Minimal (<20% relief)	4 (36.4)	6 (21.4)	1.00	2 (8.7)	4 (26.7)	0.19	0	1 (7.1)	1.00
No response	2 (18.2)	7 (25.5)	1.00	3 (13.0)	4 (26.7)	0.40	0 (0)	5 (35.7)	0.12
Treatment, n (%)									
Currently receiving NSAIDs	5 (41.7)	20 (51.3)	0.74	18 (54.5)	9 (37.5)	0.28	4 (40)	6 (18.2)	0.21
Currently receiving csDMARDs[c]	0	2 (5.1)	1.00	0	0 (0)	na	0	5 (15.2)	0.32
Previously received bioDMARDs[d]	1 (8.3)	2 (5.1)	0.56	1 (3.0)	0 (0)	1.00	5 (50)	6 (18.2)	0.09
Peripheral and extra-articular symptoms, n (%)									
Heel pain	1 (8.3)	8 (20.5)	0.67	3 (6.1)	6 (25.0)	0.06	0 (0)	5 (15.2)	0.32
History of enthesitis	1 (8.3)	11 (28.2)	0.25	5 (15.2)	3 (12.5)	1.00	1 (10)	4 (12.1)	1.00
History of peripheral arthritis	3 (25)	14 (25.9)	0.73	2 (6.1)	3 (12.5)	0.64	0 (0)	5 (15.2)	0.32
History of extra-articular symptoms									
AAU	0	2 (5.1)	1.00	33 (100)	24 (100)	na	2 (20)	1 (3)	0.13
Crohn disease colitis	0	0	na	1 (3.0)	0	1.00	4 (40.0)	19 (57.6)	0.47
Ulcerative colitis	0	0	na	0	0	na	7 (70)	14 (42.4)	0.16
PsO	12 (100)	39 (100)	na	1 (3)	1 (4.2)	1.00	0	1 (3)	1.00
Dactylitis	0	1 (2.6)	1.00	0	0	na	1 (10)	0	0.23
Physical examination									
Enthesitis, n (%)	5 (41.7)	14 (35.9)	0.74	4 (12.1)	8 (33.3)	0.10	0 (0)	8 (24.2)	0.17
Number of SPARCC enthesitis points, mean (±SD)	1.4 (±2.9)	0.9 (±1.4)	0.22	0.4 (±1.2)	1.0 (±1.5)	0.047	0 (±0)	0.7 (±1.6)	0.02
Dactylitis, n (%)	3 (25)	1 (2.6)	0.04	0	0	na	0	0	na
Hip involvement, n (%)[e]	3 (25)	4 (10.3)	0.33	5 (15.2)	1 (4.2)	0.38	1 (10)	4 (12.1)	1.00
PsO, n (%)	11 (91.7)	34 (87.2)	1.00	0 (0)	1 (4.2)	0.42	1 (10)	1 (3)	0.42
Peripheral arthritis, n (%)	4 (33.3)	6 (15.4)	0.22	1 (3.0)	2 (8.3)	0.57	0	0	na
Number of swollen joints, mean (±SD)	1.1 (±1.7)	0.3 (±0.8)	0.15	0.1 (±0.3)	0.1 (±0.3)	0.79	0 (±0)	0 (±0)	na
BASMI, mean (±SD)	2.4 (±1.0)	2.1 (±0.9)	0.36	2.2 (±1.0)	1.9 (±0.9)	0.35	3.0 (±1.2)	2.1 (±0.9)	0.009
EDASMI, mean (±SD)	2.8 (±1.1)	2.1 (±1.3)	0.08	1.9 (±1.2)	1.9 (±0.9)	0.85	2.7 (±1.4)	2.0 (±1.2)	0.15
Laboratory									
B27 positive, n (%)	5 (41.7)	2 (5.1)	0.005	26 (78.8)	15 (62.5)	0.24	5 (50)	4 (12.1)	0.02
CRP abnormal (≥6 mg/L), n (%)	3 (25.0)	2 (5.1)	0.08	8 (24.2)	1 (4.2)	0.06	7 (70)	5 (15.2)	0.002
CRP, mean (±SD)	7.9 (±11.8)	2.2 (±2.6)	0.13	6.9 (±11.5)	2.1 (±3.3)	0.03	25.7 (±32.0)	4.1 (±8.3)	0.06

* AAU, acute anterior uveitis; AS, ankylosing spondylitis; axSpA, axial spondyloarthritis; BASMI, Bath Ankylosing Spondylitis Metrology Index; bioDMARD, biologic disease-modifying antirheumatic drug; CRP, C-reactive protein; csDMARD, conventional synthetic disease-modifying antirheumatic drug; EDASMI, Edmonton Ankylosing Spondylitis Metrology Index; IBD, inflammatory bowel disease; na, not applicable; NRS, numerical rating scale; NSAID, nonsteroidal anti-inflammatory drug; PsO, psoriasis; SASPIC-2, Screening for Axial Spondyloarthritis in Psoriasis, Iritis, and Colitis cohort 2; SpA, spondyloarthritis; SPARCC, Spondyloarthritis Research Consortium of Canada.

[a] AS, PsO, AAU, and IBD are included.

[b] Severity of current back pain is measured as the amount of back and/or hip pain during the last week on a 0 to 10 (most severe) NRS.

[c] csDMARDs include methotrexate and salazopyrin.

[d] bioDMARDs include etanercept, golimumab, adalimumab, infliximab, and certolizumab.

[e] Hip involvement is defined as groin pain and/or restricted range of internal rotation.

were 41.7%, 78.8%, and 50% in SASPIC-2 (Tables 1 and 2). It was significantly more frequent in patients with axSpA versus non-axSpA among those with AAU (84.4% vs 46.4%) and IBD (37.2% vs 16.3%) in SASPIC-1 and among those with PsO (41.7% vs 5.1%) and IBD (50% vs 12.1%) in SASPIC-2. CRP was mostly higher in patients with axSpA versus non-axSpA, this being more evident in SASPIC-2, although only a minority of patients with axSpA had a level greater than normal. Among patients with IBD, there were 52 (55.3%) with Crohn disease and 42 (44.7%) with ulcerative colitis in SASPIC-1 (Supplementary Table 4) and 23 (53.5%) with Crohn disease and 20 (46.5%) with ulcerative colitis in SASPIC-2 (Supplementary Table 5). There were few differences among these subgroups according to diagnosis of axSpA, except for the level of CRP, which was significantly higher between patients with Crohn disease diagnosed with axSpA versus non-axSpA.

Imaging characteristics. Radiographic sacroiliitis meeting the mNY criteria was recorded by local readers in 42.9%, 57.8%, and 56.8% of patients diagnosed with axSpA who had PsO, AAU, or IBD, respectively, in SASPIC-1 (Table 3). The corresponding percentages in SASPIC-2 were 33.3%, 42.4%, and 60%. Values for patients with non-axSpA were <5% in SASPIC-1 and 7.7%, 16.7%, and 6.1% for patients with PsO, AAU, and IBD, respectively, in SASPIC-2. Radiographic sacroiliitis in patients with axSpA was recorded less frequently by central readers, especially in SASPIC-1 (PsO, AAU, and IBD: 15%, 33.3%, and 25.6% for SASPIC-1 and 41.7%, 36.4%, and 50% for SASPIC-2). Only two patients with non-axSpA were recorded by central readers with radiographic sacroiliitis, both being in the AAU group of SASPIC-1.

MRI of the SIJs was conducted in 132 patients (62.3%) in SASPIC-1 and in all patients of SASPIC-2 (Table 3). MRI

Table 3. Imaging features of patients presenting with undiagnosed back pain in two inception cohorts of patients recruited to SASPIC-1 and -2 according to final local rheumatologist diagnosis of axSpA versus non-axSpA*

	Patients with PsO			Patients with AAU			Patients with IBD		
Imaging variable	axSpA	Non-axSpA	*P* value	axSpA	Non-axSpA	*P* value	axSpA	Non-axSpA	*P* value
SASPIC-1 (n = 212)									
Radiography									
Total	21 (46.7)	24 (53.3)	–	45 (61.6)	28 (38.4)	–	44 (46.8)	50 (53.2)	–
Radiographic sacroiliitis by local readers[a]	9 (42.9)	1 (4.2)	0.003	26 (57.8)	1 (3.6)	<0.001	25 (56.8)	2 (4.1)	<0.001
Radiographic sacroiliitis by central readers[b]	3 (15)	0 (0)	0.086	15 (33.3)	2 (7.1)	0.010	11 (25.6)	0 (0)	<0.001
Unilateral grade 2 sacroiliitis by central readers[c]	1 (5)	2 (8.3)	1.0	9 (20)	1 (3.6)	0.078	6 (14.3)	2 (4.2)	0.139
MRI of SIJs (n = 132)									
Total	14 (43.8)	18 (56.3)	–	29 (63.0)	17 (37.0)	–	23 (42.6)	31 (57.4)	–
MRI of SIJs indicative of axSpA by central readers[d]	6 (42.9)	1 (5.6)	0.027	18 (62.1)	1 (5.9)	<0.001	9 (39.1)	0 (0)	<0.001
MRI positive by ASAS definition by central readers[e]	4 (28.6)	1 (5.6)	0.14	13 (44.8)	0 (0)	<0.001	7 (30.4)	0 (0)	0.001
MRI of the spine (n = 84)									
Total	9 (47.4)	10 (52.6)	–	17 (58.6)	12 (41.4)	–	14 (38.9)	22 (61.1)	–
MRI of the spine indicative of axSpA by central readers[f]	2 (22.2)	1 (10)	0.58	9 (52.9)	0 (0)	0.003	4 (28.6)	0 (0)	0.017
SASPIC-2 (n = 151)									
Total	12 (23.5)	39 (76.5)	–	33 (57.9)	24 (42.1)	–	10 (23.3)	33 (76.7)	–
Radiographic sacroiliitis by local readers[g]	4 (33.3)	3 (7.7)	0.044	14 (42.4)	4 (16.7)	0.039	6 (60)	2 (6.1)	<0.001
Radiographic sacroiliitis by central readers[c,h]	5 (41.7)	0 (0)	<0.001	12 (36.4)	0 (0)	0.001	5 (50)	0 (0)	<0.001
Unilateral grade 2 sacroiliitis by central readers[c]	1 (8.3)	1 (2.6)	1.0	3 (9.4)	1 (4.3)	0.632	1 (10)	1 (3)	1.0
MRI of SIJs indicative of axSpA by central readers[i]	9 (75)	0 (0)	<0.001	21 (63.6)	0 (0)	<0.001	8 (80)	0 (0)	<0.001
MRI positive by ASAS definition by central readers[j]	5 (41.7)	0 (0)	<0.001	17 (51.5)	0 (0)	<0.001	5 (50)	1 (3)	0.001

* Values are n (%) unless indicated otherwise. AAU, acute anterior uveitis; ASAS, Assessment of Spondyloarthritis International Society; axSpA, axial spondyloarthritis; CT, computed tomography; IBD, inflammatory bowel disease; MRI, magnetic resonance imaging; PsO, psoriasis; **SASPIC-1**, Screening for Axial Spondyloarthritis in Psoriasis, Iritis, and Colitis cohort 1; **SASPIC-2**, Screening for Axial Spondyloarthritis in Psoriasis, Iritis, and Colitis cohort 2; SIJ, sacroiliac joint.
[a] Included are four patients who had CT, of whom one had radiographic sacroiliitis.
[b] A total of 17 patients were adjudicated for radiographic sacroiliitis by a third central reader.
[c] Excluded are four and one patients, respectively, for whom neither CT nor x-ray were provided for central review for **SASPIC-1** and **SASPIC-2**, respectively.
[d] Nine patients were adjudicated for MRI indicative of axSpA by a third central reader.
[e] A total of 22 patients were adjudicated for ASAS positive MRI by a third central reader.
[f] Five patients were adjudicated for MRI of the spine indicative of axSpA by a third central reader.
[g] Included are three patients who had CT, of whom two had radiographic sacroiliitis.
[h] Eight patients were adjudicated for radiographic sacroiliitis by a third central reader.
[i] Eight patients were adjudicated for MRI indicative of axSpA by a third central reader.
[j] A total of 12 patients were adjudicated for ASAS positive MRI by a third central reader.

evaluation in SASPIC-1 was conducted mostly in patients who were negative for radiographic sacroiliitis (76.7%). Central readers considered the MRI indicative of axSpA in the SIJs of 42.9%, 62.1%, and 39.1% patients diagnosed with axSpA and PsO, AAU, IBD, respectively, in SASPIC-1. The corresponding percentages in patients in SASPIC-2 diagnosed with axSpA were 75%, 63.6%, and 80%.

MRI of the spine was conducted in 84 patients (39.6%) in SASPIC-1, all of whom also had MRI of the SIJs (Table 3). Spinal MRI was considered indicative of axSpA in 22.1%, 52.9%, and 28.6% of patients diagnosed with axSpA who had PsO, AAU, or IBD, respectively, and in one patient (10%) diagnosed with non-axSpA who had PsO. There were no patients with MRI indicative of axSpA confined to the spine, 11 patients for whom only the SIJs were positive, and 16 for whom both the SIJs and spine were positive. There were few differences in radiographic or MRI findings when patients with axSpA with Crohn disease and ulcerative colitis were compared (Supplementary Table 6).

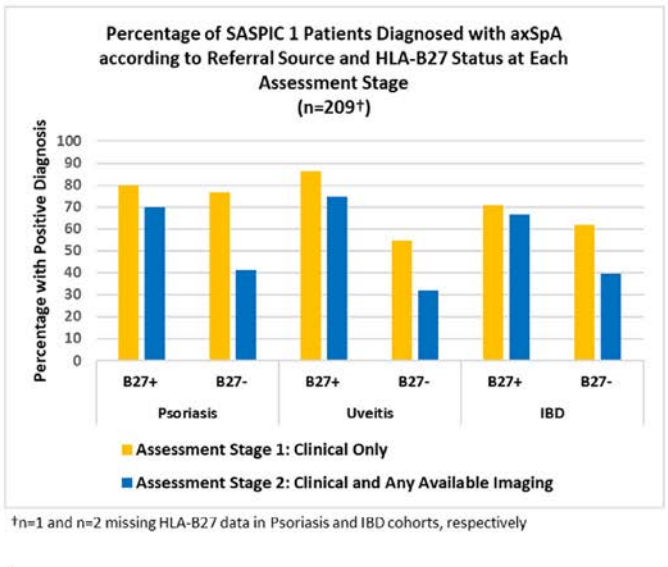

A

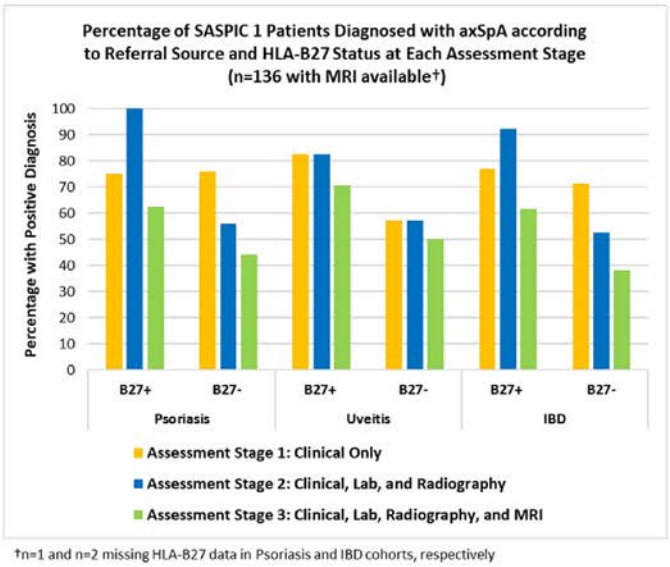

B

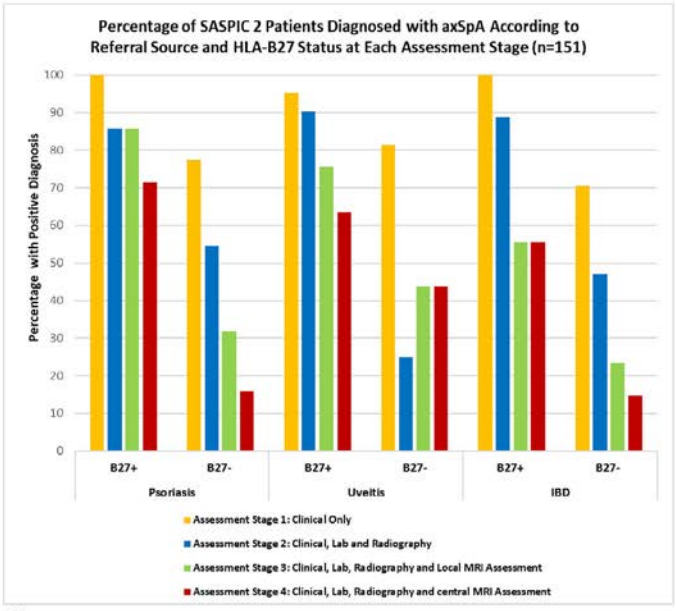

C

Figure 1. Diagnosis of axSpA by local rheumatologists according to referral source and HLA-B27 positivity at sequential stages of evaluation of patients presenting with undiagnosed back pain in two inception cohorts of patients recruited to the Screening for Axial Spondyloarthritis in Psoriasis, Iritis, and Colitis co. (A) SASPIC 1 (all patients). (B) SASPIC 1 patients with MRI scan. (C) SASPIC 2. axSpA, axial spondyloarthritis; IBD, inflammatory bowel disease; MRI, magnetic resonance imaging; SASPIC 1, Screening for Axial Spondyloarthritis in Psoriasis, Iritis, and Colitis cohort 1; SASPIC 2, Screening for Axial Spondyloarthritis in Psoriasis, Iritis, and Colitis cohort 2. Color figure can be viewed in the online issue, which is available at http://onlinelibrary.wiley.com/doi/10.1002/art.42967/abstract.

Diagnosis of axSpA at sequential stages of evaluation. For patients presenting with undiagnosed back pain who were HLA-B27 positive, axSpA was diagnosed in 70%, 74.5%, and 66.7% after final diagnostic evaluation in patients with PsO, AAU, and IBD, respectively, in SASPIC-1, and in 71.4%, 87.8%, and 55.6% after final diagnostic evaluation in patients with PsO, AAU, and IBD, respectively, in SASPIC-2 (Figure 1). The final diagnoses of axSpA in patients who were HLA-B27 negative were made in 41.2%, 31.8%, and 39.7% of patients with PsO, AAU, and IBD, respectively, in SASPIC-1, and in 15.9%, 43.8%, and 14.7% of patients with PsO, AAU, and IBD in SASPIC-2. Diagnostic ascertainment of axSpA decreased with successive stages of evaluation irrespective of referral group or B27 positivity (Figure 1). This was particularly evident in SASPIC-2 after diagnostic evaluation with MRI by local readers and in patients who were HLA-B27 negative. The frequency of patients who were positive for axSpA always decreased after local reader MRI evaluation in SASPIC-1 and -2, and a further relatively minor decrease was evident in some subgroups of SASPIC-2 after central reader evaluation, particularly patients with PsO or IBD who were HLA-B27 negative. The local rheumatologist level of confidence in ruling in and ruling out the diagnosis increased primarily after MRI evaluation (Supplementary Figure 2).

Performance of the 2009 ASAS classification criteria in SASPIC-1 and -2. Sensitivity and specificity of the ASAS classification criteria using the final rheumatologist evaluation as gold standard were 66.4% and 79.4% in SASPIC-1, and performance was somewhat better in analyses of patients with high diagnostic confidence and those with symptom duration of five years or longer (Table 4). Performance was comparable in male and female patients for the overall criteria and for the clinical arm. For the imaging arm, sensitivity in male patients (50%) was almost double that in female patients (27.3%) at the expense of slightly lower specificity (92% in male patients vs 100% in female patients). When only the subset of patients in SASPIC-1 who had MRI were analyzed, the performance of the criteria was similar to the entire SASPIC-1.

Using the final rheumatologist diagnostic evaluation after receipt of central reader imaging data as gold standard, sensitivity and specificity of the ASAS criteria were 85.5% and 82.3%, respectively, in SASPIC-2, and thereby higher than in SASPIC-1. This was mainly due to higher sensitivity, which was also evident for patients diagnosed with axSpA with high confidence (Table 4). The greatest beneficial impact of the availability of central reader imaging data was observed in female patients and the subset with symptom duration of shorter than five years. The

Table 4. Performance of the 2009 ASAS classification criteria in patients presenting with undiagnosed back pain recruited to SASPIC-1 and -2 with the final diagnosis of the rheumatologist as gold standard*

		Overall ASAS criteria[a]		Imaging arm[a]		Clinical arm	
Patient category[a]	Number	Sen	Spec	Sen	Spec	Sens	Spec
SASPIC-1							
All patients	212	66.4	79.4	40.9	97.1	53.6	81.4
Patients diagnosed with confidence >7 for axSpA and <−4 for non-axSpA (−10 to +10 scale)	163	75	82.8	51.3	97.7	59.2	85.1
Patients with symptom duration of five years or longer	132	71.8	83.6	40.8	98.4	57.7	83.6
Patients with symptom duration under five years	80	56.4	73.2	41	95.1	46.2	78
Male	108	69.7	78.6	50	92.9	53	83.3
Female	104	61.4	80	27.3	100	54.5	80
Patients with MRI in SASPIC-1							
All patients	132	65.2	75.8	43.9	98.5	48.5	77.3
Patients diagnosed with confidence >7 for axSpA and <−4 for non-axSpA (−10 to +10 scale)	99	75.6	81	58.5	98.3	53.7	82.8
Patients with symptom duration of five years or longer	78	70.7	78.4	43.9	100	51.2	78.4
Patients with symptom duration under five years	54	56	72.4	44	96.6	44	75.9
Male	66	65	76.9	55	96.2	42.5	80.8
Female	66	65.4	75	26.9	100	57.7	75
SASPIC-2							
All patients	151	85.5	82.3	69.1	99	61.8	83.3
Patients diagnosed with confidence >7 for axSpA yes and <−4 for non-axSpA (−10 to +10 scale)	126	92.3	81.6	87.2	98.9	66.7	82.8
Patients with symptom duration of five years or longer	84	90.3	75.5	67.7	98.1	80.6	77.4
Patients with symptom duration under five years	67	79.2	90.7	70.8	100	37.5	90.7
Male	75	82.1	88.9	69.2	100	59	88.9
Female	76	93.8	78.3	68.8	98.3	68.8	80

* ASAS, Assessment of Spondyloarthritis International Society; axSpA, axial spondyloarthritis; MRI, magnetic resonance imaging; **SASPIC-1**, Screening for Axial Spondyloarthritis in Psoriasis, Iritis, and Colitis cohort 1; **SASPIC-2**, Screening for Axial Spondyloarthritis in Psoriasis, Iritis, and Colitis cohort 2; Sen, Sensitivity; Spec, Specificity.
[a] Central reader assessment of radiographic sacroiliitis and ASAS positive MRI were used for the analysis of the performance of the ASAS classification criteria and clinical and imaging arms.

Table 5. Performance of the 2009 ASAS classification criteria in three groups of patients presenting with undiagnosed back pain recruited to SASPIC-1 and -2 with the final diagnosis of the rheumatologist as gold standard*

	Patients with psoriasis			Patients with AAU			Patients with IBD		
Patient category[a]	Total	Sen	Spec	Total	Sen	Spec	Total	Sens	Spec
All patients of **SASPIC-1**	45	42.9	83.3	73	51.1	92.9	94	36.4	90
Patients with MRI in SASPIC-1	32	42.9	77.8	46	55.2	100	54	30.4	87.1
SASPIC-2	51	75	94.9	57	66.7	100	43	50	90.9

* AAU, acute anterior uveitis; ASAS, Assessment of Spondyloarthritis International Society; IBD, inflammatory bowel disease; MRI, magnetic resonance imaging; SASPIC-1, Screening for Axial Spondyloarthritis in Psoriasis, Iritis, and Colitis cohort 1; SASPIC-2, Screening for Axial Spondyloarthritis in Psoriasis, Iritis, and Colitis cohort 2; Sen, Sensitivity; Spec, Specificity.
[a] Central reader assessment of radiographic sacroiliitis and ASAS positive MRI were used for the analysis of the performance of the 2009 ASAS classification criteria.

performance of the criteria varied somewhat between subgroups according to the referral source, but sensitivity was comparatively low in all three subgroups, especially in patients with IBD, and in both SASPIC-1 and -2 (Table 5). Both sensitivity and specificity were greater in SASPIC-2 for all subgroups, especially for patients with PsO, but sensitivity remained comparatively low.

DISCUSSION

Data from these two cohorts include the first data incorporating systematic evaluation using MRI, have significant implications for clinical practice, and emphasize the crucial role of MRI. First, the frequency of axSpA was about 25% in those presenting with PsO or IBD and 60% in those with AAU. Second, diagnosis was delayed by up to nine years, this being comparable to the delay reported in other cohorts of patients with axSpA[1] despite the known association with extra-articular features and the severity of back pain. These two observations support recent referral recommendations that advocate referral to a rheumatologist of patients with chronic back pain, symptom onset at younger than 45 years of age, and extra-articular features related to axSpA.[2,16] Third, musculoskeletal clinical features largely failed to discriminate between axSpA and non-axSpA, and some SpA features, such as enthesitis, were even more common in non-axSpA. IBP in patients with PsO was more common in those diagnosed without axSpA. Fourth, good response to NSAIDs did not discriminate between axSpA and non-axSpA, consistent with a recent report.[21] Fifth, family history was nondiscriminatory, a history of PsO even being higher in patients with non-axSpA. Sixth, the frequency of HLA-B27 was only 30% to 50% in patients with PsO or IBD diagnosed with axSpA, being closer to 50% of patients in SASPIC-2 with axSpA for whom MRI of the SIJs was conducted in all patients. Conversely, being positive for HLA-B27 was associated with axSpA in 56% to 88% of patients, the highest figure being evident in patients in SASPIC-2 with AAU. Seventh, MRI was almost twice as sensitive as radiography in detecting axSpA lesions in the SIJs, being positive in 60% to 80% of patients. Spine MRI was indicative of axSpA in a substantial minority, though there were no patients with only spinal involvement. MRI was especially helpful in ruling out a diagnosis of axSpA raised on clinical grounds because the frequency of axSpA diagnoses declined after MRI in both cohorts and in all subgroups. Finally, sensitivity and specificity of the ASAS classification criteria was impacted by systematic MRI assessment, and sensitivity was comparatively low in all three subgroups, consistent with the relatively low frequency of HLA-B27 in patients who were axSpA positive with concomitant PsO and IBD.

We designed this unique study to reproduce the sequential process of diagnostic decision-making in clinical practice and to document and weigh the contribution of each assessment at sequential stages in the process. The use of MRI appears to impact diagnostic decision-making for these patients in two primary ways. The majority of patients were considered to have axSpA after clinical evaluation, especially if they were HLA-B27 positive, and rheumatologists primarily ordered MRI evaluation in radiograph negative/equivocal patients in SASPIC-1.[22] In patients in SASPIC-2, a negative MRI also appeared to provide the confidence to rule out axSpA, and this is most likely the reason for the lower frequency of axSpA after MRI evaluation, especially for patients with PsO and IBD. The concept that MRI contributes to an accurate diagnosis is supported by the enhanced performance of the ASAS criteria in SASPIC-2 for which MRI was a required evaluation, especially in patients with PsO and IBD.

Two recent reports have assessed the frequency of axSpA in patients presenting with AAU, included MRI per clinical need, and stated that the ASAS criteria were used to diagnose axSpA. In the Spanish Sentinel study, 50.2% of all patients with AAU and 71.2% of patients who were HLA-B27 positive presented with axSpA.[17] The frequency of axSpA was lower than in the SASPIC cohorts, but only 44% had IBP in the Sentinel study given that all patients presenting with AAU were evaluated. The Irish Dublin Uveitis Evaluation Tool (DUET) study recruited discovery and validation cohorts for the development of a screening strategy for axSpA in patients presenting with AAU.[16] The frequency of axSpA was 38.5% and 37.8% in the discovery and validation cohorts, respectively. MRI was conducted according to clinical need, although it was not stated how many patients had MRI or what

the MRI findings were. The frequency of axSpA was lower in the DUET study versus SASPIC, but only two-thirds of patients in the DUET study had back pain. Neither of these nor additional studies evaluating axSpA in patients with AAU[23,24] systematically compared patients with back pain diagnosed with or without axSpA for discriminatory features, and none conducted systematic MRI.

A recent prospective, multicenter study conducted in Berlin applied a dermatologist-centered screening/referral tool focusing on detecting axial involvement in patients with PsO and undiagnosed chronic back pain.[25] The diagnosis of axial psoriatic arthritis (axPsA) was made in 14 of 100 patients (14%) evaluated by a rheumatologist and 9 patients (64.3%) fulfilled the ASAS classification criteria for axSpA. HLA-B27 was present in 28.6% of those diagnosed with axPsA versus 14.8% in those without axPsA. The somewhat higher frequency of axPsA in SASPIC-2 (23.5%) versus Berlin (14%) cohorts may reflect differences between Canadian and German rheumatologists in the perceived importance of a positive MRI for diagnosis (75% vs 100% in SASPIC vs Berlin cohorts, respectively). These reports are consistent with the prevalence of 5% to 28% for axPsA reported in patients with early-stage disease.[26–34] An important argument in favor of systematic MRI evaluation is that only 25% to 45% of patients with radiographic axPsA have been reported to have IBP, whereas axSpA-based IBP criteria have been shown to lack specificity for axPsA.[35–40]

There are several study limitations. First, there is no international consensus on a case definition of axPsA and little information on the sensitivity and specificity of MRI lesions in the axial skeleton. Consequently, MRI readers relied on their expertise in deciding as to the presence of a positive MRI. Second, MRI evaluation for spinal lesions was only conducted on an as-required basis by local rheumatologists in SASPIC-1, and only MRI of the SIJs was required in SASPIC-2. Third, we confined systematic radiographic assessment to the SIJs, consistent with many prior studies that have relied on defining axPsA according to the mNY criteria. It is possible that radiographic findings in the spine, particularly new bone formation, may have captured additional patients with axial disease. Fourth, our conclusions are based on patients presenting with undiagnosed back pain, and we acknowledge that prospective follow-up is likely to demonstrate higher numbers of patients diagnosed with axial inflammation. Fifth, we confined our analysis to patients presenting with back and/or buttock pain, and we acknowledge that patients who were asymptomatic may not have been detected. However, it is unclear how this might have impacted management. We also excluded patients receiving biologic DMARD for their extra-articular disease because this could obscure clinical and imaging features of axSpA, especially inflammation. However, our findings regarding the value of MRI may be further reinforced because MRI is the most sensitive means to detect structural lesions in the SIJs, which may be the only feature pointing to axSpA in such patients. In view of the importance that rheumatologists attach to MRI, particularly central reader evaluations, there could be concern regarding circular reasoning in formulating the diagnostic conclusion that a patient has axSpA. However, it is noteworthy that rheumatologists diagnosed axSpA despite negative imaging by central readers in 20% to 36% of patients diagnosed with axSpA in SASPIC-2, the cohort in which all patients had central MRI evaluation. Furthermore, the major change in local rheumatologist diagnostic conclusion occurred after local radiologist assessment of the MRI scan and not central reader evaluation. The impact of MRI assessment was mainly observed in patients who were HLA-B27 negative, and this was aimed at ruling out the diagnosis. A major strength of our study is the unique study design based on a stepwise diagnostic process that enabled evaluation of the contribution of clinical and laboratory features to diagnosis independently of information provided by imaging. We observed that the performance of the ASAS classification criteria improved in SASPIC-2, the cohort in which MRI evaluation was conducted in every patient, supporting the argument that systematic assessment of SIJs by MRI in all patients helps to correctly identify the patient with axSpA.

In conclusion, our multicenter stepwise evaluation of two Canadian cohorts of patients presenting with undiagnosed back pain and PsO, IBD, or AAU culminated in a diagnosis of axSpA in 25% of patients with PsO or IBD and 60% in patients with AAU. Diagnostic ascertainment of axSpA decreased with successive stages of evaluation irrespective of referral group or B27 status, especially after diagnostic evaluation with MRI by local readers and in patients who were HLA-B27 negative. Our data support the benefit of recent referral recommendations that advocate referral to a rheumatologist of patients with chronic back pain and extra-articular features related to axSpA. Our data also demonstrate that MRI evaluation of all patients contributes to accuracy of diagnosis and the performance of classification criteria because clinical features are not helpful in identification of axSpA, and frequency of HLA-B27 is lower than in axSpA without these features. Finally, these findings have significant implications for clinical trials that recruit patients on the basis of rheumatologist opinions that do not incorporate evaluation of MRI scans.

AUTHOR CONTRIBUTIONS

All authors contributed to at least one of the following manuscript preparation roles: conceptualization AND/OR methodology, software, investigation, formal analysis, data curation, visualization, and validation AND drafting or reviewing/editing the final draft. As corresponding author, Dr Maksymowych confirms that all authors have provided the final approval of the version to be published, and takes responsibility for the affirmations regarding article submission (eg, not under consideration by another journal), the integrity of the data presented, and the statements regarding compliance with institutional review board/Helsinki Declaration requirements.

ROLE OF THE STUDY SPONSOR

AbbVie Canada and Janssen Canada had no role in the study design or in the collection, analysis, or interpretation of the data, the writing of the manuscript, or the decision to submit the manuscript for

publication. Publication of this article was not contingent upon approval by Abbvie Canada or Janssen Canada.

REFERENCES

1. Hay CA, Packham J, Ryan S, et al. Diagnostic delay in axial spondyloarthritis: a systematic review. Clin Rheumatol 2022;41:1939–1950.
2. Poddubnyy D, van Tubergen A, Landewé R, et al. Development of an ASAS-endorsed recommendation for the early referral of patients with a suspicion of axial spondyloarthritis. Ann Rheum Dis 2015;74:1483–1487.
3. Rahman P, Elder JT. Genetic epidemiology of psoriasis and psoriatic arthritis. Ann Rheum Dis 2005;64(Suppl 2):ii37–ii39.
4. Rudwaleit M, Baeten D. Ankylosing spondylitis and bowel disease. Best Pract Res Clin Rheumatol 2006;20:451–471.
5. Karreman MC, Luime JJ, Hazes JM, et al. The prevalence and incidence of axial and peripheral spondyloarthritis in inflammatory bowel disease: a systematic review and meta-analysis. J Crohns Colitis 2017;11:631–642.
6. Chung YM, Liao HT, Lin KC, et al. Prevalence of spondyloarthritis in 504 Chinese patients with HLA-B27-associated acute anterior uveitis. Scand J Rheumatol 2009;38:84–90.
7. Monnet D, Breban M, Hudry C, et al. Ophthalmic findings and frequency of extraocular manifestations in patients with HLA-B27 uveitis: a study of 175 cases. Ophthalmology 2004;111:802–809.
8. Rosenbaum JT. Characterization of uveitis associated with spondyloarthritis. J Rheumatol 1989;16:792–796.
9. Antony A, Tillett W. Diagnosis, classification and assessment in psoriatic arthritis. Best Pract Res Clin Rheumatol 2021;35:101669.
10. Feld J, Ye JY, Chandran V, et al. Axial disease in psoriatic arthritis: the presence and progression of unilateral grade 2 sacroiliitis in a psoriatic arthritis cohort. Semin Arthritis Rheum 2021;51:464–468.
11. Gladman DD. Axial psoriatic arthritis. Curr Rheumatol Rep 2021; 23:35.
12. Chandran V. Psoriatic spondylitis or ankylosing spondylitis with psoriasis: same or different? Curr Opin Rheumatol 2019;31:329–334.
13. Feld J, Chandran V, Haroon N, et al. Axial disease in psoriatic arthritis and ankylosing spondylitis: a critical comparison. Nat Rev Rheumatol 2018;14:363–371.
14. Feld J, Ye JY, Chandran V, et al. Is axial psoriatic arthritis distinct from ankylosing spondylitis with and without concomitant psoriasis? Rheumatology (Oxford) 2020;59:1340–1346.
15. Rudwaleit M, van der Heijde D, Landewé R, et al. The development of Assessment of SpondyloArthritis international Society classification criteria for axial spondyloarthritis (part II): validation and final selection. Ann Rheum Dis 2009;68:777–783.
16. Haroon M, O'Rourke M, Ramasamy P, et al. A novel evidence-based detection of undiagnosed spondyloarthritis in patients presenting with acute anterior uveitis: the DUET (Dublin Uveitis Evaluation Tool). Ann Rheum Dis 2015;74:1990–1995.
17. Juanola X, Loza Santamaria E, Cordero-Coma M; SENTINEL Working Group. Description and prevalence of spondyloarthritis in patients with anterior uveitis: the SENTINEL Interdisciplinary Collaborative Project. Ophthalmology 2016;123:1632–1636.
18. Oliveira TL, Maksymowych WP, Lambert RG, et al. Sacroiliac joint magnetic resonance imaging in asymptomatic patients with recurrent acute anterior uveitis: a proof-of-concept study. J Rheumatol 2017; 44:1833–1840.
19. Williamson L, Dockerty JL, Dalbeth N, et al. Clinical assessment of sacroiliitis and HLA- B27 are poor predictors of sacroiliitis diagnosed by magnetic resonance imaging in psoriatic arthritis. Rheumatology 2004;43:85–88.
20. van der Linden S, Valkenburg HA, Cats A. Evaluation of diagnostic criteria for ankylosing spondylitis. A proposal for modification of the New York criteria. Arthritis Rheum 1984;27:361–368
21. Baraliakos X, Bergmann E, Tsiami S, et al. A good response to nonsteroidal antiinflammatory drugs does not discriminate patients with longstanding axial spondylo-arthritis from controls with chronic back pain. J Rheumatol 2024;51:250–256.
22. Maksymowych WP, Carmona R, Yeung J, et al. Diagnostic ascertainment of axial spondyloarthritis in patients presenting with undiagnosed back pain: what is the impact of MRI in rheumatological practice? J Rheumatol 2018;45:10.
23. Sykes MP, Hamilton L, Jones C, et al. Prevalence of axial spondyloarthritis in patients with acute anterior uveitis: a cross-sectional study utilising MRI. RMD Open 2018;4:e000553.
24. Bubova K, Hasikova L, Mintalova K, et al. The prevalence of MRI-defined sacroiliitis and classification of spondyloarthritis in patients with acute anterior uveitis: a longitudinal single-centre cohort study. Diagnostics 2022;12:161–172.
25. Proft F, Lüders S, Hunter T, et al. Early identification of axial psoriatic arthritis among patients with psoriasis: a prospective multicentre study. Ann Rheum Dis 2022;81:1534–1540.
26. Baraliakos X, Coates LC, Braun J. The involvement of the spine in psoriatic arthritis. Clin Exp Rheumatol 2015;33:S31–S35.
27. Torre Alonso JC, Rodriguez-Perez A, Arribas-Castrillo JM, et al. Psoriatic arthritis (PA): a clinical, immunological and radiological study of 180 patients. Br J Rheumatol 1991;30:245–250.
28. Yang Q, Qu L, Tian H, et al. Prevalence and characteristics of psoriatic arthritis in Chinese patients with psoriasis. J Eur Acad Dermatol Venereol 2011;25:1409–1414.
29. Moghaddassi M, Shahram F, Chams-Davatchi C, et al. Different aspects of psoriasis: analysis of 150 Iranian patients. Arch Iran Med 2009;12:279–283.
30. Coates LC, Conaghan PC, Emery P, et al. Sensitivity and specificity of the classification of psoriatic arthritis criteria in early psoriatic arthritis. Arthritis Rheum 2012;64:3150–3155.
31. Niccoli L, Nannini C, Cassara E, et al. Frequency of iridocyclitis in patients with early psoriatic arthritis: a prospective, follow up study. Int J Rheum Dis 2012;15:414–418.
32. Nossent JC, Gran JT. Epidemiological and clinical characteristics of psoriatic arthritis in Northern Norway. Scand J Rheumatol 2009;38: 251–255.
33. Chandran V, Tolusso DC, Cook RJ, et al. Risk factors for axial inflammatory arthritis in patients with psoriatic arthritis. J Rheumatol 2010; 37:809–815.
34. Mease PJ, Palmer JB, Liu M, et al. Influence of axial involvement on clinical characteristics of psoriatic arthritis: analysis from the Corrona Psoriatic Arthritis/Spondyloarthritis Registry. J Rheumatol 2018;45: 1389–1396.
35. Yap KS, Ye JY, Li S, et al. Back pain in psoriatic arthritis: defining prevalence, characteristics and performance of inflammatory back pain criteria in psoriatic arthritis. Ann Rheum Dis 2018;77:1573–1577.
36. Haroon M, Gallagher P, FitzGerald O. Inflammatory back pain criteria perform well in subset of patients with active axial psoriatic arthritis but not among patients with established axial disease. Ann Rheum Dis 2019;78:1003–1004.
37. Fernández-Sueiro JL, Willisch A, Pértega-Díaz S, et al. Validity of the Bath Ankylosing Spondylitis Disease Activity Index for the evaluation of disease activity in axial psoriatic arthritis. Arthritis Care Res (Hoboken) 2010;62:78–85.
38. Chandran V, Barrett J, Schentag CT, et al. Axial psoriatic arthritis: update on a longterm prospective study. J Rheumatol 2009;36:2744–2750.

39. Jadon DR, Sengupta R, Nightingale A, et al. Axial disease in psoriatic arthritis study: defining the clinical and radiographic phenotype of psoriatic spondyloarthritis. Ann Rheum Dis 2017;76: 701–707.

40. Maldonado-Ficco H, Sheane BJ, Thavaneswaran A, et al. Magnetic resonance imaging in psoriatic arthritis: a descriptive study of indications, features and effect on treatment change. J Clin Rheumatol 2017;23:243–245.

Arthritis & Rheumatology
Vol. 77, No. 1, January 2025, pp 59–66
DOI 10.1002/art.42964

American College of Rheumatology
Empowering Rheumatology Professionals

BRIEF REPORT

Toll-Like Receptor 8 is Expressed in Monocytes in Contrast to Plasmacytoid Dendritic Cells and Mediates Aberrant Interleukin-10 Responses in Patients With Systemic Sclerosis

Christine Ehlers,[1] Thea Thiele,[2] Hannah Biermann,[3] Stephan Traidl,[4] Luzia Bruns,[2] Annett Ziegler,[5] Matthias Schefzyk,[4] Lea M. Bartsch,[6] Ulrich Kalinke,[5] Torsten Witte,[2] and Theresa Graalmann[7]

Objective. Systemic sclerosis (SSc) is a severe rheumatic disease causing fibrotic tissue rearrangement. Aberrant toll-like receptor (TLR) 8 transcripts in plasmacytoid dendritic cells (pDCs) were recently linked to SSc pathogenesis, which is at least partially mediated by increased type I interferon (IFN-I) responses. Here, we addressed the functional role of TLR8 signaling in different immune cell subsets of patients with SSc.

Methods. Monocytes, conventional dendritic cells (cDCs), and pDCs from the blood and skin of patients with SSc were analyzed for TLR8 protein expression. To assess TLR function, cytokine responses upon TLR7 and TLR8 stimulation were studied. To identify relevant alterations specific for patients with SSc (n = 16), patients with primary Sjögren disease (pSS; n = 10) and healthy controls (HCs; n = 13) were included into the study.

Results. In all individuals, TLR8 was expressed in monocytes and cDCs but not in pDCs. The TLR8 expression levels were overall similar in patients with SSc and pSS and HCs. Additionally, in all study participants, TLR8 stimulation of pDCs did not induce IFN-I expression. In contrast, monocytes from patients with SSc revealed increased interleukin (IL)-10 responses upon TLR8 (patients with SSc vs HCs, $P = 0.0126$) and TLR7/8 stimulation (patients with SSc vs HCs, $P = 0.0170$).

Conclusion. TLR8 protein is not expressed in pDCs of patients with SSc. Accordingly, they do not respond to TLR8 stimulation. In contrast, monocytes of patients with SSc respond to TLR8 stimulation with increased IL-10 responses. Therefore, TLR8 signaling in monocytes participates in SSc pathogenesis by conferring aberrant IL-10 expression.

INTRODUCTION

Systemic sclerosis (SSc) is a complex rheumatic disease within the group of connective tissue diseases (CTDs) that is associated with high morbidity and mortality rates. The disease progression is characterized by inflammation, microvascular injury, and fibrotic tissue rearrangement of skin and internal organs such as the lungs and heart.[1] Although the complete pathomechanism of SSc remains elusive, the contribution of innate immunity to disease progression is postulated. Previous

[1]Christine Ehlers, MSc: Junior Research Group for Translational Immunology, TWINCORE Centre for Experimental and Clinical Infection Research, a joint venture between the Helmholtz Centre for Infection Research and the Hannover Medical School, Hannover, Germany; Biomedical Research in End-Stage and Obstructive Lung Disease Hannover (BREATH), German Center for Lung Research (DZL), Hannover, Germany; [2]Thea Thiele, MD, Luzia Bruns, MD, Torsten Witte, MD: Department for Rheumatology and Immunology, Hannover Medical School, Hannover, Germany; [3]Hannah Biermann, BSc: Junior Research Group for Translational Immunology, TWINCORE Centre for Experimental and Clinical Infection Research, a joint venture between the Helmholtz Centre for Infection Research and the Hannover Medical School, Hannover, Germany; [4]Stephan Traidl, MD, Matthias Schefzyk, MD: Department for Dermatology and Allergy, Hannover Medical School, Hannover, Germany; [5]Annett Ziegler, PhD, Ulrich Kalinke, PhD: Institute for Experimental Infection Research, TWINCORE, Centre for Experimental and Clinical Infection Research, a joint venture between the Helmholtz Centre for Infection Research and the Hannover Medical School, Hannover, Germany; [6]Lea M. Bartsch, MD: Department for Gastroenterology, Hepatology, Infectious Diseases and Endocrinology, Hannover Medical School, Hannover, Germany; [7]Theresa Graalmann, MD, PhD: Junior Research Group for Translational Immunology, TWINCORE, Centre for Experimental and Clinical Infection Research, a joint venture between the Helmholtz Centre for Infection Research and the Hannover Medical School, Hannover, Germany, Biomedical Research in End-Stage and Obstructive Lung Disease Hannover (BREATH), German Center for Lung Research (DZL), Hannover, Germany, and Department for Rheumatology and Immunology, Hannover Medical School, Hannover, Germany.

Additional supplementary information cited in this article can be found online in the Supporting Information section (https://acrjournals.onlinelibrary.wiley.com/doi/10.1002/art.42964).

Author disclosures and graphical abstract are available at https://onlinelibrary.wiley.com/doi/10.1002/art.42964.

Address correspondence via email to Theresa Graalmann, MD, PhD, at theresa.graalmann@twincore.de.

Submitted for publication April 29, 2024; accepted in revised form July 24, 2024.

studies reported a monocytosis in blood, accumulation of plasmacytoid dendritic cells (pDCs) in skin, and an increased type I interferon (IFN-I) signature in patients with SSc.[2–4] More specifically, increased IFN-I signaling and IFN-I–stimulated gene expression were described in blood and affected tissue in patients with SSc.[4,5] Accordingly, a clinical trial was initiated aiming at testing the efficacy of IFN-I receptor blockade with the monoclonal antibody anifrolumab in patients with SSc.

In most infections, pDCs are the main IFN-I–producing cell type in vivo with the ability of systemic IFN-I responses even without self-enhancing positive IFN-I receptor feedback loop.[6] They are equipped with several toll-like receptors (TLRs), such as TLR7, for endosomal single-stranded RNA (ssRNA) detection.[7] In contrast, TLR8, which is recognizing ssRNA as well, is not expressed in human pDCs of healthy individuals.[7–10] TLR8 is rather thought to crucially equip monocytes and conventional dendritic cells (cDCs).[7–10] Interestingly, pDCs isolated from the blood of patients with SSc were recently shown to express aberrant TLR8 transcripts.[3] Thus, IFN-I responses in patients with SSc are postulated to be at least partially derived from pDCs, expressing increased TLR8 levels.[3,4] Furthermore, increased TLR8 expression was observed in skin tissue and isolated myofibroblasts, indicating a pivotal role for TLR8 signaling in patients with SSc.[11] In this study, we aimed to precise the role of TLR8 protein expression and function in blood- and skin-derived immune cell subsets from patients with SSc.

PATIENTS AND METHODS

Patients with SSc and primary Sjögren disease. Blood samples of patients were obtained from inpatients and outpatients of the Department for Rheumatology and Immunology from Hannover Medical School after obtaining informed written consent. The study was approved by the local ethics committee (ethical approval 5582, 9700, 09_566, and 03_3362). Patients with SSc and primary Sjögren's syndrome (pSS) fulfilled EULAR disease classification criteria (detailed patient characteristics in Supplementary Table 1).[16,17]

Skin punch biopsies of patients with SSc (n = 3) were taken in local anesthesia within three months after SSc diagnosis and within six months of symptom onset. Two of three patients never had immunomodulatory therapy; one patient started mycophenolate mofetil (2 g/day) three weeks earlier. Control samples of healthy skin (n = 4) were obtained from anonymous donors from dermatological surgeries.

Flow cytometry. Peripheral blood mononuclear cells (PBMCs) were isolated from heparinized blood using density-gradient centrifugation (Histopaque-1077, Merck). For quantification of cell subsets, 1×10^6 fresh PBMCs were directly stained; for further experiments, the remaining cells were frozen in fetal bovine serum (FBS) superior (Biochrom) containing 10% DMSO and stored at −150°C. Dead cells were identified using the live/dead stain Zombie Aqua or Zombie NIR (BioLegend). Fc receptors were blocked with human polyglobulin and PBMCs were labeled with fluorochrome-conjugated monoclonal antibodies against human CD45 Phycoerythrin (PE)-Cyanine (Cy)5.5 (Thermo Fisher Scientific); CD45 Peridinin-Chlorophyll-protein (PerCP)-Cy5.5 (Invitrogen); CD14 Brilliant Ultra Violett™ (BUV)563, CD19 BUV805, and CD123 RealBlue™ (RB)780 (all BD Biosciences); and human leucocyte antigen-DR (HLA-DR) Allophycocyanine (APC)-Cy7, CD3 Spark near-infrared (NIR CD11b Brilliant Violett™ (BV)570, CD11c BV421, CD303 PE-Cy7, and CD123 PE-Cy5 (all BioLegend).

For intracellular TLR8 protein labeling and cytokine detection after stimulation, 1×10^6 PBMCs were stained with fluorochrome-conjugated monoclonal antibodies as described above. Subsequently, cells were washed, fixed, and permeabilized with Cytofix/Cytoperm (BD Biosciences). Monoclonal anti-human TLR8 fluorescein isothiocyanate (BioLegend) was used to detect intracellular TLR8 expression. Labeling of intracellular cytokines after stimulation was performed using fluorochrome-conjugated monoclonal antibodies against interferon (IFN)-α APC (Miltenyi Biotec) and interleukin (IL)-10 BV421 and IL-6 PerCP-Cy5.5 (both BioLegend). Spectral flow cytometry was performed using the ID7000 spectral analyzer (Sony Biotechnology). Flow cytometry data were analyzed with FlowJo version 10.10.0. Data were visualized as t-Distributed Stochastic Neighbor Embedding (t-SNE) plots after dimensionality reduction based on lineage marker or cytokine expression.

TLR stimulation of human PBMCs. PBMCs were seeded in a concentration of 1×10^6 cells/mL in RPMI 1640 (Capricorn Scientific) containing 1% GlutaMax (Thermo Fisher Scientific), 10% FBS superior (volume/volume [v/v]; Biochrom), and penicillin/streptomycin (Capricorn Scientific) in 24-well plates. PBMCs were stimulated for seven hours with different TLR agonists: TLR7, 5 μg/mL imiquimod (R837); TLR7/8, 5 μg/mL resiquimod (R848); TLR8, 50 ng/mL TL8-506 and 1.5 μg/mL ssRNA 40/LyoVec (ssRNA40; InvivoGen). For Golgi blocking, 2 μL/mL brefeldin A (BD Biosciences) was added after one hour. After harvesting, PBMCs were stained and analyzed as described above.

Skin cell isolation. Skin punch biopsies (diameter 4 mm) were incubated in RPMI 1640 (Capricorn Scientific) containing 1% GlutaMax (Thermo Fisher Scientific), 10% FBS superior (v/v; Biochrom), penicillin/streptomycin (Capricorn Scientific), and 320 U/mL collagenase type IV (Gibco) for 18 hours. A single-cell suspension was obtained by mechanical dissociation of remaining tissue followed by filtration of the complete suspension (100 μm). Skin cells were stained and analyzed by spectral flow cytometry as described above with the additional use of monoclonal antibodies against CD1a VioBlue (Miltenyi Biotec) and CD141 BV711, IL-10 BV785, and CD1c BV605 (all BioLegend).

TLR stimulation of skin cells. For stimulation of skin cells, the TLR8 agonist 250 ng/mL TL8-506 was added during the 18-hour incubation. For Golgi blocking 0.5 µl/mL brefeldin A (BD Biosciences) was added after two hours. After harvesting, skin cells were stained and analyzed as described above.

Statistical analysis. Statistical tests were performed in GraphPad Prism version 10.1.0 (GraphPad Software) as indicated in the figure legends. Differences were considered statistically significant at *P* values less than 0.05.

RESULTS

TLR8 is expressed in monocytes and cDCs but not pDCs of patients with SSc. In this study, we aimed at assessing the functional role of TLR8 expression in patients with SSc. Using spectral flow cytometry, intracellular TLR8 protein expression was measured in different immune cell subsets within PBMCs. Besides patients with SSc, patients with pSS and healthy controls (HCs) were analyzed as controls (detailed patient characteristics in Supplementary Table 1). Based on their surface marker distribution, different immune cell subsets were identified

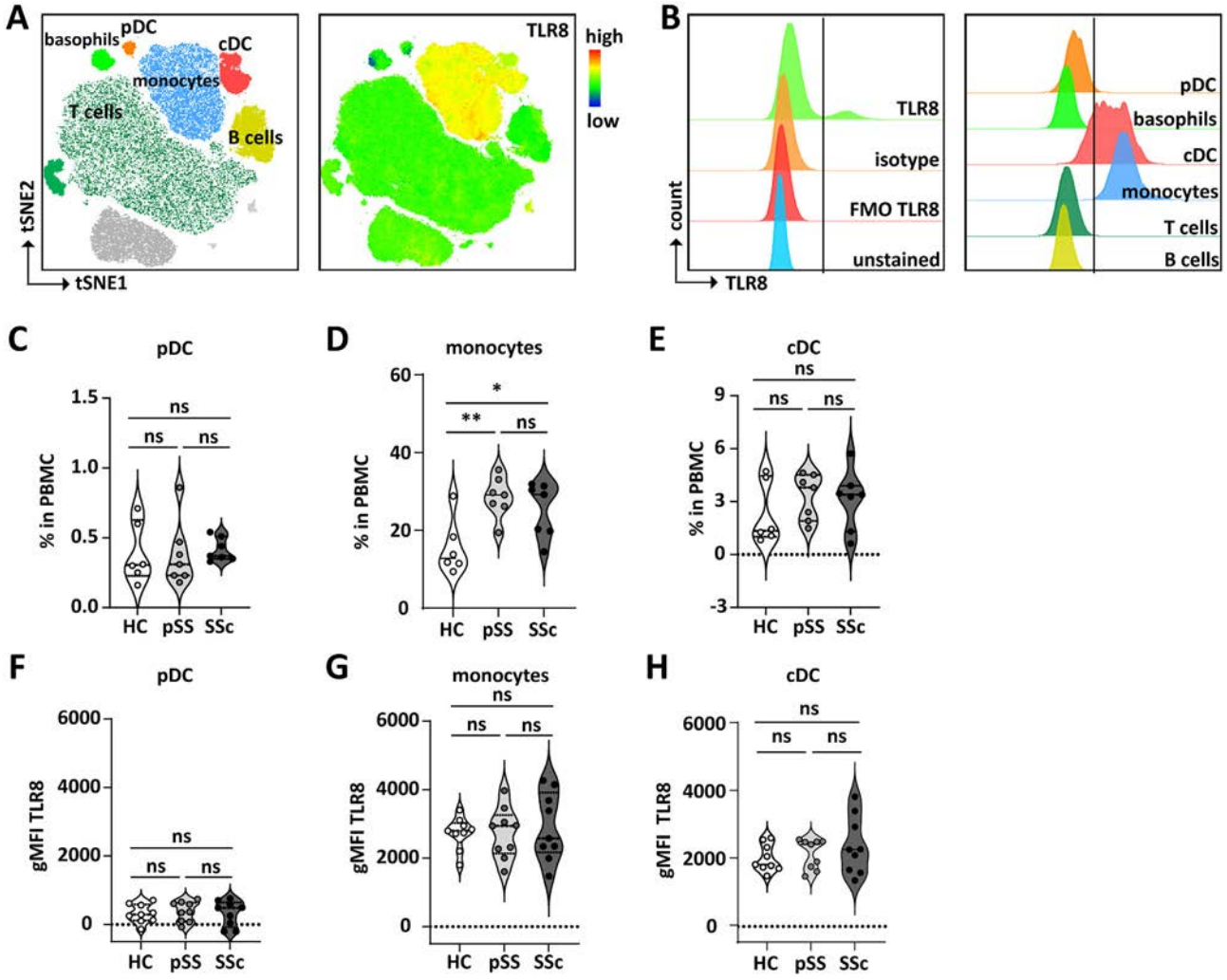

Figure 1. TLR8 is expressed in monocytes and cDCs but not pDCs of patients with systemic sclerosis (SSc). Peripheral blood mononuclear cells (PBMCs) from patients with SSc and primary Sjögren's syndrome (pSS) and healthy controls (HCs) were analyzed for lineage marker and intracellular toll-like receptor (TLR) 8 expression by spectral flow cytometry. (A) The clustering upon t-SNE-based dimensionality reduction of several immune cell subsets is shown for one representative HC (left plot). TLR8 protein expression is detected in monocytes and cDCs, as indicated as a heat map (right plot). (B) Histograms of labeling controls (isotype control, fluorescence minus one [FMO], and unstained control) are shown for one representative HC (left plot). Histograms of TLR8 protein expression in indicated cell subsets are shown for one representative HC (right plot). (C) pDCs, (D) monocytes, and (E) cDCs were quantified within PBMCs (HCs n = 6, patients with pSS n = 7, patients with SSc n = 7). $^{*}P < 0.05$, $^{**}P < 0.01$, by one-way analysis of variance (ANOVA) followed by Tukey's multiple comparisons test. Geometric mean of fluorescence intensity (gMFI) of TLR8 expression is quantified in (F) pDCs, (G) monocytes, and (H) cDCs (HCs n = 9, patients with pSS n = 9, patients with SSc n = 9). cDC, conventional dendritic cell; ns, not significant; pDC, plasmacytoid dendritic cell; t-SNE, t-Distributed Stochastic Neighbor Embedding.

(Figure 1A; Supplementary Figure 1A), and intracellular TLR8 protein expression was assessed (Figure 1B). Similar percentages of pDCs and cDCs were observed within PBMCs of all study groups (Figure 1C and E). Interestingly, monocytes were significantly enriched in patients with SSc (mean SSc 25.36%, patients with SSc vs HCs, $P = 0.0376$) and with pSS (mean 28.57%, patients with pSS vs HCs, $P = 0.0059$) compared with HCs (mean HCs 15.60%; Figure 1D). The intracellular TLR8 protein expression was subsequently assessed within the identified immune cell populations. TLR8 was expressed in monocytes and cDCs but not in pDCs of all tested individuals (Figure 1F–H). In addition, basophils, B cells, and T cells did not mount TLR8 protein expression (Supplementary Figure 1B–D). Besides the distribution, the level of TLR8 expression was also very similar in patients with SSc and pSS and HCs. In summary, TLR8 protein expression was not altered in different immune cell subsets and was particularly absent in the pDCs of patients with SSc.

TLR8 stimulation induces aberrant IL-10 expression in monocytes of patients with SSc. To analyze TLR function, PBMCs were stimulated with agonists for TLR7 (R837), TLR7/8 (R848), or TLR8 (TL8-506), respectively. Intracellular cytokine responses of individual cell subsets were measured by spectral flow cytometry (Supplementary Figure 2A–C). Upon selective TLR7 and simultaneous TLR7 and TLR8 stimulation, but not upon selective TLR8 stimulation, pDCs mounted robust IFN-I responses. IFN-I expression upon TLR7 stimulation was significantly increased in the pDCs of patients with SSc, whereas upon simultaneous TLR7/TLR8 stimulation, IFN-I was significantly expressed in all study groups (Figure 2A and B). Moreover, upon simultaneous TLR7/TLR8 stimulation, low levels of IL-6 were detected in pDCs derived from patients with SSc (Figure 2C). The frequencies of IFN-I– and IL-6–expressing pDCs were overall similar in patients with SSc and pSS and HCs (Figure 2B and C). Also, of note, the human TLR8–specific ssRNA oligonucleotide ssRNA40 did not induce either IFN-vα or IL-6 expression in the pDCs of all study groups (Supplementary Figure 3A and B). In the cDCs, simultaneous TLR7 and TLR8 stimulation induced only minor amounts of IFN-I and IL-6 responses, whereas IL-10 expression was absent (Supplementary Figure 2D–G). Monocytes did not mount IFN-I responses upon either stimulation (Figure 2D). However, upon TLR8 and TLR7/8, but not upon TLR7 stimulation alone, monocytes mounted significant amounts of IL-6 and IL-10 (Figure 2D–F). Both cytokines were expressed in two distinct monocyte subsets (Figure 2D). Most interestingly, although IL-6 levels were similar, IL-10 responses were significantly increased upon TLR8 (SSc vs HC, $P = 0.0126$) or combined TLR7/8 (SSc vs HC, $P = 0.0170$) stimulation in monocytes of patients with SSc but not pSS when compared with HCs (Figure 2E and F). Because the expression level of certain TLRs can be induced during stimulation, the TLR8 protein expression in monocytes and pDCs was monitored upon stimulation (Supplementary Figure 3C and D). Neither in HCs nor in patients with SSc did the expression of TLR8 in pDCs change upon TLR7 or TLR8 stimulation. In contrast, in monocytes, selective TLR8 and simultaneous TLR7/8 but not selective TLR7 stimulation induced a slight increase of TLR8 protein expression.

Thus, in line with the finding that TLR8 protein is absent in the pDCs of patients with SSc, TLR8 stimulation did not induce IFN-I or other cytokine responses in the pDCs of patients with SSc. Most interestingly, TLR8 stimulation induces aberrant IL-10 expression in the monocytes of patients with SSc, indicating an important role for TLR8 in SSc pathogenesis.

Skin-isolated pDCs of patients with SSc do not express TLR8. SSc is a systemic disease; however, the vast majority of inflammation occurs inside affected tissue. Consequently, we further investigated the expression and function of TLR8 in the affected skin of patients with SSc and HC skin samples. Upon flow cytometry of isolated immune cells, tissue-resident pDCs; $CD1a^+$, $CD1c^+$, or $CD141^+$ cDC subsets; and $CD11b^+$HLA-DR^+CD14^+ macrophages could be identified, and their expression level of TLR8 protein was analyzed (Figure 3A and B). Similar frequencies of pDCs, cDC subsets, and macrophages (Figure 3C–G) as well as similar levels or TLR8 protein were detected when comparing skin samples from controls and patients with SSc (Figure 3H–L). Importantly, no TLR8 protein was detectable in pDCs, albeit the cell counts of such rare cell subsets are very small. Upon stimulation of skin punch biopsies with the selective TLR8 agonist TL8-506 macrophages but not pDCs showed a robust IL-6 response. Except for one healthy donor, this effect was similar between patients with SSc and HCs (Figure 3M and N). Only low IL-10 expression was detectable in skin cell subsets before and after TLR8 stimulation (Figure 3O). Interestingly, one patient with SSc showed a high frequency of IL-10–expressing macrophages already before stimulation (Figure 3O). In conclusion, TLR8 protein is absent in blood- and skin-homing pDCs of patients with SSc and therefore does not contribute to aberrant IFN-I expression. In contrast, the role of TLR8-induced aberrant IL-10 expression in monocytes and differentiated tissue macrophages definitely needs further attention.

DISCUSSION

In this study, we aimed at assessing the functional role of TLR8 expression in patients with SSc. TLR8 protein expression was not detected in the blood-derived pDCs of patients with SSc or pSS or HCs or in the skin-derived pDCs of patients with SSc or HCs. Accordingly, TLR8 stimulation did not induce IFN-I or IL-6 responses in the pDCs derived from blood or skin, suggesting that TLR8 does not contribute to aberrant systemic or local IFN-I responses in patients with SSc. This finding is in contrast to the well cited study performed by Ah Kioon et al[3] that reported TLR8 messenger RNA expression in isolated pDCs from

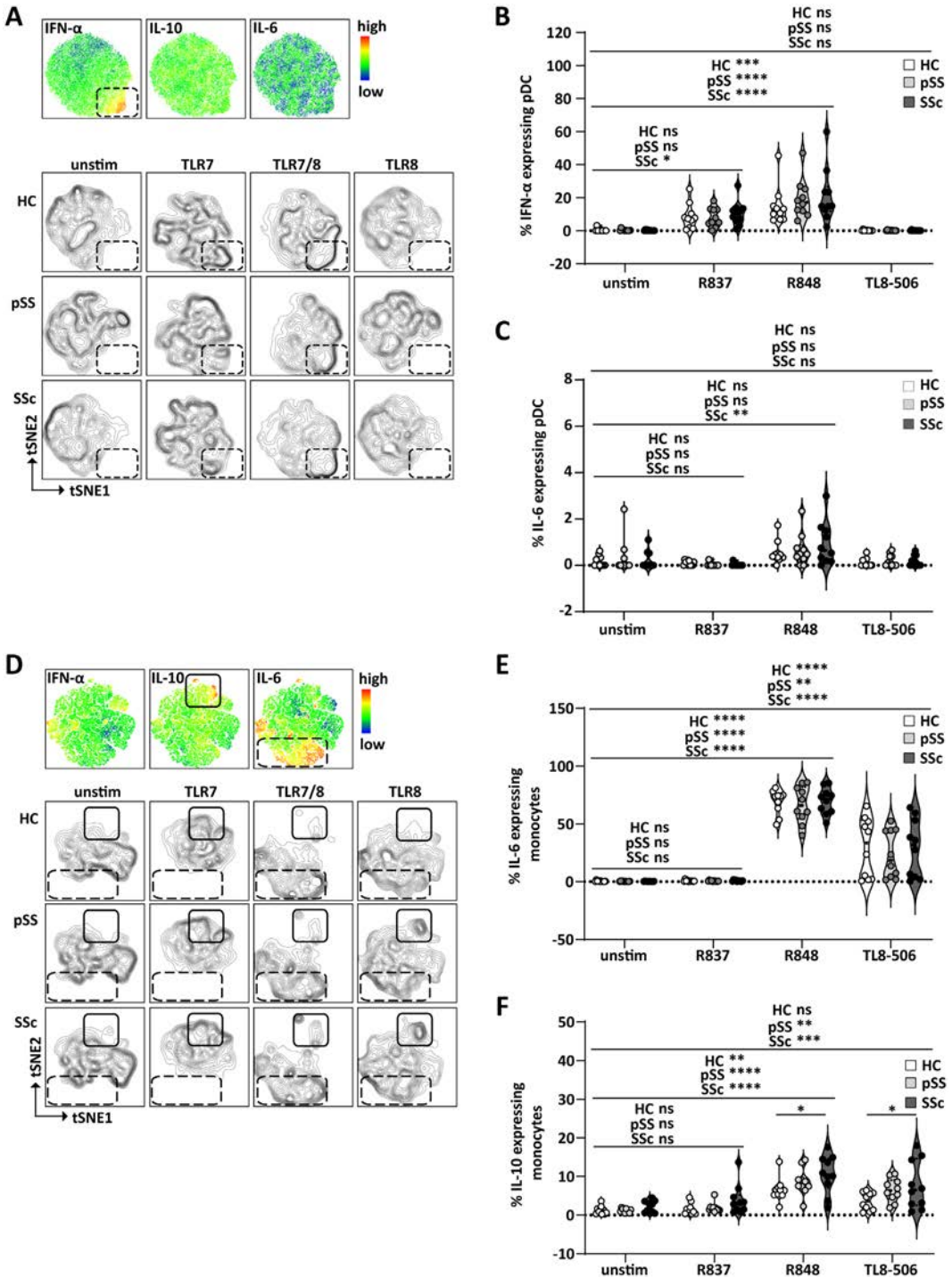

Figure 2. TLR8 stimulation induces aberrant IL-10 expression in monocytes of patients with systemic sclerosis (SSc). Peripheral blood mononuclear cells from patients with SSc and primary Sjögren disease (pSS) and healthy controls (HCs) were stimulated with specific agonists for TLR7 (R837), TLR7/8 (R848), and TLR8 (TL8-506), respectively. Percentages of cell subsets expressing IFN-α, IL-10, and IL-6 were quantified by spectral flow cytometry. (A) Pooled pDCs from all stimulation conditions and all donors are shown as t-SNE plots in dimensionality reduction based on their cytokine expression. Percentages of (B) IFNα- and (C) IL-6–expressing pDCs are depicted. *$P < 0.05$, **$P < 0.01$, ***$P < 0.001$, ****$P < 0.0001$, by two-way analysis of variance followed by Tukey's multiple comparisons test. (D) Pooled monocytes from all stimulation conditions and all donors are shown as t-SNE plots in dimensionality reduction based on their cytokine expression. Percentages of (E) IL-6– and (F) IL-10–expressing monocytes are depicted (HCs n = 10, patients with pSS n = 10, patients with SSc n = 10). *$P < 0.05$, **$P < 0.01$, ***$P < 0.001$, ****$P < 0.0001$, by two-way analysis of variance followed by Tukey's multiple comparisons test. solid line indicates gate for IL-10 expressing cells, dotted line indicates gate for IL-6 expressing cells. IFN, interferon; IL, interleukin; ns, not significant; pDC, plasmacytoid dendritic cell; TLR, toll-like receptor; t-SNE, t-Distributed Stochastic Neighbor Embedding; unstim, unstimulated.

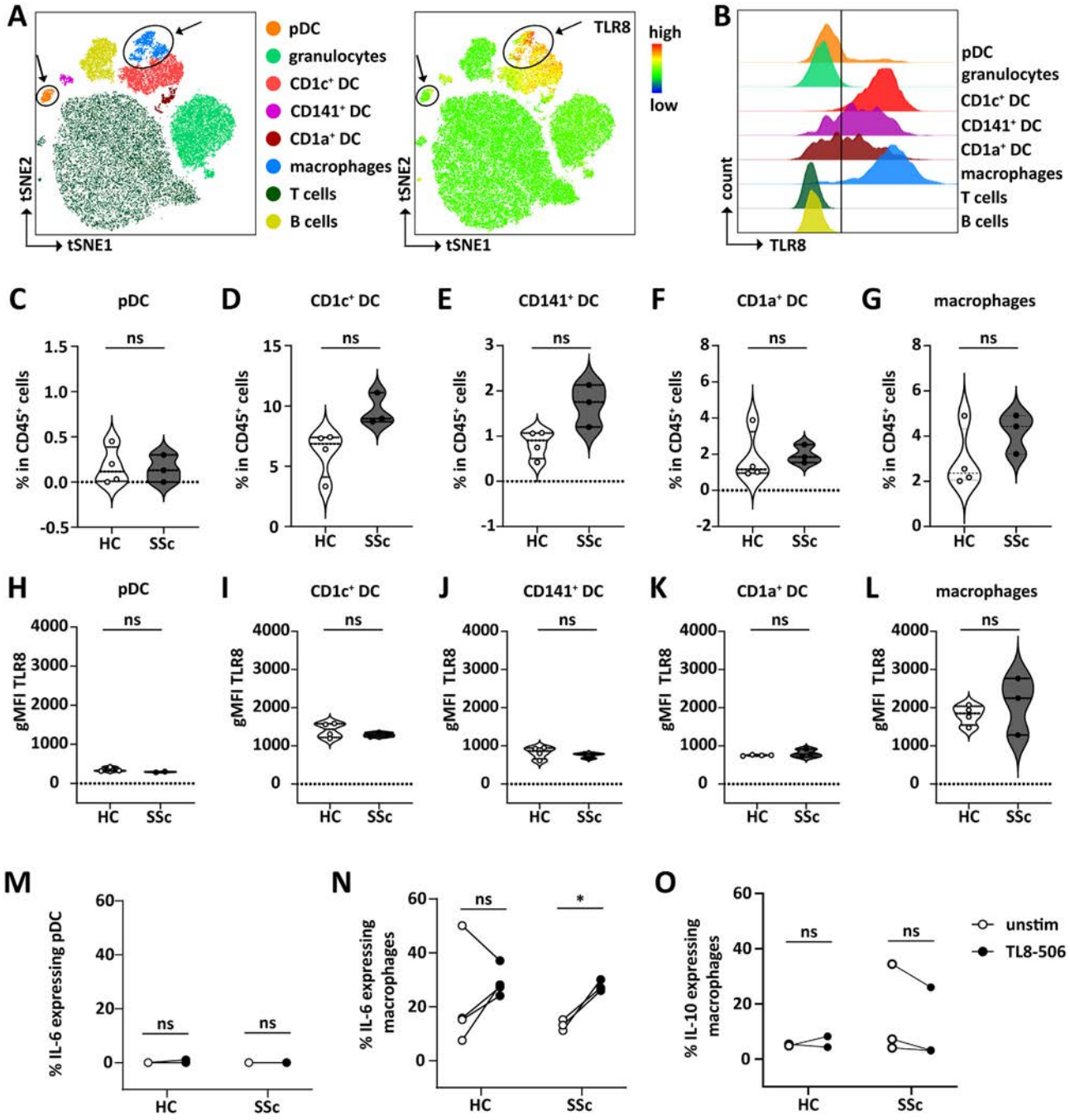

Figure 3. TLR8 is expressed in skin-derived conventional DC subsets and macrophages but not skin-derived pDCs of patients with systemic sclerosis (SSc). Skin punch biopsies from patients with SSc and healthy controls (HCs) were analyzed for lineage marker and intracellular toll-like receptor (TLR) 8 expression by spectral flow cytometry. (A) Clustering upon tSNE-based dimensionality reduction of immune cell subsets is shown for one representative HC (left plot). The orange pDC cluster and the blue cluster of macrophages are marked by a black arrow. TLR8 protein expression is detected in conventional skin DC subsets and macrophages, as indicated as a heat map (right plot). (B) Histograms of TLR8 protein expression in indicated cell subsets are shown for one representative HC. (C) pDCs, (D) $CD1c^+$ DCs, (E) $CD141^+$ DCs, (F) $CD1a^+$ DCs, and (G) $HLA\text{-}DR^+CD14^+CD11b^+$ macrophages were quantified within isolated $CD45^+$ skin cells. Geometric mean of fluorescence intensity (gMFI) of TLR8 expression is quantified in (H) pDCs, (I) $CD1c^+$ DCs, (J) $CD141^+$ DCs, (K) $CD1a^+$ DCs, and (L) macrophages (HCs n = 4, patients with SSc n = 3) Mann–Whitney test was performed. Skin punch biopsies from patients with SSc and HCs were stimulated with specific agonists for TLR8 (TL8-506). Percentages of cell subsets expressing IL-6 were quantified by spectral flow cytometry. Percentages of (M) IL-6–expressing pDCs, (N) IL-6–expressing macrophages, and (O) IL-10–expressing macrophages are depicted (HCs n = 4, patients with SSc n = 3). *$P < 0.05$, by paired *t*-test. DC, dendritic cell; HLA-DR, human leucocyte antigen-DR; IL, interleukin; ns, not significant; pDC, plasmacytoid DC; tSNE, t-Distributed Stochastic Neighbor Embedding; unstim, unstimulated.

patients with SSc.[5] However, it is in accordance with the majority of previous reports, showing that human pDCs of healthy individuals do not express TLR8. In those reports, no significant levels of TLR8 transcripts were detected in blood-derived pDCs obtained via enrichment of BDCA4$^+$ cells from healthy individuals.[7–9,12] The isolation of pDCs in the study performed by Ah Kioon et al[3] was performed via sorting of HLA-DR$^+$, CD123$^+$, and BDCA4$^+$ cells, followed by bulk RNA sequencing. All three individual markers can also be expressed by other cell types. The authors showed that the sorted pDCs express the rather specific marker BDCA2$^+$, which makes cross-contamination with other TLR8-expressing cells unlikely but not impossible. In fact, expression of some TLR8 transcript might even be possible in the pDCs of patients with SSc; however, our study suggests that translated protein is still absent and is also not increased in blood- or skin-derived pDCs upon stimulation. In a second study analyzing RNA expression in whole blood, no TLR8 transcripts were detected in patients with SSc.[7–9,12] All studies mentioned above analyzed TLR8 expression on the RNA level. In contrast, we analyzed TLR8 protein expression via flow cytometry and function upon stimulation, which might explain the different results.

We observed a robust IFN-I response upon TLR7 stimulation in the pDCs of patients with SSc. This is in strong contrast to patients with systemic lupus erythematosus (SLE) in whom pDCs are significantly impaired in responding to TLR7 stimulation.[13] Interestingly, SLE keratinocytes were shown as the nonhematopoietic cell type to express the IFN-I subtype IFN-κ.[13] The phenotype and function of pDCs and, probably as a consequence, the primary source of aberrant IFN-I responses might thus differ significantly among different CTDs and should be further investigated.

In line with previous literature, monocyte frequency in patients with SSc was increased in our cohort, which is indicative for a worse clinical prognosis.[2] Most interestingly, TLR8 stimulation induced significantly increased frequencies of IL-10–expressing monocytes in patients with SSc. This is of utmost interest because IL-10–expressing M2-like macrophages play a key role for fibrotic tissue rearrangement in skin as well as for the establishment of interstitial lung disease (ILD) in patients with SSc.[2,14] Interestingly, treatment with nintedanib, a potent antifibrotic drug for ILD, was recently shown to down-modulate the M2-like phenotype in monocyte-derived macrophages from patients with SSc.[15] Moreover, TLR8 is known to be able to reverse the immunomodulatory properties of regulatory T cells.[8] Within our skin stimulation model, the IL-10 expression in CD11b$^+$ HLA-DR$^+$ CD14$^+$ macrophages was unclear even though the analyzed macrophages expressed significantly increased IL-6 amounts after TLR8 stimulation. Of note, we could not discriminate between M1- and M2-polarized subpopulations in our staining. A reason could be that IL-10 is usually expressed in rather low amounts and our method was not sensitive enough for tissue macrophages. Indeed, aberrant IL-10 responses detected in the monocytes of patients with SSc could also deteriorate upon infiltration and differentiation inside the skin. The importance of TLR8 in subtypes of tissue macrophages as well as tissue-infiltrating monocytes should be addressed in future studies accordingly. In contrast to the previously published hypothesis of aberrant TLR8 expression in pDCs, we suggest that in patients with SSc, TLR8 signaling in monocytes results in increased IL-10 levels and thus contributes to SSc pathogenesis.

ACKNOWLEDGMENTS

We thank all blood and skin donors for their participation in this study. We also thank Christine Jänke and Kira Baumann for technical help and Elisabeth Janecek-Erfurth for the team coordination.

AUTHOR CONTRIBUTIONS

All authors contributed to at least one of the following manuscript preparation roles: conceptualization AND/OR methodology, software, investigation, formal analysis, data curation, visualization, and validation AND drafting or reviewing/editing the final draft. As corresponding author, Dr Theresa Graalmann confirms that all authors have provided the final approval of the version to be published, and takes responsibility for the affirmations regarding article submission (eg, not under consideration by another journal), the integrity of the data presented, and the statements regarding compliance with institutional review board/Helsinki Declaration requirements.

DATA AVAILABILITY STATEMENT

The data that support the findings of this study are available on request from the corresponding author. The data are not publicly available due to privacy or ethical restrictions.

REFERENCES

1. Volkmann ER, Andréasson K, Smith V. Systemic sclerosis. Lancet 2023;401:304–318.
2. Higashi-Kuwata N, Jinnin M, Makino T, et al. Characterization of monocyte/macrophage subsets in the skin and peripheral blood derived from patients with systemic sclerosis. Arthritis Res Ther 2010;12:R128.
3. Ah Kioon MD, Tripodo C, Fernandez D, et al. Plasmacytoid dendritic cells promote systemic sclerosis with a key role for TLR8. Sci Transl Med 2018;10:eaam8458.
4. Skaug B Assassi S. Type I interferon dysregulation in systemic sclerosis. Cytokine 2020;132:154635.
5. Barrat FJ, Crow MK, Ivashkiv LB. Interferon target-gene expression and epigenomic signatures in health and disease. Nat Immunol 2019;20:1574–1583.
6. Barchet W, Cella M, Odermatt B, et al. Virus-induced interferon alpha production by a dendritic cell subset in the absence of feedback signaling in vivo. J Exp Med 2002;195:507–516.
7. Hornung V, Rothenfusser S, Britsch S, et al. Quantitative expression of toll-like receptor 1-10 mRNA in cellular subsets of human peripheral blood mononuclear cells and sensitivity to CpG oligodeoxynucleotides. J Immunol 2002;168:4531–4537.
8. Sun H, Li Y, Zhang P, et al. Targeting toll-like receptor 7/8 for immunotherapy: recent advances and prospectives. Biomark Res 2022;10:89.

9. Guiducci C, Gong M, Cepika AM, et al. RNA recognition by human TLR8 can lead to autoimmune inflammation. J Exp Med 2013;210: 2903–2919.
10. Eigenbrod T, Pelka K, Latz E, et al. TLR8 senses bacterial RNA in human monocytes and plays a nonredundant role for recognition of *Streptococcus pyogenes*. J Immunol 2015;195:1092–1099.
11. Kong X, Jiang S, He Q, et al. TLR8 aggravates skin inflammation and fibrosis by activating skin fibroblasts in systemic sclerosis. Rheumatology (Oxford) 2024;63:1710–1719.
12. Paradowska-Gorycka A, Wajda A, Stypinska B, et al. Variety of endosomal TLRs and interferons (IFN-α, IFN-β, IFN-γ) expression profiles in patients with SLE, SSc and MCTD. Clin Exp Immunol 2021;204:49–63.
13. Psarras A, Alase A, Antanaviciute A, et al. Functionally impaired plasmacytoid dendritic cells and non-haematopoietic sources of type I interferon characterize human autoimmunity. Nat Commun 2020;11: 6149.
14. Soldano S, Trombetta AC, Contini P, et al. Increase in circulating cells coexpressing M1 and M2 macrophage surface markers in patients with systemic sclerosis. Ann Rheum Dis 2018;77:1842–1845.
15. Soldano S, Smith V, Montagna P, et al. Nintedanib downregulates the profibrotic M2 phenotype in cultured monocyte-derived macrophages obtained from systemic sclerosis patients affected by interstitial lung disease. Arthritis Res Ther 2024;26:74.
16. van den Hoogen F, Khanna D, Fransen J, et al. 2013 classification criteria for systemic sclerosis: an American college of rheumatology/European league against rheumatism collaborative initiative. Ann Rheum Dis 2013;72:1747–1755.
17. Shiboski CH, Shiboski SC, Seror R, et al. 2016 American College of Rheumatology/European League Against Rheumatism Classification Criteria for Primary Sjogren's Syndrome: A Consensus and Data-Driven Methodology Involving Three International Patient Cohorts Arthritis Rheumatol. 2017;69:35–45.

Arthritis & Rheumatology
Vol. 77, No. 1, January 2025, pp 67–79
DOI 10.1002/art.42975

American College of Rheumatology
Empowering Rheumatology Professionals

Diversity and Epitope Spreading of Anti–RNA Polymerase III Antibodies in Systemic Sclerosis: A Potential Biomarker for Skin and Lung Involvement

Hirohito Kotani,[1] Kazuki M. Matsuda,[1] Kei Yamaguchi,[2] Chihiro Ono,[2] Emi Kogo,[2] Koji Ogawa,[2] Yuki Kobayashi,[2] Teruyoshi Hisamoto,[1] Ruriko Kawanabe,[1] Ai Kuzumi,[1] Takemichi Fukasawa,[1] Asako Yoshizaki-Ogawa,[1] Naoki Goshima,[3] Shinichi Sato,[1] and Ayumi Yoshizaki[1]

Objective. Epitope spreading (ES), involving autoantibodies, plays a crucial role in the development and persistence of autoimmune reactions in various autoimmune diseases. This study aimed to investigate the relationship between ES of anti–RNA polymerase III (RNAP III) antibodies (ARAs) and the clinical manifestations of systemic sclerosis (SSc).

Methods. We investigated whether intermolecular ES occurs in the subunits of the RNAP III complex and whether intramolecular ES targets the major antigen, RNA polymerase III subunit A (RPC1), in patients with SSc. To achieve this, we synthesized 17 full-length subunit proteins of the RNAP III complex and 5 truncated forms of RPC1 in vitro using a wheat germ cell-free translation system. Subsequently, we prepared antigen-binding plates and measured autoantibodies in the serum of patients with SSc.

Results. Autoantibodies against different RNAP III complex subunits were found in patients who were ARA-positive with SSc. The intermolecular ES indicators significantly correlated with the modified Rodnan skin thickness score (mRSS) and surfactant protein-D, a biomarker of interstitial lung disease. However, the extent of disease on high-resolution computed tomography or pulmonary function tests did not show any significant correlation. Intramolecular ES indicator against RPC1 were significantly correlated with mRSS and renal crisis. Furthermore, longitudinal assessment of ES in RNAP III complex subunits correlated with mRSS and exhibited potential as a disease activity biomarker.

Conclusion. Our findings indicate a correlation between ES levels and the severity of skin sclerosis or the risk of other complications in SSc. This study suggests that measuring ES in SSc serves as a novel biomarker for disease activity.

INTRODUCTION

Autoimmune diseases are caused by dysregulation of the immune system, leading to the immune system attacking the body's own tissues and organs. In numerous autoimmune conditions, patients' sera exhibit disease-specific autoantibodies directed against self-antigens.[1] Notably, systemic autoimmune diseases, such as systemic sclerosis (SSc) and systemic lupus erythematosus (SLE), are characterized by the presence of autoantibodies recognizing nuclear antigens. Consequently, antinuclear antibody testing (ANA) stands as the gold-standard screening method for systemic autoimmune diseases.[2] The clinical significance of disease-specific autoantibodies is that they play a pivotal role in diagnosis, prognostication of complications, and prediction of outcomes. Despite their clinical relevance, these autoantibodies are generally considered nonpathogenic because of their inability to traverse the cell membrane and access the nucleus in vivo. The persistent challenge lies in reconciling this clinical association with the purported lack of pathogenicity, hindering a comprehensive understanding of the pathogenesis of systemic autoimmune

[1]Hirohito Kotani, MD, PhD, Kazuki M. Matsuda, MD, PhD, Teruyoshi Hisamoto, MD, PhD, Ruriko Kawanabe, MD, PhD, Ai Kuzumi, MD, PhD, Takemichi Fukasawa, MD, PhD, Asako Yoshizaki-Ogawa, MD, PhD, Shinichi Sato, MD, PhD, Ayumi Yoshizaki MD, PhD: University of Tokyo, Bunkyo-ku, Japan; [2]Kei Yamaguchi, PhD, Chihiro Ono, MS, Emi Kogo,••, Koji Ogawa, MS, Yuki Kobayashi, PhD: ProteoBridge Corporation, Koto-ku, Japan; [3]Naoki Goshima, PhD: ProteoBridge Corporation and the University of Musashino, Koto-ku, Japan.

Additional supplementary information cited in this article can be found online in the Supporting Information section (https://acrjournals.onlinelibrary.wiley.com/doi/10.1002/art.42975).

Author disclosures and graphical abstract are available at https://onlinelibrary.wiley.com/doi/10.1002/art.42975.

Address correspondence via email to Ayumi Yoshizaki, MD, PhD at ayuyoshi@me.com.

Submitted for publication March 25, 2024; accepted in revised form August 19, 2024.

diseases. In contrast, organ-specific autoimmune diseases manifest autoantibodies against membrane proteins, exemplified by anti–aquaporin-4 antibodies in neuromyelitis optica and anti–desmoglein 1 and 3 antibodies in pemphigus, which possess pathogenic properties and serve as biomarkers for disease activity.[3–5]

Epitope spreading (ES) delineates the process of antibody diversification from an initial dominant epitope to a secondary epitope over time. ES can exhibit within a single antigen (intramolecular) or across different antigens (intermolecular), contributing to the perpetuation and exacerbation of autoimmune responses in autoimmune diseases.[6] The mechanism of ES in autoimmune diseases is classified into independent and dependent processes.[6,7] The independent process is triggered by increased autoantigen exposure due to tissue damage from chronic inflammation, malignancy, and persistent viral infections, leading to antigen-presenting cells presenting self-antigens to helper T cells (Th cells). The dependent process involves the activation of Th cells and B cells through autoantigen processing and presentation. Activated autoreactive B cells enhance antibody affinity through endocytic processing, which involves antigen endocytosis and re-presentation by major histocompatibility complex class II, and somatic hypermutation (SHM), which induces mutations in immunoglobulins to select higher affinity antibodies.[8–11] In bullous pemphigoid, an organ-specific autoimmune disease of skin and mucous, intramolecular ES occurs against BP180, a major autoantigen, and intermolecular ES occurs against BP270, located near BP180.[7,12] The extent of ES correlates with the severity and activity of bullous disease, underscoring its clinical relevance.[13] Therefore, unraveling ES in autoimmune diseases is imperative for developing therapies targeting or modulating these broader immune responses, with the potential to support the control or management of autoimmune disease progression. Long-term observational studies suggest that even in patients with systemic autoimmune diseases, such as SLE and SSc, the target antigens of autoantibodies are increasingly diverse as the disease progresses.[14] However, how ES is involved in autoantibody diversity in these diseases is largely unknown.

SSc, a refractory autoimmune disease, is characterized by vasculopathy, fibrosis, and immune abnormalities, leading to skin sclerosis and diverse organ involvements.[15,16] Representative disease-specific autoantibodies are anti-centromere (ACAs), anti–topoisomerase I (ATAs), and anti–RNA polymerase III (RNAP III) antibodies (ARAs). ARAs are the most prevalent antinuclear antibodies in SSc after ACAs and ATAs[17] and exhibit a prevalence of 11% (95% confidence interval [95% CI] 8–14%) in patients with SSc, influenced significantly by geographic factors.[18] ARA-positive SSc is characterized by rapidly progressive diffuse skin sclerosis and a high incidence of complications such as synchronous malignancies, renal crisis, and gastric antral vascular ectasia.[19–23] The prevalence of interstitial lung disease (ILD) in ARA-positive SSc is conflicting, with some cohort studies reporting a lower frequency and others indicating a higher prevalence exceeding 50%.[18,20,24–26] Generally, ILD in ARA-positive SSc is considered milder compared with ATA-positive SSc. However, a single-center prospective study reported the ILD progression in some patients who are ARA-positive, and follow-up is necessary.[27] The RNAP III complex, comprising 17 subunits with RPC1 as the core subunit,[28] is the focus of this study. Previous research has identified RPC1 as the major antigen of ARAs and the one used for the diagnosis of ARA-positive SSc.[24,29] Although some studies have shown the detection of autoantibodies against several RNAP III complex subunits other than RPC1,[30,31] no studies have examined the correlation between ES against RNAP III complex subunits and the clinical manifestations of SSc. Hence, we retrospectively analyze patients who are ARA-positive with SSc and evaluate intermolecular ES for RNAP III complex subunits and intramolecular ES for RPC1 subunits, seeking to elucidate their relationship with severity and disease activity in SSc.

MATERIALS AND METHODS

Patients. Serum samples were obtained from 75 Japanese patients with SSc visited at Tokyo University Hospital between 2013 and 2022. Samples were typically collected at the patient's first visit and during follow-up as deemed necessary by the physician. All patients with SSc fulfilled the classification criteria established by the American College of Rheumatology and EULAR.[32] Patients with SSc were categorized into four groups based on specific autoantibodies detected using tests covered by Japanese health insurance: ARA-positive (n = 34), ATA-positive (n = 13), ACA-positive (n = 7), and specific autoantibodies unknown (n = 21). The "specific autoantibodies unknown" group included patients who tested negative for ARAs (MESACUP Anti-RNA polymerase III; MBL), ATAs (MEBLux Scl-70; MBL), and ACAs (MEBLux CENP-B; MBL), regardless of their ANA test results. Additionally, serum samples from nine healthy Japanese individuals were obtained from BioIVT and used as controls to determine cut-off values. All serum samples were stored at −80°C before use. The study was conducted in accordance with the Declaration of Helsinki and approved by The University of Tokyo Ethical Committee (approval no. 695). Written informed consent was obtained from all participants.

Clinical data acquisition. The clinical data of patients with SSc were collected by a retrospective review of medical records. All patients received medical histories, physical examinations, and laboratory analyses at their first visit, and follow-up was continued every one to three months. The severity of skin sclerosis was examined by the modified Rodnan skin thickness score (mRSS).[33] ILD was defined as the presence of pulmonary interstitial fibrosis, such as ground-glass opacities, reticular shadows, and honeycombing, in the bibasilar regions and elsewhere on high-resolution computed tomography (HRCT). The extent of ILD lesions was scored as HRCT extent, evaluating HRCT scans

as previously described.[34] Pulmonary function tests, including the percentage of predicted forced lung vital capacity (%FVC) and percentage of predicted lung diffusing capacity for carbon monoxide (%DLCO), and serum biomarkers for ILD, including Krebs von den Lungen-6 (KL-6) and surfactant protein-D (SP-D), were performed for evaluating lung dysfunction.[35,36] Renal crisis was defined as new onset malignant hypertension with blood pressure >140/90 mm Hg or a >30 mm Hg rise in blood pressure from baseline and rising serum creatinine levels.[37] Pulmonary hypertension was defined as mean pulmonary artery pressure ≥25 mm Hg on right heart catheterization. Gastroesophageal manifestations were defined as symptoms caused by upper gastrointestinal tract disorders such as gastroesophageal reflux, substernal burning pain, dysphagia and dyspepsia.[38,39] Malignancy was diagnosed concurrently with SSc or within the three years after SSc diagnosis or if a preceding malignancy occurred within the three years before diagnosis of SSc. We gathered the patient's basic information (age, disease duration), clinical manifestations (Raynaud phenomenon, nail fold bleeding, pitting scar/digital ulcers, telangiectasia, calcinosis, and gastroesophageal manifestations), medication history, and complications of SSc as of the date of serum collection. Laboratory findings and mRSS were obtained from the closest point to the serum collection date.

In vitro protein expression. We synthesized 17 full-length subunit proteins of RNA polymerase III complex and 5 truncated forms of RPC1 in vitro using a wheat germ cell-free translation system. Target clones of antigens in the human proteome expression resource and complete sets of protein-encoding open reading frames entry clone library (Supplementary Table 1) and polymerase chain reaction products of truncated forms were recombined into an expression vector for producing N-terminal FLAG–glutathione S-transferase (GST)-tag proteins with the GATEWAY cloning system (Thermo Fisher Scientific).[40,41] In vitro protein translation was performed by reacting the transcripts synthesized from the expression vectors with wheat germ extract (WEPRO7240G; CellFree Sciences), as previously described.[40,41] The synthesized proteins were confirmed to match the target size by sodium dodecyl sulfate–polyacrylamide gel electrophoresis and Coomassie Brilliant Blue staining (Supplementary Figure 1).

Antigen-binding plate preparation. Antigen-binding plates were prepared under wet conditions. The translation reaction solution containing the FLAG-GST–tagged target proteins was diluted five times with phosphate-buffered saline (PBS) and attached on 96-well plates coated with 50 mM glutathione (GSH) via Sulfo-SMPB (22317, Thermo Fisher Scientific) by its affinity with glutathione S-transferase (GST) tags. The translation reaction solution was mixed in equal portions when preparing plates containing the RNAP III complex subunit mixtures. The plates were incubated at room temperature for 60 minutes and washed with Tris-buffered saline containing 0.1% Tween 20 (Tris buffered saline–Tween [TBST]; 9997S, Cell Signaling Technology). The plates were then incubated in blocking buffer (50 mM HEPES pH 7.5, 200 mM NaCl, 0.08% Triton-X, 25% Glycerol, 5 mM GSH, 0.3% skim milk, and 1 mM DTT) and stored at –80°C until use. The antigen binding to the plate was confirmed by measuring the fluorescence of wells reacted with Alexa Fluor 647-conjugated anti-FLAG Ab (MBL) (Supplementary Figure 2).

Autoantibody detection. The blocking buffer on the plates was thawed at room temperature and discarded. The plates were treated with Alexa Fluor 647–conjugated anti-FLAG Ab diluted 1:3,000 or serum diluted 1:150 in the reaction buffer, which was PBS containing 0.1% skim milk, 0.1% Tween 20, and 1× Synthetic Block (PA017, Invitrogen). After the reaction at room temperature for one hour, the plates were washed three times with TBST and incubated with the secondary antibody, which was goat anti-human IgG (H+L) Alexa Flour 647 conjugate (A-21445, Invitrogen) diluted 1:1,000 in the reaction buffer. TBST was added in place of the secondary antibody to wells reacted with Alexa Fluor 647-conjugated anti-FLAG Ab. Finally, after the reaction at room temperature for one hour, the plates were washed three times with TBST, and fluorescence was measured by a fluorescence imager (Typhoon FLA 9500). The negative control spots were prepared using the translation reaction mixture containing distilled water (10977015, Invitrogen) instead of messenger RNA. The positive control spots were prepared using the human immunoglobulin heavy constant gamma 1 (IGHG1) tagged with FLAG-GST.

Autoantibody quantification. The level of autoantibody was quantified based on the fluorescent values obtained from reactions of serum with the protein spots. The level of each autoantibody was calculated as below:

$$Index\ value = \frac{F_{autoantigen} - F_{negative\ control}}{F_{flag} \times \left(F_{positive\ control} - F_{negative\ control}\right)} \times 10^5$$

where $F_{autoantigen}$ is the fluorescent intensity of autoantigen spot, $F_{negative\ control}$ is the fluorescence intensity of negative control spot, F_{flag} is the fluorescence intensity of anti-FLAG antibody, and $F_{positive\ control}$ is the fluorescence intensity of positive control spot. The cut-off value for autoantibody positivity was defined as an index value of three or higher, above the mean +3 SD for all antigens in healthy controls.

Harr plot analysis. Harr plot analysis was performed to evaluate the homology among the subunits of the RNAP III complex. Harr plots of amino acid sequences between all RNAP III complex subunits were created by Python. A black dot represents the homology of four amino acids between subunits.

Statistical analysis. Statistical analyses were performed by the Mann–Whitney *U* test for comparison of continuous variables and Fisher's exact test for comparing categorical variables. *P* values lower than 0.05 were considered statistically significant. Spearman's *r* was calculated to produce the correlation matrix. All the analyses were performed using Prism 10 (GraphPad Software).

RESULTS

Baseline characteristics of ARA-positive patients with SSc. Clinical characteristics of patients who were ARA-positive with SSc (6 men and 28 women) are summarized in Table 1. The median (IQR) age was 69 (61–72), with a female predominance (28 of 34; 82%). LeRoy's classification rule categorized patients into 27 diffuse cutaneous SSc (dcSSc) and 7 limited cutaneous SSc (lcSSc). Consistent with previous studies, patients with dcSSc exhibited a more frequent presence of ILD (78% vs 29%, $P = 0.02$) and gastroesophageal manifestations (89% vs 43%, $P = 0.02$) than patients with lcSSc. Furthermore, only patients with dcSSc exhibited a higher prevalence of renal crisis (6 of 27; 22%) and malignancy (5 of 27; 19%), the hallmark feature of ARA-positive patients with SSc.

Autoantibodies against various subunits of the RNAPIII complex in ARA-positive patients with SSc. We investigated whether intermolecular ES is observed for the RNAP III complex subunits and intramolecular ES for the major antigen, RPC1, in patients with SSc (Figure 1A). To detect autoantibodies against the target antigen, we prepared antigen-binding plates and reacted them with patient serum samples, followed by fluorescence measurement using a fluorescence-labeled secondary antibody (Figure 1B). Amino acid homology was examined by Harr plot analysis to determine cross-reactivity between subunits of the RNAP III complex. No homology of >10 amino acids, the length required for antibody recognition, was observed between all subunits (Figure 1C). Antigen-binding plates were used to measure autoantibodies in patients with SSc and healthy controls (ARA-positive: n = 34, ATA-positive: n = 13, ACA-positive: n = 7, unknown: n = 21, and healthy control: n = 9). The "unknown"

Table 1. Clinical characteristics of patients who were ARA-positive with SSc*

Basic demographics	Total (n = 34)	dcSSc (n = 27)	lcSSc (n = 7)	*P* values
Age, median (IQR), y	69 (61–72)	69 (61–72)	68 (59–70)	0.81
Female, n (%)	28 (82)	22 (81)	6 (86)	>0.99
Disease duration, median (IQR), months	45 (10–171)	45 (10–180)	24 (5–168)	0.88
Disease classification, n (%)				
dcSSc	27 (79)	–	–	–
lcSSc	7 (21)	–	–	–
Cutaneous involvement				
mRSS, median (IQR)	13 (10–21)	16 (12–24)	8 (2–13)	<0.01
Raynaud phenomenon, n (%)	27 (79)	20 (74)	7 (100)	0.3
Nail fold bleeding, n (%)	23 (68)	16 (59)	7 (100)	0.07
Pitting scar/digital ulcers, n (%)	11 (32)	9 (33)	2 (29)	>0.99
Telangiectasia, n (%)	12 (35)	10 (37)	2 (29)	>0.99
Calcinosis, n (%)	6 (18)	5 (19)	1 (14)	>0.99
Lung involvement				
ILD, n (%)	23 (68)	21 (78)	2 (29)	0.02
HRCT extent, median (IQR)	6 (3–18)	–	–	–
1%∼20%, n (%)	20 (59)	19 (70)	1 (14)	0.01
20%, n (%)	3 (9)	2 (7)	1 (14)	0.51
%FVC, median (IQR)	89 (84–97)	89 (82–93)	106 (86–108)	0.24
%DLco, median (IQR)	96 (81–107)	96 (80–106)	98 (72–118)	0.49
KL-6, U/mL, median (IQR)	396 (278–656)	390 (278–671)	401 (322–536)	0.9
SP-D, ng/mL, median (IQR)	111 (83–253)	111 (85–259)	112 (79–140)	0.64
Other involvement				
Gastroesophageal manifestations, n (%)	27 (79)	24 (89)	3 (43)	0.02
Pulmonary hypertension, n (%)	4 (12)	3 (11)	1 (14)	>0.99
Renal crisis, n (%)	6 (18)	6 (22)	0 (0)	0.31
Malignancy, n (%)	5 (15)	5 (19)	0 (0)	0.56
Medication history				
Oral prednisolone, n (%)	15 (44)	13(48)	2 (29)	0.43
Dose, median (IQR), mg/d	5 (5–8)	5 (5–9)	7 (5–8)	0.89
Immunosuppressive agents, n (%)	2 (6)	2 (7)	0 (0)	>0.99
Tocilizumab, n (%)	3 (9)	3 (11)	0 (0)	>0.99

* %DLco, percentage of predicted lung diffusing capacity for carbon monoxide; %FVC, percentage of predicted forced lung vital capacity; ARA, anti-RNA polymerase antibody; dcSSC, diffuse cutaneous systemic sclerosis; HRCT, high-resolution computed tomography; ILD, interstitial lung disease; IQR, interquartile range; KL-6, Krebs von den Lungen-6; lcSSc, limited cutaneous systemic sclerosis; mRSS, modified Rodnan skin thickness score; SP-D, surfactant protein-D.

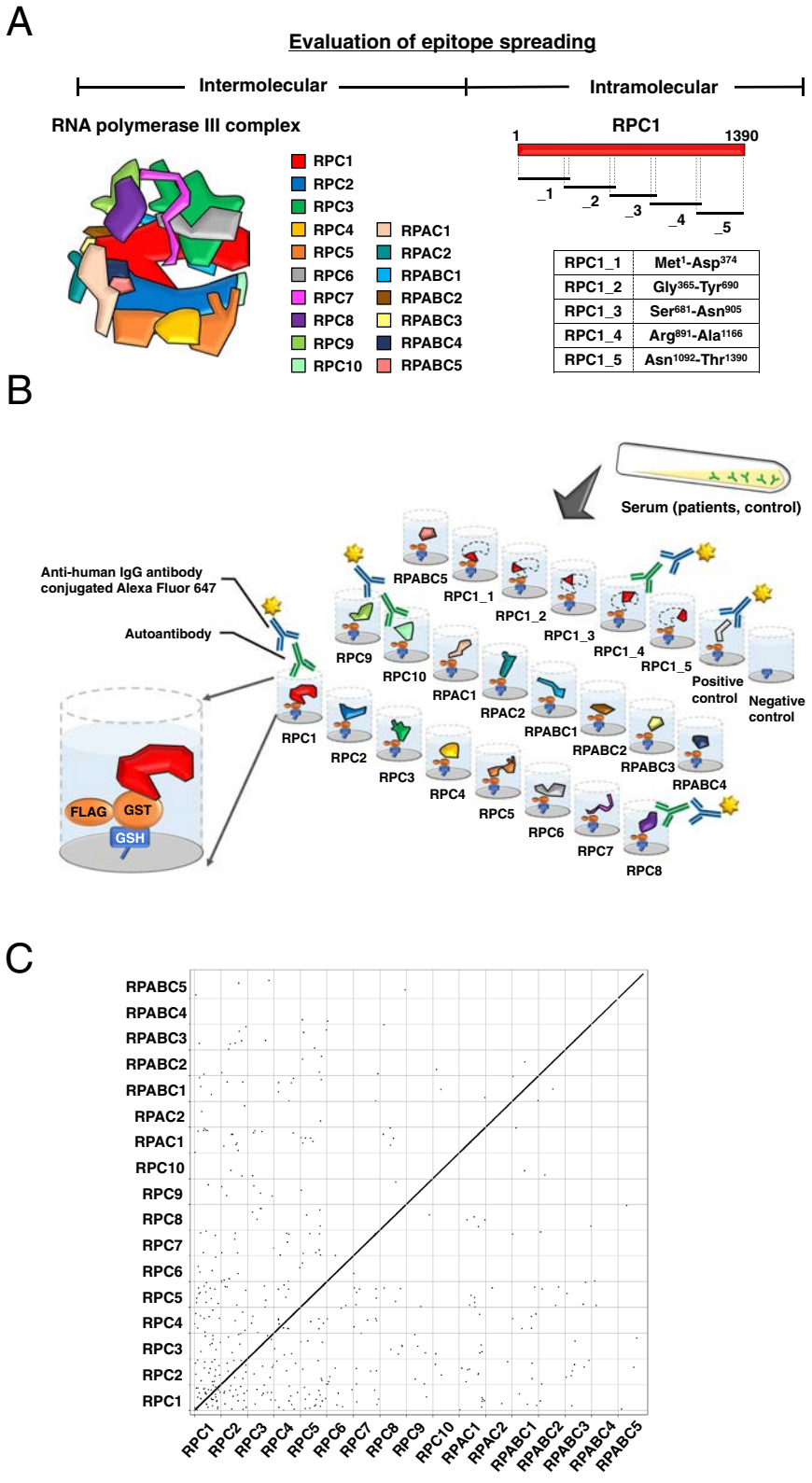

Figure 1. Evaluation of ES of ARAs against RNAP III complex: schematic of human RNAP III complex and truncated forms of RPC1 for evaluation of ES. (A) Schematic flow chart of autoantibody detection is shown. Antigen proteins were attached to antigen-binding plates via binding of GSH and GST tags and reacted with patient serum. (B) Autoantibodies bound to the antigen were detected with Alexa Flour 647–labeled secondary antibodies. (C) Harr plots of the homology of amino acids between the RNAP III complex subunits are shown. The homology of four amino acids between subunits is represented by a black dot. ARA, anti-RNA polymerase antibody; ES, epitope spreading; GSH, glutathione; GST, glutathione S-transferase; RNAP III, RNA polymerase III; RPAC, RNA polymerase I and III subunit; RPABC, RNA polymerase I, II, and III subunit; RPC1, RNA polymerase III subunit A.

group is patients with SSc who tested negative for ARAs, ATAs, and ACAs, regardless of their ANA test results. All ARA-positive patients with SSc had autoantibodies to RPC1_4, including the epitope used in the current test, indicating the validity of our methods. Interestingly, various autoantibodies were detected with high frequency against subunits of the RNAP III complex other than RPC1_4 (Figure 2A–C). In contrast, ATA-positive and ACA-positive patients with SSc and healthy controls were negative for all other autoantibodies against subunits of the RNAP III complex, except for autoantibodies against RPC4 (Figure 2B and C). Moreover, one patient with SSc with unknown specific antibodies showed autoantibodies with higher index values against several subunits of the RNAP III complex than RPC1 (Figure 2D). This patient's ANA patterns by indirect immunofluorescence on Hep-2 cells were Speckled pattern (1:320), but ARAs, ATAs, and ACAs were negative on current testing. These results suggest that some patients who were ARA-negative by the current test may include some ARA-positive individuals by evaluating autoantibodies against the RNAP III complex subunits.

Clinical correlation between ES levels and symptoms of SSc. The positivity rate of anti-RPC4 antibodies was almost the same among patients who were ARA-positive with SSc, other patients with SSc, and healthy controls. There was no significant difference in the indicators of ES of autoantibodies against the other subunits in patients who were ARA-positive with SSc with or without anti-RPC4 antibodies (Supplementary Figure 3). Therefore, we evaluated the intermolecular ES against 16 subunit antigens of the RNAP III complex, excluding RPC4. First, we defined the number of autoantibodies and the sum of the index as the indicators of intermolecular ES, then analyzed the correlations with skin sclerosis, ILD, renal crisis, and malignancy in ARA-positive SSc. Interestingly, both the number of autoantibodies and the sum of the index showed a significant positive correlation with mRSS (number of autoantibodies, r = 0.44, P = 0.012; sum of the index, r = 0.49, P = 0.005) (Figure 3A and B). No significant correlation was observed with HRCT extent, %FVC, %DLco, or KL-6, but a significant positive correlation was recognized with SP-D (number of autoantibodies, r = 0.34, P = 0.049; sum of the index, r = 0.43, P = 0.011) (Figure 3A and B). Moreover, the number of autoantibodies and the sum of the index showed no significant differences between patients with or without renal crisis and malignancy (Figure 3A and B). Next, we analyzed the correlation among intramolecular ES against RPC1, the major antigen of the RNAPIII complex, and the clinical findings. Most patients had autoantibodies only to RPC1_4, the major epitope of RPC1, but those with autoantibodies to regions other than RPC1_4 showed significantly higher mRSS (median [IQR], 12 [8–17] vs 18 [14.5–34]; P = 0.007) (Figure 3C). On the other hand, there were no significant differences in ILD-related laboratory findings. Intriguingly, the number of autoantibodies (RPC1_1–5) was significantly increased in patients with SSc with renal crisis compared with patients without a renal crisis (median [IQR], 2 [1–3.5] vs 1 [1–1]; P = 0.014) (Figure 3C). The intermolecular/intramolecular ES indicators were not significantly associated with or without other clinical manifestations of SSc (Supplementary Figure 4). These findings suggest that the severity of SSc can be predicted by evaluating intermolecular ES for the RNAP III complex and intramolecular ES for RPC1.

Correlation with clinical course of SSc and longitudinal changes in ES levels. We investigated the correlation between disease duration and ES at the time of blood collection in patients who were ARA-positive. Although ES indicators tended to decrease as disease duration increased, no significant correlation was observed in patients who were ARA-positive with SSc (Supplementary Figure 5). These results might be due to individual differences in ES indicators among patients with early-stage SSc and the fact that each patient was evaluated only once. Therefore, we examined the clinical course and ES in a patient who was ARA-positive with SSc. This 68-year-old female patient was diagnosed with SLE and rheumatoid arthritis (RA) at age 36 and was under long-term control with oral prednisolone at 6 mg/day. During follow-up, she developed skin sclerosis and muscle weakness, leading to a diagnosis of SSc-myositis overlap. Throughout the course of her disease, there were no signs of SLE or RA relapse. Autoantibodies against RNAP III complex subunits were found before the onset of SSc. After onset, the number of autoantibodies and the sum of the index increased along with worsening mRSS. However, immunosuppressive therapy with tocilizumab improved the mRSS and tended to decrease the number of autoantibodies and the sum of the index (Figure 4A). Interestingly, the index values of autoantibodies to most individual subunits changed in parallel with the sum of index, whereas those to RPC3 and RPC9 showed a decreasing trend over time (Figure 4B). Next, a longitudinal analysis was performed between intermolecular ES and skin sclerosis. Longitudinal data were available for 12 patients with SSc who were ARA-positive. The median (IQR) follow-up duration among these patients was 21 (8–39) months. We examined the correlation between change in mRSS (ΔmRSS) and change in intermolecular ES levels (Δnumber of autoantibodies and Δsum of the index). Correlation analyses showed that ΔmRSS was not significantly positively correlated with Δnumber of antibody, but only with Δsum of the index (Δnumber of autoantibodies, r = 0.45, P = 0.14; Δsum of the index, r = 0.66, P = 0.022) (Figure 4C). These findings suggest that the longitudinal change in indicators of intermolecular ES is useful as disease biomarkers for SSc.

Correlation of individual autoantibodies against the subunits of RNAPIII complex with clinical findings. To investigate the correlation between individual autoantibodies

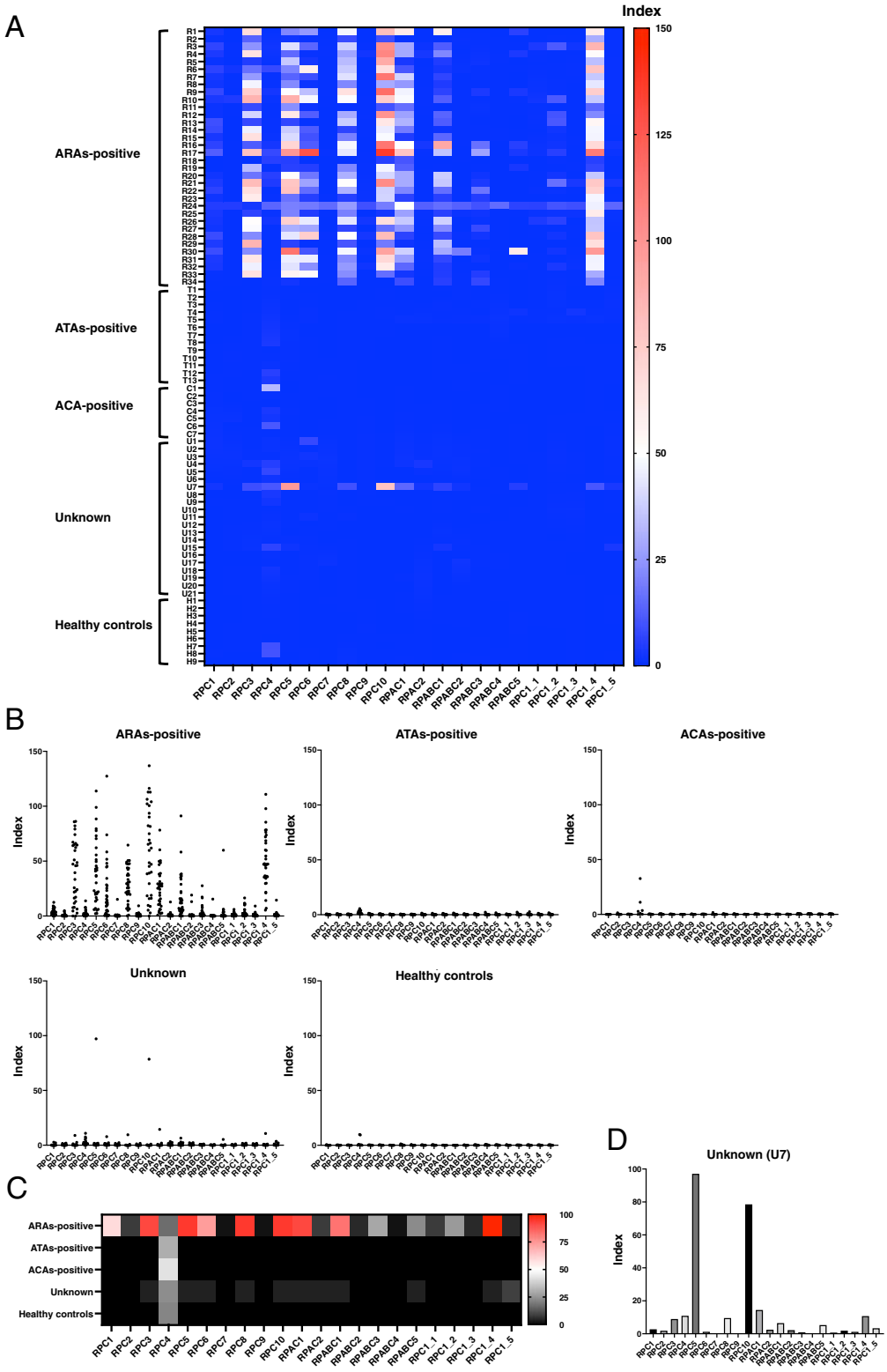

Figure 2. Detection of various autoantibodies against the RNAP III complex subunits in patients who are ARA-positive with SSc. Heatmap (A) and dot plots (B) of autoantibody index against RNAP III complex subunits and truncated forms of RPC1 in individual serum of SSc and healthy controls are shown. Patients with SSc were divided into ARA-positive, ATA-positive, ACA-positive, and specific antibodies unknown patients. (C) Autoantibody positivity rate against RNAP III complex subunits and truncated forms of RPC1 in SSc (ARA-, ATA-, and ACA-positive and specific antibodies unknown patients) and healthy controls is shown. (D) Autoantibody index against RNAP III complex subunits and truncated forms of RPC1 in one patient with SSc (U7) with unknown specific antibodies is shown. ACA, anti-centromere antibody; ARA, anti-RNA polymerase antibody; ATA, anti-Topoisomerase I antibody; RNAP III, RNA polymerase III; RPC1, RNA polymerase III subunit A; SSc, systemic sclerosis. Color figure can be viewed in the online issue, which is available at http://onlinelibrary.wiley.com/doi/10.1002/art.42975/abstract.

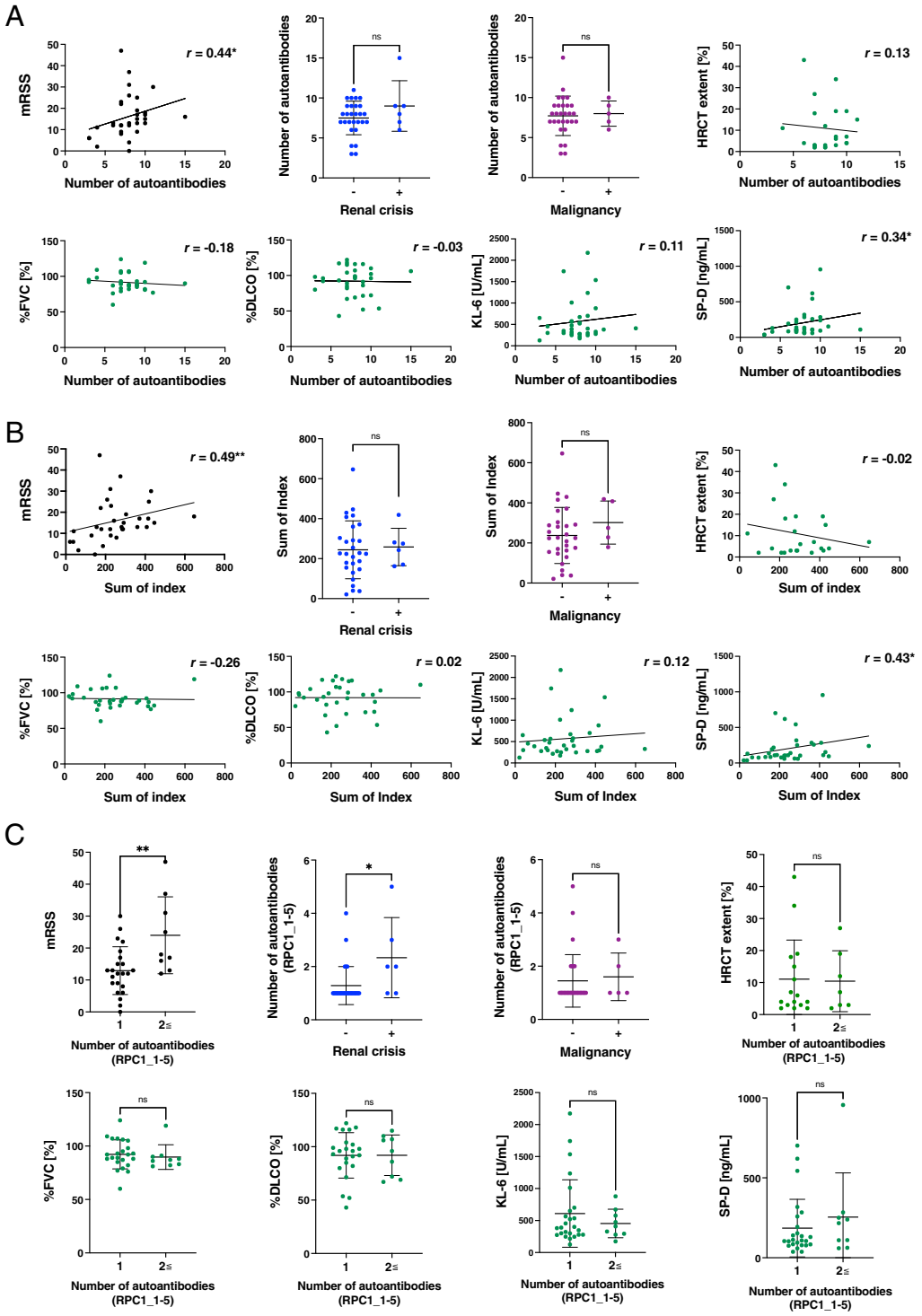

Figure 3. Levels of intermolecular/intramolecular ES and clinical findings in patients who are ARA-positive with SSc. Correlation between the number of autoantibodies (A) or the sum of the index and mRSS, HRCT extent, PFTs, and ILD markers (B) is shown. *P* values were calculated by estimating *r*. The solid line shows regression lines. The number of autoantibodies (A) or the sum of the index (B) were compared between patients with or without renal crisis and malignancy. *P* values were calculated by Mann–Whitney *U* test. (C) mRSS, HRCT extent, PFTs, and ILD markers were compared between patients with 1 or ≥2 of the number of autoantibodies (RPC1_1–5). The number of autoantibodies (RPC1_1–5) were compared between patients with or without renal crisis and malignancy. *P* values were calculated by Mann–Whitney *U* test. Error bars indicate SD, and longer horizontal lines in the middle of the bars indicate mean values. $^{*}P < 0.05$, $^{**}P < 0.01$. ARA, anti-RNA polymerase antibody; ES, epitope spreading; HRCT, high-resolution computed tomography; ILD, interstitial lung disease; mRSS, modified Rodnan skin thickness score; ns, not significant; PFT, pulmonary function tests; *r*, Spearman's correlation coefficient; RPC, RNA polymerase C subunit 1; SP-D, surfactant protein-D; SSc, systemic sclerosis. Color figure can be viewed in the online issue, which is available at http://onlinelibrary.wiley.com/doi/10.1002/art.42975/abstract.

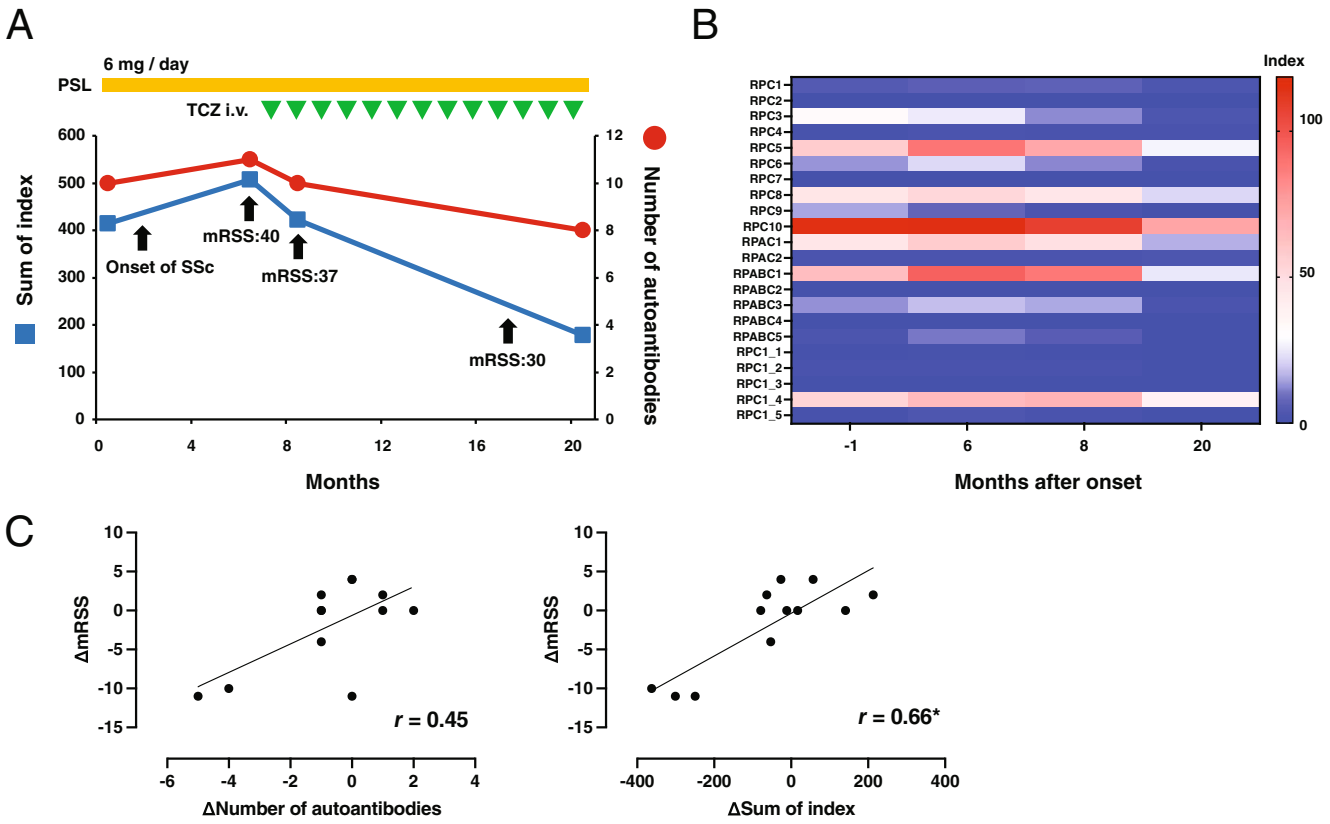

Figure 4. Longitudinal associations between the ES levels and the clinical course in patients who are ARA-positive with SSc. (A) Serial measurements of the intermolecular ES levels and skin thickness score in a 68-year-old woman with SSc, myositis, RA, and SLE are given. Scales for the number of autoantibodies and the sum of index are shown on the right and left, respectively. (B) Heatmap of longitudinal autoantibodies index against RNAP III complex subunits in the 68-year-old patient with SSc is shown. (C) Correlation between change in mRSS (ΔmRSS) and change in intermolecular ES levels (Δnumber of autoantibodies and Δsum of the index) is shown. *P* values were calculated by estimating *r*. The solid line shows regression lines. ARA, anti-RNA polymerase antibody; ES, epitope spreading; mRSS, modified Rodnan skin thickness score; *r*, Spearman's correlation coefficient; RA, rheumatoid arthritis; SLE, systemic lupus erythematosus; TCZ i.v., intravenous tocilizumab. Color figure can be viewed in the online issue, which is available at http://onlinelibrary.wiley.com/doi/10.1002/art.42975/abstract.

against the RNAP III complex subunits and clinical findings of SSc, we created a heatmap by dividing patients into two groups: lcSSc, a mild type of skin sclerosis, and dcSSc, a severe type of sclerosis. Patients with dcSSc had higher positivity and index values against more subunits of RNAP III complex than lcSSc. However, there was significant variation in the combinations of autoantibodies, even among patients with the same disease type (Figure 5A). Next, we selected the top eight autoantibodies against the RNAP III complex subunit at a positive rate and investigated the correlation between these individual autoantibodies and mRSS and laboratory findings of ILD. Interestingly, the correlation with clinical findings varied for each individual autoantibody (Figure 5B). To determine which autoantibodies correlate best with clinical findings of skin and lung involvements, the absolute value of Spearman's correlation coefficient for mRSS, %FVC, and SP-D was defined as the sum of Spearman's *r* (mRSS, % FVC, SP-D). The sum of Spearman's *r* (mRSS, %FVC, SP-D) for anti-RPC8 antibody was the highest rank (Supplementary Figure 6A). Subsequently, the top six autoantibodies (anti-RPC1_4, RPC5, RPC8, RPC10, RPAC1, and RPABC1) of the sum of Spearman's *r* (mRSS, %FVC, SP-D) were selected. The sum of the index (the selected six autoantibodies) was defined and correlated with clinical findings in ARA-positive SSc. As we expected, the sum of the index (the selected six autoantibodies) showed a significant correlation with mRSS, %FVC, and SP-D (mRSS, $r = 0.57$, $P < 0.001$; %FVC, $r = -0.40$, $P = 0.039$; SP-D, $r = 0.45$, $P = 0.007$) (Supplementary Figure 6B). These results suggested that the correlation with clinical findings differs depending on the autoantibodies against the subunits of RNAP IIII complex, and the accuracy of ES as a biomarker may be enhanced by focusing on autoantibodies that have a strong correlation.

The mixture of RNAP III complex subunit antigens enhanced the sensitivity for detection of ARAs. We examined the possibility of improving the detection sensitivity of ARAs by mixing RNAP III complex subunit antigens and reacting them with patient serum samples. Antigen mixtures of eight antigens with a positive rate of over 70% (RPC1_4, RPC3, RPC5, RPC6, RPC8, RPC10, RPAC1, RPABC1) or five antigens, specific subunits of the RNAPIII complex with a positive rate of over 90%

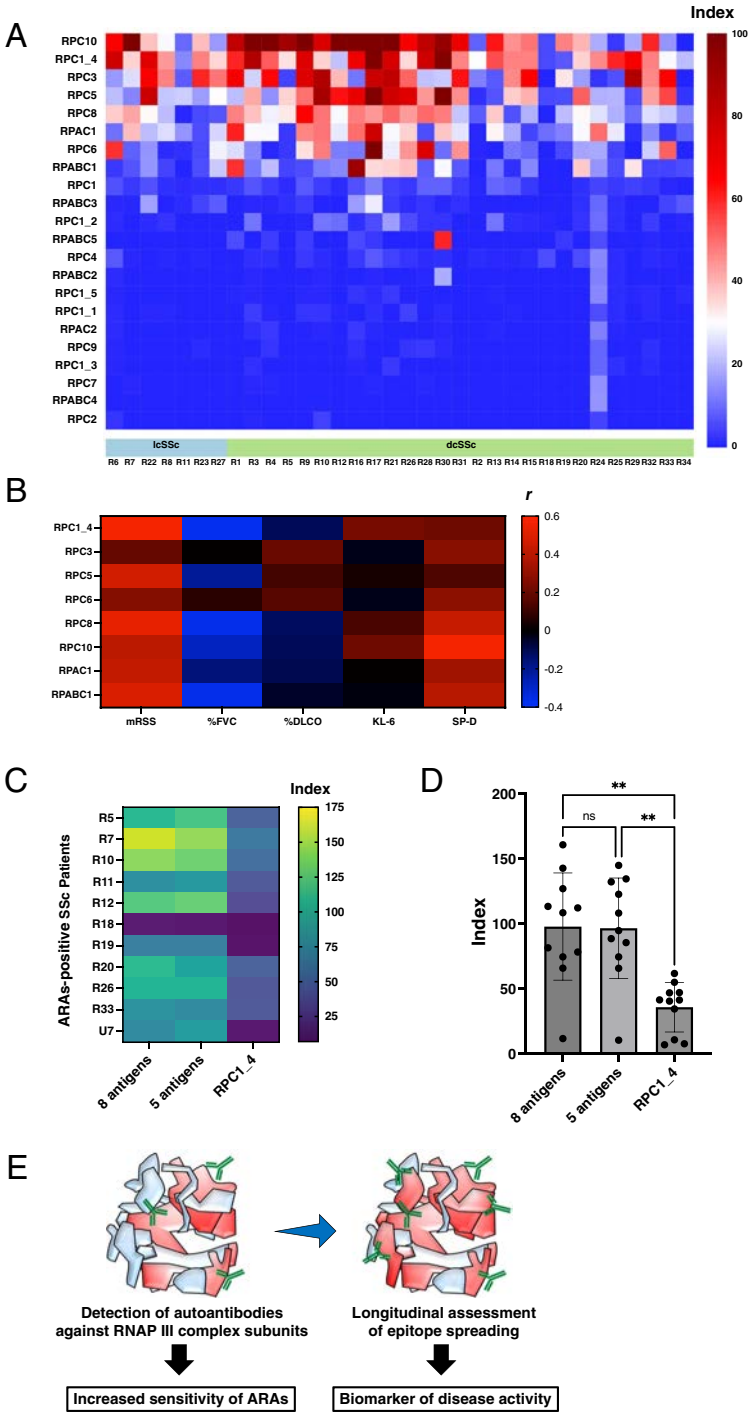

Figure 5. Individual autoantibodies against the RNAP III complex subunits and clinical findings in patients who are ARA-positive with SSc. (A) Heatmap of autoantibodies index against RNAP III complex subunits and truncated forms of RPC1 in patients who are ARA-positive with SSc is shown. Patients with SSc were divided into lcSSc and dcSSc. (B) Heatmap of Spearman's correlation coefficient between each autoantibody index of the top eight positive rate and skin score, pulmonary function, and ILD markers is given. (C) Heatmap of autoantibodies index against eight-antigen mixtures, five-antigen mixtures, and RPC1_4 is given. (D) Autoantibody index against eight antigens, five antigens, and RPC1_4 was compared. *P* values were calculated by Dunn's multiple comparisons test. (E) Schematic of ES of ARAs against RNAP III complex is shown. The sensitivity of ARAs was increased by detecting each RNAP III complex subunit. Longitudinal assessment of ES in RNAP IIII complex has the potential as a biomarker of disease activity. $^{**}P < 0.01$. %DLco, percentage of predicted lung diffusing capacity for carbon monoxide; %FVC, percentage of predicted forced lung vital capacity; ARA, anti-RNA polymerase antibody; dcSSC, diffuse cutaneous systemic sclerosis; ES, epitope spreading; HRCT, high-resolution computed tomography; ILD, interstitial lung disease; KL-6, Krebs von den Lungen-6; lcSSc, limited cutaneous systemic sclerosis; mRSS, modified Rodnan skin thickness score; ns, not significant; PFT, pulmonary function tests; *r*, Spearman's correlation coefficient; RPC1, RNA polymerase C subunit 1; SP-D, surfactant protein-D; SSc, systemic sclerosis. Color figure can be viewed in the online issue, which is available at http://onlinelibrary.wiley.com/doi/10.1002/art.42975/abstract.

(RPC1_4, RPC3, RPC5, RPC8, RPC10), were prepared and reacted with patient with SSc serum samples found to be ARA-positive in this study with low levels of autoantibodies against RPC1_4. Interestingly, the index values of autoantibodies against mixtures of eight antigens or five antigens were markedly increased compared with autoantibodies against RPC1_4 (Figure 5C and D). This result suggested that the detection sensitivity of ARAs is improved by examining autoantibodies against a mixture of RNAP III complex subunits. These findings suggest that examining autoantibodies against each RNAP III complex subunit can improve the detection sensitivity of ARAs and predict the severity and risk of complications in patients who are ARA-positive with SSc. Moreover, the longitudinal assessment of ES in RNAP III complex subunits showed potential to be used as a biomarker of disease activity (Figure 5E).

DISCUSSION

In this study, we demonstrated the occurrence of intermolecular ES among RNAP III complex subunits and intramolecular ES within RPC1. Subsequently, we observed a correlation between ES levels and the severity of skin sclerosis and serum biomarker of ILD in patients who were ARA-positive with SSc (Figures 2–4). Furthermore, longitudinal assessment revealed a correlation between intermolecular ES levels and skin score (Figure 4C). These findings propose that ES mechanisms in ARAs are intricately linked to the development of SSc and reflect disease activity. In a previous study, an enzyme-linked immunosorbent assay (ELISA) using the major epitope antigen of RPC1 indicated that skin sclerosis was more severe in patients with higher levels of ARAs and that changes in ARA levels correlated with changes in skin score.[24,42] Consistent with previous studies, we observed a strong correlation between the levels of autoantibodies against RPC1_4 and the severity of skin score (Figure 5B). Additionally, we found that patients with intramolecular ES within RPC1 not only had more severe skin sclerosis but also a higher risk of renal crisis (Figure 3C). These findings indicate that autoreactive B cells are highly activated in patients with severe SSc, potentially leading to SHM and endocytic processing, which contribute to intramolecular ES. Although it is generally acknowledged that an independent process governs intermolecular ES and a dependent process underlies intramolecular ES, recent research indicates that bridging autoreactive B cells with distinct Th cells can enable intermolecular ES for various antigens.[43] Consequently, intermolecular ES may also involve dependent processes such as intramolecular ES, possibly reflecting B cell activity in SSc.

Previous studies have emphasized the pivotal role of immunologic abnormalities, particularly in B cells, in SSc pathogenesis.[44,45] Recently, rituximab, a B cell elimination therapy, demonstrated significant improvement in skin sclerosis and lung vital capacity reduction in SSc due to ILD, affirming the importance of B cells.[46] Autoreactive B cells with high-affinity B cell receptors produce inflammatory cytokines such as interleukin-6 (IL-6), which has been implicated in SSc pathogenesis.[47] IL-6 has been shown to enormously enhance ES via SHM and disruption of immune tolerance in germinal center B cells.[10,48,49] In our study, a patient with SSc who was treated with tocilizumab, an IL-6 inhibitor, showed that the number of autoantibodies and the sum of the index decreased parallel with mRSS improvement (Figure 4A). Further studies are required to confirm whether inflammatory cytokines such as IL-6 are involved in the mechanism by which affinity maturation of autoreactive B cells and ES occur in SSc. These findings suggest that the correlation between the degree of ES and clinical findings such as mRSS in ARA-positive SSc may be because ES reflects the activity of B cells, which are considered crucial in the pathogenesis of SSc, and consequently linked to the disease activity of SSc. Interestingly, autoantibodies targeting nuclear antigens, previously thought to be nonpathogenic, have recently been reported to be internalized into the nucleus. In patients with anti–PM-Scl antibodies, known to be specific for SSc-myositis overlap syndrome, it is suggested that IgG is internalized into the nucleus of myositis muscle, causing dysfunction of the nuclear RNA exosome complex.[50] If IgG internalizes into the nucleus and inhibits RNA transcription in ARA-positive SSc, thereby exerting pathogenicity, intermolecular ES may be directly involved in the disease activity of SSc. Further studies on the pathogenicity of ARAs are needed.

The sensitivity of the detection of ARAs was increased by measuring autoantibodies against various subunits of the RNAP III complex. We identified an patient with SSc initially diagnosed with unknown specific antibodies, later identified as ARA-positive because of positive autoantibodies against multiple RNAP III complex subunits (Figure 2D). To avoid missing patients with SSc who were ARA-positive, comprehensive evaluation of autoantibodies against all RNAP III complex subunits is crucial. However, the positivity rate of anti-RPC4 antibodies was the same in patients who were ARA-positive with SSc as well as in other SSc serogroups and healthy controls, raising the possibility of detecting a nonspecific antigen-antibody reaction, resulting in false positive results. To ensure the accuracy of this autoantibody detection system, the homology with other proteins should be evaluated by epitope analysis of anti-RPC4 antibodies in future studies. In our cohort, anti-RPC8 antibodies exhibited the strongest correlation with skin sclerosis and ILD, suggesting variable correlations with clinical findings depending on the autoantibody detected (Figure 5A and B and Supplementary Figure 6A). Although further investigations are warranted, a detailed autoantibody assessment in the RNAP III complex may facilitate the subgrouping of ARA-positive SSc, enabling tailored treatment and follow-up.

Accurate and reproducible autoantibody assays are essential for the precise evaluation of ES. Our methods have several technical advantages compared with conventional ELISA and line blot methods. First, all processes, from antigen synthesis to autoantibody measurement, occur under wet conditions, preserving protein structure without denaturation by drying, enabling high-sensitivity autoantibody measurement. Previous studies have

validated the equivalence of this autoantibody assay technique to the immunoprecipitation method.[51] Second, reproducibility and quantitativeness are ensured by correcting for antigen content using an anti-FLAG antibody against the FLAG tag attached to the antigen and interassay variation correction using positive control IGHG1. This process allows for an accurate assessment of ES changes over time. Third, the mixture of RNAP III complex subunit antigens enhances ARA detection sensitivity in patients with SSc. Measuring ARAs with antigen mixtures not only improves detection rates but also allows simultaneous ES evaluation.

The major limitations of the present study include its indistinct patient selection criteria and retrospective design. In this study, in addition to the intermolecular ES against the RNAP III complex correlating with clinical findings (Figure 3A–C), autoantibodies to individual subunits showed different correlations with complications (Figure 5A). However, ARA positivity and complication frequency in SSc vary among racial groups, necessitating further investigation with prospective recruitment across multiple hospitals and ethnicities to validate these findings. Furthermore, it is essential to note that the analysis was performed in a patient population with varying disease durations and treatments at the time the serum was sampled. Because patients who are ARA-positive with SSc tend to progress rapidly in the early stages of the disease, it would be beneficial to prospectively follow them from the early onset to assess the correlation between ES and disease activity accurately. Another limitation of this study is that only RNAP III was evaluated for autoantibodies among the three RNA polymerases (RNAP I, II, and III). Previous reports indicated autoantibodies against RNAP I and RNAP II in SSc.[31,52] Notably, patients who are ARA-positive with SSc with autoantibodies against RPA1, a specific RNAP I subunit, were reported to have a lower malignancy complication risk.[53] For a more detailed classification of patients who are ARA-positive with SSc, assessing autoantibodies against RNAP I and RNAP II specific subunits may be necessary.

In conclusion, we assessed intermolecular ES for RNAP III complex subunits and intramolecular ES for RPC1 in patients with SSc. Examining autoantibodies against each RNAP III complex subunit was found to enhance ARAs detection sensitivity, with ES levels correlating with complication severity in patients with SSc. Furthermore, subunit antigens could be made into a mixture and measured autoantibodies by ELISA or other methods to easily evaluate ES and improve the detection sensitivity of ARAs, indicating the possibility of immediate clinical application. Although additional studies are needed for comprehensive validation, evaluating ES against RNAP III complex subunits holds promise as a biomarker for disease activity in SSc.

ACKNOWLEDGMENTS

We thank Ms Maiko Enomoto, Ms Teruko Tani, and their colleagues for their technical assistance and secretary work.

AUTHOR CONTRIBUTIONS

All authors contributed to at least one of the following manuscript preparation roles: conceptualization AND/OR methodology, software, investigation, formal analysis, data curation, visualization, and validation AND drafting or reviewing/editing the final draft. As corresponding author, Dr Yoshizaki confirms that all authors have provided the final approval of the version to be published and takes responsibility for the affirmations regarding article submission (eg, not under consideration by another journal), the integrity of the data presented, and the statements regarding compliance with institutional review board/Helsinki Declaration requirements.

REFERENCES

1. Elkon K, Casali P. Nature and functions of autoantibodies. Nat Clin Pract Rheumatol 2008;4(9):491–498.
2. Agmon-Levin N, Damoiseaux J, Kallenberg C, et al. International recommendations for the assessment of autoantibodies to cellular antigens referred to as anti-nuclear antibodies. Ann Rheum Dis 2014; 73(1):17–23.
3. Pollmann R, Schmidt T, Eming R, et al. Pemphigus: a comprehensive review on pathogenesis, clinical presentation and novel therapeutic approaches. Clin Rev Allergy Immunol 2018;54(1):1–25.
4. Papadopoulos MC, Verkman AS. Aquaporin 4 and neuromyelitis optica. Lancet Neurol 2012;11(6):535–544.
5. Ludwig RJ, Vanhoorelbeke K, Leypoldt F, et al. Mechanisms of autoantibody-induced pathology. Front Immunol 2017;8:603.
6. Cornaby C, Gibbons L, Mayhew V, et al. B cell epitope spreading: mechanisms and contribution to autoimmune diseases. Immunol Lett 2015;163(1):56–68.
7. Didona D, Di Zenzo G. Humoral epitope spreading in autoimmune bullous diseases. Front Immunol 2018;9:779.
8. Binder M, Müller F, Jackst A, et al. B-cell receptor epitope recognition correlates with the clinical course of chronic lymphocytic leukemia. Cancer 2011;117(9):1891–1900.
9. McGovern EM, Moquin AE, Caballero A, et al. The effect of B cell receptor signaling on antigen endocytosis and processing. Immunol Invest 2004;33(2):143–156.
10. Muhammad K, Roll P, Seibold T, et al. Impact of IL-6 receptor inhibition on human memory B cells in vivo: impaired somatic hypermutation in preswitch memory B cells and modulation of mutational targeting in memory B cells. Ann Rheum Dis 2011;70(8):1507–1510.
11. Chi X, Li Y, Qiu X. V(D)J recombination, somatic hypermutation and class switch recombination of immunoglobulins: mechanism and regulation. Immunology 2020;160(3):233–247.
12. Recke A, Rose C, Schmidt E, et al. Transition from pemphigus foliaceus to bullous pemphigoid: intermolecular B-cell epitope spreading without IgG subclass shifting. J Am Acad Dermatol 2009;61(2): 333–336.
13. Di Zenzo G, Thoma-Uszynski S, Calabresi V, et al. Demonstration of epitope-spreading phenomena in bullous pemphigoid: results of a prospective multicenter study. J Invest Dermatol 2011;131(11): 2271–2280.
14. Arbuckle MR, McClain MT, Rubertone MV, et al. Development of autoantibodies before the clinical onset of systemic lupus erythematosus. N Engl J Med 2003;349(16):1526–1533.
15. LeRoy EC, Black C, Fleischmajer R, et al. Scleroderma (systemic sclerosis): classification, subsets and pathogenesis. J Rheumatol. 1988; 15(2):202–205.
16. Volkmann ER, Andréasson K, Smith V. Systemic sclerosis. Lancet 2023;401(10373):304–318.

17. Cavazzana I, Vojinovic T, Airo' P, et al. Systemic sclerosis-specific antibodies: novel and classical biomarkers. Clin Rev Allergy Immunol 2023;64(3):412–430.
18. Sobanski V, Dauchet L, Lefèvre G, et al. Prevalence of anti-RNA polymerase III antibodies in systemic sclerosis: new data from a French cohort and a systematic review and meta-analysis. Arthritis Rheumatol 2014;66(2):407–417.
19. Jaafar S, Lescoat A, Huang S, et al. Clinical characteristics, visceral involvement, and mortality in at-risk or early diffuse systemic sclerosis: a longitudinal analysis of an observational prospective multicenter US cohort. Arthritis Res Ther 2021;23(1):170.
20. Lazzaroni MG, Cavazzana I, Colombo E, et al; EUSTAR co-authors. Malignancies in patients with anti-RNA polymerase III antibodies and systemic sclerosis: analysis of the EULAR scleroderma trials and research cohort and possible recommendations for screening. J Rheumatol 2017;44(5):639–647.
21. Igusa T, Hummers LK, Visvanathan K, et al. Autoantibodies and scleroderma phenotype define subgroups at high-risk and low-risk for cancer. Ann Rheum Dis 2018;77(8):1179–1186.
22. Moinzadeh P, Fonseca C, Hellmich M, et al. Association of anti-RNA polymerase III autoantibodies and cancer in scleroderma. Arthritis Res Ther 2014;16(1):R53.
23. Wirz EG, Jaeger VK, Allanore Y, et al; EUSTAR co-authors. Incidence and predictors of cutaneous manifestations during the early course of systemic sclerosis: a 10-year longitudinal study from the EUSTAR database. Ann Rheum Dis 2016;75(7):1285–1292.
24. Kuwana M, Okano Y, Pandey JP, et al. Enzyme-linked immunosorbent assay for detection of anti-RNA polymerase III antibody: analytical accuracy and clinical associations in systemic sclerosis. Arthritis Rheum 2005;52(8):2425–2432.
25. Castelino FV, VanBuren JM, Startup E, et al. Baseline characteristics of systemic sclerosis patients with restrictive lung disease in a multi-center US-based longitudinal registry. Int J Rheum Dis 2022;25(2):163–174.
26. Motegi S, Toki S, Yamada K, et al. Demographic and clinical features of systemic sclerosis patients with anti-RNA polymerase III antibodies. J Dermatol 2015;42(2):189–192.
27. Hoffmann-Vold AM, Midtvedt Ø, Tennøe AH, et al. Cardiopulmonary disease development in anti-RNA polymerase III-positive systemic sclerosis: comparative analyses from an unselected, prospective patient cohort. J Rheumatol 2017;44(4):459–465.
28. Girbig M, Misiaszek AD, Vorländer MK, et al. Cryo-EM structures of human RNA polymerase III in its unbound and transcribing states. Nat Struct Mol Biol 2021;28(2):210–219.
29. Kuwana M, Kimura K, Kawakami Y. Identification of an immunodominant epitope on RNA polymerase III recognized by systemic sclerosis sera: application to enzyme-linked immunosorbent assay. Arthritis Rheum 2002;46(10):2742–2747.
30. Kuwana M, Okano Y, Kaburaki J, et al. Autoantibodies to RNA polymerases recognize multiple subunits and demonstrate cross-reactivity with RNA polymerase complexes. Arthritis Rheum 1999; 42(2):275–284.
31. Xu GJ, Shah AA, Li MZ, et al. Systematic autoantigen analysis identifies a distinct subtype of scleroderma with coincident cancer. Proc Natl Acad Sci USA 2016;113(47):E7526–E7534.
32. van den Hoogen F, Khanna D, Fransen J, et al. 2013 classification criteria for systemic sclerosis: an American College of Rheumatology/ European League against Rheumatism collaborative initiative. Arthritis Rheum 2013;65(11):2737–2747.
33. Khanna D, Furst DE, Clements PJ, et al. Standardization of the modified Rodnan skin score for use in clinical trials of systemic sclerosis. J Scleroderma Relat Disord 2017;2(1):11–18.
34. Goh NS, Desai SR, Veeraraghavan S, et al. Interstitial lung disease in systemic sclerosis: a simple staging system. Am J Respir Crit Care Med 2008;177(11):1248–1254.
35. Györfi AH, Filla T, Dickel N, et al. Performance of serum biomarkers reflective of different pathogenic processes in systemic sclerosis-associated interstitial lung disease. Rheumatology (Oxford) 2024;63(4):962–969.
36. Elhai M, Hoffmann-Vold AM, Avouac J, et al. Performance of candidate serum biomarkers for systemic sclerosis-associated interstitial lung disease. Arthritis Rheumatol 2019;71(6):972–982.
37. Woodworth TG, Suliman YA, Li W, et al. Scleroderma renal crisis and renal involvement in systemic sclerosis. Nat Rev Nephrol 2016;12(11): 678–691.
38. Ntoumazios SK, Voulgari PV, Potsis K, et al. Esophageal involvement in scleroderma: gastroesophageal reflux, the common problem. Semin Arthritis Rheum 2006;36(3):173–181.
39. Lahcene M, Oumnia N, Matougui N, et al. Esophageal involvement in scleroderma: clinical, endoscopic, and manometric features. ISRN Rheumatol 2011;2011:325826.
40. Sawasaki T, Ogasawara T, Morishita R, et al. A cell-free protein synthesis system for high-throughput proteomics. Proc Natl Acad Sci USA 2002;99(23):14652–14657.
41. Goshima N, Kawamura Y, Fukumoto A, et al. Human protein factory for converting the transcriptome into an in vitro-expressed proteome. Nat Methods 2008;5(12):1011–1017.
42. Nihtyanova SI, Parker JC, Black CM, et al. A longitudinal study of anti-RNA polymerase III antibody levels in systemic sclerosis. Rheumatology (Oxford) 2009;48(10):1218–1221.
43. Fahlquist-Hagert C, Wittenborn TR, Terczyńska-Dyla E, et al. Antigen presentation by B cells enables epitope spreading across an MHC barrier. Nat Commun 2023;14(1):6941.
44. Yoshizaki A, Fukasawa T, Ebata S, et al. Involvement of B cells in the development of systemic sclerosis. Front Immunol 2022;13:938785.
45. Matsushita T, Kobayashi T, Mizumaki K, et al. BAFF inhibition attenuates fibrosis in scleroderma by modulating the regulatory and effector B cell balance. Sci Adv 2018;4(7):eaas9944.
46. Ebata S, Yoshizaki A, Oba K, et al. Safety and efficacy of rituximab in systemic sclerosis (DESIRES): a double-blind, investigator-initiated, randomised, placebo-controlled trial. Lancet Rheumatol 2021;3(7):e489–e497.
47. Fukasawa T, Yoshizaki A, Ebata S, et al. Single-cell-level protein analysis revealing the roles of autoantigen-reactive B lymphocytes in autoimmune disease and the murine model. eLife 2021;10:e67209.
48. Wu Y, El Shikh MEM, El Sayed RM, et al. IL-6 produced by immune complex-activated follicular dendritic cells promotes germinal center reactions, IgG responses and somatic hypermutation. Int Immunol 2009;21(6):745–756.
49. Yan Y, Wang YH, Diamond B. IL-6 contributes to an immune tolerance checkpoint in post germinal center B cells. J Autoimmun 2012; 38(1):1–9.
50. Pinal-Fernandez I, Muñoz-Braceras S, Casal-Dominguez M, et al. Pathogenic autoantibody internalization in myositis. medRxiv Preprint posted online January 17, 2024. https://doi.org/10.1101/2024.01.15.24301339
51. Kuzumi A, Norimatsu Y, Matsuda KM, et al. Comprehensive autoantibody profiling in systemic autoimmunity by a highly-sensitive multiplex protein array. Front Immunol 2023;14:1255540.
52. Hamaguchi Y, Kodera M, Matsushita T, et al. Clinical and immunologic predictors of scleroderma renal crisis in Japanese systemic sclerosis patients with anti-RNA polymerase III autoantibodies. Arthritis Rheumatol 2015;67(4):1045–1052.
53. Shah AA, Laiho M, Rosen A, et al. Protective effect against cancer of antibodies to the large subunits of both RNA polymerases I and III in scleroderma. Arthritis Rheumatol 2019;71(9):1571–1579.

Arthritis & Rheumatology
Vol. 77, No. 1, January 2025, pp 80–91
DOI 10.1002/art.42973

American College of Rheumatology
Empowering Rheumatology Professionals

Targeting CD13/Aminopeptidase N as a Novel Therapeutic Approach for Scleroderma Fibrosis

Sei Muraoka,[1] William D. Brodie,[2] Megan N. Mattichak,[2] Mikel Gurrea-Rubio,[2] Yuzo Ikari,[3] Caroline Foster,[2] M. Asif Amin,[2] Neha Khanna,[2] Hafsa Amin,[2] Phillip L. Campbell,[2] Sirapa Vichaikul,[2] Ellen N. Model,[2] Morgan M. Omara,[2] Steven Petrovski,[2] Karly Kozicki,[2] Camilia Amarista,[2] Anna Webber,[2] Mustafa Ali,[2] Pamela J. Palisoc,[2] Jonatan Hervoso,[2] Jeffrey H. Ruth,[2] Lam C. Tsoi,[2] John Varga,[2] Johann E. Gudjonsson,[2] Dinesh Khanna,[2] David A. Fox,[2] and Pei-Suen Tsou[2]

Objective. Systemic sclerosis (SSc) is an autoimmune multisystem disease with poorly understood pathogenesis and ineffective treatment options. Soluble CD13 (sCD13), generated by the cleavage of cell surface CD13 via matrix metalloproteinase 14 (MMP14), signals through the bradykinin receptor B1 (B1R) to elicit pro-inflammatory, pro-arthritic, and pro-angiogenic responses. In this study, we explored the antifibrotic potential of targeting the sCD13-B1R axis in SSc.

Methods. The expression of CD13, B1R, and MMP14 was examined in SSc skin and explanted dermal fibroblasts. The efficacy of B1R antagonists in the inhibition on fibrosis was determined in vitro and in vivo.

Results. Expression of the genes for CD13, B1R, and MMP14 was elevated in skin biopsies from patients with diffuse cutaneous (dc) SSc. Notably, single-cell analysis of SSc skin biopsies revealed the highest *BDKRB1* expression in *COL8A1*-positive myofibroblasts, a population exclusively seen in SSc. Transforming growth factor beta (TGFβ) induced the expression of *BDKRB1* and production of sCD13 by dcSSc skin fibroblasts. Treatment of dcSSc fibroblasts with sCD13 promoted fibrotic gene expression, signaling, cell proliferation, migration, and gel contraction. The pro-fibrotic responses of sCD13 or TGFβ were prevented by a B1R antagonist. Mice lacking *Cd13* or *Bdkrb1* were resistant to bleomycin-induced skin fibrosis and inflammation. Pharmacological B1R inhibition had a comparable anti-fibrotic effect.

Conclusion. These results are the first to demonstrate a key role for sCD13 in SSc skin fibrosis and suggest that targeting the sCD13-B1R signaling axis is a promising novel therapeutic approach for SSc.

INTRODUCTION

Systemic sclerosis (SSc) is a chronic progressive autoimmune disease characterized by microvascular damage and irreversible fibrosis of organs including the skin, lungs, heart, kidney, and gastrointestinal tract.[1] Skin fibrosis, a hallmark of SSc, is correlated with disease severity and poor quality of life. The etiology of SSc is unknown, and currently no effective disease-modifying treatment exists.[2] Methotrexate, cyclophosphamide, mycophenolate, and tocilizumab have shown only limited efficacy along

Supported by the Japan Research Foundation for Clinical Pharmacology (to Dr Muraoka), the NIH (training grant T32-AR-007080 to Dr Gurrea-Rubio; grant R01-AI-183620 to Drs Gudjonsson, Khanna, and Tsou; and grant R56-AR076384 to Dr Fox), the University of Michigan Skin Biology and Diseases Resource-Based Center (grant P30-AR-075043 to Drs Gudjonsson and Tsou), the University of Michigan Clinical Autoimmunity Center of Excellence (grants U19-AI-110483 and A706890 to Drs Khanna and Fox), the National Scleroderma Foundation (to Dr Fox), the Frederick G. L. Huetwell and William D. Robinson Professorship in Rheumatology at the University of Michigan (to Dr Fox), the Beverley and Michael Townsley Fund for Scleroderma Biorepository (to Drs Khanna and Tsou), the Edward T. and Ellen K. Dryer Early Career Professor of Rheumatology (to Dr Tsou), the Frederick G. L. Huetwell Professorship in Rheumatology (to Dr Tsou), the Department of Defense (to Dr Tsou), and the Brian and Rosaline Chamberlain Research Fund (to Dr Tsou).

[1]Sei Muraoka, MD, PhD: University of Michigan, Ann Arbor, and Toho University School of Medicine, Tokyo, Japan; [2]William D. Brodie, BSc, Megan N. Mattichak, BSc, Mikel Gurrea-Rubio, PhD, Caroline Foster, BA, M. Asif Amin, MD, Neha Khanna, Hafsa Amin, Phillip L. Campbell, BSc, Sirapa Vichaikul, BSc, Ellen N. Model, BSc, Morgan M. Omara, BSc, Steven Petrovski, Karly Kozicki, Camilia Amarista, Anna Webber, BSc, Mustafa Ali, MD, Pamela J. Palisoc, BSc, Jonatan Hervoso, BSc, Jeffrey H. Ruth, PhD, Lam C. Tsoi, PhD, John Varga, MD, Johann E. Gudjonsson, MD, PhD, Dinesh Khanna, MD, David A. Fox, MD, Pei-Suen Tsou, PhD: University of Michigan, Ann Arbor; [3]Yuzo Ikari, MD, PhD: University of Michigan, Ann Arbor and Showa University School of Medicine, Tokyo, Japan.

Drs Fox and Tsou contributed equally to this work.

Additional supplementary information cited in this article can be found online in the Supporting Information section (https://acrjournals.onlinelibrary.wiley.com/doi/10.1002/art.42973).

Author disclosures and graphical abstract are available at https://onlinelibrary.wiley.com/doi/10.1002/art.42973.

Address correspondence via email to David A. Fox, MD, at dfox@umich.edu; or to Pei-Suen Tsou, PhD, at ptsou@umich.edu.

Submitted for publication January 19, 2024; accepted in revised form August 7, 2024.

with various safety concerns.[3] There is a need to better elucidate the pathogenesis of SSc to develop new, targeted, safe, and effective therapeutic agents.

Aminopeptidase N (CD13) is a ubiquitously expressed metallopeptidase originally described as a myeloid cell marker that functions as an ectoenzyme with multiple substrates.[4,5] Notably, CD13 can be shed from the cell membrane via its cleavage catalyzed by matrix metalloproteinase 14 (MMP14). Soluble CD13 (sCD13) binds to a G-protein–coupled receptor on activated T cells, monocytes, endothelial cells, and fibroblasts and acts as a chemoattractant for monocyte and T cell migration.[6–8] Moreover, CD13 acts on endothelial cells to promote angiogenesis.[8] Very recently, we identified the bradykinin receptor B1 (B1R) as a surface receptor of sCD13 on a variety of cell types and demonstrated that the sCD13/B1R axis plays a pivotal role in inflammatory arthritis.[9] However, the role of CD13 in other inflammatory diseases remains largely unknown.

Previous studies investigated the expression of CD13 in the skin. In particular, prominent CD13 expression was demonstrated on fibroblasts and blood vessels in the papillary dermis in both healthy and SSc skin.[10] Importantly, Dan et al demonstrated elevated CD13 enzymatic activity in both bronchoalveolar lavage fluid and sera from patients with SSc compared with healthy controls.[11] Moreover, it was shown that blocking CD13 using monoclonal anti-CD13 antibodies inhibited skin fibroblast migration.[12]

We have previously demonstrated that sCD13 signals by binding to a bradykinin receptor.[9] Interestingly, an earlier study showed reduced levels of bradykinin receptors in SSc skin fibroblasts compared with healthy fibroblasts,[13] associated with impaired bradykinin-induced Ca^{2+} release and defective formation of inositol 1,4,5-trisphosphate.[14,15] Despite these intriguing observations, the role of sCD13 and B1R in SSc remains unknown. Notably, inhibiting CD13 using actinonin was shown to reduce chemokine secretion in the lung and mitigate silica-induced lung fibrosis.[16] Moreover, deletion or inactivation of B1R in mice reduced the severity of kidney fibrosis.[17–19] Taken together, these studies suggest that the sCD13/B1R signaling axis might play a pathogenic role in SSc, and its targeting might have the potential to treat SSc fibrosis. In this study, we sought to assess the role of the sCD13-B1R axis in SSc fibrosis, focusing on patient-derived dermal fibroblasts and a mouse model of skin fibrosis. Our results provide compelling evidence for a previously unsuspected pathogenic role for CD13 in SSc and identify the sCD13-B1R axis as a novel target for therapy.

MATERIALS AND METHODS

Animal model, histology, and analysis. All animal protocols were approved by the Institutional Animal Care & Use Committee at the University of Michigan. The *Cd13* and *Bdkrb1* knockout mice were obtained and bred as described in Tsou et al.[9] The bleomycin skin fibrosis model was performed as previously described.[20,21] Briefly, skin fibrosis in both C57BL/6 mice (Jackson Laboratory) and *Cd13* or *Bdkrb1* knockout mice was induced by intracutaneous injection of bleomycin (0.5 mg/mL in phosphate buffered saline [PBS], Hospira) in a defined area on the upper back daily for 2 weeks. PBS injections were used as negative controls. In experiments evaluating the antifibrotic properties of the B1R inhibitor SSR240612 in C57BL/6 mice, one group of mice received intracutaneous PBS injections alone, one group was challenged with bleomycin via intracutaneous injections on the back in conjunction with intraperitoneal (IP) injections of SSR240612 (2 mg/kg, Cayman Chemical), and the third group received bleomycin injections with IP injections of vehicle control (2.2% DMSO/97.8% PBS). After 2 weeks, skin tissues from the defined areas were harvested for histology, hydroxyproline analysis, and messenger RNA (mRNA) extraction. To evaluate the effect of B1R blockade in established fibrosis, in a separate experiment, fibrosis in C57BL/6 mice was induced first by repeated intracutaneous injections of bleomycin for 2 weeks followed by IP injections of SSR240612 (2 mg/kg) for another 2 weeks.

For histology, paraffin-embedded tissues were stained with hemtoxylin and eosin and Masson's trichrome. Dermal thickness was determined using ImageJ.[22] To measure monocytes and macrophages in the skin, immunofluorescence was performed after antigen retrieval using rat antimouse F4/80 (Thermo Fisher Scientific) antibody followed by Alexa Fluor 488–tagged antibodies (Thermo Fisher Scientific). The quantification of F4/80-positive cells was done using ImageJ. To measure hydroxyproline content in the skin, weighed skin sections were hydrolyzed in concentrated HCl at 120°C for 3 hours. A hydroxyproline analysis kit (Abcam) was then used to measure hydroxyproline. The resultant absorbance at 560 nm was assayed using a Synergy HT microplate reader. Tissue weight was used to normalize the hydroxyproline values, which are presented as μg/mg tissue weight.

Human subjects. All protocols involving human subjects were approved by the University of Michigan Institutional Review Board and performed upon obtaining written informed consents. Patients fulfilling the American College of Rheumatology classification for SSc[23] and age-, sex-, and ethnicity-matched healthy controls were recruited. Patient characteristics are summarized in Supplementary Table 1.

Cell culture. Punch biopsies were obtained from the dorsal forearm from all enrolled subjects. Dermal fibroblasts were isolated from skin biopsies from healthy volunteers and patients with diffuse cutaneous (dc) SSc as previously described.[20,21] Isolated dermal fibroblasts were cultured in RPMI1640 supplemented with 10% fetal bovine serum (FBS), L-glutamine, and antibiotics. Cells between passages 3 and 6 were used in all experiments. In some experiments, fibroblasts from healthy subjects were treated with 10 ng/mL transforming growth factor (TGF) β1 (Cell Signaling) for up to 72 hours in RPMI1640 with 1% FBS. Dermal fibroblasts from

patients with dcSSc were treated with various concentrations of sCD13 (R&D Systems) for 72 hours in the presence or absence of B1R inhibitor SSR240612 (Cayman Chemical). For signaling experiments, healthy or dcSSc dermal fibroblasts were serum starved overnight in RPMI1640 media with 1% FBS then incubated with 10 ng/mL TGFβ1 for 60 min, or 500 ng/mL of sCD13 for 25 min, with or without pretreatment of the cells with B1R inhibitor SSR240612 for 60 min. Knockdown of MMP14 or B1R in dermal fibroblasts was done by Accell siRNA reagents from Horizon Discovery (Cambridge, United Kingdom).

GEO, RNA, and single-cell transcriptome analysis. To determine the expression of the genes of interest, publicly available data sets (GEO GSE58095 and GSE130955) generated from skin biopsies of healthy controls and patients with SSc were analyzed. To quantitatively evaluate the expression of the genes of interest, real-time polymerase chain reaction was performed, as described.[24]

To examine the expression of ANPEP (gene encoding CD13), MMP14, and BDKRB1 at a single-cell scale, single-cell RNA sequencing (RNA-seq) results previously generated from skin biopsies from 18 healthy controls and 22 patients with early dcSSc[25,26] were analyzed.

Immunolabelling and immunofluorescence. After treatments, fibroblasts were fixed in formalin and blocked. The cells were then immunolabelled with antibodies to p-ERK1/2 (Cell Signaling Technology 4376S; clone 20G11) or phosphorylated SMAD2 (Cell Signaling Technology 18338S; clone E8F3R) followed by Alexa Fluor antibodies (Thermo Fisher Scientific). The slides were mounted with antifade mounting medium with DAPI (Thermo Fisher Scientific) and visualized under an Olympus microscope (Olympus, Tokyo, Japan).

Western blotting. Equal amounts of protein were separated by sodium dodecyl sulfate-polyacrylamide gel electrophoresis then transferred onto a nitrocellulose membrane. The blots were probed with antibodies against B1R (LS Bio; clone 3A2), collagen I (Abcam ab138492; clone EPR7785), or α smooth muscle actin (SMA) (Abcam ab5694). Antibodies against β-actin (Sigma-Aldrich A2066) or GAPDH (Cell Signaling Technology 2118; clone 14C10) were used as loading controls.

Myofibroblast functional analysis and sCD13 quantification. To evaluate the myofibroblast phenotype of dcSSc fibroblasts, the following endpoints were examined: cell proliferation, migration, and gel contraction, as previously described.[20] The sCD13 in culture media was quantified using the Human Aminopeptidase N/CD13 DuoSet Enzyme-Linked Immunosorbent Assay (R&D Systems).

Skin immunolabelling. Skin biopsies from patients with dcSSc and healthy volunteers were embedded in OCT compound, cryosectioned, and immunolabelled using either anti-human B1R (LSBio clone 3A2), anti–α-SMA (Abcam ab5694), anti-COL8A1 antibody (LSBio), or purified IgG (Thermo Fisher Scientific). Cryosections were incubated with Alexa Fluor secondary antibodies (Thermo Fisher Scientific) for 1 hour at 37°C. Sections were mounted with antifade mounting medium with DAPI (Thermo Fisher Scientific) and visualized under an Olympus microscope (Olympus, Tokyo, Japan).[9]

Statistical analysis. A normality test was first performed to determine the distribution of the data. To determine the differences between groups, Student's 2-tailed *t*-test, Mann-Whitney test, Kruskal-Wallis test, one-way analysis of variance, or two-way analysis of variance were performed using GraphPad Prism version 10 (GraphPad Software, Inc). The Pearson correlation coefficient was used for correlation analysis for gene expression and modified Rodnan skin score (mRSS) or forced vital capacity (percent predicted). *P* values of <0.05 were considered statistically significant. Unless specified, results were expressed as mean ± SD. The values underlying graphed data and reported means in this study are available from the corresponding authors upon request.

RESULTS

Mice lacking *Cd13* are protected from bleomycin-induced skin fibrosis. To test the effect of CD13 on skin fibrosis, we intracutaneously injected bleomycin or PBS into *Cd13*$^{-/-}$ and sex- and age-matched wildtype mice. After 2 weeks, *Cd13*$^{-/-}$ mice injected with bleomycin had reduced dermal thickness ($P < 0.001$) (Figure 1A and B) and skin hydroxyproline content ($P < 0.01$) (Figure 1B) compared with similarly treated wildtype mice. Because sCD13 induces monocyte migration by binding to B1R,[9] we measured monocyte/macrophage infiltration in the lesional skin. We found that *Cd13*$^{-/-}$ mice injected with bleomycin had lower numbers of F4/80-positive cells in the skin compared with wildtype mice ($P < 0.05$) (Figure 1C and Supplementary Figure 1A). We then investigated the effect of *Cd13* loss on the expression of fibrotic and inflammatory genes. In bleomycin-treated *Cd13*$^{-/-}$ mice, *Col1a1, Col8a1*, *Acta2, and Tgfb1* expression were decreased compared with wildtype mice injected with bleomycin, with *Col1a1, Col8a1*, and *Tgfb1* reaching statistical significance (Figure 1D). Moreover, *Ccl2* and *Il6* expression was significantly elevated in bleomycin-treated wildtype but not in *Cd13*$^{-/-}$ mice.

CD13, MMP14, and B1R are abundantly expressed in the skin. To characterize the sCD13 signaling axis in SSc, we analyzed a transcriptome data set (GEO GSE58095)[27] generated from skin biopsies. We found significantly higher expression levels of *ANPEP* ($P < 0.01$) and *MMP14* ($P < 0.05$) in SSc compared with healthy skin biopsies (Figure 2A). Furthermore, the expression of both *ANPEP* and *MMP14* significantly correlated with

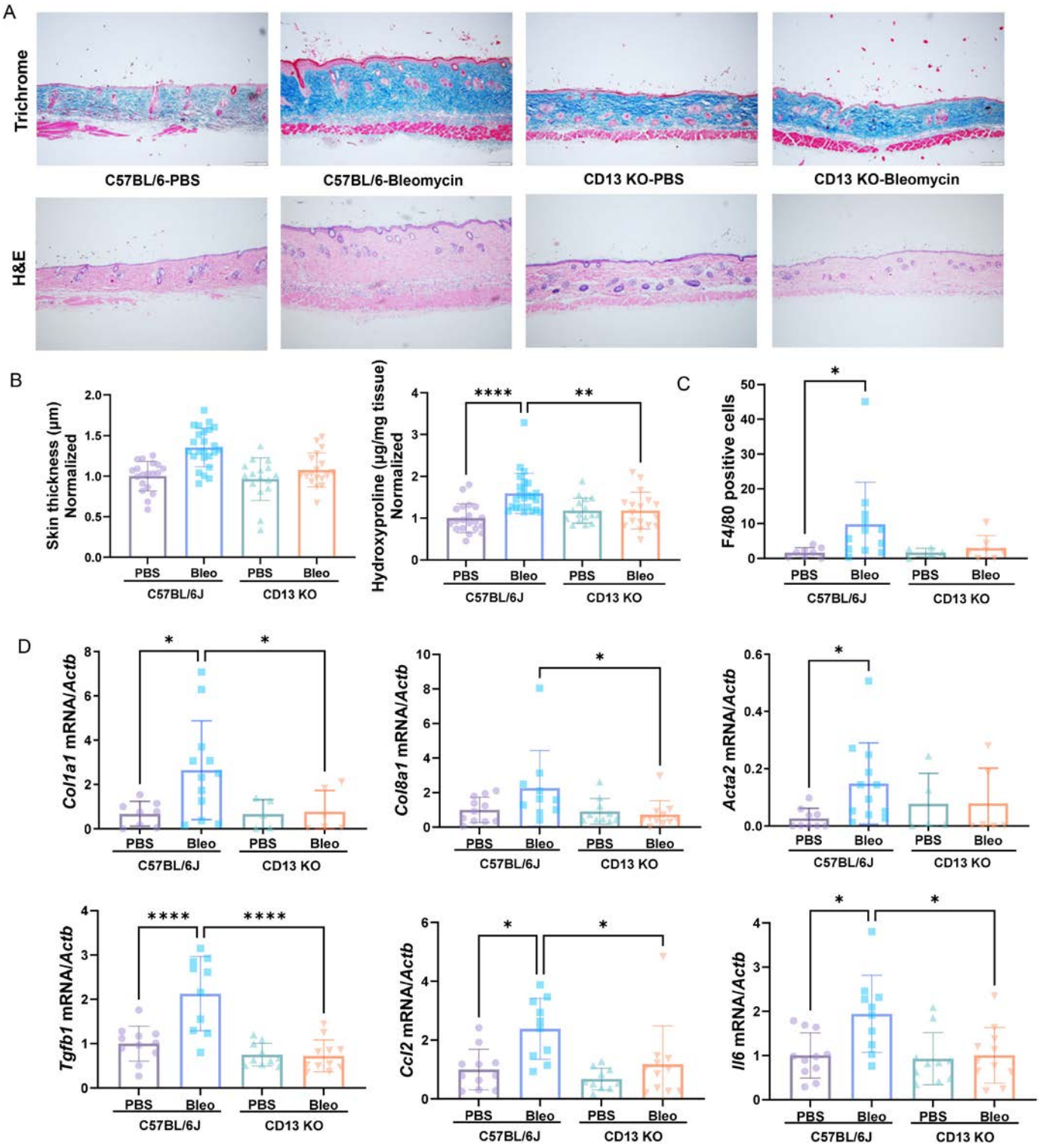

Figure 1. *Cd13* knockout mice are protected from bleomycin-induced skin fibrosis. (A and B) *Cd13*$^{-/-}$ mice injected with bleomycin showed less skin thickness than wildtype C57BL/6 mice injected with bleomycin ($P < 0.001$). Hydroxyproline content in skin tissues was significantly reduced in bleomycin-injected *Cd13*$^{-/-}$ mice compared with bleomycin-injected wildtype mice ($P < 0.01$). Original magnification ×10. (C) Significantly higher number of F4/80-positive monocytes/macrophages were present in skin sections of bleomycin-injected wildtype mice compared with PBS-injected mice ($P < 0.05$); this difference was not observed in *Cd13*$^{-/-}$ mice. (D) Bleomycin induced significant upregulation of fibrotic and pro-inflammatory genes in wildtype mice ($P < 0.05$), whereas in *Cd13*$^{-/-}$ mice bleomycin failed to increase these genes. Results are expressed as mean ± SD. *$P < 0.05$; **$P < 0.01$; ***$P < 0.001$; ****$P < 0.0001$. Significance was determined by (B-D) one-way analysis of variance or (D) Kruskal-Wallis test. Bleo, bleomycin; H&E, hemtoxylin and eosin; KO, knockout; mRNA, messenger RNA; PBS, phosphate buffered saline.

mRSS (Figure 2B). In contrast, *BDKRB1* expression was comparable between healthy and dcSSc skin biopsies and showed no significant correlation with mRSS (Figure 2A and B). In an independent SSc skin biopsy data set (GEO GSE130955),[28] we observed significant elevation of *MMP14* and *BDKRB1* expression in patients with SSc compared with healthy controls (Supplementary Figure 2A). However, the expression levels for the three genes examined did not corelate with mRSS. We noted that *BDKRB1* expression levels trended with mRSS at the site of the biopsy (Supplementary Figure 2B). Importantly, expression levels significantly correlated with forced vital capacity (percentage predicted).

To gain further insights into cell type–specific gene expression, single-cell analysis on skin biopsies from 22 patients with

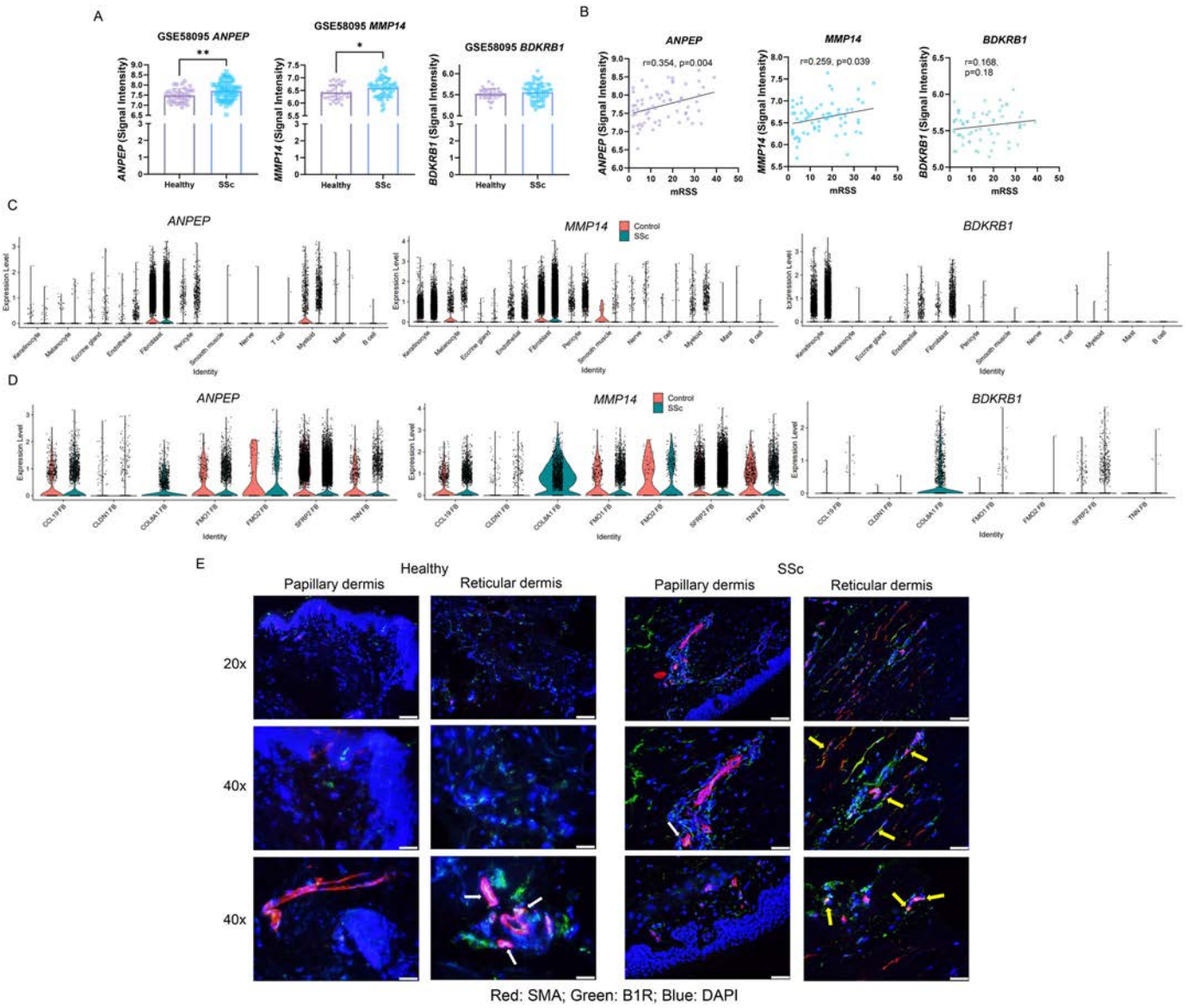

Figure 2. CD13, MMP14, and B1R are abundantly expressed in the skin. (A) Increased expression of *ANPEP* ($P < 0.01$) and *MMP14* ($P < 0.05$) was observed in skin biopsies from patients with SSc compared with healthy controls, and *BDKRB1* levels were similar in the two groups. Data were extracted from GEO GSE58095. (B) Analyzing the same GEO dataset, *ANPEP* and *MMP14* expression correlated significantly with modified Rodnan skin score (mRSS), and *BDKRB1* did not. (C) The expression of *ANPEP*, *MMP14*, and *BDKRB1* was observed in various cell types in the skin, analyzing single-cell RNA-seq results generated in 18 healthy controls and 22 patients with diffuse cutaneous SSc. (D) The expression of *ANPEP*, *MMP14*, and *BDKRB1* was observed in various fibroblast subsets. (E) Co-expression of B1R (green) and α-SMA (red) was observed in SSc skin mainly in the reticular dermis, whereas in healthy skin, B1R expression was low, with some staining in the blood vessels. White arrows point to blood vessels, and yellow arrows point to myofibroblasts. Original magnification ×20–40. Results are expressed as mean ± SD. $^{*}P < 0.05$; $^{**}P < 0.01$. Significance was determined by (A) unpaired *t*-test and (B) Pearson correlation. B1R, bradykinin receptor B1; MMP14, matrix metalloproteinase 14; SMA, smooth muscle actin; SSc, systemic sclerosis.

SSc and 18 healthy adults was performed. In this analysis, 12 distinct cell types were identified in the skin.[25,26] Remarkably, the expression of all three genes involved in the sCD13 signaling axis was elevated in multiple cell populations in SSc skin biopsies compared with healthy controls (Figure 2C). *ANPEP* was abundantly expressed on fibroblasts and myeloid cells and was also expressed on endothelial cells and pericytes. *MMP14* was expressed on various cell types, most abundantly on fibroblasts, keratinocytes, endothelial cells, and pericytes. *BDKRB1* was mainly expressed in keratinocytes, fibroblasts, and endothelial cells. Because we had previously noted multiple distinct subpopulations of fibroblasts in the skin,[26] we next sought to identify the expression of *ANPEP*, *MMP14*, and *BDKRB1* in fibroblast subpopulations (Figure 2D). *ANPEP* and *MMP14* were expressed in all seven fibroblast subpopulations identified in the skin, whereas the expression of *BDKRB1* was most abundantly expressed in *COL8A1*+ fibroblasts, a subpopulation exclusively seen in SSc biopsies,[26] and a low-level expression on the *SFRP2*+ subset. Furthermore, expression of all the genes in the identified fibroblast subsets was elevated in patients with SSc compared with controls. Importantly, *ANPEP*, *MMP14*, and *BDKRB1* were all highly expressed on SSc-exclusive myofibroblast *COL8A1*+ fibroblasts.

To validate the findings of the single-cell RNA-seq analysis, we immunolabelled B1R in skin biopsies. Because *BDKRB1* was abundantly expressed on myofibroblasts (Figure 2D), α-SMA, which is expressed by vascular smooth muscle cells and myofibroblasts, was also included. In skin biopsies from healthy controls, B1R expression was overall low and predominantly seen in dermal blood vessels (Figure 2E, white arrows). In sharp contrast, B1R expression was remarkably abundant in SSc skin compared with healthy skin, specifically in the reticular dermis (Figure 2E, yellow arrows). Although B1R was expressed in blood vessels, it was also frequently observed in α-SMA–positive myofibroblasts. Here we found that COL8A1 was expressed mainly in the blood vessels in normal skin but was abundantly expressed in SSc skin, in both blood vessels (white arrows) and myofibroblasts (yellow arrows, Supplementary Figure 3). Co-expression of B1R with α-SMA and COL8A1 in SSc skin biopsies suggests a functional relationship between myofibroblast differentiation and B1R expression.

We have previously demonstrated that MMP14 generates the soluble form of CD13 in fibroblast-like synoviocytes.[7] To determine whether similar CD13 cleavage also occurs in dermal fibroblasts, we performed MMP14 knockdown in dcSSc dermal fibroblasts and measured sCD13 levels in the culture media. The results showed that knocking down MMP14 in dcSSc fibroblasts significantly reduced sCD13 in the culture media (Supplementary Figure 4A). These results therefore indicate that MMP14 acts as the sheddase for sCD13 in skin fibroblasts similar to fibroblast-like synoviocytes.

To determine the expression of *ANPEP*, *MMP14*, and *BDKRB1* in explanted fibroblasts, we performed quantitative polymerase chain reaction and immunoblotting using fibroblasts isolated from skin biopsies of healthy controls and patients with dcSSc. We found that the expression of *BDKRB1* was significantly elevated in dcSSc fibroblasts compared with those of healthy controls ($P < 0.05$) (Figure 3A), whereas the expression of *ANPEP* and *MMP14* was comparable. Elevated protein levels of B1R in dcSSc dermal fibroblasts were also observed (Figure 3B).

Because TGFβ plays a key role in SSc fibrosis, we next sought to determine the effect of TGFβ1 on *ANPEP*, *MMP14*, and *BDKRB1* expression in normal fibroblasts. We found that *ANPEP* expression was significantly down-regulated by TGFβ1 (Figure 3C). In contrast, *MMP14* and *BDKRB1* were up-regulated by TGFβ1, as early as 6 hours for *BDKRB1*. Next, we determined the effect of TGFβ1 on the secretion of CD13. sCD13 released from TGFβ1-treated dcSSc fibroblasts, as measured in the culture media, was significantly higher compared with cells from healthy controls (Figure 3D). These results suggest that TGFβ1, an essential cytokine in this disease, upregulates sCD13 and B1R in SSc dermal fibroblasts.

Blockade of sCD13 by B1R inhibition or knockdown alleviates myofibroblast phenotypes and signaling in dcSSc fibroblasts. Next, we examined how sCD13 and B1R affect the phenotype of SSc fibroblasts. We investigated whether sCD13 and the B1R inhibitor SSR240612 affected fibrotic genes, including *COL1A1* and *ACTA2*. sCD13 increased *COL1A1* and *ACTA2* expression and protein production in dcSSc fibroblasts in a dose-dependent manner. The inhibition of B1R by SSR240612 down-regulated both gene expression and protein levels (Figure 4A and B). Furthermore, we observed that cell proliferation was promoted by sCD13 in a dose-dependent manner and significantly suppressed by the addition of higher concentrations of SSR240612 (Figure 4C). Gel contraction by myofibroblasts was enhanced in dcSSc compared with healthy controls.[29] We determined that gel contraction was enhanced by sCD13 in dcSSc fibroblasts and inhibited by SSR240612 (Figure 4D). Consistent with these results, fibroblast migration was enhanced by sCD13 and inhibited by SSR240612 (Figure 4E).

We had previously shown that sCD13 induces the phosphorylation of ERK1/2 in various cell types.[9] Therefore, we next investigated whether sCD13 similarly activates this signaling pathway in SSc dermal fibroblasts. Immunolabelling and immunofluorescence showed that sCD13 stimulation of SSc fibroblasts led to significant phosphorylation of ERK1/2, which could be blocked by pretreatment with the B1R inhibitor SSR240612 (Figure 4F). Notably, sCD13 treatment also induced phosphorylation of SMAD2 in dcSSc fibroblasts, and this effect was also inhibited by B1R blockade (Figure 4G). Furthermore, in a separate series of experiments, we noted that sCD13 failed to stimulate expression of *COL1A1* and *ACTA2* in dcSSc dermal fibroblasts with

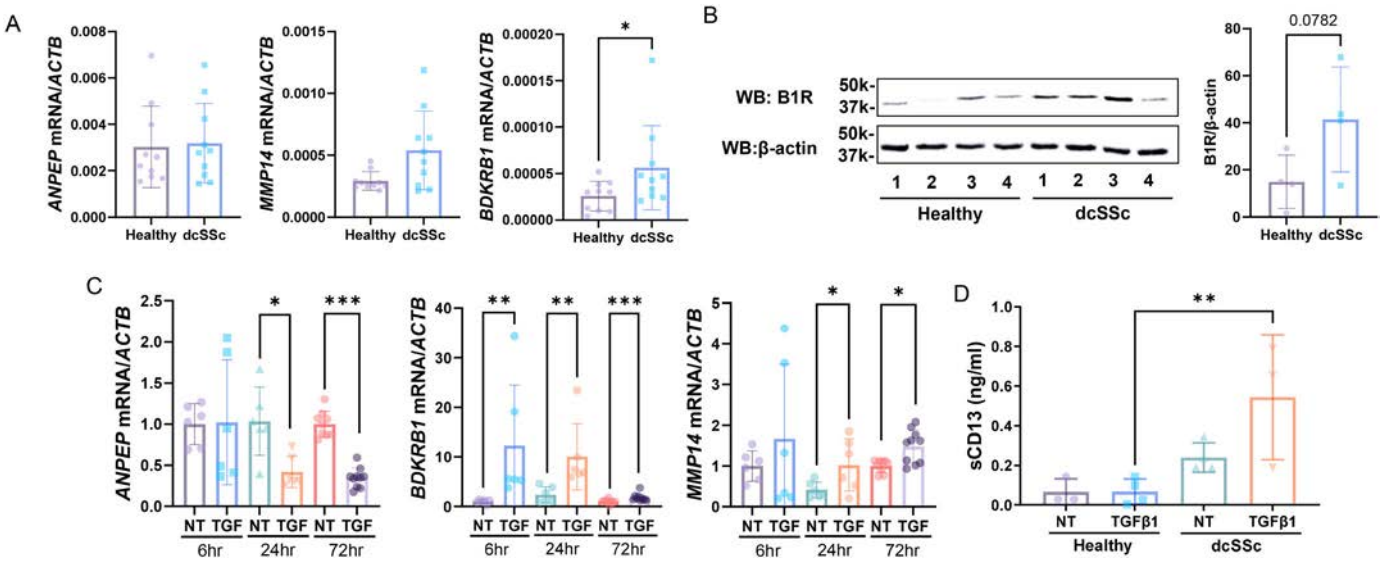

Figure 3. CD13, MMP14, and B1R are increased in dermal fibroblasts isolated from patients with dcSSc. (A) In cultured dcSSc dermal fibroblasts, increased expression of *BDKRB1* was detected compared with that from healthy controls ($P < 0.05$), whereas *ANPEP* and *MMP14* levels were similar. (B) Increased B1R levels were shown in dermal fibroblasts from patients with dcSSc compared with healthy controls. (C) TGFβ suppressed the expression of *ANPEP* and increased *MMP14* and *BDKRB1* mRNA in fibroblasts isolated from healthy controls. (D) TGFβ increased sCD13 levels in culture media from dcSSc dermal fibroblasts compared with those of healthy controls. Results are expressed as mean ± SD. *$P < 0.05$; **$P < 0.01$; ***$P < 0.001$. Significance was determined by (A-B) unpaired *t*-test, (C) Mann-Whitney test, and (D) one-way analysis of variance. B1R, bradykinin receptor B1; dcSSc, diffuse cutaneous systemic sclerosis; MMP14, matrix metalloproteinase 14; mRNA, messenger RNA; NT, Not-treated; sCD13, soluble CD13; TGFβ, transforming growth factor β; WB, Western blot.

B1R knockdown (Figure 4H and Supplementary Figure 4B), and this effect was consistent at the protein level as well (Figure 4I). These results suggest that the B1R blockade ameliorates a myofibroblast phenotype that is exacerbated by sCD13.

B1R inhibition mitigates the pro-fibrotic effects of TGFβ1 in healthy dermal fibroblasts. Treatment with TGFβ1 stimulates the expression of both sCD13 and its receptor B1R in SSc dermal fibroblasts. Therefore, we next sought to determine if B1R inhibition could counteract the pro-fibrotic effects of TGFβ1. Treatment of healthy dermal fibroblasts with TGFβ1 induced robust fibrotic gene expression at both the mRNA and protein levels; however, in the presence of the B1R inhibitor SSR240612, the TGFβ1 induction of these genes was substantially attenuated (Figure 5A and B). Notably, SSR240612 significantly blocked TGFβ1-induced sCD13 secretion from healthy dermal fibroblasts (Figure 5C). Moreover, B1R inhibition significantly prevented TGFβ1-induced cell proliferation and migration in these fibroblasts (Figure 5D and E). B1R inhibition with SSR240612 also blocked the TGFβ1-induced phosphorylation of SMAD2 (Figure 5F).

B1R blockade in mice attenuates bleomycin-induced skin fibrosis. To further determine whether B1R is a potential therapeutic target for SSc fibrosis, we evaluated the anti-fibrotic efficacy of B1R inhibitor SSR240612 in a bleomycin skin fibrosis mice model. In the prevention model in which B1R inhibition was initiated concurrently with the start of bleomycin injections, we noted that SSR240612 significantly attenuated bleomycin-induced skin thickness, including fibrotic area, and reduced skin hydroxyproline content (Figure 6A and B). We also observed that the number of F4/80-positive monocytes/macrophages in the skin was promoted by injection of bleomycin and significantly suppressed by SSR240612 (Figure 6C and Supplementary Figure 1B). The expression of fibrotic genes, including *Col1a1*, *Col8a1*, *Acta2*, and *Tgfb1* was up-regulated by bleomycin and significantly down-regulated by treatment with SSR240612 (Figure 6D). Similar results were observed for inflammatory genes *Ccl2* and *Il6*. Comparable results were observed in the therapeutic model, in which fibrosis was first established before administering the B1R inhibitor, with reductions in dermal thickness and hydroxyproline content (Figure 6E and F).

To confirm the role of B1R in bleomycin-induced fibrosis, we used *Bdkrb1* knockout mice. Consistent with the findings from SSR240612 treatment, *Bdkrb1* knockout mice exhibited reduced bleomycin-induced skin thickness and lower hydroxyproline levels (Figure 6G and H). In addition, *Bdkrb1* knockout mice injected with bleomycin had lower numbers of F4/80-positive cells in the skin compared with wildtype mice injected with bleomycin (Figure 6I and Supplementary Figure 1C). And finally, fibrotic genes, including *Col1a1*, *Col8a1*, *Acta2*, and *Tgfb1*, as well as inflammatory genes *Ccl2* and *Il6* were significantly lower in

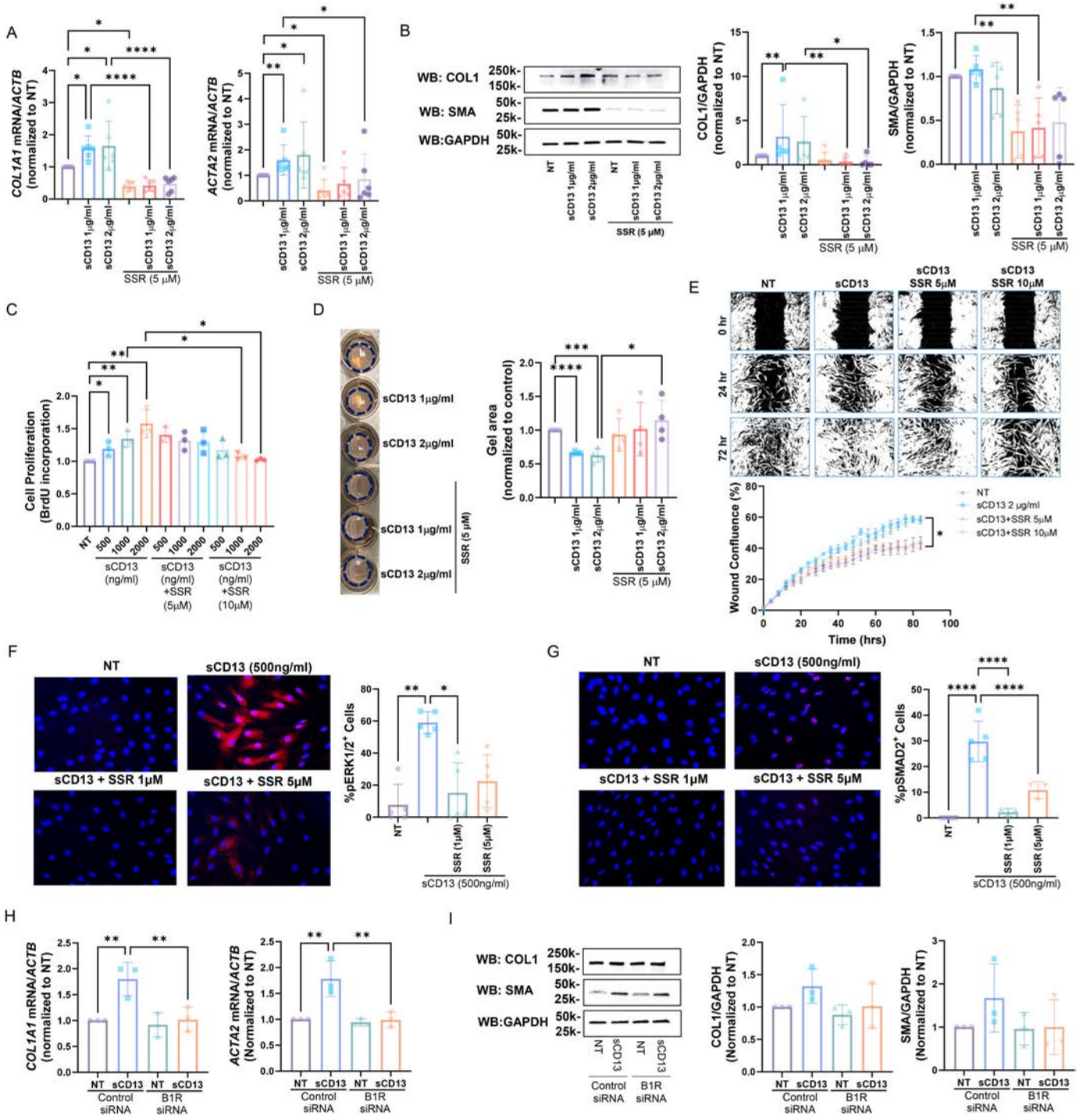

Figure 4. sCD13 and B1R promote myofibroblast phenotypes and signaling in dcSSc fibroblasts. (A and B) B1R inhibitor SSR240612 suppressed sCD13-induced both mRNA and protein levels of COL1 and α-SMA in dcSSc fibroblasts. (C–E) SSR240612 inhibited sCD13-induced cell proliferation, gel contraction, and migration of dcSSc fibroblasts ($P < 0.05$). (F–G) sCD13 induced phosphorylation of ERK1/2 (red) or SMAD2 (red) in dcSSc fibroblasts, which were blocked by SSR240612 ($P < 0.05$). Results were presented as the percentage of red-positive cells/DAPI-stained nucleus. (H and I) B1R knockdown suppressed sCD13-induced fibrotic genes in dcSSc fibroblasts. Results are expressed as mean ± SD or (E) mean ± SEM. *$P < 0.05$; **$P < 0.01$; ***$P < 0.001$; ****$P < 0.0001$. Significance was determined by (A–D, F) Kruskal-Wallis test, (G–I) one-way analysis of variance, and (E) two-way analysis of variance. B1R, bradykinin receptor B1; dcSSc, diffuse cutaneous systemic sclerosis; mRNA, messenger RNA; NT, not-treated; sCD13, soluble CD13; siRNA, small interfering RNA; SMA, smooth muscle actin; SSR, SSR240612; WB, Western blot.

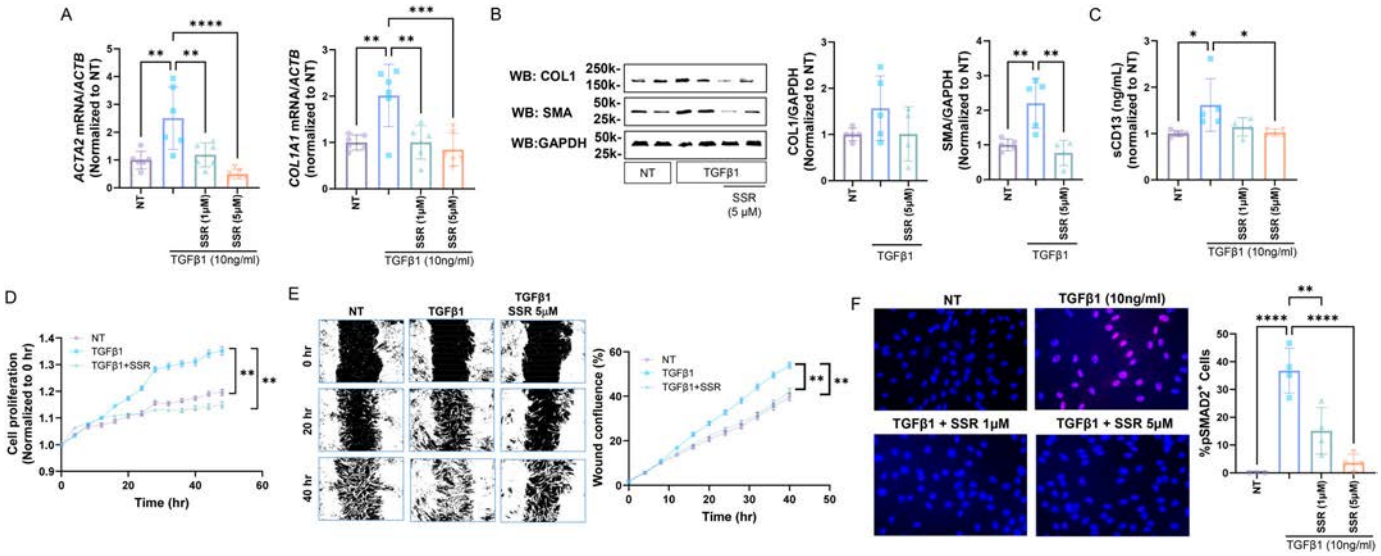

Figure 5. B1R inhibition alleviates the pro-fibrotic effects of TGFβ1 in dcSSc fibroblasts. (A and B) B1R inhibitor SSR240612 suppressed TGFβ1 induced both mRNA and protein levels of COL1 and α-SMA in dcSSc fibroblasts. (C) SSR240612 inhibited TGFβ-induced sCD13 shedding in dcSSc fibroblasts ($P < 0.05$). (D and E) TGFβ1-induced cell proliferation and migration was blocked by B1R inhibitor SSR240612 ($P < 0.05$). (F) TGFβ1-induced phosphorylation of SMAD2 (red) in dcSSc fibroblasts was blocked by SSR240612 ($P < 0.05$). Results are expressed as mean ± SD or (D and E) mean ± SEM. *$P < 0.05$; **$P < 0.01$; ***$P < 0.001$; ****$P < 0.0001$. Significance was determined by (A–C, F) one-way analysis of variance and (D and E) two-way analysis of variance. B1R, bradykinin receptor B1; dcSSc, diffuse cutaneous systemic sclerosis; mRNA, messenger RNA; NT, not-treated; sCD13, soluble CD13; SMA, smooth muscle actin; SSR, SSR240612; TGFβ, transforming growth factor β; WB, Western blot.

bleomycin-treated *Bdkrb1* knockout mice compared with bleomycin-treated wildtype mice (Figure 6J).

DISCUSSION

In this study, we sought to determine the expression and role of the widely expressed aminopeptidase CD13 in SSc. CD13 is increasingly implicated in inflammatory diseases and promotes inflammatory cell adhesion, migration, and aggregation.[4] Previous studies have demonstrated important roles for CD13 in rheumatoid arthritis, psoriasis, and connective tissue diseases.[11,30,31] We showed that MMP14 cleaves off the soluble form of CD13 from the cell surface.[7] Significantly, using a series of orthogonal experimental approaches, we recently identified B1R as the cellular receptor for sCD13.[9] These observations highlight the significance of the sCD13-B1R signaling axis in the pathogenesis of multiple inflammatory conditions. In the present study, we demonstrated, for the first time, the importance of this pathway in SSc by showing the antifibrotic efficacy of B1R blockade in vitro and in vivo, complemented with the demonstration that mice lacking either *Cd13* or *Bdkrb1* were protected from bleomycin-induced skin fibrosis. We believe that these results identify a novel and promising therapeutic target for SSc fibrosis.

We found abundant expression of *ANPEP*, *MMP14*, and *BDKRB1* in SSc skin as well as in isolated dermal fibroblasts. According to our single-cell RNA-seq analysis, *ANPEP* was highly expressed on fibroblasts and myeloid cells, whereas *MMP14* was widely expressed on various cell types (Figures 2 and 3). Interestingly, *BDKRB1* was highly expressed on *COL8A1*+ fibroblasts. This subset is the myofibroblast cluster observed exclusively in dcSSc skin.[25,26] Indeed, we confirmed in SSc skin that B1R is expressed mainly on myofibroblasts in the deep dermis and that its expression is also significantly elevated in isolated SSc dermal fibroblasts. This could possibly explain the discrepancy we found regarding *BDKRB1* expression in whole-skin biopsies and dermal fibroblasts (Figure 2 and 3). It could also explain why *BDKRB1* expression does not correlate with skin score, whereas *ANPEP* and *MMP14* correlate significantly in the GEO data analysis (Figure 2B). Nonetheless, the consistent observation that B1R is highly expressed on SSc-specific myofibroblasts, and that CD13 and MMP14 are expressed in the skin, suggest that sCD13, which is shed by MMP14 in SSc skin, acts on myofibroblasts via B1R locally. This notion supports our findings that sCD13 is significantly more abundant in supernatants from SSc fibroblast cultures compared with healthy fibroblasts (Figure 3D).

We further demonstrated that sCD13-treated SSc fibroblasts exhibited characteristic myofibroblast features, and myofibroblast transition by sCD13 could be suppressed by a B1R antagonist (Figure 4). Notably, B1R inhibition also blocked the pro-fibrotic effects of TGFβ1 in healthy dermal fibroblasts (Figure 5). Furthermore, mice null of Cd13 or B1R, or wildtype mice treated with SSR240612, were protected from bleomycin-

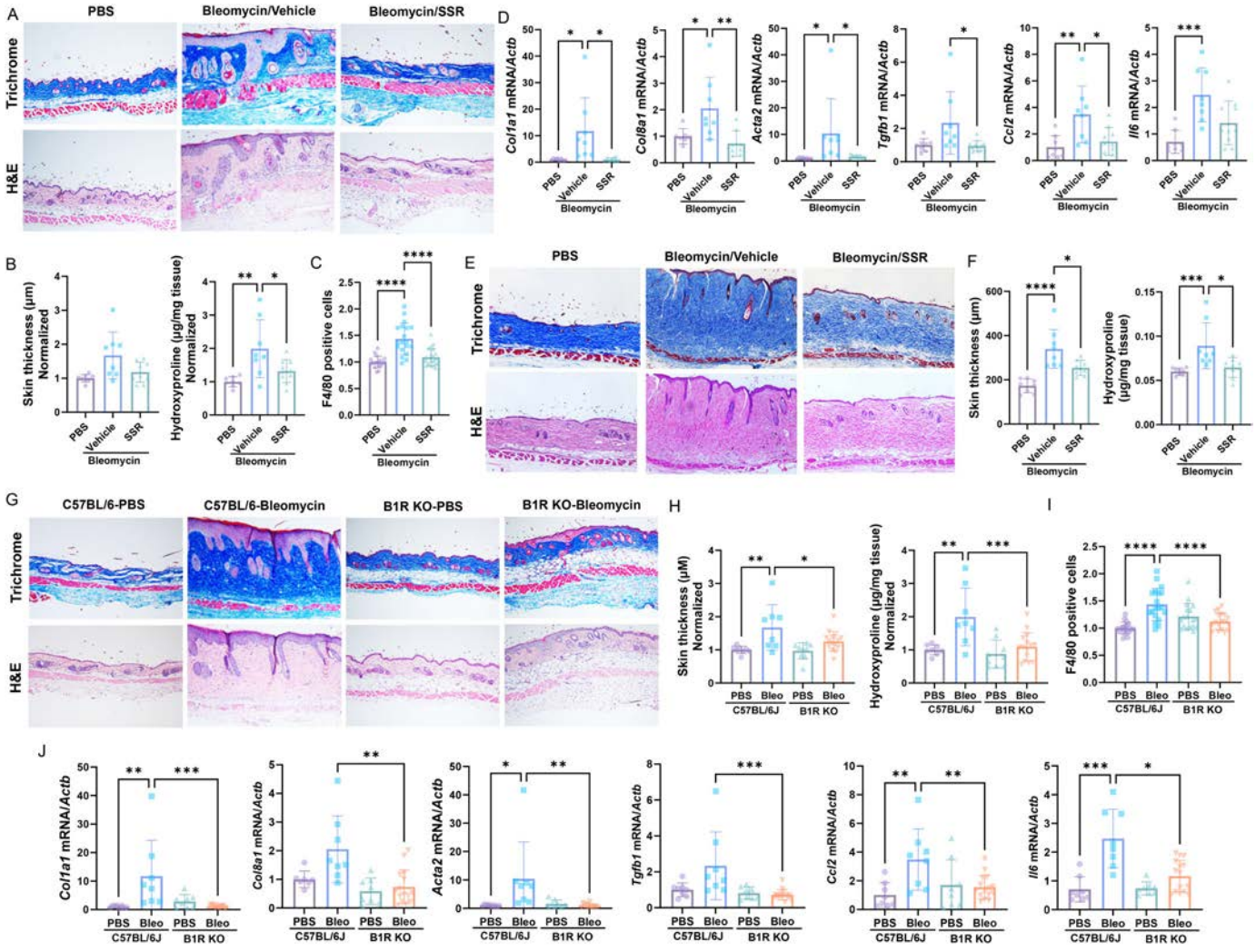

Figure 6. B1R blockade in mice attenuates bleomycin-induced skin fibrosis. (A and B) B1R inhibitor SSR240612 attenuated bleomycin-induced skin thickness and hydroxyproline content ($P < 0.05$) in wildtype C57BL/6 mice in the prevention model. (C) SSR240612 reduced bleomycin-induced F4/80 positive cells in skin tissue ($P < 0.0001$). (D) SSR240612 decreased bleomycin-induced expression of pro-fibrotic and pro-inflammatory genes in mice skin ($P < 0.05$). (E and F) Significant fibrosis was established by bleomycin injection in mice for 2 weeks, and SSR240612 treatment for the following 2 weeks blocked skin fibrosis significantly. (G and H) Bleomycin-induced skin fibrosis was less prominent in B1R knockout mice compared with wildtype mice as shown by significant reduction in skin thickness and hydroxyproline content ($P < 0.05$). (I) B1R knockout mice showed fewer F4/80-positive cells in the skin compared with wildtype mice injected with bleomycin ($P < 0.0001$). (J) B1R knockout mice showed lower levels of bleomycin-induced fibrotic and inflammatory genes in the skin compared with wildtype mice. Original magnification ×10. Results are expressed as mean ± SD. $^{*}P < 0.05$; $^{**}P < 0.01$; $^{***}P < 0.001$; $^{****}P < 0.0001$. Significance was determined by (B–D, F, H–J) one-way analysis of variance and (D, F, J) Kruskal-Wallis test. B1R, bradykinin receptor B1; Bleo, bleomycin; H&E, hemtoxylin and eosin; KO, knockout; mRNA, messenger RNA; PBS, phosphate buffered saline; SSR, SSR240612.

induced skin fibrosis, including attenuated induction of *Col8a1* and pro-inflammatory genes, indicating that the sCD13-B1R axis plays a pivotal role in SSc fibrosis and could be a potential therapeutic target.

In the present study, we showed that B1R is abundant in dcSSc skin, specifically in myofibroblasts. We further demonstrated that this elevation is mediated, at least in part, by TGFβ1. Although TGFβ1 down-regulated CD13 at the transcriptional level (Figure 3C), we showed that TGFβ1 significantly promoted sCD13 release from dcSSc fibroblasts. This could be mediated by the significant increase of *MMP14* observed in various stromal cell populations in dcSSc skin, including various fibroblast subsets (Figure 2D). The upregulation of MMP14 also appears to be TGFβ1-dependent (Figure 3C). We also confirmed that MMP14 is the sheddase for generating sCD13 in dermal fibroblasts (Supplementary Figure 4A).

Because sCD13 activates the ERK signaling pathway via B1R,[8,9] we posit that the pro-fibrotic effect of the sCD13-B1R axis could also be mediated via the ERK pathway. Indeed, we showed that sCD13 induced significant ERK1/2 phosphorylation

in dcSSc dermal fibroblasts (Figure 4F). There is growing evidence that ERK1/2 is involved in fibrosis in SSc. In fact, ERK1/2 has been documented to be involved in fibroblast proliferation,[32] and IL11-dependent ERK1/2 signaling is required for TGFβ to induce a pro-fibrotic response in dermal fibroblasts.[33] Interestingly, PTP4A1 is reported to be a key promoter of TGFβ signaling in primary skin fibroblasts and bleomycin-induced fibrosis in vivo.[34] PTP4A1 promotes TGFβ signaling in human fibroblasts through enhanced ERK1/2 activity, which stimulates SMAD3 expression and nuclear migration. These findings support the possibility that the pro-fibrotic effect of sCD13 is mediated in part by activating ERK1/2 in fibroblasts.

There are some limitations of this study. Although our goal is to treat systemic fibrosis in SSc, we focused exclusively on skin fibrosis in this study. Interestingly, B1R expression in various lung diseases has been reported.[35,36] Further investigation is needed to assess the effect of inhibition of sCD13-B1R in other organs or fibrotic conditions. Second, we only focused on specimens from patients with dcSSc. Because B1R expression depends highly on stimuli such as TGFβ1, the expression pattern of this receptor on other SSc disease subtypes requires further examination. B1R could be a potential target for precision medicine approaches for this disease.

Based on our findings, the role of the sCD13-B1R axis in dcSSc skin lesions is depicted in Supplementary Figure 5. CD13 is distributed mainly in myeloid cells and fibroblasts in SSc skin. MMP14 is widely expressed in the skin, including keratinocytes, endothelial cells, and fibroblasts, and serves to cleave CD13 off from cell membranes. B1R is specifically expressed on both *SFRP2*+ and *COL8A1*+ fibroblasts. Interestingly, from our pseudotime analysis there is evidence that the *SFRP2*+ fibroblasts differentiate into the *COL8A1*+ fibroblasts.[26] Therefore, it is possible that the sCD13-B1R pathway on these cells promotes and maintains myofibroblast differentiation in the deep dermis. Furthermore, suppression of B1R may indirectly inhibit myofibroblast transformation by suppressing the migration of monocytes or macrophages to the cutaneous loci. We have previously shown that sCD13 induces angiogenesis in endothelial cells.[8] Because B1R is expressed on SSc endothelial cells, yet angiogenesis is impaired in SSc, this apparent disconnection requires further investigation and may reflect abnormal responses to angiogenic stimuli in SSc endothelial cells. Taken together, our results provide evidence that sCD13 is involved in skin fibrosis via B1R by promoting myofibroblast transformation and that the blockade of the sCD13-B1R axis warrants evaluation as a potential therapeutic option for SSc fibrosis.

AUTHOR CONTRIBUTIONS

All authors contributed to at least one of the following manuscript preparation roles: conceptualization AND/OR methodology, software, investigation, formal analysis, data curation, visualization, and validation AND drafting or reviewing/editing the final draft. As corresponding authors, Drs Fox and Tsou confirm that all authors have provided the final approval of the version to be published, and take responsibility for the affirmations regarding article submission (eg, not under consideration by another journal), the integrity of the data presented, and the statements regarding compliance with institutional review board/Helsinki Declaration requirements.

REFERENCES

1. Allanore Y, Simms R, Distler O, et al. Systemic sclerosis. Nat Rev Dis Primers 2015;1(1):15002.
2. Bhattacharyya S, Wei J, Varga J. Understanding fibrosis in systemic sclerosis: shifting paradigms, emerging opportunities. Nat Rev Rheumatol 2011;8(1):42–54.
3. Volkmann ER, Varga J. Emerging targets of disease-modifying therapy for systemic sclerosis. Nat Rev Rheumatol 2019;15(4):208–224.
4. Lu C, Amin MA, Fox DA. CD13/aminopeptidase N is a potential therapeutic target for inflammatory disorders. J Immunol 2020;204(1):3–11.
5. Mina-Osorio P. The moonlighting enzyme CD13: old and new functions to target. Trends Mol Med 2008;14(8):361–371.
6. Morgan R, Endres J, Behbahani-Nejad N, et al. Expression and function of aminopeptidase N/CD13 produced by fibroblast-like synoviocytes in rheumatoid arthritis: role of CD13 in chemotaxis of cytokine-activated T cells independent of enzymatic activity. Arthritis Rheumatol 2015;67(1):74–85.
7. Morgan RL, Behbahani-Nejad N, Endres J, et al. Localization, shedding, regulation and function of aminopeptidase N/CD13 on fibroblast like synoviocytes. PLoS One 2016;11(9):e0162008.
8. Du Y, Lu C, Morgan RL, et al. Angiogenic and arthritogenic properties of the soluble form of CD13. J Immunol 2019;203(2):360–369.
9. Tsou PS, Lu C, Gurrea-Rubio M, et al. Soluble CD13 induces inflammatory arthritis by activating the bradykinin receptor B1. J Clin Invest 2022;132(11):132.
10. Bou-Gharios G, Osman J, Atherton A, et al. Expression of ectopeptidases in scleroderma. Ann Rheum Dis 1995;54(2):111–116.
11. Dan H, Tani K, Hase K, et al. CD13/aminopeptidase N in collagen vascular diseases. Rheumatol Int 2003;23(6):271–276.
12. Lai A, Ghaffari A, Ghahary A. Inhibitory effect of anti-aminopeptidase N/CD13 antibodies on fibroblast migration. Mol Cell Biochem 2010;343(1-2):191–199.
13. Ozeki T, Osada K, Seishima M, et al. Decreased bradykinin binding sites in fibroblasts from progressive systemic scleroderma. Arch Dermatol Res 1994;286(3-4):133–136.
14. Seishima M, Kudo Y, Nagao S, et al. Alterations in intracellular calcium transients of fibroblasts from progressive systemic sclerotic patients: a digital imaging microscopic study. Arch Dermatol Res 1991;283(2):96–99.
15. Seishima M, Yada Y, Nagao S, et al. Defective formation of inositol 1,4,5-trisphosphate in bradykinin-stimulated fibroblasts from progressive systemic sclerotic patients. Biochem Biophys Res Commun 1988;156(3):1077–1082.
16. Kühlmann UC, Chwieralski CE, van den Brule S, et al. Modulation of cytokine production and silica-induced lung fibrosis by inhibitors of aminopeptidase N and of dipeptidyl peptidase-IV-related proteases. Life Sci 2009;84(1-2):1–11.
17. Wang PH, Cenedeze MA, Campanholle G, et al. Deletion of bradykinin B1 receptor reduces renal fibrosis. Int Immunopharmacol 2009;9(6):653–657.
18. Huart A, Klein J, Gonzalez J, et al. Kinin B1 receptor antagonism is equally efficient as angiotensin receptor 1 antagonism in reducing renal fibrosis in experimental obstructive nephropathy, but is not additive. Front Pharmacol 2015;6:8.

19. Klein J, Gonzalez J, Duchene J, et al. Delayed blockade of the kinin B1 receptor reduces renal inflammation and fibrosis in obstructive nephropathy. FASEB J 2009;23(1):134–142.
20. Vichaikul S, Gurrea-Rubio M, Amin MA, et al. Inhibition of bromodomain extraterminal histone readers alleviates skin fibrosis in experimental models of scleroderma. JCI Insight 2022;7(9):7.
21. Tsou PS, Campbell P, Amin MA, et al. Inhibition of EZH2 prevents fibrosis and restores normal angiogenesis in scleroderma. Proc Natl Acad Sci USA 2019;116(9):3695–3702.
22. Schneider CA, Rasband WS, Eliceiri KW. NIH image to ImageJ: 25 years of image analysis. Nat Methods 2012;9(7):671–675.
23. van den Hoogen F, Khanna D, Fransen J, et al. 2013 classification criteria for systemic sclerosis: an American College of Rheumatology/European League Against Rheumatism collaborative initiative. Ann Rheum Dis 2013;72(11):1747–1755.
24. Tsou PS, Palisoc PJ, Ali M, et al. Genome-wide reduction in chromatin accessibility and unique transcription factor footprints in endothelial cells and fibroblasts in scleroderma skin. Arthritis Rheumatol 2021;73(8):1501–1513.
25. Shi B, Tsou PS, Ma F, et al. Senescent cells accumulate in systemic sclerosis skin. J Invest Dermatol 2023;143(4):661–664.e5.
26. Ma F, Tsou PS, Gharaee-Kermani M, et al. Systems-based identification of the Hippo pathway for promoting fibrotic mesenchymal differentiation in systemic sclerosis. Nat Commun 2024;15(1):210.
27. Assassi S, Swindell WR, Wu M, et al. Dissecting the heterogeneity of skin gene expression patterns in systemic sclerosis. Arthritis Rheumatol 2015;67(11):3016–3026.
28. Skaug B, Khanna D, Swindell WR, et al. Global skin gene expression analysis of early diffuse cutaneous systemic sclerosis shows a prominent innate and adaptive inflammatory profile. Ann Rheum Dis 2020;79(3):379–386.
29. Shiwen X, Stratton R, Nikitorowicz-Buniak J, et al. A role of myocardin related transcription factor-a (MRTF-A) in scleroderma related fibrosis. PLoS One 2015;10(5):e0126015.
30. Shimizu T, Tani K, Hase K, et al. CD13/aminopeptidase N-induced lymphocyte involvement in inflamed joints of patients with rheumatoid arthritis. Arthritis Rheum 2002;46(9):2330–2338.
31. Thielitz A, Ansorge S, Bank U, et al. The ectopeptidases dipeptidyl peptidase IV (DP IV) and aminopeptidase N (APN) and their related enzymes as possible targets in the treatment of skin diseases. Front Biosci 2008;13(13):2364–2375.
32. Ihn H, Tamaki K. Oncostatin M stimulates the growth of dermal fibroblasts via a mitogen-activated protein kinase-dependent pathway. J Immunol 2000;165(4):2149–2155.
33. Adami E, Viswanathan S, Widjaja AA, et al. IL11 is elevated in systemic sclerosis and IL11-dependent ERK signalling underlies TGFβ-mediated activation of dermal fibroblasts. Rheumatology (Oxford) 2021;60(12):5820–5826.
34. Sacchetti C, Bai Y, Stanford SM, et al. PTP4A1 promotes TGFβ signaling and fibrosis in systemic sclerosis. Nat Commun 2017;8(1):1060.
35. Tidjane N, Hachem A, Zaid Y, et al. A primary role for kinin B1 receptor in inflammation, organ damage, and lethal thrombosis in a rat model of septic shock in diabetes. Eur J Inflamm 2015;13(1):40–52.
36. Phagoo SB, Reddi K, Silvallana BJ, et al. Infection-induced kinin B1 receptors in human pulmonary fibroblasts: role of intact pathogens and p38 mitogen-activated protein kinase-dependent signaling. J Pharmacol Exp Ther 2005;313(3):1231–1238.

Arthritis & Rheumatology
Vol. 77, No. 1, January 2025, pp 92–98
DOI 10.1002/art.42979

American College of Rheumatology
Empowering Rheumatology Professionals

BRIEF REPORT

Mutual Amplification of GLI2/Hedgehog and Transcription Factor JUN/AP-1 Signaling in Fibroblasts in Systemic Sclerosis: Potential Implications for Combined Therapies

Christina Bergmann,[1] Sara Chenguiti Fakhouri,[1] Thuong Trinh-Minh,[2] Tim Filla,[2] Aleix Rius Rigau,[1] Arif B. Ekici,[3] Benita Merlevede,[1] Ludwig Hallenberger,[1] Honglin Zhu,[4] Clara Dees,[1] Alexandru-Emil Matei,[2] Janina Auth,[1] Andrea-Hermina Györfi,[2] Xiang Zhou,[2] Simon Rauber,[1] Aline Bozec,[1] Nicholas Dickel,[5] Chunguang Liang,[5] Meik Kunz,[6] Georg Schett,[1] and Jörg H.W. Distler[2]

Objective. Deregulation of the cJUN/AP-1 and hedgehog/GLI2 signaling pathways has been implicated in fibroblast activation in systemic sclerosis (SSc). However, the consequences of their concomitant up-regulation are unknown. Here, we tested the hypothesis that mutual amplification of both pathways might drive persistent fibroblast activation.

Methods. Cultured fibroblasts and skin sections of patients with diffuse SSc and healthy volunteers were analyzed. cJUN/AP-1 signaling and hedgehog/GLI2 signaling were inhibited using knockdown and pharmacologic approaches. Hedgehog signaling was activated in mice by fibroblast-specific overexpression of constitutively active Smoothened.

Results. cJUN and GLI2 are concomitantly up-regulated and colocalize in fibroblasts of patients with SSc compared to healthy controls. Activation of hedgehog/GLI2 signaling induces the expression of cJUN in vitro and in vivo, whereas inactivation of GLI2 inhibits cJUN expression. Likewise, inactivation of cJUN impairs the expression of GLI2. This mutual regulation occurs at the level of transcription with binding of cJUN and GLI2 to specific binding motifs. Interference with this mutual amplification of cJUN signaling and GLI2 signaling inhibits fibroblast activation and collagen release: Inhibition of cJUN/AP-1 signaling ameliorates hedgehog-induced fibroblast activation and skin fibrosis in Smo^{ACT} mice with a reduction of skin thickness of 103% (P = 0.0043) in the treatment group compared to the fibrotic control group. Moreover, combined pharmacologic inhibition of cJUN/AP-1 and hedgehog/GLI2 exerts additive antifibrotic effects in a model of TGFβ-driven experimental fibrosis (TBR^{ACT} mice).

Conclusion. The transcription factors cJUN and GLI2 reinforce each other's activity to promote fibroblast activation in SSc. Interruption of this crosstalk by combined inhibition of both pathways exerts additive antifibrotic effects at well-tolerated doses.

Supported by the German Research Foundation (grants DI 1537/17-1, DI 1537/20-1, DI 1537/22-1, DI 1537/23-1, BE 7036/2-1, and BE 7036/5-1), Sonderforschungsbereich (SFB) CRC1181 (project A01 and C01) and SFB TR221/project number 324392634 (B04), German Research Foundation project 441730715 (Leica Stellaris 8 Microscope), German Research Foundation project number 324392634 (Drs Dickel, Liang, and Kunz), and Graduiertenkolleg (GRK) 2740 (B02 to Dr Kunz), German Research Foundation project 424726560 (imaging CyTOF), the Wilhelm-Sander-Stiftung (grant 2013.056.1), the Else-Kröner-Fresenius-Foundation (grants 2014_A47 and 2014_A184), the ELAN-Foundation Erlangen (grant 21-11-09-1-Bergmann), the Research Committee of the Medical Faculty of the Heinrich-Heine University Düsseldorf (Forschungskommission ID 2023-33 to Dr Matei, ID 2022-18 to Dr Györfi, and ID 2023-31 to Dr Distler), and the German Federal Ministry of Education and Research (BMBF): MASCARA program, TP 2 (01EC1903A), and iIMMUNE_ACS (01EO2105). Drs Auth and Bergmann's work was supported by NOTICE (RA 2506/7-21), Clinician Scientist Program of the German Research Foundation. Dr Bergmann's work was supported by the Clinician Scientist Program of IZKF Erlangen. Dr Matei's work was supported by the German Research Foundation (grant MA 9219/2-1), the Else-Kröner-Fresenius-Foundation (grants 2021_EKEA.03 and 2022_EKMS.02), and The Edith Busch and World Scleroderma Foundation Research Grant Program 2022–2023. The work of Drs Kunz and Dickel was supported by the CompLS program (grant 031L0262C). Dr Kunz's work was supported by the Fraunhofer Cluster of Excellence Immune-Mediated Diseases. Dr Distler's work was supported by an unrestricted research grant from the Hiller-Foundation.

[1]Christina Bergmann, MD, Sara Chenguiti Fakhouri, MS, Aleix Rius Rigau, PhD, Benita Merlevede, MD, Ludwig Hallenberger, MD, Clara Dees, PhD, Janina Auth, MD, Simon Rauber, PhD, Aline Bozec, PhD, Georg Schett, MD: Deutsches Zentrum für Immuntherapie, Friedrich-Alexander-Universität Erlangen-Nürnberg and Uniklinikum Erlangen, Erlangen, Germany; [2]Thuong Trinh-Minh, PhD, Tim Filla, MS, Alexandru-Emil Matei, MD, Andrea-Hermina Györfi, MD, Xiang Zhou, PhD, Jörg H.W. Distler, MD: Hiller Research Center,

INTRODUCTION

Systemic sclerosis (SSc) is a chronic fibrosing connective tissue disorder that affects the skin and various inner organs.[1,2] A central hallmark of SSc is the uncontrolled and persistent activation of fibroblasts, which results in the excessive release of extracellular matrix. Myofibroblasts are key effectors of pathologic tissue remodeling and tissue fibrosis. In normal wound healing, myofibroblasts occur transiently to promote repair. In contrast, myofibroblasts persist in the pathologic context of fibrotic diseases such as SSc[1,2] and promote chronic fibrotic remodeling. Although the mechanisms of aberrant fibroblast activation are incompletely understood, several core transcription factors of fibrotic tissue remodeling, such as the activator protein 1 (AP-1) member cJUN or the hedgehog transcription factor GLI2, have been identified. Activation of cJUN and GLI2 are common denominators of fibrotic diseases: Both pathways have been shown to be sufficient and required for the development of fibrosis in preclinical models.[3–10] Thus, both pathways are potential candidates for targeted antifibrotic therapies. cJUN is centrally involved in homeostatic functions such as cell proliferation and survival, while hedgehog signaling plays a critical role for stem cell revival.[11,12] Although small molecule inhibitors are in clinical development (for cJUN/AP-1) or are already in clinical use (for hedgehog signaling), prolonged inhibition of cJUN/AP-1 and hedgehog signaling with higher doses of inhibitors in a chronic disease such as SSc might be complicated by dose-limiting adverse events.

Combinations of synergistic therapies may enable dose reduction of individual drugs, resulting in reduced toxicity but comparable or even improved efficacy. This concept might be particularly critical for targets with major homeostatic functions such as cJUN and GLI2, as low-grade residual activity is often sufficient to maintain tissue homeostasis, but the achieved extent of inhibition might still be effective in breaking the pathologic signaling output caused by uncontrolled activation in pathologic conditions. First evidence of the mutual interaction of cJUN and GLI2 has been described in keratinocytes,[13] and a previous study demonstrated that cJun induces skin fibrosis through the hedgehog-mediated multiplication of CD26+, Sca– fibroblasts in a murine, cJun-driven fibrosis model.[14]

The aim of this study was to characterize the mutual interaction of cJUN/AP-1 and hedgehog/GLI2 signaling in human fibroblasts and different murine models of SSc as a prototypical chronic fibrosing disorder and to test the hypothesis that combination therapies with lower doses of inhibitors of cJUN/AP-1 and hedgehog/GLI2 signaling may have additive antifibrotic effects and better tolerability than high-dose monotherapies.

MATERIALS AND METHODS

Patients and fibroblasts. Human dermal fibroblasts were isolated from skin biopsies of 7 patients with SSc and 12 healthy volunteers. All patients fulfilled the 2013 American College of Rheumatology/EULAR criteria for SSc.[15] Four patients were female; three were male. The median age of patients with SSc was 48 years (range: 32–62 years), and their median disease duration was 6.3 years (range: 0.6–23 years). All patients and volunteers signed a consent form approved by the local institutional review board. Patients with active and inactive skin disease were included in the study. Active skin disease was defined as progression of skin fibrosis (increase of modified Rodnan Skin Score >5 within 12 months).[16]

Fibroblast-specific overexpression of Smo (Smo^{ACT}; Col1a2-Cre-ER transgenic mice). To analyze the effects of activated hedgehog signaling in vivo, we generated a mouse model with fibroblast-specific overexpression of active Smoothened (Smo^{ACT} mice). Briefly, Col1a2-Cre-ER mice, expressing a tamoxifen-sensitive Cre recombinase CreERT under the control of a 6 kbp, fibroblast-specific Col1a2 promoter fragment,[17] were cross-bred with Smo^{ACT} mice that harbor a Cre-inducible Smo^{ACT} mutation (W539L point mutation) to generate Smo^{ACT} Col1a2-Cre-ER double transgenic mice. Upon induction of recombination by tamoxifen at the age of 4 weeks, these mice overexpress Smo^{ACT} selectively in fibroblasts, resulting in increased dermal thickness, myofibroblast counts, and collagen content after 8 weeks. Treatment with the cJUN/AP-1 inhibitor T5224 was performed in a preventive manner and started 1 week after tamoxifen application at the age of 5 weeks. Control mice were injected with oil, the solvent of T5224.

TBR^{ACT} mice. To induce dermal fibrosis by selective activation of transforming growth factor β (TGFβ) signaling, attenuated adenoviruses encoding for a constitutively active TGFβ receptor type I (adTBR) were injected at a concentration of 6.67 ×

University Hospital Düsseldorf and Heinrich Heine University, Düsseldorf, Germany; [3]Arif B. Ekici, PhD: Institute of Human Genetics, Friedrich Alexander Universität Erlangen-Nürnberg, and Uniklinikum Erlangen, Erlangen, Germany; [4]Zhu Honglin, MD: Xiangya Hospital, Central South University, Changsha, China; [5]Nicholas Dickel, MS, Chunguang Liang, PhD: Friedrich-Alexander Universität Erlangen-Nürnberg, Erlangen, Germany; [6]Meik Kunz, PD: Friedrich-Alexander Universität Erlangen-Nürnberg, Erlangen, and Fraunhofer Institute for Toxicology and Experimental Medicine and Fraunhofer Cluster of Excellence Immune-Mediated Diseases, Hannover, Germany.

Additional supplementary information cited in this article can be found online in the Supporting Information section (https://acrjournals.onlinelibrary.wiley.com/doi/10.1002/art.42979).

Author disclosures are available at https://onlinelibrary.wiley.com/doi/10.1002/art.42979.

Address correspondence via email to Christina Bergmann, MD, at christina.bergmann@uk-erlangen.de.

Submitted for publication January 8, 2023; accepted in revised form August 20, 2024.

10^7 infectious units into the upper back of 4-week-old male C57BL/6 mice. Injections of transgene beta-galactosidase (lacZ) by replication-deficient adenoviral vectros (adLacZ) served as controls.[18] Injections were performed four times with two weekly intervals. Mice were treated with T5224 (3 or 30 mg/kg/day, oral gavage), GANT-61 (2 or 20 mg/kg/day, intraperitoneally) or solvents in a preventive manner. The application of T5224 and GANT-61 was started in parallel with the first injection of adTBR or adLacZ.

Fibroblast-specific knockdown of Gli2. Mice with conditional alleles of GLI2 ($GLI2^{fl/fl}$) were cross-bred with Col1a2-Cre-ER mice to generate $GLI2^{fl/fl}$;Col1a2-Cre-ER mice. Cre-mediated recombination was induced at the age of 4 weeks by injection of tamoxifen (100 mg/kg for 5 days); oil, the solvent of tamoxifen, was used for controls. In addition, $GLI2^{fl/fl}$;Col1a2-Cre-ER mice were injected with attenuated adenoviruses encoding for a constitutively active TGFβ receptor type I (adTBR) as described in the previous section.[3] Injections of adLacZ served to control for the adTBR virus injections.[18] Further methods are described in Supplementary Materials and Methods.

RESULTS

Concurrent up-regulation of cJUN and GLI2 in fibroblasts in SSc skin. cJUN is the AP-1 family member with the highest expression levels in SSc fibroblasts, and GLI2 is the predominant hedgehog transcription factor in SSc.[3,5] We thus analyzed the expression patterns of cJUN and GLI2 as readouts for activation of both pathways in SSc skin. The expression of cJUN and GLI2 were both significantly increased in patients with SSc with progressive skin fibrosis as compared to matched healthy individuals with increased numbers of cJUN- and GLI2-positive fibroblasts (Figure 1A). Of particular note, the numbers of cJUN- and GLI2-double-positive fibroblasts were highly increased in SSc, with >50% of SSc fibroblasts coexpressing cJUN and GLI2 compared to 27% of fibroblasts in healthy controls. Confocal microscopy confirmed the concomitant up-regulation of cJUN and GLI2 in fibroblasts in SSc compared to normal skin (Figure 1B), confirming simultaneous activation of cJUN/AP-1 and hedgehog/GLI2 signaling in SSc fibroblasts. In addition to fibroblasts, we investigated the expression of cJUN and GLI2 in relation to CD31+ cells and CD45+ cells using imaging mass cytometry (Supplementary Figure S1). We observed a tendency of up-regulation of cJUN and GLI2 in both CD31+ cells and CD45+ cells; however, the differences were not statically significant and not as pronounced as in fibroblasts. Although the lack of statistically significant differences in expression levels does not exclude functional effects, we thus focused our studies on fibroblasts that demonstrate higher expression levels and statistically significant differences between patients and controls.

Mutual induction of cJUN and GLI2 signaling in fibroblasts. Next, we aimed to analyze whether GLI2 and cJUN regulate each other. Thus, we overexpressed cJUN and GLI2 in cultured fibroblasts, respectively, and analyzed the expression of GLI2 and cJUN by Western blot: Overexpression of cJUN resulted in the up-regulation of GLI2, and overexpression of GLI2 induced cJUN expression (Figure 1C). Consistently, we observed a down-regulation of GLI2 upon knockdown of cJUN and, vice versa, a down-regulation of cJUN upon GLI2 knockdown (Figure 1D). These results indicate that cJUN and GLI2 mutually regulate the expression of each other. To confirm the mutual regulation of cJun and Gli2 in vivo, we analyzed the expression of cJun and the number of cJun-positive fibroblasts in a mouse model characterized by the fibroblast-specific overexpression of a constitutively active Smoothened mutant (Smo^{ACT}): Messenger RNA (mRNA) levels of *cJun* and the number of cJun-positive mesenchymal cells was significantly increased in Smo^{ACT} mice compared to control mice (Figure 1E and Supplementary Figure 2). Other members of the AP-1 family such as JunB, JunD, FosB, FosC, and Fra2 were not differentially expressed in Smo^{ACT} mice (Supplementary Figure 3), highlighting the specific interaction of Gli2 with cJun. Consistently, fibroblast-specific knockout of Gli2 prevented the induction of cJun in mice overexpressing a constitutively active TGFβ receptor type I ($TBRI^{ACT}$) (Supplementary Figure 4A). In contrast to cJun knockout mice, mice overexpressing cJun under a ubiquitous $H2k^B$ promoter do not demonstrate a clinical phenotype,[11] indicating that the overexpression of cJun can be compensated by endogenous mechanisms. Thus, overexpression models may not be suitable options to study the effects of chronic activation of cJun. However, we have previously shown that TGFβ induces the expression of cJUN in SSc fibroblasts.[3] We thus used mice with overexpression of a constitutively active TGFβ receptor 1 (TBR^{ACT} mice) upon treatment with adTBR virus to activate cJun/AP-1 signaling. The number of Gli2-positive mesenchymal cells was increased in TBR^{ACT} mice compared to control mice treated with adLacZ virus (Figure 1F). The inhibition of cJun signaling by the selective AP-1 inhibitor T5224[6] prevented the increase in the number of Gli2-positive mesenchymal cells in the skin of TBR^{ACT} mice (Figure 1F). Moreover, treatment with T5224 also reduced the levels of *Ptch2* mRNA, a prototypical GLI-target gene, in murine skin of SMO^{ACT} mice (Supplementary Figure 4B). These results support the regulatory role of cJun/AP-1 signaling on Gli2/hedgehog signaling.

Mechanisms of mutual amplification of cJUN and GLI2. We next tested the hypothesis that cJUN and GLI2 may activate the transcription of each other by binding to specific binding motifs in their promoters. We found 12 GLI2 binding sites in

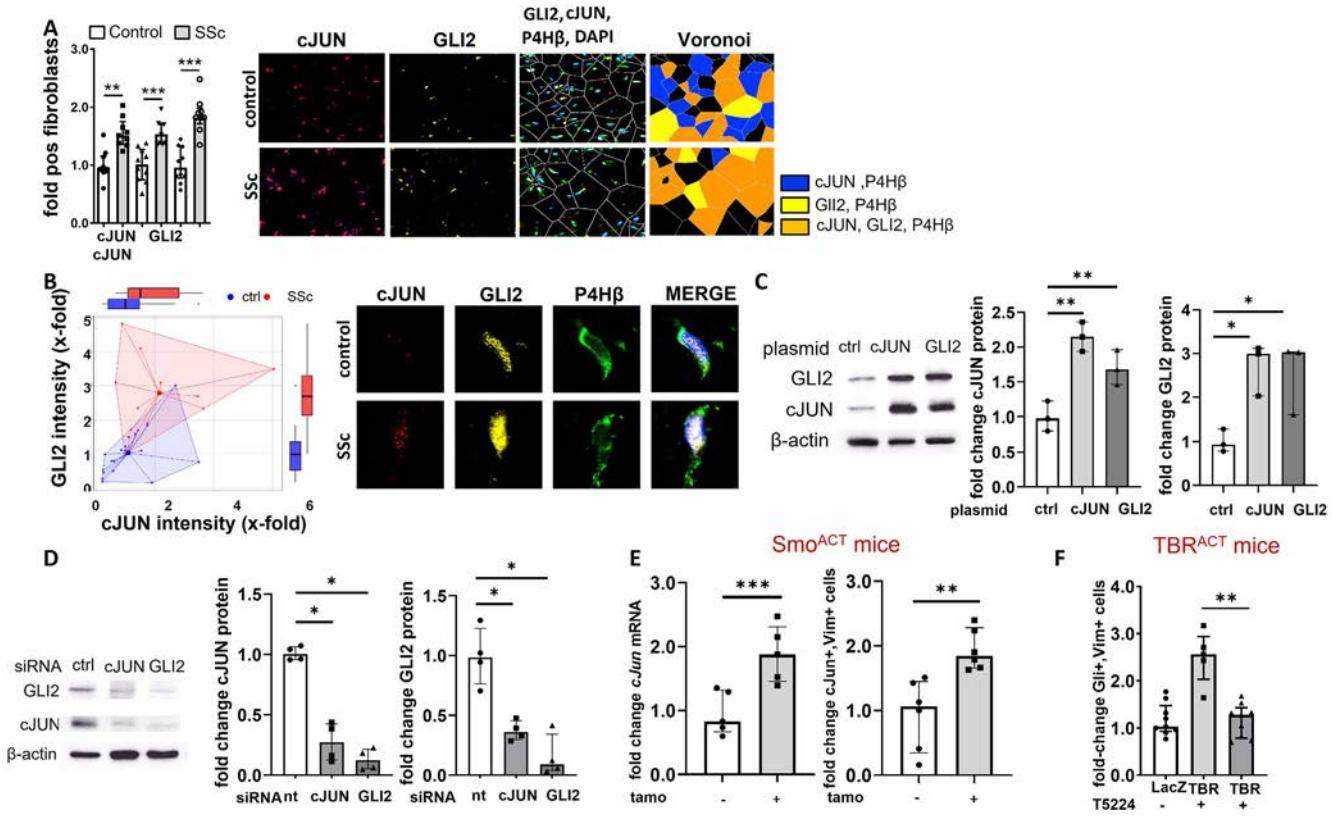

Figure 1. cJUN and GLI2 are concomitantly overexpressed in SSc and induce their mutual expression. (A) Concomitant up-regulation of cJUN and GLI2 in lesional fibroblasts in SSc versus healthy participants. Representative images of immunofluorescence staining for cJUN (red), GLI2 (yellow), and co-staining with P4Hβ (green) and DAPI (blue) in the dermis of healthy donors (n = 5; 1–2 technical replicates) and patients with dcSSc (n = 5; 1–2 technical replicates) patients at 1,000-fold magnification. Voronoi diagrams and quantification of cJUN-positive fibroblasts, GLI2-positive fibroblasts, and cJUN/GLI2-double-positive fibroblasts are included as bar graphs. (B) Representative fibroblast at 10,000-fold magnification using confocal microscopy. Quantification: Dots represent individual cells from a total of four patients and four controls. (C,D) Mutual regulation of expression levels of cJUN and GLI2 in fibroblasts upon overexpression (panel C; n = 3 per group) or knockdown by siRNA (panel D; n = 4 per group). (E) Increased expression of cJun in Smo^{ACT} mice compared to control mice on mRNA level (n = 5/group) and protein level as assessed by quantification of cJun,Vim+ mesenchymal cells (n = 6/group). (F) Decreased numbers of Gli2-positive mesenchymal cells in TBR^{ACT} mice upon inhibition of cJun/AP-1 signaling by T5224 (n = 5; 1–2 technical replicates). Data are presented as median with interquartile range. *P < 0.05; **P < 0.01; ***P < 0.001. ctrl, control; dcSSc, diffuse Systemic Sclerosis; LacZ, transgene beta-galactosidase; mRNA, messenger RNA; nt, nontargeting; siRNA, small interfering RNA; SSc, systemic sclerosis; tamo, tamoxifen; TBR, TGFβ receptor I.

the cJUN promotor (–1,000 to +5,000 kb) (Supplementary Figure 4). AP-1-dependent reporter assays experimentally confirmed an increase in AP-1 reporter activity upon stimulation with sonic hedgehog cytokine (SHH).

We also identified seven JUN binding sites in the GLI2 promotor. Moreover, inhibition of cJUN signaling by treatment with T5224 prevented the induction of GLI-reporter activity by TGFβ in Light2 reporter cells (Supplementary Figure 5). In extension to these experiments, we analyzed DNA binding of GLI2 upon overexpression of cJUN with or without TGFβ stimulation using chromatin immunoprecipitation sequencing (ChIPSeq). We also analyzed DNA binding of cJUN upon GLI2 overexpression by ChIPSeq. Overexpression of cJUN resulted in a 4.6-fold increase in DNA binding/gene detection of GLI2 (Supplementary Figure 6A). Overexpression of GLI2 had milder effects on DNA binding/gene detection of cJUN, with 1.5-fold increases (Supplementary Figure 6A), which might be due to higher DNA binding of cJUN in general. Gene ontology term enrichment analysis indicated that DNA binding occurred at genes with relevance to fibrotic tissue remodeling, such as "extracellular matrix organization," "Notch signaling," and "vascular smooth muscle cell differentiation" (upon GLI2 overexpression and precipitation for cJUN) and "cytoskeletal organization" and "cell-cell junction" (upon cJUN overexpression and precipitation for GLI2; Supplementary Figure 6B).

Inhibition of cJUN/AP-1 signaling ameliorates hedgehog-induced fibroblast activation and skin fibrosis. Overexpression of constitutively active smoothened (Smo) induced a selective activation of hedgehog signaling with increased mRNA levels of the hedgehog target gene *Ptch2* in the skin of mice, without effects on other developmental pathways such as Wnt signaling with its target genes *Axin2* and

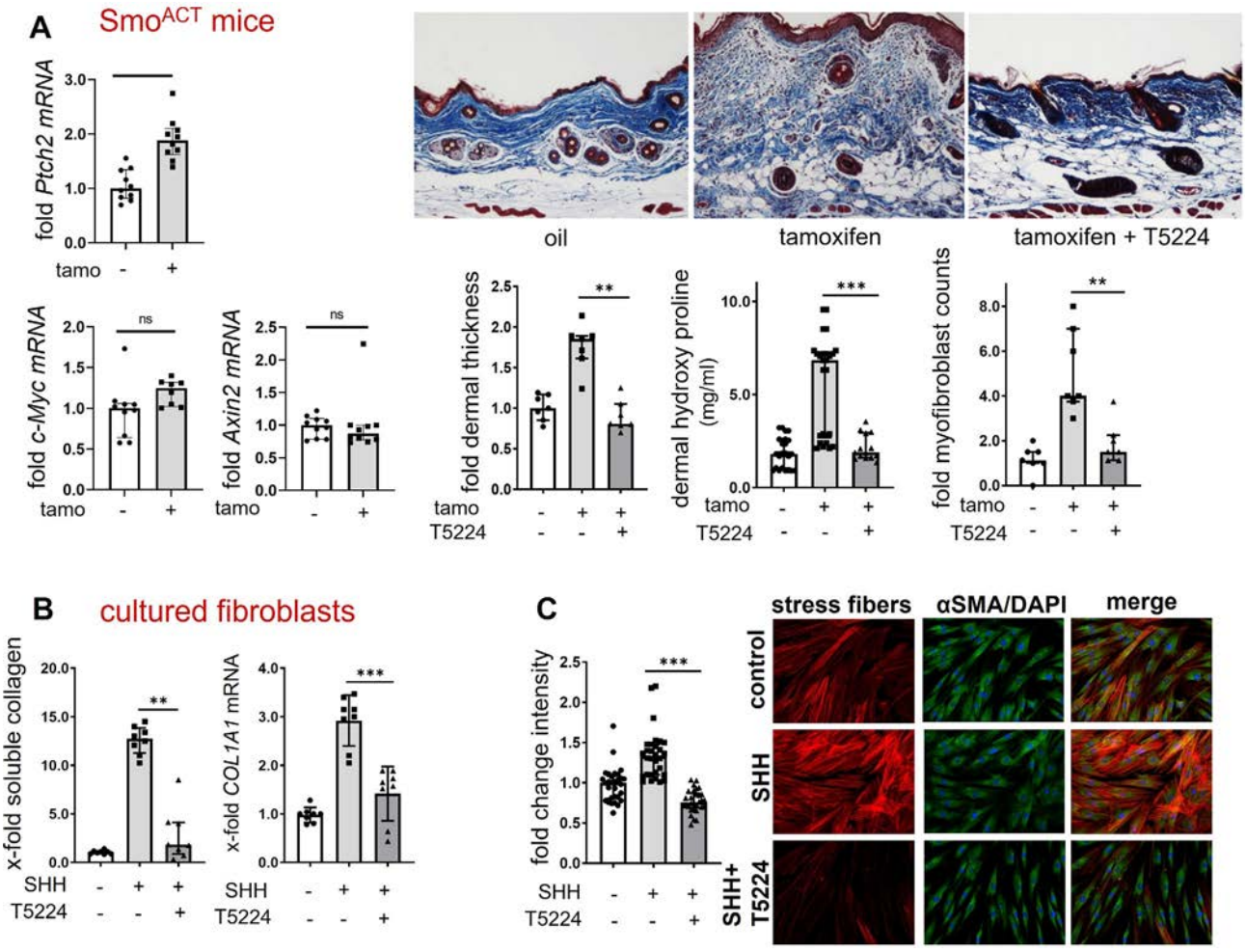

Figure 2. Pharmacologic inhibition of cJUN/AP-1 ameliorates hedgehog-induced fibroblast activation and skin fibrosis. (A) Increased mRNA levels of the hedgehog target gene *Ptch2* compared to other target genes (n = 4–5, technical duplicates) in Smo^{ACT} mice. Effects of treatment with the cJun/AP-1 inhibitor T5224 on dermal thickness (n = 7/group), dermal hydroxyproline content (n = 7/group; 1–2 technical duplicates), and dermal myofibroblast counts (n = 7/group) in Smo^{ACT} mice. Representative images (200-fold magnification; staining: Masson-Trichrome) are shown. (B) Treatment with T5224 reduces the release of soluble collagen and the mRNA levels of *COL1A1* in cultured fibroblasts stimulated with SHH (n = 4, technical duplicates). (C): T5224 ameliorates the formation of stress fibers in SHH-stimulated fibroblasts (n = 3 cell lines with 10 random high-power fields quantified each). Representative images of stress fibers visualized by rhodamine-phalloidin staining (red), α-smooth muscle actin (green), and DAPI (blue) are shown at 2,000-fold magnification. Data are presented as median with interquartile range. *$P < 0.05$; **$P < 0.01$; ***$P < 0.001$. mRNA, messenger RNA; tamo, tamoxifen; SHH, Sonic Hedgehog; αSMA, αSmooth Muscle Actin. Color figure can be viewed in the online issue, which is available at http://onlinelibrary.wiley.com/doi/10.1002/art.42979/abstract.

c-Myc (Figure 2A). The selective activation of hedgehog signaling in Smo^{ACT} mice by tamoxifen was sufficient to induce skin fibrosis with increased dermal thickness, accumulation of myofibroblasts, and higher hydroxyproline content compared to control littermates injected with corn oil (Figure 2A) 8 weeks after the application of tamoxifen. Of note, the concomitant inhibition of cJun/AP-1 signaling using the cJun/AP-1 inhibitor T5224, which was applied daily starting from the day of the first application of tamoxifen, completely prevented Smo^{ACT}-induced skin fibrosis with dermal thickness, myofibroblast counts, and hydroxyproline content comparable to those in nonfibrotic control mice (Figure 2A). Skin thickening was reduced by 103% (p=0.0043) in Smo^{ACT} mice treated with T5224 compared to Smo^{ACT} mice treated with corn oil.

Inhibition of cJUN/AP-1 signaling also blocked GLI2-induced fibroblast activation and collagen release in human dermal fibroblasts. Incubation of cultured human fibroblasts with recombinant SHH increased the levels of *COL1A1* mRNA and the release of collagen protein and induced fibroblast-to-myofibroblast transition with increased expression of αSmooth Muscle Actin (αSMA) and of stress fibers (Figure 2B and 2C). These profibrotic effects of SHH were blocked by treatment with cJUN/AP-1 inhibitor T5224, which returned the levels of collagen and the expression of myofibroblast markers to those of resting fibroblasts (Figure 2B and 2C).

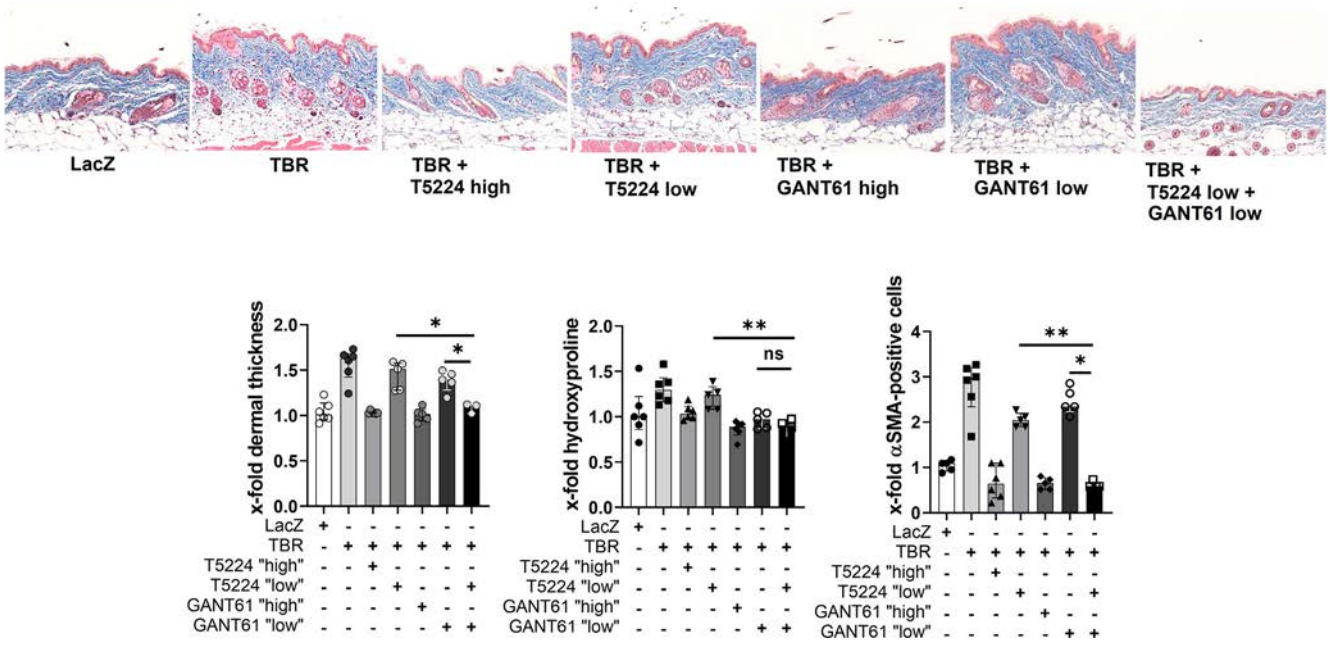

Figure 3. Combined inhibition of cJun/AP-1 and Gli2/hedgehog signaling exerts additive antifibrotic effects. Treatment of TBR^{ACT} mice with T5224 high (30 mg/kg), T5224 low (3 mg/kg), GANT61 high (20 mg/kg), GANT61 low (2 mg/kg/d), or a combination of T5224 low and GANT61 low (n = 3-6 per group). Representative images of trichrome staining at 200-fold magnification are shown. Quantification of dermal thickness, hydroxyproline content, and myofibroblasts are shown as bar graphs. Data are presented as median with interquartile range. $^{*}P < 0.05$; $^{**}P < 0.01$; $^{***}P < 0.001$. LacZ, transgene beta-galactosidase; αSMA, αSmooth Muscle Actin; TBR, TGFβ receptor I. Color figure can be viewed in the online issue, which is available at http://onlinelibrary.wiley.com/doi/10.1002/art.42979/abstract.

Effects of combined inhibition of cJUN and GLI2 signaling in experimental fibrosis. Selective inhibitors of cJUN and of GLI2 are in advanced clinical development[3,5]; however, long-term application of these inhibitors, as would be required in chronic fibrotic diseases such as SSc, may be complicated by adverse events.[19,20] We thus evaluated whether the combined inhibition of cJun/AP-1 and Gli2/hedgehog at lower doses may exert additive antifibrotic effects and better tolerability as compared to monotherapies with higher doses of cJun/AP-1 or Gli2/hedgehog inhibitors.

Treatment with T5224 ameliorated adTBR-induced fibrosis in a dose-dependent manner. Dose-dependent antifibrotic effects were also observed for the Gli2 inhibitor GANT61 (Figure 3). Combination therapy with lower doses of T5224 and of GANT61 were more effective than monotherapies, with the same doses of T5224 or GANT61 with more pronounced reductions in dermal thickening, in myofibroblast counts, and in hydroxyproline content (Figure 3). The antifibrotic effect of the combination therapy of low doses of T5224 and GANT61 was comparable to that of higher doses of T5224 or GANT-61 (Figure 3).

DISCUSSION

Our study demonstrates that simultaneous induction and amplification of two core pathways of fibrotic tissue remodeling, cJUN/AP-1 and GLI2/hedgehog signaling, enables fibroblasts to escape their physiologic regulation.

The mutual activation of cJUN/AP-1 signaling and GLI2/hedgehog signaling is of direct relevance for fibroblast activation and tissue fibrosis. We show that breaking the mutual activation loop by inhibition of cJun in Smo^{ACT} mice with hyperactive hedgehog/Gli2 signaling normalizes Gli2/hedgehog-induced fibroblast activation and tissue fibrosis. Moreover, we also demonstrate that the combined pharmacologic inhibition of cJun and of Gli2 exerts additive antifibrotic effects. Combination therapies are standard regimens in numerous diseases, including rheumatic diseases, as they offer potential for additive efficacy or for dose reduction of individual drugs to allow better tolerability.[21,22] However, despite those potential advantages and their widespread use in other diseases, combination therapies are not yet part of the clinical concept in fibrotic disorders. Our study provides first evidence for positive effects of a combination of cJun/AP-1 inhibitors with Gli2/hedgehog inhibitors in a preclinical model of SSc. Combined inhibition of both pathways demonstrated more potent antifibrotic effects than application of individual inhibitors. The antifibrotic effects of combination therapies with lower doses of inhibitors are comparable to higher doses of monotherapies, but they may not be complicated by their potential adverse events such as increased apoptosis and stem cell depletion, even upon long-term treatment, as is required for antifibrotic treatment. Indeed, combination therapies of T5224 and GANT-61 were well-tolerated in our study, without clinical or histopathologic evidence of obvious toxicity in the preclinical model.

Our study has some limitations: SSc is a complex and heterogenous disease, which is difficult to model in preclinical models. Here, we analyzed the antifibrotic effects of combined inhibition of Gli2/hedgehog signaling and cJun/AP-1 signaling in a mouse model characterized by the constitutive activation of TGFβ signaling, a central mediator of fibrotic disease. However, other features of SSc such as autoimmunity or inflammation are not predominantly reflected by this model. To address potential additive effects of combined inhibition of Gli2/hedgehog signaling and cJun/AP-1 signaling on these disease characteristics would require additional models. Moreover, advanced humanized in vitro models such as three-dimensional vascularized skin grafts have recently become available that may allow us to characterize the combined inhibition of cJUN/AP-1 and GLI2/hedgehog signaling in an additional setting[23] in the future. Despite these limitations, the concept of mutual dependence of profibrotic pathways and the rationale of their combined inhibition is clearly supported by our study.

In summary, our findings of the mutual activation and perturbation of cJUN/AP-1 signaling and GLI2/hedgehog in SSc, its role in fibroblast activation and tissue fibrosis, and the demonstration of additive antifibrotic effects of combined inhibition of cJun/AP-1 signaling and Gli2/hedgehog signaling may have translational implications, as cJUN/AP-1-inhibiting drugs are in clinical testing and hedgehog inhibitors are already in clinical use.

ACKNOWLEDGMENTS

We thank Katja Dreißigacker, Regina Kleinlein, Saskia de Visser van Bloemen, and Wolfgang Espach for excellent technical assistance. Open Access funding enabled and organized by Projekt DEAL.

AUTHOR CONTRIBUTIONS

All authors contributed to at least one of the following manuscript preparation roles: conceptualization AND/OR methodology, software, investigation, formal analysis, data curation, visualization, and validation AND drafting or reviewing/editing the final draft. As corresponding author, Dr Bergmann confirms that all authors have provided the final approval of the version to be published, and takes responsibility for the affirmations regarding article submission (eg, not under consideration by another journal), the integrity of the data presented, and the statements regarding compliance with institutional review board/Helsinki Declaration requirements.

REFERENCES

1. Distler JHW, Györfi AH, Ramanujam M, et al. Shared and distinct mechanisms of fibrosis. Nat Rev Rheumatol 2019;15:705–730.
2. Denton CP, Khanna D. Systemic sclerosis. Lancet 2017;390:1685–1699.
3. Liang R, Šumová B, Cordazzo C, et al. The transcription factor GLI2 as a downstream mediator of transforming growth factor-β-induced fibroblast activation in SSc. Ann Rheum Dis 2017;76:756–764.
4. Horn A, Palumbo K, Cordazzo C, et al. Hedgehog signaling controls fibroblast activation and tissue fibrosis in systemic sclerosis. Arthritis Rheum 2012;64:2724–2733.
5. Avouac J, Palumbo K, Tomcik M, et al. Inhibition of activator protein 1 signaling abrogates transforming growth factor β-mediated activation of fibroblasts and prevents experimental fibrosis. Arthritis Rheum 2012;64:1642–1652.
6. Zhang F, Hao M, Jin H, et al. Canonical hedgehog signalling regulates hepatic stellate cell-mediated angiogenesis in liver fibrosis. Br J Pharmacol 2017;174:409–423.
7. Schulien I, Hockenjos B, Schmitt-Graeff A, et al. The transcription factor c-Jun/AP-1 promotes liver fibrosis during non-alcoholic steatohepatitis by regulating Osteopontin expression. Cell Death Differ 2019;26:1688–1699.
8. Cui L, Chen SY, Lerbs T, et al. Activation of JUN in fibroblasts promotes pro-fibrotic programme and modulates protective immunity. Nat Commun 2020;11:2795.
9. Wernig G, Chen SY, Cui L, et al. Unifying mechanism for different fibrotic diseases. Proc Natl Acad Sci U S A 2017;114:4757–4762.
10. Wasson CW, Ross RL, Wells R, et al. Long non-coding RNA HOTAIR induces GLI2 expression through Notch signalling in systemic sclerosis dermal fibroblasts. Arthritis Res Ther 2020;22:286.
11. Jochum W, Passegué E, Wagner EF. AP-1 in mouse development and tumorigenesis. Oncogene 2001;20:2401–2412.
12. Kopinke D, Norris AM, Mukhopadhyay S. Developmental and regenerative paradigms of cilia regulated hedgehog signaling. Semin Cell Dev Biol 2021;110:89–103.
13. Laner-Plamberger S, Kaser A, Paulischta M, et al. Cooperation between GLI and JUN enhances transcription of JUN and selected GLI target genes. Oncogene 2009;28:1639–1651.
14. Lerbs T, Cui L, King ME, et al. CD47 prevents the elimination of diseased fibroblasts in scleroderma. JCI Insight 2020;5:e140458.
15. van den Hoogen F, Khanna D, Fransen J, et al. 2013 classification criteria for systemic sclerosis: an American College of Rheumatology/European League Against Rheumatism Collaborative Initiative. Ann Rheum Dis 2013;72:1747–1755.
16. Wu W, Jordan S, Graf N, et al. Progressive skin fibrosis is associated with a decline in lung function and worse survival in patients with diffuse cutaneous systemic sclerosis in the European Scleroderma Trials and Research (EUSTAR) cohort. Ann Rheum Dis 2019;78:648–656.
17. Denton CP, Zheng B, Shiwen X, et al. Activation of a fibroblast-specific enhancer of the proalpha2(I) collagen gene in tight-skin mice. Arthritis Rheum 2001;44:712–722.
18. Zehender A, Li YN, Lin NY, et al. TGFβ promotes fibrosis by MYST1-dependent epigenetic regulation of autophagy. Nat Commun 2021;12:4404.
19. Grund-Gröschke S, Stockmaier G, Aberger F. Hedgehog/GLI signaling in tumor immunity—new therapeutic opportunities and clinical implications. Cell Commun Signal 2019;17:172.
20. Gurzov EN, Bakiri L, Alfaro JM, et al. Targeting c-Jun and JunB proteins as potential anticancer cell therapy. Oncogene 2008;27:641–652.
21. Melero I, Berman DM, Aznar MA, et al. Evolving synergistic combinations of targeted immunotherapies to combat cancer. Nat Rev Cancer 2015;15:457–472.
22. Aletaha D, Smolen JS. Diagnosis and management of rheumatoid arthritis: a review. JAMA 2018;320:1360–1372.
23. Matei AE, Kubánková M, Xu L, et al. Identification of a distinct monocyte-driven signature in systemic sclerosis using biophysical phenotyping of circulating immune cells. Arthritis Rheumatol 2023:75:768–781.

Arthritis & Rheumatology
Vol. 77, No. 1, January 2025, pp 99–106
DOI 10.1002/art.42972

American College of Rheumatology
Empowering Rheumatology Professionals

BRIEF REPORT

Muscle Tissue Transcriptome of Idiopathic Inflammatory Myopathy Reflects the Muscle Damage Process by Monocytes and Presence of Skin Lesions

Shinji Izuka,[1] Natsuka Umezawa,[2] Toshihiko Komai,[1] Yusuke Sugimori,[1] Naoki Kimura,[2] Fumitaka Mizoguchi,[2] Yuichiro Fujieda,[3] Keita Ninagawa,[3] Takeshi Iwasaki,[4] Katsuya Suzuki,[5] Tsutomu Takeuchi,[5] Koichiro Ohmura,[4] Tsuneyo Mimori,[4,6] Tatsuya Atsumi,[3] Eiryo Kawakami,[7] Akari Suzuki,[7] Yuta Kochi,[7] Kazuhiko Yamamoto,[1,7] Shinsuke Yasuda,[2] Tomohisa Okamura,[1,8] Mineto Ota,[1,8] and Keishi Fujio[1]

Objective. We aim to investigate transcriptomic and immunophenotypic features of muscle specimens from patients with idiopathic inflammatory myopathy (IIM).

Methods. Bulk RNA-sequencing was performed on muscle biopsy samples from 16 patients with dermatomyositis (DM) and 9 patients with polymyositis (PM). Seven tested positive for anti-aminoacyl transfer RNA synthetase antibodies in the patients with DM (ARS-DM). We conducted weighted gene coexpression network analysis (WGCNA), differentially expressed gene (DEG) analysis, and gene set variation analysis to assess contributions of specific pathways. Cell proportions in muscle specimens were estimated using a deconvolution approach.

Results. WGCNA revealed significant positive correlations between serum creatine kinase (CK) levels and gene modules involved in cellular respiration, phagocytosis, and oxidative phosphorylation (OXPHOS). Significant positive correlations were also observed between CK levels and proportions of CD16-positive and negative monocytes and myeloid dendritic cells. Notably, patients with DM demonstrated enrichment of complement and interferon-α and γ pathway genes compared with those with PM. Furthermore, ARS-DM demonstrated a higher proportion of Th1 cells and DEGs related to OXPHOS. Additionally, serum Krebs von den Lungen-6 levels correlated with gene modules associated with extracellular matrix and the transforming growth factor-β signaling pathway.

Conclusion. Our study highlights a significant involvement of monocytes in muscle damage and delineates pathologic differences among IIM subtypes. DM was characterized by complement and interferon-α and γ signaling, whereas ARS-DM was associated with OXPHOS. Distinctive gene expression variations in muscle specimens suggest that different pathologic mechanisms underlie muscle damage in each IIM phenotype.

Supported by the Japan Agency for Medical Research and Development (grant 19ek0410047).

[1]Shinji Izuka, MD, Toshihiko Komai, MD, PhD, Yusuke Sugimori, MD, PhD, Kazuhiko Yamamoto, MD, PhD, Tomohisa Okamura, MD, PhD, Mineto Ota, MD, PhD, Keishi Fujio, MD, PhD: Department of Allergy and Rheumatology, Graduate School of Medicine, The University of Tokyo, Tokyo, Japan; [2]Natsuka Umezawa, MD, PhD, Naoki Kimura, MD, PhD, Fumitaka Mizoguchi, MD, PhD, Shinsuke Yasuda, MD, PhD: Department of Rheumatology, Graduate School of Medical and Dental Sciences, Tokyo Medical and Dental University (TMDU), Tokyo, Japan; [3]Yuichiro Fujieda, MD, PhD, Keita Ninagawa, MD, PhD, Tatsuya Atsumi, MD, PhD: Department of Rheumatology, Endocrinology and Nephrology, Graduate School of Medicine and Faculty of Medicine, Hokkaido University, Sapporo, Japan; [4]Takeshi Iwasaki, MD, PhD, Tsuneyo Mimori, MD, PhD, Department of Rheumatology and Clinical Immunology, Graduate School of Medicine, Koichiro Ohmura, MD, PhD: Kyoto University, Kyoto, Japan; [5]Katsuya Suzuki, MD, PhD, Tsutomu Takeuchi, MD, PhD: Division of Rheumatology, Department of Internal Medicine, Keio University School of Medicine, Tokyo, Japan; [6]Tsuneyo Mimori, MD, PhD: Takeda Clinic for Rheumatic Diseases, Kyoto, Japan; [7]Eiryo Kawakami, MD, PhD, Akari Suzuki, PhD, Yuta Kochi, MD, PhD, Kazuhiko Yamamoto, MD, PhD: Center for Integrative Medical Sciences, the Institute of Physical and Chemical Research (RIKEN), Yokohama City, Kanagawa, Japan; [8] Tomohisa Okamura, MD, PhD, Mineto Ota, MD, PhD: Department of Functional Genomics and Immunological Diseases, Graduate School of Medicine, The University of Tokyo, Tokyo, Japan.

Additional supplementary information cited in this article can be found online in the Supporting Information section (https://acrjournals.onlinelibrary.wiley.com/doi/10.1002/art.42972).

Author disclosures and graphical abstract are available at https://onlinelibrary.wiley.com/doi/10.1002/art.42972.

Address correspondence via email to Toshihiko Komai, MD, PhD, at KOMAIT-INT@h.u-tokyo.ac.jp; or to Keishi Fujio, MD, PhD, at FUJIOK-INT@h.u-tokyo.ac.jp.

Submitted for publication April 30, 2024; accepted in revised form August 8, 2024.

INTRODUCTION

Idiopathic inflammatory myopathy (IIM) encompasses several heterogeneous phenotypes, including polymyositis (PM), dermatomyositis (DM), and antisynthetase syndrome (ASyS). The underlying mechanisms of muscle damage remain poorly understood. Although IIM can present with extramuscular symptoms, such as skin rash, interstitial lung disease (ILD), and arthritis, muscle damage is the major problem and impairs patients' quality of life.[1] Because of its clinical and pathologic heterogeneity, muscle biopsy has been used to differentiate the phenotypes of IIM based on distinct histologic findings. For instance, the histologic features of DM include infiltrations of $CD4^+$ T cells, B cells, major histocompatibility complex class I expression on muscle fibers, and membrane attack complex depositions in capillaries. In contrast, the histologic features of PM are characterized by the infiltration of $CD8^+$ T cells.[1]

Recent transcriptomic studies of muscle biopsies have provided invaluable insights into the inflammatory milieu of IIM,[2] revealing distinct expression of type I interferon (IFN)-inducible genes, particularly in DM and, to a lesser extent, in ASyS.[3] Furthermore, application of machine learning analysis to muscle biopsy transcriptomics has yielded diagnostic models for the disease phenotypes with high predictive accuracy, delineating the unique pathophysiologic signatures of each myositis phenotype.[4] Recently, single-cell RNA-sequencing (RNA-seq) analysis of muscle biopsies focused on muscle-infiltrating T cells. The study identified a distinct subset of tissue-resident memory T cells characterized by the expression of *HOBIT*, *XCL1*, and *CXCR6*.[5] Nonetheless, single-cell data on myositis are limited within T-cell subsets. It is of great importance to elucidate the association between immune cells not limited to T cells and muscle damage. Moreover, an association between transcriptomic features and clinical parameters is still under exploration.

Especially, the association between the complication of skin lesions and the inflammatory process in muscles remains a significant unresolved issue. Myxovirus-resistant protein A (MxA), a type I IFN surrogate marker, is now one of the definite DM muscle biopsy criteria in the new 2018 European Neuromuscular Centre classification of DM.[6] Given the strong link between myxovirus-resistant protein A positivity and perifascicular atrophy, it was proposed that the sarcoplasmic expression of a type I IFN surrogate marker, in conjunction with the presence of myositis-specific antibodies, supports the diagnosis of DM even when skin manifestations are absent. Considering this, it is possible that processes other than type I IFN may be related to the presence or absence of skin lesions, that is, the difference between classic DM and PM. To address these challenges, we conducted bulk RNA-seq, a more cost-effective yet robust approach that permits the analysis of gene expression across an entire tissue sample. Moreover, we used a deconvolution approach to estimate cell proportions from bulk RNA-seq data,[7] a strategic method that approximates the resolution of single-cell RNA-seq, enabling the identification of immune cell subsets infiltrating the muscle tissue in IIM. These data also elucidated clinical relevance and provided transcriptomic data.

MATERIALS AND METHODS

Detailed materials and methods are provided in the Supplementary Methods section. Briefly, muscle biopsies were obtained from patients with IIM. We performed RNA-seq, and infiltrated cell proportions were estimated by a deconvolution approach. Because of the lack of publicly available single-cell RNA-seq data on muscle tissue from patients with IIM that are applicable to deconvolution analysis, we conducted deconvolution analysis using data from lymphocytes and myeloid cells from patients with immune-mediated diseases, including IIM, and healthy human peripheral blood mononuclear cells (PBMCs) from the Immune Cell Gene Expression Atlas from the University of Tokyo.[8] Additionally, we included age-associated helper T cells, specifically the $CXCR3^{mid}CD4^+$ T-cell subset, which we recently identified and found to be associated with humoral immunity in IIM,[9] as well as myocytes from the Genotype-Tissue Expression (GTEx) database.[10] We then performed weighted gene coexpression network analysis (WGCNA), differentially expressed gene (DEG) analysis, enrichment analysis of gene ontology terms, and gene set variation analysis (GSVA) to identify the differences in individual IIM phenotypes. This study was approved by the ethics committees of the University of Tokyo (approval number: G10137), and written informed consent was obtained from all enrolled patients.

RESULTS

Patient characteristics. We enrolled a total of 25 patients with IIM. Within that cohort, 16 patients were diagnosed with DM, and 9 patients were diagnosed with PM. The median levels of serum creatine kinase (CK) were 1,291.5 U/L (interquartile range [IQR] 123.8–4,187.3) in DM and 710.0 IU/mL (IQR 406.0–806.0) in PM. Among the patients with DM, 62.5% (10 of 16) showed positivity for myositis specific autoantibodies (MSAs); these patients included seven with anti-aminoacyl transfer RNA synthetase (ARS) antibody, one with the anti-Mi-2 antibody, one with the anti–transcriptional intermediary factor 1-γ antibody, and one with the anti–signal recognition particle antibody (Supplementary Table 1). Only one patient with PM showed positivity for the anti-ARS antibody. Muscle biopsies from these patients were subjected to RNA-seq.

WGCNA of muscle biopsies of patients with IIM. We investigated possible correlations between gene expression profiles in muscle biopsies and clinical biomarkers of muscle damage, such as CK and aldolase. Thus, we applied WGCNA to analyze the RNA-seq of muscle biopsies from patients with IIM. We discerned 24 distinct modules of co-expressed genes (Figure 1A; Supplementary Table 2). Notably, five modules

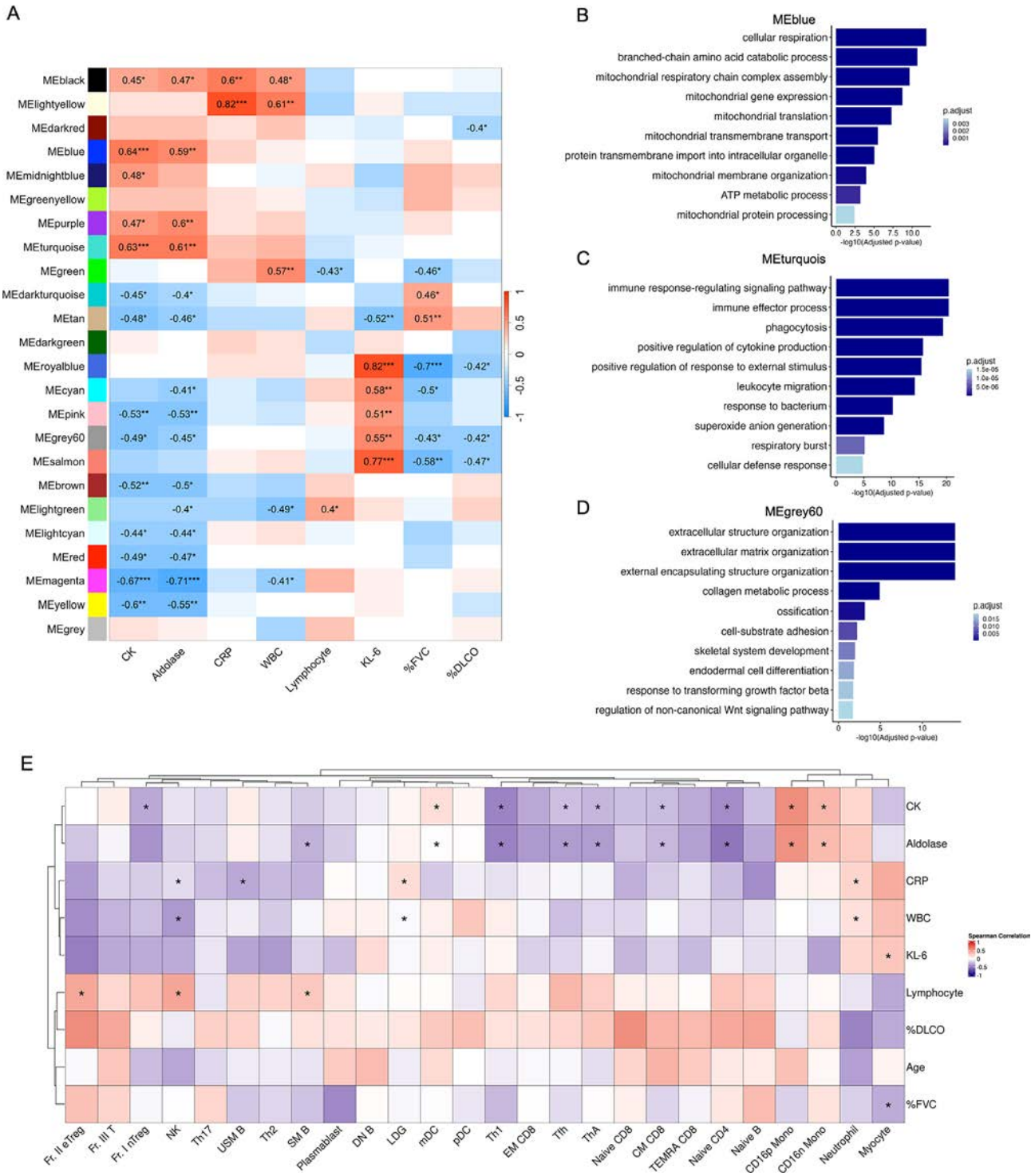

Figure 1. Relationships between clinical parameters and the transcriptome in muscle biopsies. (A) Heatmap of weighted gene correlation network analysis showing the Pearson correlation coefficient matrix among MEs and clinical parameters. (B) Gene ontology enrichment analysis of biologic process terms in MEblue modules correlated with CK and aldolase. (C) Gene ontology enrichment analysis of biologic process terms in MEturquois modules correlated with CK and aldolase. (D) Gene ontology enrichment analysis of biologic process terms in MEgrey60 modules correlated with KL-6 levels, %FVC, and %DLco. (E) Heatmap showing the Spearman correlation coefficients between estimated cell proportions and clinical parameters. Statistically significant correlations are marked with an asterisk (*$P < 0.05$; **$P < 0.01$). CK, creatine kinase; CRP, C-reactive protein; DLco, diffusing capacity of the lung for carbon monoxide; DN B, double negative B cells; EM CD8, effector memory CD8 T cells; FVC, forced vital capacity; KL-6, Krebs von den Lungen-6; LDG, low-density granulocytes; mDC, myeloid dendritic cells; ME, module eigengene; NK, natural killer; pDC, plasmacytoid dendritic cells; SM B, switched memory B cells ; TEMRA CD8, T effector memory CD45RA$^+$ CD8 T cells; Th, T helper cell; USM B, unswitched memory B cells; WBC, white blood cell.

exhibited significant positive correlations with serum CK levels, and four modules paralleled aldolase levels.

The module eigengene ME blue module, which was highly correlated with CK, was enriched for genes implicated in cellular respiration, mitochondrial function, and mitochondrial gene expression (Figure 1B). Concurrently, the MEturquoise module, which was correlated with both CK and aldolase, was associated with genes involved in immune effector processes, phagocytosis, and cytokine production (Figure 1C). Moreover, MEmidnightblue and MEpurple, which also correlated with CK, were linked to muscle contraction and oxidative phosphorylation, respectively (Supplementary Figure 1). These positive correlations indicate that muscle damage in IIM may have both immunologic and metabolic underpinnings. We also identified three specific gene modules—MEroyalblue, MEgrey60, and MEsalmon—that showed a positive correlation with serum Krebs von den Lungen-6 (KL-6) levels and an inverse relationship with the percentage forced vital capacity and percentage diffusing capacity of the lung for carbon monoxide (Figure 1D; Supplementary Figure 2). Notably, the MEgrey60 module included genes pivotal in extracellular matrix organization and the transforming growth factor-β (TGF-β) response pathway (Figure 1D).

Correlations between immunophenotypes and clinical features. Next, we used the bulk RNA-seq data to predict the proportions of cell types infiltrating the muscle tissue. This analysis used a deconvolution approach. These data predicted the infiltrated immune cell subsets and their potential association with clinical manifestations of IIM. We found that serum CK and aldolase levels were positively correlated

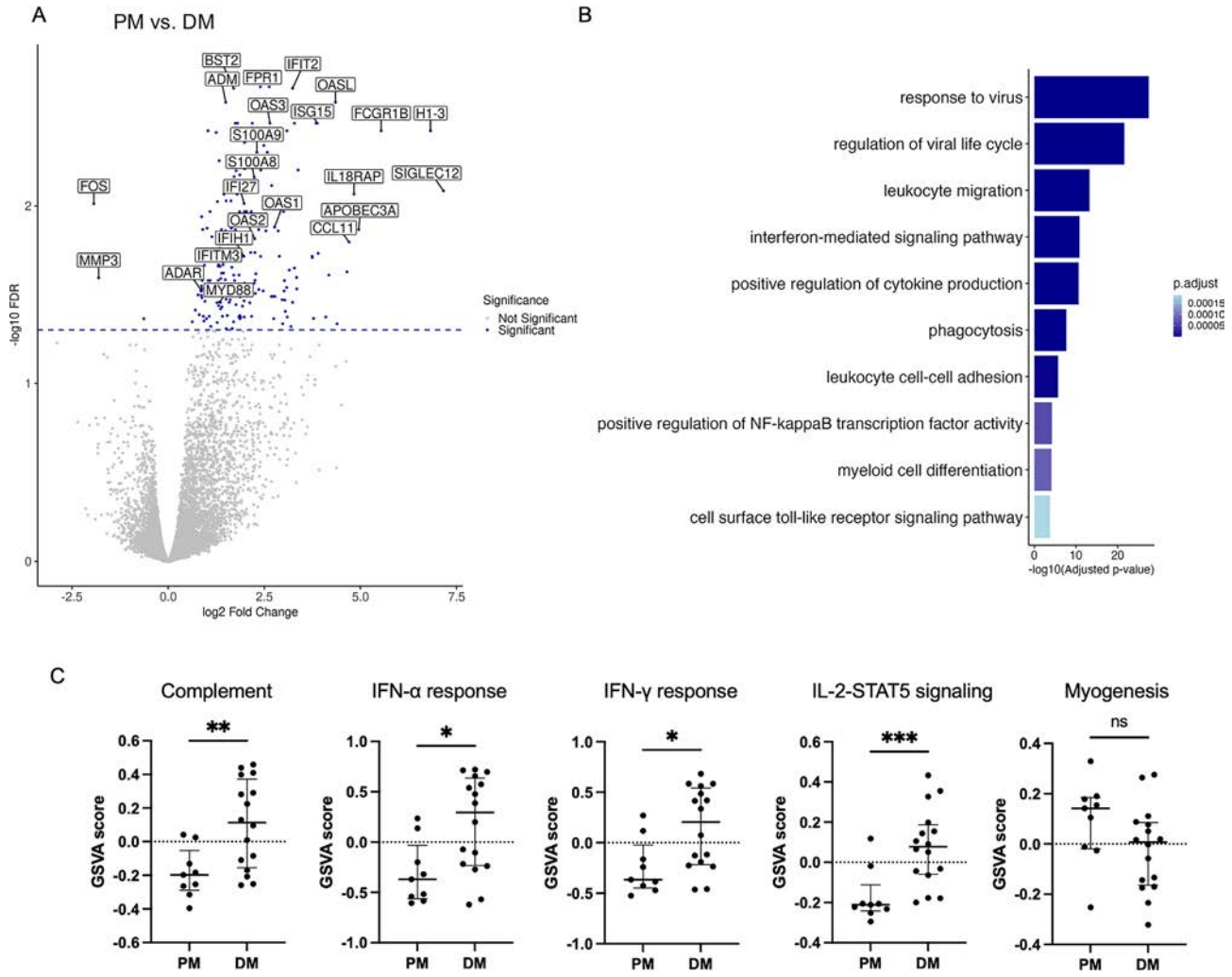

Figure 2. Transcriptomic features in muscle specimens of DM and PM. (A) Volcano plot representing differences in gene expression between PM and DM. Genes to the left are more expressed in PM, and genes to the right are more expressed in DM, with an FDR of <0.05 set as the threshold for statistical significance. (B) Gene ontology enrichment analysis of biologic process terms in differentially expressed genes of DM. (C) Box plots comparing GSVA scores between two phenotypes in DM versus PM. Statistically significant differences between conditions are denoted by asterisks (*$P < 0.05$; **$P < 0.01$; ***$P < 0.001$). DM, dermatomyositis; FDR, false discovery rate; GSVA, gene set variation analysis; IFN, interferon; IL, interleukin; ns, not significant; PM, polymyositis; STAT5, signal transducer and activator of transcription 5. Color figure can be viewed in the online issue, which is available at http://onlinelibrary.wiley.com/doi/10.1002/art.42972/abstract.

with the proportions of CD16-negative monocytes (CD16n Mono) ($\rho = 0.357$, $P < 0.001$ and $\rho = 0.342$, $P < 0.001$), CD16-positive monocytes (CD16p Mono) ($\rho = 0.564$, $P < 0.001$ and $\rho = 0.545$, $P = 0.001$), and myeloid dendritic cells (mDC) ($\rho = 0.166$, $P = 0.023$ and $\rho = 0.01$, $P = 0.030$), suggesting a link between myeloid cell infiltration and muscle damage (Figure 1E). Additionally, neutrophils and low-density granulocytes (LDG) showed positive correlations with serum C-reactive protein levels ($\rho = 0.213$, $P < 0.001$ and $\rho = 0.168$, $P < 0.001$, respectively) (Figure 1E), suggesting their involvement in muscle and systemic inflammation.

Transcriptomic and immunophenotypic features differ between PM and DM. We then explored the transcriptomic characteristics in IIM, distinguishing between those with and without skin rash by comparing DM and PM. To address the differences depending on the presence of a skin rash, we conducted a DEG analysis of DM versus PM, indicating that patients with DM exhibited greater enrichment of several IFN-related genes (*IFIT2*, *OASL*, and *BST2*) and innate immunity-related genes (*IL18RAP*, *APOBEC3A*, and *LYN*) (Figure 2A and B), whereas patients with PM demonstrated increased expression of genes associated with oxidative stress pathways, such as *MMP3* and *FOS*. To delve further into potential pathogenic processes, we performed GSVA and revealed that DM had significantly higher scores for complement, IFN-α response, IFN-γ response, and interleukin-2 signal transducer and activator of transcription 5 signaling pathways compared with PM (Figure 2C). In contrast, GSVA scores for myogenesis showed a trend toward higher values in PM, although this did not reach statistical significance ($P = 0.11$; Figure 2C). There were no significantly different estimated cell proportions between PM and DM (Supplementary Figure 3; Supplementary Table 3). The proportions of CD16n Mono, CD16p Mono, and mDC were positively correlated with CK, even for patients with DM (Supplementary Figure 4).

Difference of immunophenotypes and transcriptomic features between non–ARS-DM and ARS-DM. Finally, in delineating the immunopathological features of ASyS, which is often differentiated from other DM subtypes,[1] we contrasted patients with anti–ARS antibody-positive DM (ARS-DM; n = 7) and patients with anti–ARS antibody–negative DM (non–ARS-DM; n = 9) (Supplementary Tables 4 and 5). DEG analysis between these subgroups unveiled a pronounced expression of IFN-associated genes, such as *ISG15*, *CXCL10*, and *IFI6*, in the non–ARS-DM group (Figure 3A), suggesting a predominant role of IFN pathways in non–ARS-DM pathogenesis.

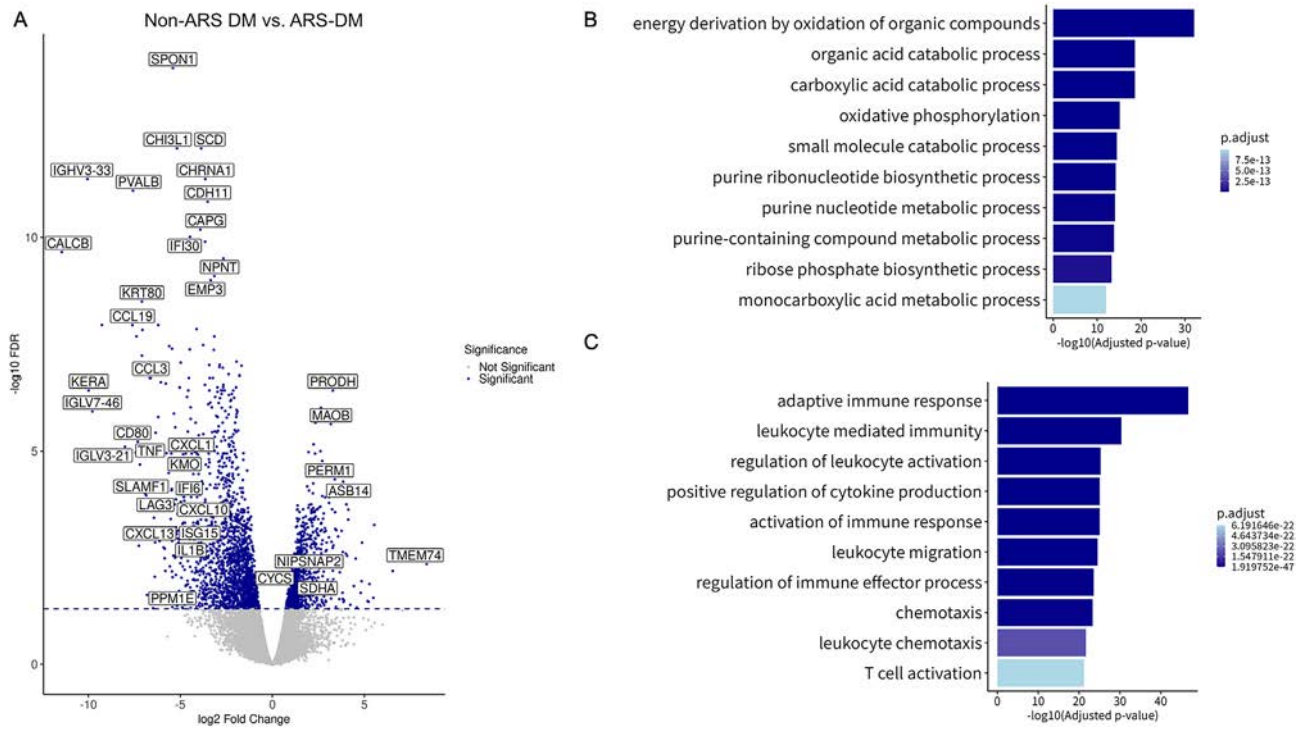

Figure 3. Transcriptomic features in muscle specimens of ARS-DM. (A). Volcano plot representing differential gene expression between non–ARS-DM and ARS-DM. Genes to the left are more expressed in non–ARS-DM, and genes to the right are more expressed in ARS-DM, with an FDR of <0.05 set as the threshold for statistical significance. (B) Gene ontology enrichment analysis of biologic process terms in differentially expressed genes of ARS-DM. (C) Gene ontology enrichment analysis of biologic process terms in differentially expressed genes of non–ARS-DM. ARS-DM, anti-aminoacyl transfer RNA synthetase antibody-positive dermatomyositis; DM, dermatomyositis; FDR, false discovery rate. Color figure can be viewed in the online issue, which is available at http://onlinelibrary.wiley.com/doi/10.1002/art.42972/abstract.

Enrichment analysis of the DEGs underscored the predominance of oxidative phosphorylation and ATP metabolic processes in ARS-DM (Figure 3B), whereas non–ARS-DM exhibited enhanced adaptive immune responses and immune effector processes (Figure 3C). Cell proportion analysis revealed a greater presence of Th1 cells in ARS-DM (0.0576 [IQR 0.0561–0.0589] vs 0.0533 [IQR 0.0479–0.0562]; P = 0.039), whereas non–ARS-DM was characterized by an increased proportion of CD16p Mono (0.0267 [IQR 0.0245–0.0296] vs 0.0200 [IQR 0.0193–0.0207]; P = 0.013) (Supplementary Figure 5; Supplementary Table 5). Despite not being significantly different, follicular helper T cells and age-associated helper T cells were also increased in ARS-DM (0.0461 [IQR 0.0459–0.0469] vs 0.0443 [IQR 0.0426–0.0452]; P = 0.0502 and 0.0572 [IQR 0.0558–0.0587] vs 0.0545 [IQR 0.0489–0.0564]; P = 0.0502, respectively) (Supplementary Figure 5; Supplementary Table 5). Notably, CD16n Mono levels were positively correlated with CK for all examined IIM phenotypes, as well as within non–ARS-DM and ARS-DM (Figure 1C; Supplementary Figure 6).

DISCUSSION

We used muscle biopsies in IIM to study transcriptomic and immunophenotypic alterations associated with muscle damage. They revealed complex interplays between metabolic and immunologic pathways. Consistent with prior research, our findings underscore the heterogeneity of IIM and offer novel insights into its pathogenesis.

There is relatively little information regarding the specific immune cell subsets infiltrating the muscles in patients with myositis. In fact, existing data rely on histologic studies. Currently, there is only one study employing single-cell RNA-seq analysis of muscle tissue and it focused on T cells.[5] Our application using cell-type deconvolution demonstrated that CD16p and CD16n Mono, as well as mDC, were positively correlated with serum CK levels. Previously, histopathological examination of muscle tissue has revealed the associations between immune cell infiltration and muscle damage, and our findings supplement those studies. For instance, it has been postulated that the macrophages that infiltrate injured tissue originate from circulating monocytes.[11] Moreover, the infiltration of $CD68^+$ macrophages within the endomysium was identified in anti-Mi2 antibody-positive DM and immune-mediated necrotizing myopathy. Both of these showed higher serum CK levels.[12] Also, DCs that differentiate from monocytes promote myoblast proliferation and migration as well as enhance the expression of HLA-ABC, DR, VLA-5, and VLA-6 by myoblasts.[13] Given that mDCs are a primary source of type I IFN within muscle tissues, particularly in DM, and considering the role of type I IFN in promoting the differentiation of monocytes into macrophages,[14] these observations and our studies suggest that monocytes and mDCs synergistically contribute to muscle damage.

Our research has revealed muscle transcriptomic distinctions between patients with and without skin rash by comparing DM and PM. The well-documented role of complement-mediated microangiopathy in DM pathogenesis[15] is further substantiated by our findings of a pronounced complement signature at the transcriptional level. This discovery reinforces the potential therapeutic impact of complement inhibitors, as well as that of intravenous Ig, which can bind to C1q, C3, and C4, thereby preventing the triggering of the complement pathway.[15] Moreover, tissue deposition of the C5b-9 membranolytic attack complex within endothelial cells of capillaries was observed in DM.[15] Such an activation of the C5b-9 membranolytic attack complex may precipitate the migration of both macrophages and DCs.[15] Consequently, we suggest that the muscle damage observed in DM could result from the combined effects of an activated system and the infiltration of monocytes and DCs.

In addition, previous investigations into muscle biopsies of patients with DM have shown elevated expression of type 1 IFN-inducible genes, with DM exhibiting more pronounced levels than ASyS.[3] Significant genes, such as *ISG15*, *IFI6*, and *MX1*, previously identified in DM, were also prominent in our DEG comparisons of DM versus PM and non–ARS-DM versus ARS-DM. These findings suggest exploring the targeting of IFN signaling as a therapeutic option, particularly for patients with non–ARS-DM. In addition, chemotaxis pathways were enriched in non–ARS-DM (Figure 3C). More specifically, the DEGs included in these pathways were *CXCL10*, *CXCL13*, and *TNF* (Figure 3A). Furthermore, the DEGs also included many Ig genes, such as *IGHV3-33*, *IGLV7-46*, and *IGLV3-21* (Figure 3A). These chemokines and cytokines, possibly produced by monocytes or T cells, are involved in B cell chemoattraction as well as tissue inflammation. This suggests a hypothesis for muscle damage in non–ARS-DM.

ILD is a critical condition for patients with myositis, with KL-6 recognized as a prognostic biomarker for mortality in PM-/DM-associated ILD.[1] Our data revealed a notable positive correlation between serum KL-6 levels and the expression of genes related to the extracellular matrix as well as the TGF-β signaling pathway, including *TGFB2, COL11A1, COL6A3, ECM2*, and *FN1*, which occur concurrently with impaired pulmonary function. The absence of a correlation between disease duration and serum KL-6 levels suggests that chronic muscle changes do not account for this observation. Thus, fibrotic activity likely occurs simultaneously in muscle and lung tissues. In ASyS, the immune response against endothelial cells may be a key pathologic process that causes damage to both muscle and lung tissues.[1,16]

Additionally, the MEroyalblue and MEsalmon modules demonstrated significant correlations with KL-6, percentage forced vital capacity, and percentage diffusing capacity of the lung for carbon monoxide, showing positive, negative, and negative correlations, respectively (Figure 1A). The MEroyalblue module included CX3CL1 and CX3CR1, both of which have been

reported to be associated with ILD.[17,18] CX3CL1 is primarily enriched in inflamed endothelial cells and promotes the recruitment of monocytes and T cells. Notably, CX3CL1 concentrations in lung tissue were increased in systemic sclerosis–associated ILD, suggesting that CX3CL1 and its receptor CX3CR1 play significant roles in ILD.[17] Increased CX3CL1 levels were identified in both PBMCs and lung tissue in ILD and have been suggested as a driver of the migration of $CX3CR1^+$ nonclassical monocytes into lung tissue, leading to fibrotic changes.[18] The MEsalmon module encompassed genes related to oxidative phosphorylation, mammary gland epithelial cell differentiation, and mitochondrial gene expression (Supplementary Figure 2). Abnormalities in oxidative phosphorylation have been identified in senescent fibroblasts of idiopathic pulmonary fibrosis,[19] suggesting a potential role of the MEsalmon module genes in the pathogenesis of pulmonary fibrosis in IIM. Although further investigation is needed to fully understand the implications of these novel associations, common fibrotic pathways in muscle and lung tissues could contribute to the respective organ damage.

In our analysis of ARS-DM, oxidative phosphorylation pathways were notably enriched in muscle biopsy specimens. Given that CD16n Mono was positively correlated with CK levels both in ARS-DM and non–ARS-DM, this immune cell subset may be a key subset being associated with muscle damage. In ARS-DM, the oxidative phosphorylation pathway was enriched compared with non–ARS-DM (Figure 3B). In tissue-resident macrophages, such as alveolar macrophages and adipose tissue macrophages, oxidative phosphorylation has a significant homeostatic function by stabilizing lipid-handling capacity.[20] Therefore, the enrichment of the oxidative phosphorylation pathway in the muscles of patients with ARS-DM can explain the higher activity of monocytes in muscle tissue, which may lead to muscle damage. In addition, we have previously demonstrated the upregulation of genes associated with oxidative phosphorylation in plasmablasts within the peripheral blood of patients with an active ASyS.[21] Interestingly, these mature B cell populations were reduced in the peripheral blood during the active phase of the disease.[21] Taken together, these data may imply that metabolic alterations in B cell subsets also contribute to the pathogenesis of ASyS. Additionally, a pronounced increase in Th1 was detected in ARS-DM muscle biopsies.

In contrast with these tissue findings, single-cell RNA-seq of peripheral blood from patients with ASyS indicated a decreased proportion of Th1 cells.[22] Furthermore, bronchoalveolar lavage fluid from patients positive for anti-histidyl transfer RNA synthetase, a specific autoantibody in ASyS, exhibited a significantly elevated percentage of Th1 ($CD4^+CD3^+CXCR3^+$ T cells) compared with peripheral blood samples.[16] Although these observations were confirmed in bronchoalveolar lavage studies, they suggest the possibility that Th1 infiltration in muscular tissues can also contribute to the mechanism of tissue damage.

The limitations of this study include a modest sample size and a lack of more precise clinical data, such as manual muscle testing. However, whereas previous studies[2–4] included larger numbers of muscle samples and identified distinct pathogenesis in each phenotype, we were able to identify biologically plausible associations between transcriptomic signatures and clinical features of IIM. We also adhered to the recommended guidelines for RNA-seq experiment design,[23] including the number of samples, the methods used, and the fold-change threshold. Furthermore, we conducted a principal component analysis of gene expression levels, which confirmed the relative homogeneity within each IIM phenotype (Supplementary Figure 7), supporting the robustness of the results despite the small sample sizes. Recent transcriptome analyses of muscles have elucidated unique signatures using fewer than eight samples.[5,24,25] Our analysis, with a sample size of 25, exceeds the recommended minimum of 20 for WGCNA,[26] potentially providing more precise analysis than previous muscle transcriptome studies.

Secondly, cell proportions were estimated using the deconvolution approach, referencing immune cells from PBMCs obtained from a wide variety of diseases[8,9] and myocytes from the GTEx database.[10] Although most deconvolution methods use data from PBMCs to estimate tissue-infiltrated immune cells,[27,28] it is important to note that these estimations are predictions based on non–single-cell RNA-seq data from IIM muscle. Therefore, future single-cell RNA-seq, as well as pathologic analyses, such as confocal microscopy, are anticipated to provide a deeper understanding of the immunophenotyping of muscle specimens from patients with myositis.

In summary, our findings suggest distinct pathogenic mechanisms in subgroups of IIM. Of note, CD16n Mono appears to play a crucial role in muscle damage in all subgroups of myositis. Targeting IFN pathways and complement systems may offer viable therapeutic strategies for patients with DM, particularly in non–ARS-DM, and oxidative phosphorylation may be related to the pathophysiology of ASyS.

ACKNOWLEDGMENTS

We would like to express gratitude toward the patients, medical staff, technicians, and many others who helped with this study.

AUTHOR CONTRIBUTIONS

All authors contributed to at least one of the following manuscript preparation roles: conceptualization AND/OR methodology, software, investigation, formal analysis, data curation, visualization, and validation AND drafting or reviewing/editing the final draft. As corresponding authors, Drs Komai and Fujio confirm that all authors have provided the final approval of the version to be published, and take responsibility for the affirmations regarding article submission (eg, not under consideration by another journal), the integrity of the data presented, and the statements regarding compliance with institutional review board/Helsinki Declaration requirements.

REFERENCES

1. Lundberg IE, Fujimoto M, Vencovsky J, et al. Idiopathic inflammatory myopathies. Nat Rev Dis Primers 2021;7(1):86.
2. Pinal-Fernandez I, Milisenda JC, Pak K, et al. Transcriptional derepression of CHD4/NuRD-regulated genes in the muscle of patients with dermatomyositis and anti-Mi2 autoantibodies. Ann Rheum Dis 2023;82(8):1091–1097.
3. Pinal-Fernandez I, Casal-Dominguez M, Derfoul A, et al. Identification of distinctive interferon gene signatures in different types of myositis. Neurology 2019;93(12):e1193–e1204.
4. Pinal-Fernandez I, Casal-Dominguez M, Derfoul A, et al. Machine learning algorithms reveal unique gene expression profiles in muscle biopsies from patients with different types of myositis. Ann Rheum Dis 2020;79(9):1234–1242.
5. Argyriou A, Horuluoglu B, Galindo-Feria AS, et al. Single-cell profiling of muscle-infiltrating T cells in idiopathic inflammatory myopathies. EMBO Mol Med 2023;15(10):e17240.
6. Tanboon J, Uruha A, Stenzel W, et al. Where are we moving in the classification of idiopathic inflammatory myopathies? Curr Opin Neurol 2020;33(5):590–603.
7. Nakajima S, Tsuchiya H, Ota M, et al. Synovial tissue heterogeneity in Japanese patients with rheumatoid arthritis elucidated using a cell-type deconvolution approach. Arthritis Rheumatol 2023;75(12): 2130–2136.
8. Ota M, Nagafuchi Y, Hatano H, et al. Dynamic landscape of immune cell-specific gene regulation in immune-mediated diseases. Cell 2021;184(11):3006–3021.e17.
9. Goto M, Takahashi H, Yoshida R, et al. Age-associated CD4+ T cells with B cell-promoting functions are regulated by ZEB2 in autoimmunity. Sci Immunol 2024;9(93):eadk1643.
10. Ardlie KG, Deluca DS, Segrè AV, et al; GTEx Consortium. Human genomics. The Genotype-Tissue Expression (GTEx) pilot analysis: multitissue gene regulation in humans. Science 2015;348(6235): 648–660.
11. Wang X, Zhou L. The many roles of macrophages in skeletal muscle injury and repair. Front Cell Dev Biol 2022;10:952249.
12. Fornaro M, Girolamo F, Cavagna L, et al. Severe muscle damage with myofiber necrosis and macrophage infiltrates characterize anti-Mi2 positive dermatomyositis. Rheumatology (Oxford) 2021;60(6): 2916–2926.
13. Ladislau L, Portilho DM, Courau T, et al. Activated dendritic cells modulate proliferation and differentiation of human myoblasts. Cell Death Dis 2018;9(5):551.
14. Miller FW, Lamb JA, Schmidt J, et al. Risk factors and disease mechanisms in myositis. Nat Rev Rheumatol 2018;14(5):255–268.
15. Dalakas MC. Complement in autoimmune inflammatory myopathies, the role of myositis-associated antibodies, COVID-19 associations, and muscle amyloid deposits. Expert Rev Clin Immunol 2022;18(4): 413–423.
16. Galindo-Feria AS, Albrecht I, Fernandes-Cerqueira C, et al. Proinflammatory histidyl-transfer RNA synthetase-specific CD4+ T cells in the blood and lungs of patients with idiopathic inflammatory myopathies. Arthritis Rheumatol 2020;72(1):179–191.
17. Hoffmann-Vold AM, Weigt SS, Palchevskiy V, et al. Augmented concentrations of CX3CL1 are associated with interstitial lung disease in systemic sclerosis. PLoS One 2018;13(11):e0206545.
18. Greiffo FR, Viteri-Alvarez V, Frankenberger M, et al. CX3CR1-fractalkine axis drives kinetic changes of monocytes in fibrotic interstitial lung diseases. Eur Respir J 2020;55(2):1900460.
19. Álvarez D, Cárdenes N, Sellarés J, et al. IPF lung fibroblasts have a senescent phenotype. Am J Physiol Lung Cell Mol Physiol 2017; 313(6):L1164–L1173.
20. Wculek SK, Heras-Murillo I, Mastrangelo A, et al. Mar Oxidative phosphorylation selectively orchestrates tissue macrophage homeostasis. Immunity 2023;56(3):516–530.
21. Sugimori Y, Iwasaki Y, Takeshima Y, et al. Transcriptome profiling of immune cell types in peripheral blood reveals common and specific pathways involved in the pathogenesis of myositis-specific antibody-positive inflammatory myopathies. ACR Open Rheumatol 2023;5(2): 93–102.
22. Zhu L, Cao Z, Wang S, et al. Single-cell transcriptomics reveals peripheral immune responses in anti-synthetase syndrome-associated interstitial lung disease. Front Immunol 2022;13:804034.
23. Schurch NJ, Schofield P, Gierliński M, et al. How many biological replicates are needed in an RNA-seq experiment and which differential expression tool should you use? RNA 2016;22(6):839–851.
24. Ye Y, Chen Z, Jiang S, et al. Single-cell profiling reveals distinct adaptive immune hallmarks in MDA5+ dermatomyositis with therapeutic implications. Nat Commun 2022;13(1):6458.
25. Makinde HM, Dunn JLM, Gadhvi G, et al. Three distinct transcriptional profiles of monocytes associate with disease activity in scleroderma patients. Arthritis Rheumatol 2023;75(4):595–608.
26. Langfelder P, Horvath S. WGCNA: an R package for weighted correlation network analysis. BMC Bioinformatics 2008;9(1):559.
27. Pontarini E, Sciacca E, Chowdhury F, et al; Trial for anti–B cell therapy in patients with primary Sjögren syndrome study research group. serum and tissue biomarkers associated with composite of relevant endpoints for Sjögren syndrome (CRESS) and Sjögren tool for assessing response (STAR) to B cell-targeted therapy in the trial of anti-B cell therapy in patients with primary Sjögren syndrome (TRACTISS). Arthritis Rheumatol 2024;76(5):763–776.
28. Aran D, Hu Z, Butte AJ. xCell: digitally portraying the tissue cellular heterogeneity landscape. Genome Biol 2017;18(1):220.

Arthritis & Rheumatology
Vol. 77, No. 1, January 2025, pp 107–115
DOI 10.1002/art.42969

American College of Rheumatology
Empowering Rheumatology Professionals

Novel Genetic Loci in Early-Onset Gout Derived From Whole-Genome Sequencing of an Adolescent Gout Cohort

Aichang Ji,[1] Yang Sui,[2] Xiaomei Xue,[1] Xiapeng Ji,[1] Wenrui Shi,[2] Yongyong Shi,[3] Robert Terkeltaub,[4] Nicola Dalbeth,[5] Riku Takei,[6] Fei Yan,[1] Mingshu Sun,[7] Maichao Li,[1] Jie Lu,[1] Lingling Cui,[1] Zhen Liu,[1] Can Wang,[1] Xinde Li,[1] Lin Han,[1] Zhanjie Fang,[2] Wenyan Sun,[1] Yue Liang,[2] Yuwei He,[1] Guangmin Zheng,[2] Xuefeng Wang,[1] Jiayi Wang,[8] Hui Zhang,[9] Lei Pang,[1] Han Qi,[1] Yushuang Li,[1] Zan Cheng,[1] Zhiqiang Li,[10] Jingfa Xiao,[2] Changqing Zeng,[2] Tony R. Merriman,[11] Hongzhu Qu,[12] Xiangdong Fang,[12] and Changgui Li[13]

Objective. Mechanisms underlying the adolescent-onset and early-onset gout are unclear. This study aimed to discover variants associated with early-onset gout.

Methods. We conducted whole-genome sequencing in a discovery adolescent-onset gout cohort of 905 individuals (gout onset 12 to 19 years) to discover common and low-frequency single-nucleotide variants (SNVs) associated with gout. Candidate common SNVs were genotyped in an early-onset gout cohort of 2,834 individuals (gout onset ≤30 years old), and meta-analysis was performed with the discovery and replication cohorts to identify loci associated with early-onset gout. Transcriptome and epigenomic analyses, quantitative real-time polymerase chain reaction and RNA sequencing in human peripheral blood leukocytes, and knock-down experiments in human THP-1 macrophage cells investigated the regulation and function of candidate gene *RCOR1*.

Results. In addition to *ABCG2*, a urate transporter previously linked to pediatric-onset and early-onset gout, we identified two novel loci ($P_{meta} < 5.0 \times 10^{-8}$): rs12887440 (*RCOR1*) and rs35213808 (*FSTL5-MIR4454*). Additionally, we found associations at *ABCG2* and *SLC22A12* that were driven by low-frequency SNVs. SNVs in *RCOR1* were linked to elevated blood leukocyte messenger RNA levels. THP-1 macrophage culture studies revealed the potential of decreased RCOR1 to suppress gouty inflammation.

Conclusion. This is the first comprehensive genetic characterization of adolescent-onset gout. The identified risk loci of early-onset gout mediate inflammatory responsiveness to crystals that could mediate gouty arthritis. This study will contribute to risk prediction and therapeutic interventions to prevent adolescent-onset gout.

INTRODUCTION

Gout is a polygenic inflammatory arthritis and mostly occurs in adult men, with an average age at onset >45 years.[1] Although rare, gout can occur in adolescents and young adults,[2,3] and the mechanism of early-onset gout is still unknown. Adolescents with gout have higher urate levels and faster development of tophi, and they are more likely to have a family history of gout compared with

Supported by the National Key R&D Program of China (grants 2022YFC2503300, 2022YFC2503304 and 2022YFE0107600), National Natural Science Foundation of China (grants 82220108015 and 82201957), and Natural Science Foundation of Shandong Province (grant ZR2022QH065).

[1]Aichang Ji, PhD, Xiaomei Xue, PhD, Xiaopeng Ji, MS, Fei Yan, PhD, Maichao Li, MS, Jie Lu, PhD, Lingling Cui, PhD, Zhen Liu, PhD, Can Wang, MS, Xinde Li, PhD, Lin Han, MS, Wenyan Sun, PhD, Yuwei He, PhD, Xuefeng Wang, MS, Lei Pang, PhD, Han Qi, MS, Yushuang Li, MS, Zan Cheng, BS: Affiliated Hospital of Qingdao University, Qingdao, China; [2]Yang Sui, PhD, Wenrui Shi, BS, Zhanjie Fang, BS, Yue Liang, MS, Guangmin Zheng, MS, Jingfa Xiao, PhD, Changqing Zeng, PhD: China National Center for Bioinformation, Beijing Institute of Genomics, Chinese Academy of Sciences, and University of Chinese Academy of Sciences, Beijing, China; [3]Yongyong Shi, PhD: Affiliated Hospital of Qingdao University and Biomedical Sciences Institute of Qingdao University (Qingdao Branch of SJTU Bio-X Institutes), Qingdao University, Qingdao, China, and Bio-X Institutes, Key Laboratory for the Genetics of Developmental and Neuropsychiatric Disorders (Ministry of Education), Collaborative Innovation Center for Brain Science, Shanghai Jiao Tong University, Shanghai, China; [4]Robert Terkeltaub, MD, PhD: University of California San Diego School of Medicine, La Jolla; [5]Nicola Dalbeth, MD, PhD: University of Auckland, Auckland, New Zealand; [6]Riku Takei, MS: Asia Pacific Gout Consortium and University of Alabama at Birmingham; [7]Mingshu Sun, MD, PhD: Shandong Provincial Clinical Research Center for Immune Diseases and Gout & Shandong Provincial Key Laboratory of Metabolic Diseases, The Affiliated Hospital of Qingdao University, Qingdao, China; [8]Jiayi Wang, PhD: Development Center for Medical Science & Technology, National Health Commission of the People's Republic of China, Beijing, China; [9]Hui Zhang, PhD: Institute of Metabolic Diseases, Qingdao University, Qingdao, China; [10]Zhiqiang Li, PhD: The Biomedical Sciences Institute and The Affiliated Hospital of Qingdao University, Qingdao University, Qingdao, Shandong, China; [11]Tony R. Merriman, PhD: Asia Pacific Gout Consortium, University of Alabama at Birmingham, Institute of Metabolic Diseases, Qingdao University, Qingdao, China, and University of Otago, Dunedin, New Zealand; [12]Hongzhu Qu, PhD, Xiangdong Fang, MD, PhD: China National Center for Bioinformation, Beijing Institute of Genomics, Chinese Academy of Sciences, University of Chinese Academy of Sciences, and Beijing Key Laboratory of Genome and Precision Medicine Technologies,

those who develop disease in adulthood.[4,5] The percentage of patients with adolescent-onset gout and a family history of gout is 38.7% to 43.8%,[4,5] compared with 25.9% to 30% in gout with onset in early adulthood[6–8] and 11% to 23.8% in gout with the most common pattern of onset later in adulthood.[5,6,8] This supports that the adolescent-onset gout population is more likely to have a stronger genetic background basis. The early onset of complex disease is often familial, with genetic risk factors having a relatively large impact on risk in younger patients.[9] Therefore, genetic studies of adolescent-onset gout can provide novel insights into the mechanisms of gout and also may allow identification of new therapeutic targets for adolescents and adults with gout.

Most studies of the genetics of gout have focused on adult-onset disease. Hundreds of genetic variants associated with gout and serum urate levels have been identified by genome-wide association studies (GWASs) in adults (mean age 37.6 to 76.4 years old).[10–12] Other than rare mutations that cause hypoxanthine guanine phosphoribosyltransferase deficiency or phosphoribosylpyrophosphate synthetase superactivity and major perturbations in purine metabolism,[13] gene variants previously associated with gout with adult onset before age 40 have only been described in *ABCG2*,[14] a high-capacity urate transporter that promotes intestinal and renal excretion of urate. Moreover, in a Czechia study of 31 patients with pediatric-onset gout, 2 common (p.V12M, p.Q141K) and 3 very rare (p.K360del, p.T421A, p.T434M) allelic *ABCG2* variants were detected.[15]

Routine array-based GWASs are common in adult patients with gout, usually focusing on common variants, and the imputation quality to study less common variants depends on the reference panel size and genetic distance from the target population.[16] Deep whole-genome sequencing (WGS) is the gold standard to fully capture genetic variation, which provides the means to comprehensively analyze common variants, uncommon variants, and indels to discover etiological variants associated with disease.[17] Here, we conducted WGS, association analysis, and replication in an adolescent-onset gout and an early-onset gout cohort (a total of 3,739 individuals) to discover loci associated with early-onset gout.

METHODS

Study cohort. Gout onset between the ages of 12 and 19 years old was defined as adolescent-onset gout. The adolescent-onset gout cohort included 280 individuals diagnosed with adolescent-onset gout, 191 individuals with hyperuricemia, and 434 normouricemic individuals. The independent early-onset gout replication cohort, defined as having gout with onset at ≤30 years of age, comprised 824 individuals with early-onset gout, 926 who were hyperuricemic, and 1,084 who were normouricemic. Normouricemic individuals are controls who do not develop hyperuricemia or gout beyond the period of adolescence. All participants in this study are male because gout rarely occurs in girls and young premenopausal women in the absence of monogenic syndromes such as Lesch-Nyhan syndrome. All participants were recruited from the Affiliated Hospital of Qingdao University except 332 normouricemic individuals from Beijing Institute of Genomics, Chinese Academy of Sciences/China National Center for Bioinformation (BIG). All patients with gout analyzed in the study were examined by rheumatologists and met the 2015 American College of Rheumatology/EULAR classification criteria for gout.[18] Hyperuricemia was defined as serum urate concentration >7 mg/dL (>420 μmol/L). The normouricemic control participants were attained via site survey. Practice lists of normouricemic control participants were screened for potentially suitable participants by excluding those with hyperuricemia, diabetes, cancer, and other arthritis-related illnesses.

Ethics statement. All participants in this study provided written informed consent. In concordance with the Declaration of Helsinki, this study was reviewed and approved by the ethics committee of the Affiliated Hospital of Qingdao University (QYFYKYLL923011921) and BIG (2015H023).

WGS and data processing. DNA of the GWAS cohort was extracted from whole blood by the Qiagen Blood Midi Kit (Qiagen, Hilden, Germany). Qingdao data were generated by BGISEQ-500 WGS library preparation[19] and BGISEQ-500 (PE 100) platform. Data from BIG were generated by NEXTflex Rapid DNA-seq Kit (catalog no. 5144-08, Bioo Scientific Corporation, Austin, TX) library preparation and Hi-Seq X Ten, Hi-Seq 3000, and Hi-Seq 4000 platforms. Adapter sequences and low-quality bases were removed using SOAPnuke (version 1.5.6),[20] and filtered reads were aligned to human reference genome (hg19) using BWA (Burrows-Wheeler Aligner, version 0.7.12) with default parameters.[21] The duplicated reads of polymerase chain reaction (PCR) amplification were removed using the Picard tool (http://broadinstitute.github.io/picard/). GATK (version 3.3)[22]

Beijing, China; [13]Changgui Li, MD, PhD: The Affiliated Hospital of Qingdao University, Qingdao, China, Asia Pacific Gout Consortium, and Institute of Metabolic Diseases, Qingdao University, Qingdao, China.

Authors A. Ji, Sui, Xue, X. Ji, W. Shi, Y. Shi contributed equally to this work.

Additional supplementary information cited in this article can be found online in the Supporting Information section (https://acrjournals.onlinelibrary.wiley.com/doi/10.1002/art.42969).

Author disclosures are available at https://onlinelibrary.wiley.com/doi/10.1002/art.42969.

Address correspondence via email to Tony R. Merriman, PhD, at tony.merriman@otago.ac.nz, Hongzhu Qu, PhD, at quhongzhu@big.ac.cn, Xiangdong Fang, MD, PhD, at fangxd@big.ac.cn, or Changgui Li, MD, PhD, at changguili@vip.163.com.

Submitted for publication June 20, 2024; accepted in revised form August 5, 2024.

HaplotypeCaller was used for variants calling, and variants were further filtered in confidence level 99.0 with variant quality score recalibration; then, the variants were annotated with ANNOVAR (version 2018-04-16).[23] The novel single-nucleotide variants (SNVs) and novel indels were obtained by comparing to other public data sets, including dbSNP (version 150), ExAC (version 0.3), the gnomAD genome collection (version 2.1.1), the NHLBI Exome Sequencing Project, and the 1000 Genomes Project.

GWAS. Individuals were first classified into the G-NG group (individuals with gout vs individuals without gout) and the G-H group (individuals with gout vs individuals with hyperuricemia). The GWAS was performed using the PLINK software package (version 1.9)[24] in each group. Individuals with ambiguous sex, genotype missing rate >0.05, heterozygosity rate exceeding ±3 SDs, and kinship coefficients >0.0884, as well as outliers that greatly departed from other samples detected by principal component analysis, were excluded (Supplementary Figure 1). Variants with genotype missing rate >0.05, minor allele frequency (MAF) <0.05, and departures from Hardy-Weinberg equilibrium ($P < 1 \times 10^{-6}$) were also removed. For principal component (PC) analysis, we intersected autosomal variants outside the high linkage disequilibrium (LD) region and pruned variants by PLINK2 software with –indep-pairwise option 1000 100 0.2. Using these genotypes, we calculated the first 10 PCs by PLINK2 software –pca option. Multivariable-adjusted logistic regression association analysis was performed with the first 10 PCs as covariables. To correct the influence of different sequencing platforms, sequencing platform batches were also included as covariables. The online tool LocusZoom (http://locuszoom.sph.umich.edu/)[25] was used to visualize specific regions.

Gene-based SKAT. Sequence kernel association test (SKAT)[26] on common and low-frequency variants was performed using the R-package SKAT (http://www.hsph.harvard.edu/lin-lab/skat/). SKAT CommonRare methods was used to evaluate the effect of common (MAF ≥0.05) or low-frequency variants (MAF <0.05 and minor allele counts ≥ 2) separately.

TWAS. Transcriptome-wide association study (TWAS) was performed by MetaXcan framework and the GTEx version 0.8 expression quantitative trait locus (eQTL) multivariate adaptive shrinkage (MASHR) models (https://predictdb.org/).[27] In addition, eQTL data from the ImmuNexUT database built with Japanese immune cells, combined with Hapmap3 Chinese and Japanese genotype data, were used for ImmuNexUT eQTL MASHR model construction.[28] GTEx version 0.8 TWAS was performed for data from five tissues implicated in gout and serum urate,[1] including whole blood, kidney cortex, colon sigmoid, colon transverse, and liver, separately. ImmuNexUT TWAS was performed for data from four types of immune cells, including plasmacytoid dendritic cells, myeloid dendritic cells, nonclassical monocytes, and double negative B cells. Finally, meta-analysis across these different tissues and cell types were performed separately by S-Multixcan to test the joint effect of genes on phenotype under different models.

Replication. Candidate common SNVs for replication were selected using the following criteria: (1) lead SNVs with a $P \leq 1 \times 10^{-4}$ in either the G-NG group or G-H group (LD, $r^2 < 0.2$); (2) four SNVs, including rs2273406, rs41303970, rs7515191, and rs6680315, located in the *GCLM* region from the TWAS analysis, and three SNVs, including rs8009475, rs35258120, and rs35785423, in the *RCOR1* region from the TWAS analysis. DNA of the replication cohort was extracted from whole blood by the Magnetic Whole Blood Genome Extraction Kit (NanoMagBio, Wuhan, China), and NEXTflex Rapid DNA-seq Kit (catalog no. 5144-08, Bioo Scientific Corporation, Austin, TX) was used to prepare libraries. Candidate common SNVs were genotyped by targeted sequencing using an Illumina Nova seq 6000. Case-control association analysis of the variants was conducted using the same model as the GWAS. Cochran's Q test and the I^2 index were used to quantify the degree of heterogeneity. The meta-analyses using a fixed-effects model were conducted in METAL software[29] using the standard error SE (STDERR) model, which takes into account effect size estimate and the association results for each SNV across GWASs, and replication data sets were combined.

Functional analysis of *RCOR1*. Firstly, functional annotation of *RCOR1* risk loci was performed using epigenome data (Supplementary Material). Secondly, quantitative real-time polymerase chain reaction (RT-qPCR) and RNA sequencing (RNA-seq) in peripheral blood leukocytes of patients with gout were conducted to quantify the relative expression of *RCOR1*, and gene ontology (GO; https://geneontology.org/) enrichment analyses of differentially expressed genes (DEGs) in different genotypes of the *RCOR1* risk loci was performed. The RT-qPCR primers are in Supplementary Table 1. Thirdly, a human monocyte leukemia cell line (THP-1) was cultured, and the lentiviral knock-down vector of RCOR1 was produced. Lastly, knock-down experiments in human THP-1 macrophage cells were performed and protein concentrations measured by Western blot for RCOR1 and pro–interleukin-1β (IL-1β), as well as protein concentrations of IL-1β in supernatants determined by enzyme-linked immunosorbent assay to investigate the regulation and functions of candidate gene *RCOR1*. The Supplementary Methods provide further details.

Statistical analysis. All experimental data with a normal distribution were presented as mean ± SD and analyzed with the aid of SPSS17.0 statistical software. Statistical significance was determined by one-way analysis of variance (ANOVA). For data with equal variances assumed, ANOVA followed by the least

significance difference test was applied. For data with equal variances not assumed, ANOVA followed by Dunnett's T3 test was used. Data in bar graphs are expressed as means ± SEM. A probability of <0.05 was considered to be statistically significant.

RESULTS

Genomic resource of Chinese adolescent-onset gout cohort. We enrolled 905 male participants including 280 people with gout, 191 people with hyperuricemia, and 434 normouricemic individuals as the Chinese adolescent-onset gout cohort. The urate concentration in patients with adolescent-onset gout was significantly higher than that in individuals with hyperuricemia and normouricemia (Supplementary Figure 2A). The positive family history of gout in adolescents was 40.36%, and 11.28% of individuals had palpable tophi (Supplementary Table 2). A total of 31.36 million SNVs and 4.22 million indels were obtained after WGS with a median sequencing coverage of 25× (Supplementary Figure 3) and quality control on variants. Of them, 11.14 million SNVs and 3.47 million indels were novel (Supplementary Figure 2B). Of the 35.58 million genetic variants, 80.65% were located in intronic and intergenic regions; only 0.34 million SNVs were found in protein-coding regions. The distributions of the genetic variants were 20.15% common SNVs (MAF ≥0.05, 7.17 million), 79.85% low-frequency SNVs (MAF <0.05, 28.41 million), and 72.71% uncommon SNVs (MAF <0.01, 25.87 million) (Supplementary Figure 2C).

Identification of risk loci from common variants. We first performed GWAS on common SNVs in the G-NG group (270 gout vs 608 individuals without gout) and the G-H group (270 gout vs 183 individuals with hyperuricemia) after the quality control. A total of 571 and 550 gout-associated SNVs were identified as putative associations ($P_{discovery} < 1.0 \times 10^{-4}$) from the G-NG and G-H groups, respectively (Supplementary Tables 3 and 4). Among these, all SNVs that reached nominal genome-wide significance ($P_{discovery} < 5.0 \times 10^{-8}$) were located in the 4q22.1 region (Figure 1A and B), which contains the *ABCG2* locus, also established in adult gout.

We performed both TWAS and gene-based SKAT on common SNVs to evaluate the joint effect of SNVs at the gene level. Four genes were all discovered from the results of GTEx version 0.8 TWAS, SKAT, and GWAS ($P_{TWAS} < 5 \times 10^{-4}$, $P_{GWAS} < 1 \times 10^{-4}$, and $P_{SKAT} < 5 \times 10^{-4}$), including the known genes *ABCG2* and *PKD2*, a novel gene *GCLM* significant in both the G-NG and G-H groups (Figure 1C and D), and a novel gene *RCOR1* significant only in the G-H group (Figure 1D). After further validation by ImmuNexUT TWAS (East Asian population, $P_{TWAS} < 5 \times 10^{-4}$), genes *PKD2* in the G-NG group and *RCOR1* in the G-H group were still significant (Supplementary Figure 4).

For validation, 166 independent association signals (LD, $r^2 < 0.2$), combined with 7 SNVs in *GCLM* (rs7515191, rs6680315, rs2273406, and rs41303970) and *RCOR1* (rs8009475, rs35258120, and rs35785423) included in the TWAS were genotyped in an independent Chinese case-control cohort (n = 2,834; gout = 824, hyperuricemia = 926, and normouricemia = 1,084). Due to the low prevalence of adolescent-onset gout, we recruited patients with gout with age at onset ≤30. The ages of participants in the replication stage were mean ± SD 24.92 ± 4.44, 18.30 ± 0.54, and 16.70 ± 2.23 years for gout, hyperuricemia, and normouricemia, respectively. The sequencing depths of the 173 variants were more than 50×, and all variants were detected in the cohorts (Supplementary Figure 5). Using the same criteria of quality control as that in discovery stage, a total of 2,417 participants were included in further analysis, including 699 with gout, 802 with hyperuricemia, and 916 with normouricemia. After conducting association analysis in the replication data set, we performed meta-analysis combining the results from the discovery and replication data sets. At the genome-wide significance level ($P < 5.0 \times 10^{-8}$), in addition to SNVs that had already been reported for gout-associated loci (*ABCG2* and *PKD2*, Supplementary Table 5), we identified three novel associations in the G-H group: rs35213808 of *FSTL5-MIR4454* ($P_{meta} = 1.99 \times 10^{-11}$; odds ratio $[OR]_{meta} = 1.92$), rs12887440 of *RCOR1* ($P_{meta} = 1.32 \times 10^{-10}$; $OR_{meta} = 1.65$), and rs8009475 of *RCOR1* ($P_{meta} = 3.43 \times 10^{-10}$; $OR_{meta} = 1.63$; $r^2 = 0.90$ with rs12887440) (Figure 1E and F, Table 1). However, the locus *GCLM* detected in the discovery stage did not reach the genome-wide significance level in the replication stage (Supplementary Table 6). No significant loci were identified in the G-NG group. The sequence qualities of the final three novel associated single-nucleotide polymorphisms in the discovery and replication data sets are listed in Supplementary Table 7 and Supplementary Table 8, respectively. Cochran's Q test and the I^2 index showed that these three loci had no significant heterogeneity (I^2 <75%, Supplementary Table 9).[30]

Functional regulation of RCOR1 by identified SNVs. Because *RCOR1*, identified by the analysis of GWAS, TWAS, and SKAT in the discovery stage, also reached the genome-wide significance level after meta-analysis, we functionally annotated the SNVs in *RCOR1*. The two maximally associated SNVs were located in the promoter (rs8009475) and the second intron (rs12887440) of *RCOR1*. The region harboring rs12887440 was enriched with active histone modification markers (H3K4me1 and H3K27ac) in gout-relevant cells and tissues, including E029 (primary monocytes from peripheral blood), E124 (monocytes-$CD14^+$ RO01746 primary cells), E066 (liver), E062 (primary mononuclear cells from peripheral blood), and E034 (primary T cells from peripheral blood). Furthermore, Hi-C evidence[31] suggested that this region regulates the promoter (harboring rs8009475) by a long-range chromatin conformation interaction. In addition, we observed that rs12887440 associated with 14 DNA methylation (DNAm) sites ($P < 1 \times 10^{-5}$) in a whole-blood DNA methylation QTL data set.[32] Of the 14 DNAm sites, cg10501036 (511 bp from rs8009475) was located in the *RCOR1* promoter

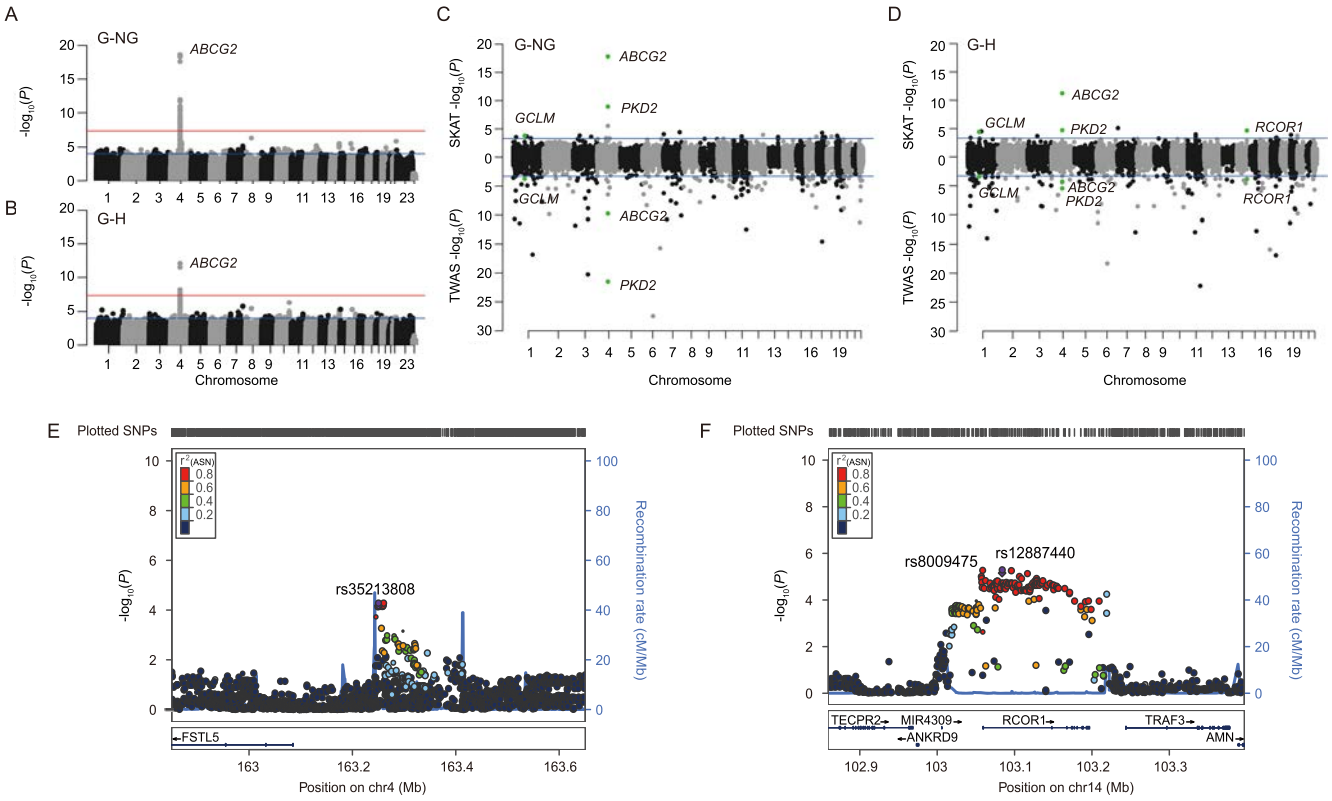

Figure 1. Manhattan plots and regional association plots for the loci identified from GWAS, SKAT, and TWAS. Manhattan plot of GWAS in the G-NG group (A) and the G-H group (B) is given. The upper red horizontal line indicates the genome-wide significance threshold ($P = 5.0 \times 10^{-8}$). The lower blue horizontal line indicates the cut-off level for selecting SNVs for replication ($P = 1.0 \times 10^{-4}$). Gene-level Manhattan plot from SKAT (upper) and TWAS (lower) of G-NG group (C) and G-H group (D) is given. The blue solid horizontal line indicates the cut-off level for selecting genes ($P = 5.0 \times 10^{-4}$). Regional association plot is shown for two novel loci identified from meta-analysis: *FSTL5-MIR4454* (E) and *RCOR1* (F). The vertical axis represents –log10(*P* value) for the test of SNV association with gout in the GWAS stage. The SNV with the lowest *P* value is depicted as a pink diamond, and neighboring SNVs are colored according to the extent of linkage disequilibrium (measured in r^2) based on 1000 Genomes phase 3. Genomic coordinates are based on NCBI human genome reference sequence build 37. AMN, amnion associated transmembrane protein; ANKRD, ankyrin repeat domain; ASN, asian; chr, chromosome; GWAS, genome-wide association study; G-H, gout vs individuals with hyperuricemia; G-NG, gout vs individuals without gout; MIR4309, microRNA 4309; RCOR1, REST corepressor 1; SKAT, sequence kernel association test; SNP, single-nucleotide polymorphism; SNV, single-nucleotide variant; TECPR2, tectonin beta-propeller repeat containing 2; TRAF3, tnf receptor associated 3; TWAS, transcriptome-wide association study.

Table 1. Novel SNVs associated with gout at a genome-wide level of significance in G-H group*

rs id	Gene	A1/A2[a]	Stage (n)	No. of participants		A1 frequency		OR (95% CI)	*P* value
				Cases	Controls	Cases	Controls		
rs35213808	*FSTL5-MIR4454*	T/A	Discovery (453)	270	183	0.756	0.623	1.89 (1.38–2.58)	6.59×10^{-5}
			Replication (1,501)	699	802	0.720	0.658	1.93 (1.52–2.46)	6.97×10^{-8}
			Meta (1,954)	969	985			1.92 (1.59–2.34)	1.99×10^{-11}
rs8009475	*RCOR1*	G/A	Discovery (453)	270	183	0.686	0.544	2.02 (1.49–2.74)	7.31×10^{-6}
			Replication (1,501)	699	802	0.669	0.600	1.52 (1.27–1.81)	2.96×10^{-6}
			Meta (1,954)	969	985			1.63 (1.40–1.89)	3.43×10^{-10}
rs12887440	*RCOR1*	A/G	Discovery (453)	270	183	0.676	0.530	1.98 (1.47–2.66)	7.00×10^{-6}
			Replication (1,501)	699	802	0.664	0.594	1.54 (1.29–1.84)	1.57×10^{-6}
			Meta (1,954)	969	985			1.65 (1.41–1.92)	1.32×10^{-10}

* G-H, gout vs individuals with hyperuricemia; OR, odds ratio; SNV, single-nucleotide variant; 95% CI, 95% confidence interval.
[a] Allele A1 is the risk-associated allele, and allele A2 is the non–risk-associated allele.

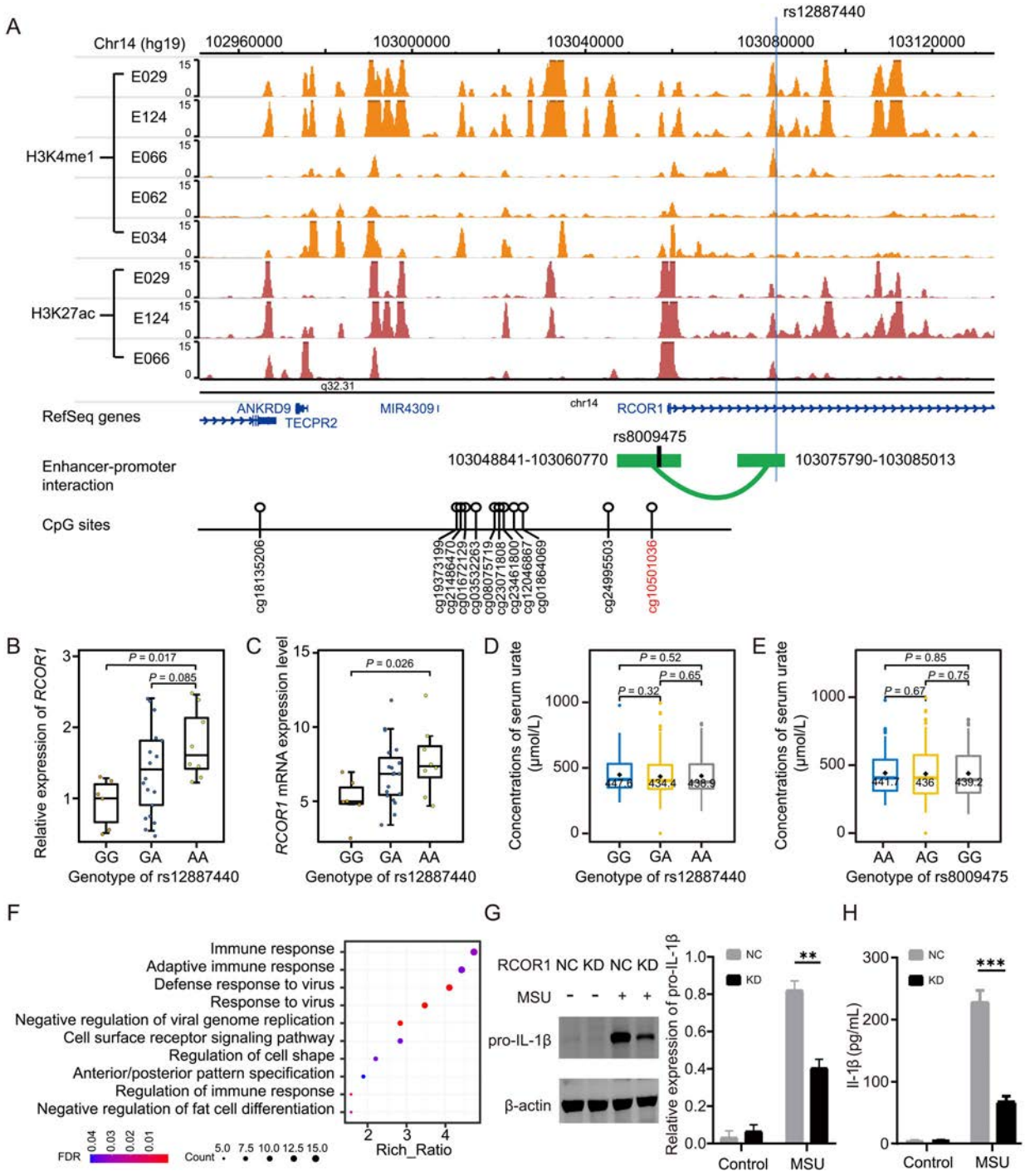

Figure 2. *RCOR1* is involved in the immune process of gout. (A) Functional annotation of rs12887440. The locus where rs12887440 resides is enriched with both H3K4me1 (orange) and H3K27ac (brown) modifications, suggesting an enhancer function of this region. The interaction of rs12887440-residing region with the promoter of *RCOR1* where rs8009475 was located as revealed by Hi-C schematic representation (green curve) is shown in 3D Genome browser. The CpG residing in the promoter of *RCOR1* is marked in red. The expression of *RCOR1* was significantly increased in the rs12887440 AA carriers (n = 8) compared with GG carriers (n = 6; $P < 0.05$) by RT-qPCR (B) and RNA-seq (C). A is the risk allele. Association between serum urate concentration and rs12887440 alleles (D) and rs8009475 alleles (E) is shown. (F) Top 10 biologic process terms enriched by differentially expressed genes in whole blood of rs12887440-AA carriers compared with that of rs12887440-GG carriers are shown. The protein expression of pro–IL-1β via Western blotting, using β-actin as an internal control (G) and the levels of IL-1β secretion in the supernatant via ELISA (H) in *RCOR1*-KD THP-1 cells after MSU crystal treatment as indicated. –, MSU untreated; +, MSU treated; NC, negative control THP-1 cells without *RCOR1* treatment (n = 3). Data are mean ± SEM. *P* values were determined by *t*-test. $^{*}P < 0.05$; $^{**}P < 0.01$; $^{***}P < 0.001$. ANKRD9, ankyrin repeat domain 9; chr, chromosome; ELISA, enzyme-linked immunosorbent assay; FDR, false discovery rate; IL, interleukin; KD, knock-down; MIR4309, microRNA 4309; MSU, monosodium urate; RCOR1, REST corepressor 1; RNA-seq, RNA sequencing; RT-qPCR, quantitative real-time polymerase chain reaction; TECPR2, tectonin beta-propeller repeat containing 2. Color figure can be viewed in the online issue, which is available at http://onlinelibrary.wiley.com/doi/10.1002/art.42969/abstract.

(Figure 2A). These findings suggest that rs12887440 may influence *RCOR1* expression. To confirm this, we measured the expression of *RCOR1* in the whole blood of 32 individuals from the adolescent gout cohort with the genotype of GG (n = 6), GA (n = 18), or AA (n = 8) at rs12887440. The homozygous risk allele carriers (AA allele) displayed significantly higher *RCOR1* messenger RNA levels in their whole blood compared with the noncarriers (GG allele) through both RT-qPCR and RNA-seq (Figure 2B and C), which suggests that rs12887440 is associated with the expression of *RCOR1*.

***RCOR1* involvement in the inflammatory process of gout.** Because *RCOR1* was identified as being associated with gout in the G-H group, we hypothesized that its role was in the immune process and not via urate homeostasis. To confirm this, we first performed an association analysis between *RCOR1* SNVs and serum urate concentrations in all participants included in the discovery and replication stages, and we found that different genotypes of rs12887440 and rs8009475 were not associated with serum urate concentrations ($P > 0.05$, Figure 2D and E). Furthermore, through RNA-seq on individuals with different genotypes of rs12887440, we identified 404 DEGs in rs12887440 AA allele carriers compared with the rs12887440 GG carriers. As the top 10 GO biologic process terms showed, these DEGs were involved in immune-related pathways such as immune system process, immune response, adaptive immune response, and regulation of immune response (Figure 2F), suggesting that *RCOR1* is possibly involved in the inflammatory process of gout.

Monosodium urate (MSU) crystals interact with resident macrophages to activate the NOD-, LRR-, and pyrin domain-containing protein 3 (NLRP3) inflammasome, leading to release of bioactive IL-1β.[1] To examine whether RCOR1 suppresses or promotes inflammation in gout development, we used THP-1–derived macrophages in which RCOR1 was knocked down (RCOR1-KD) to determine the function of RCOR1 in MSU crystal–induced inflammation. The cells did not express pro–IL-1β and IL-1β when there was no inflammatory stimulus, regardless of the expression level of RCOR1. However, after exposure to MSU crystals to stimulate the immune response, the protein levels of intracellular pro–IL-1β and IL-1β levels in the supernatant were significantly reduced in RCOR1-KD cells compared with control cells (Figure 2G and H). These findings demonstrate that RCOR1 could be actively involved in development of gouty inflammation.

Gene-based SKAT for low-frequency SNVs. To determine whether low-frequency SNVs (MAF < 0.05) are associated with gout and hyperuricemia in adolescents, we conducted gene-based SKAT on low-frequency SNVs with minor allele counts ≥2. As anticipated, *ABCG2* reached the genome-wide significance level in the G-NG group ($P_{ABCG2} = 1.81 \times 10^{-8}$) after Bonferroni correction ($P_{\text{Bonferroni}} < 2.09 \times 10^{-6}$, 23,869 gene sets). Solute carrier family 22 member 12 (*SLC22A12*), which is associated with serum urate levels,[33] was also significant in the G-NG group ($P_{SLC22A12} = 1.06 \times 10^{-8}$), consistent with multiple previous reports of association of uncommon variants with hypouricemia.[12,34] There were no genes with significant association in the G-H group (Supplementary Table 10).

DISCUSSION

This study comprehensively characterized adolescent-onset gout genomes. In addition to the gout risk locus *ABCG2*, which was previously linked in a small Czech Republic study to pediatric-onset gout,[15] and to *ABCG2* and *PKD2* identified in previous GWASs of gout,[12] genetic analyses of the WGS data allowed us to identify two novel common risk loci and two genes driven by low-frequency variants associated with gout. These results provide more insights into the genetic basis of gout than traditional array-based genotyping analyses by using deep sequencing data in people with early-onset gout, who are expected to have a stronger genetic contribution to disease.

Genetic variants related to immune response were identified in the adolescent-onset gout cohort. Regarding common variants, two novel candidate gout risk loci (*RCOR1* and *FSTL5-MIR4454*) were identified, of which one (*RCOR1*) may have a role in inflammation and immunity. REST corepressor 1 (*RCOR1* or CoREST), which we identified as associated with gout in the G-H group, is a protein that binds to the C-terminal domain of repressor element-1 silencing transcription factor (REST) and regulates diverse immune and inflammatory responses.[35] *Rcor1* deletion disrupts Foxp3-dependent recruitment of the CoREST complex to the promoters of T-bet, IL-2, and interferon-γ, leading to impaired Treg function in vivo and promoting antitumor immunity in mice.[36] T-bet deficiency alleviates MSU crystal–induced inflammatory cell infiltration in peritonitis and air pouch models in vivo, in addition to reducing the IL-1β levels of air pouch lavage fluid.[37] In our study, the risk allele A of the lead SNV rs12887440 in *RCOR1* had a higher allele frequency in patients with gout compared with hyperuricemia, and we observed that the risk allele increases the expression of *RCOR1*. The A allele of rs12887440 and the G allele of rs8009475 were not associated with serum urate levels (Figure 2C and D). Functional experiments in THP-1 macrophage cells indicated that *RCOR1* has a role in promoting gouty inflammation. These findings suggest that the *RCOR1* locus is proinflammatory and contributes to the progression from hyperuricemia to gout. We also identified rs35213808, an SNV in the intergenic region between *FSTL5* and *MIR4532*. *FSTL5* inhibits the Wnt/β-catenin signaling pathway in a hepatocellular carcinoma cell line.[38] In this study, rs35213808 in *FSTL5-MIR4454* was not associated with serum urate levels (Supplementary Figure 6), suggesting that it may play a role by affecting inflammation in the development of gout in adolescents.

Besides common variants, we also found low-frequency SNVs associated with adolescent gout. Low-frequency SNVs were associated with adolescent gout at *ABCG2* and *SLC22A12*, which have previously been reported to be associated with hyperuricemia and gout.[12,15,39] Our results will improve our understanding of the role of uncommon variants in gout progression.

The genetic risk variants in patients with adolescent-onset gout may contribute to clinical manifestations such as faster development of tophi and the earlier onset of gout. In this adolescent-onset gout study, we discovered a novel locus, *RCOR1*, involved in immune response. Immune-associated genetic variants for gout in adolescence may result in individuals being more sensitive to the inflammatory response to MSU crystals, leading to early onset of gout. Because our experiments found that the knock-down of RCOR1 caused lower IL-1β levels, this shows that RCOR1 has a role in promoting gouty inflammation in THP-1 cells after MSU crystal treatment. Greater sensitivity to MSU crystal inflammatory responses may be a major cause of early onset of gout.

However, due to the low prevalence of gout in adolescents, this study had limitations in discovering more gout-related genes and uncommon variants in adolescents. Although we used East Asian immune cell data to construct MASHR models to avoid differences in LD structure or variance covariance matrix due to different ancestry, the lack of available data on gene expression and genotypes in East Asian gout-related tissues prevented us from using TWAS to explore additional genes that might be associated with gout. In addition, our study shows that the newly discovered adolescent-onset gout risk genes mainly have the potential to regulate gout inflammation and immunity, but the specific regulatory mechanisms remain to be elucidated. The functional RCOR1 experiments in THP-1 macrophage cells probed effects on the inflammatory phenotype of the disease. However, a much larger scope of studies would be needed to examine the etiology, once hyperuricemia is achieved, of developing gout, which requires MSU crystal deposition in the joint. That process involves the joint surface lubrication by lubricin, collagen II release from cartilage, and homeostasis of articular cartilage, synovium, and other tissues in the joint, which is disrupted by several proteases released by inflammatory cells.[40] Moreover, there are 16,419 target genes of the RCOR1 transcription factor repressor in chromatin immunoprecipitation sequencing data sets from the ENCODE Transcription Factor Targets data set (https://www.ncbi.nlm.nih.gov/gene/23186). They include not only NLRP3, IL-1β, and IL-6, but also multiple genes that regulate lubricin proteolytic turnover (*ITIH3*, *THBS1*, *ELANE*, *TLR2*, *SERPINB6*).[40] Notably, RCOR1 also modulates articular chondrocyte homeostasis and cartilage integrity.[41]

This is the first report of comprehensive characterization of adolescent-onset gout genomes, and risk loci of early-onset gout were identified. Novel loci involved in inflammatory response may contribute to early-onset gout. This study will contribute to a better understanding of the mechanisms of adolescent-onset gout and be helpful for drug development, risk prediction, and intervention to prevent adolescent-onset gout and early-onset gout.

ACKNOWLEDGMENTS

We are grateful to all anonymous participants in the adolescent cohort, including part of the healthy control cohort, which was supported by a grant from the Key Program of the Chinese Academy of Sciences (KJZD-EW-L14).

AUTHOR CONTRIBUTIONS

All authors were involved in drafting the article or revising it critically for important intellectual content, and all authors approved the final version to be published. Dr C. Li, X. Fang, Qu, and Merriman had full access to all of the data in the study and take responsibility for the integrity of the data and the accuracy of the data analysis.

Study conception and design. Y. Shi, Terkeltaub, Dalbeth, M. Sun, Merriman, Qu, X. Fang, C. Li.

Acquisition of data. A. Ji, Sui, Xue, X. Ji, Yan, Lu, Cui, Liu, C. Wang, X. Li, Han, Z. Fang, W. Sun, Liang, He, Zheng, X. Wang, J. Wang, Zhang, Pang, Qi, Y. Li, Cheng, Xiao, Zeng.

Analysis and interpretation of data. A. Ji, Sui, Xue, W. Shi, Takei, Yan, M. Li, Z. Li, Qu, X. Fang, C. Li.

REFERENCES

1. Dalbeth N, Gosling AL, Gaffo A, et al. Gout. Lancet 2021;397(10287):1843–1855.
2. Kuo CF, Grainge MJ, Mallen C, et al. Rising burden of gout in the UK but continuing suboptimal management: a nationwide population study. Ann Rheum Dis 2015;74(4):661–667.
3. Ito S, Torii T, Nakajima A, et al. Prevalence of gout and asymptomatic hyperuricemia in the pediatric population: a cross-sectional study of a Japanese health insurance database. BMC Pediatr 2020;20:481.
4. Zheng S, Lee PY, Huang Y, et al. Clinical characteristics of juvenile gout and treatment response to febuxostat. Ann Rheum Dis 2022;81(4):599–600.
5. Chen SY, Shen ML. Juvenile gout in Taiwan associated with family history and overweight. J Rheumatol 2007;34(11):2308–2311.
6. Gao Q, Cheng X, Merriman TR, et al. Trends in the manifestations of 9754 gout patients in a Chinese clinical center: a 10-year observational study. Joint Bone Spine 2021;88:105078.
7. Yu KH, Luo SF. Younger age of onset of gout in Taiwan. Rheumatology (Oxford) 2003;42(1):166–170.
8. Li Y, Piranavan P, Sundaresan D, et al. Clinical characteristics of early-onset gout in outpatient setting. ACR Open Rheumatol 2019;1(7):397–402.
9. Schrag A, Schott JM. Epidemiological, clinical, and genetic characteristics of early-onset parkinsonism. Lancet Neurol 2006;5(4):355–363.
10. Köttgen A, Albrecht E, Teumer A, et al; LifeLines Cohort Study; CARDIoGRAM Consortium; DIAGRAM Consortium; ICBP Consortium; MAGIC Consortium. Genome-wide association analyses identify 18 new loci associated with serum urate concentrations. Nat Genet 2013;45(2):145–154.
11. Major TJ, Takei R, Matsuo H, et al. A genome-wide association analysis of 2,622,830 individuals reveals new pathogenic pathways in gout. medRxiv Preprint posted online November 29, 2022. https://doi.org/10.1101/2022.11.26.22281768

12. Tin A, Marten J, Halperin Kuhns VL, et al; German Chronic Kidney Disease Study; Lifelines Cohort Study; V. A. Million Veteran Program. Target genes, variants, tissues and transcriptional pathways influencing human serum urate levels. Nat Genet 2019;51(10):1459–1474.
13. Dewulf JP, Marie S, Nassogne MC. Disorders of purine biosynthesis metabolism. Mol Genet Metab 2022;136(3):190–198.
14. Matsuo H, Ichida K, Takada T, et al. Common dysfunctional variants in ABCG2 are a major cause of early-onset gout. Sci Rep 2013;3:2014.
15. Stiburkova B, Pavelcova K, Pavlikova M, et al. The impact of dysfunctional variants of ABCG2 on hyperuricemia and gout in pediatric-onset patients. Arthritis Res Ther 2019;21(1):77.
16. Quick C, Anugu P, Musani S, et al. Sequencing and imputation in GWAS: cost-effective strategies to increase power and genomic coverage across diverse populations. Genet Epidemiol 2020;44(6):537–549.
17. Turro E, Astle WJ, Megy K, et al; NIHR BioResource for the 100,000 Genomes Project. Whole-genome sequencing of patients with rare diseases in a national health system. Nature 2020;583(7814):96–102.
18. Neogi T, Jansen TLTA, Dalbeth N, et al. 2015 Gout classification criteria: an American College of Rheumatology/European League Against Rheumatism collaborative initiative. Arthritis Rheum 2015;67(10):2557–2568.
19. Huang J, Liang X, Xuan Y, et al. BGISEQ-500 WGS library construction. Protocols.io. 2018. Accessed [May 10, 2018]. https://www.protocols.io/view/bgiseq-500-wgs-library-construction-dm6gpn5jlzpn
20. Chen Y, Chen Y, Shi C, et al. SOAPnuke: a MapReduce acceleration-supported software for integrated quality control and preprocessing of high-throughput sequencing data. Gigascience 2018;7(1):gix120.
21. Li H, Durbin R. Fast and accurate long-read alignment with Burrows–Wheeler transform. Bioinformatics 2010;26(5):589–595.
22. DePristo MA, Banks E, Poplin R, et al. A framework for variation discovery and genotyping using next-generation DNA sequencing data. Nat Genet 2011;43(5):491–498.
23. Wang K, Li M, Hakonarson H. ANNOVAR: functional annotation of genetic variants from high-throughput sequencing data. Nucleic Acids Res 2010;38(16):e164.
24. Purcell S, Neale B, Todd-Brown K, et al. PLINK: a tool set for whole-genome association and population-based linkage analyses. Am J Hum Genet 2007;81(3):559–575.
25. Pruim RJ, Welch RP, Sanna S, et al. LocusZoom: regional visualization of genome-wide association scan results. Bioinformatics 2010;26(18):2336–2337.
26. Ionita-Laza I, Lee S, Makarov V, et al. Sequence kernel association tests for the combined effect of rare and common variants. Am J Hum Genet 2013;92(6):841–853.
27. Barbeira AN, Dickinson SP, Bonazzola R, et al; GTEx Consortium. Exploring the phenotypic consequences of tissue specific gene expression variation inferred from GWAS summary statistics. Nat Commun 2018;9(1):1825.
28. Ota M, Nagafuchi Y, Hatano H, et al. Dynamic landscape of immune cell-specific gene regulation in immune-mediated diseases. Cell 2021;184(11):3006–3021.e17.
29. Willer CJ, Li Y, Abecasis GR. METAL: fast and efficient meta-analysis of genomewide association scans. Bioinformatics 2010;26(17):2190–2191.
30. Li HJ, Zhang C, Hui L, et al; GeseDNA Research Team. Novel risk loci associated with genetic risk for bipolar disorder among Han Chinese individuals: a genome-wide association study and meta-analysis. JAMA Psychiatry 2021;78(3):320–330.
31. Wang Y, Song F, Zhang B, et al. The 3D Genome Browser: a web-based browser for visualizing 3D genome organization and long-range chromatin interactions. Genome Biol 2018;19(1):151.
32. Min JL, Hemani G, Hannon E, et al. Genomic and phenotypic insights from an atlas of genetic effects on DNA methylation. Nat Genet 2021;53(9):1311–1321.
33. Tin A, Woodward OM, Kao WH, et al; CARe and CHARGE Consortia. Genome-wide association study for serum urate concentrations and gout among African Americans identifies genomic risk loci and a novel URAT1 loss-of-function allele. Hum Mol Genet 2011;20(20):4056–4068.
34. Tin A, Li Y, Brody JA, et al. Large-scale whole-exome sequencing association studies identify rare functional variants influencing serum urate levels. Nat Commun 2018;9(1):4228.
35. Saijo K, Winner B, Carson CT, et al. A Nurr1/CoREST pathway in microglia and astrocytes protects dopaminergic neurons from inflammation-induced death. Cell 2009;137(1):47–59.
36. Xiong Y, Wang L, Di Giorgio E, et al. Inhibiting the coregulator CoREST impairs Foxp3+ Treg function and promotes antitumor immunity. J Clin Invest 2020;130(4):1830–1842.
37. Yang QB, He YL, Zhang QB, et al. Downregulation of transcription factor T-Bet as a protective strategy in monosodium urate-induced gouty inflammation. Front Immunol 2019;10:1199.
38. Zhang D, Ma X, Sun W, et al. Down-regulated FSTL5 promotes cell proliferation and survival by affecting Wnt/β-catenin signaling in hepatocellular carcinoma. Int J Clin Exp Pathol 2015;8(3):3386–3394.
39. Major TJ, Dalbeth N, Stahl EA, et al. An update on the genetics of hyperuricaemia and gout. Nat Rev Rheumatol 2018;14(6):341–353.
40. Elsaid K, Merriman TR, Rossitto LA, et al. Amplification of inflammation by lubricin deficiency implicated in incident, erosive gout independent of hyperuricemia. Arthritis Rheumatol 2023;75(5):794–805.
41. Xiao J, Li T, Wu Z, et al. REST corepressor (CoREST) repression induces phenotypic gene regulation in advanced osteoarthritic chondrocytes. J Orthop Res 2010;28(12):1569–1575.

American College of Rheumatology
Empowering Rheumatology Professionals

Arthritis & Rheumatology
Vol. 77, No. 1, January 2025, pp 116–117

LETTER

DOI 10.1002/art.42981

Refining research on systemic lupus erythematosus with key considerations: comment on the article by Xing et al

Qing Zhou, PhD
bayyzq@sina.com
The People's Hospital of Baoan Shenzhen
Shenzhen, China

To the Editor:

The study by Xing et al has made a significant contribution to the understanding of the environmental and genetic factors that influence the development of systemic lupus erythematosus (SLE).[1] However, it is necessary to emphasize a few points that warrant further discussion.

Although this study employs a land-use regression model to estimate air pollution exposure, it could not fully reflect the actual exposure levels of individuals. Factors such as indoor air pollution, personal activity patterns, and short-term exposure peaks are not considered. A representative cohort of participants could be selected and provided with portable air quality monitoring equipment in a future study. Each participant's exposure level to specific pollutants would be recorded at varying times and locations.[2]

The present study does not provide sufficient detail regarding the various subtypes of SLE. SLE is a highly heterogenous disease, and the etiology can vary considerably among patients.[3] The authors are encouraged to gather multidimensional data related to the disease, including clinical characteristics, genetic background, environmental exposure, and so forth. Thereafter, a hierarchical cluster analysis would be selected for the purpose of performing cluster analysis, which would facilitate the identification of distinct subtypes.[4]

The authors have not considered the impact of mental health factors on the development of SLE. Prior research has demonstrated that individuals with a history of depression are at an elevated risk of subsequently developing SLE.[5] The present study does not address the impact of other physiologic diseases on the occurrence of SLE. A previous study has identified a total of 38 comorbidities associated with the incidence of SLE.[6] The research fails to account for the participants' family history of SLE, which is associated with a markedly elevated risk of developing SLE.[7] It would be beneficial to collect information on participants' mental health, comorbidities, family health history, and other relevant confounding variables from the UK Biobank, which could then be incorporated into the statistical model for adjusted analysis.

Author disclosures are available at https://onlinelibrary.wiley.com/doi/10.1002/art.42981.

1. Xing M, Ma Y, Cui F, et al. Air pollution, genetic susceptibility, and risk of incident systemic lupus erythematosus: a prospective cohort study. Arthritis Rheumatol 2024;76(10):1530–1537.
2. Bernasconi S, Angelucci A, Aliverti A. A scoping review on wearable devices for environmental monitoring and their application for health and wellness. Sensors (Basel) 2022;22:5994.
3. Siegel CH, Sammaritano LR. Systemic lupus erythematosus: a review. JAMA 2024;331:1480–1491.
4. Jung JY, Lee HY, Lee E, et al. Three clinical clusters identified through hierarchical cluster analysis using initial laboratory findings in Korean patients with systemic lupus erythematosus. J Clin Med 2022;11:2406.
5. Roberts AL, Kubzansky LD, Malspeis S, et al. Association of depression with risk of incident systemic lupus erythematosus in women assessed across 2 decades. JAMA Psychiatry 2018;75:1225–1233.
6. Chen JH, Lee CTC. Explore comorbidities associated with systemic lupus erythematosus: a total population-based case-control study. QJM 2022;115:17–23.
7. Ulff-Møller CJ, Simonsen J, Kyvik KO, et al. Family history of systemic lupus erythematosus and risk of autoimmune disease: nationwide cohort study in Denmark 1977-2013. Rheumatology (Oxford) 2017;56:957–964.

DOI 10.1002/art.42980

Reply

To the Editor:

We appreciate the author for his letter to the editor regarding our recently published article "Air pollution, genetic susceptibility and risk of incident systemic lupus erythematosus: a prospective cohort study."[1] The author emphasized several points for further discussion, and we address them below.

We aimed to explore the associations between long-term exposure to outdoor air pollution and incidence systemic lupus erythematosus (SLE), and we applied a land-use regression model for exposure assessment, which is a mainstream method in a related field.[2–4] In addition, we also estimated air pollution exposure level at participants' home addresses using data from the UK Department for Environment, Food and Rural Affairs in the sensitivity analysis. Admittedly, considering the precision of exposure assessment, using portable air quality monitoring equipment would be a desirable choice in future research.

Table 1. Associations between long-term exposure to air pollutants and risk of SLE*

Air pollutants	Patients with SLE/total participants	HR (95% CI)
$PM_{2.5}$ per IQR increase	399/459,815	1.16 (1.03–1.30)
PM_{10} per IQR increase	399/459,815	1.22 (1.09–1.38)
NO_2 per IQR increase	399/459,815	1.24 (1.11–1.39)
NO_x per IQR increase	399/459,815	1.11 (1.01–1.22)

* Model 3: Adjusted for age, sex, ethnicity, household income, employment status, smoking status, drinking status, BMI, depression, rheumatoid arthritis, dermatopolymyositis, systemic sclerosis, and Sjögren disease. BMI, body mass index; HR, hazard ratio; IQR, interquartile range; PM, particulate matter; SLE, systemic lupus erythematosus; 95% CI, 95% confidence interval.

Currently, the newly diagnosed patients with SLE in the UK Biobank (UKB) were derived from hospital inpatient data coding International Statistical Classification of Diseases and Related Health Problems, Tenth Revision, and most of them were diagnosed with an unspecified form of SLE. Besides, there were no available data about SLE laboratory values and clinical manifestations in the UKB, so we could not perform hierarchical cluster analysis to identify different clusters. Future studies with multidimensional detailed data could incorporate this analysis and further compare different characteristics among different clusters.

The covariates adjusted in this analysis were generally in line with previous studies.[5] As you suggested, we added baseline depression status and several comorbidities into the model for adjusted analysis, and the results are shown below (Table 1). The prior research found 38 comorbidities associated with incident SLE, of which diffuse diseases of connective tissue exhibited the most robust association.[6] We then selected several characteristic diseases among them, including dermatopolymyositis, systemic sclerosis, Sjögren disease, and another significantly associated disease called rheumatoid arthritis as the adjusted comorbidities. We considered incorporating the family history of SLE as a covariate; however, the UKB only provides family history data for several main diseases now. We failed to get this information on SLE for adjusted analysis.

Meiqi Xing, MASc
Yudiyang Ma, PhD
Feipeng Cui, PhD
Dankang Li, PhD
Jianing Wang, MASc
Linxi Tang, MASc
Lei Zheng, MASc
Tongji Medical College
Huazhong University of Science and Technology
Wuhan, China
Jian Yang, PhD
The First College of Clinical Medical Science, China Three Gorges University & Yichang Central People's Hospital and Hubei Key Laboratory of Ischemic Cardiovascular Disease and Hubei Provincial Clinical Research Center for Ischemic Cardiovascular Disease
Yichang, China
Yaohua Tian, PhD
yaohua_tian@hust.edu.cn
Tongji Medical College
Huazhong University of Science and Technology
Wuhan, China

1. Zhou Q. Refining research on systemic lupus erythematosus with key considerations: comment on the article by Xing et al. Arthritis Rheumatol 2025; 77(1):116.
2. Huang Y, Zhu M, Ji M, et al. Air pollution, genetic factors, and the risk of lung cancer: a prospective study in the UK Biobank. Am J Respir Crit Care Med 2021;204:817–825.
3. Cui F, Sun Y, Xie J, et al. Air pollutants, genetic susceptibility and risk of incident idiopathic pulmonary fibrosis. Eur Respir J 2023;61:2200777.
4. Ma Y, Zhang J, Li D, et al. Genetic susceptibility modifies relationships between air pollutants and stroke risk: a large cohort study. Stroke 2024;55:113–121.
5. Parks CG, de Souza Espindola Santos A, Barbhaiya M, et al. Understanding the role of environmental factors in the development of systemic lupus erythematosus. Best Pract Res Clin Rheumatol 2017; 31(3):306–320.
6. Chen JH, Lee CTC. Explore comorbidities associated with systemic lupus erythematosus: a total population-based case-control study. QJM 2022;115:17–23.

American College of Rheumatology
Empowering Rheumatology Professionals

Arthritis & Rheumatology
Vol. 77, No. 1, January 2025, pp 118

DOI 10.1002/art.42970

Clinical Images: Painless subcutaneous swellings in a middle-aged man

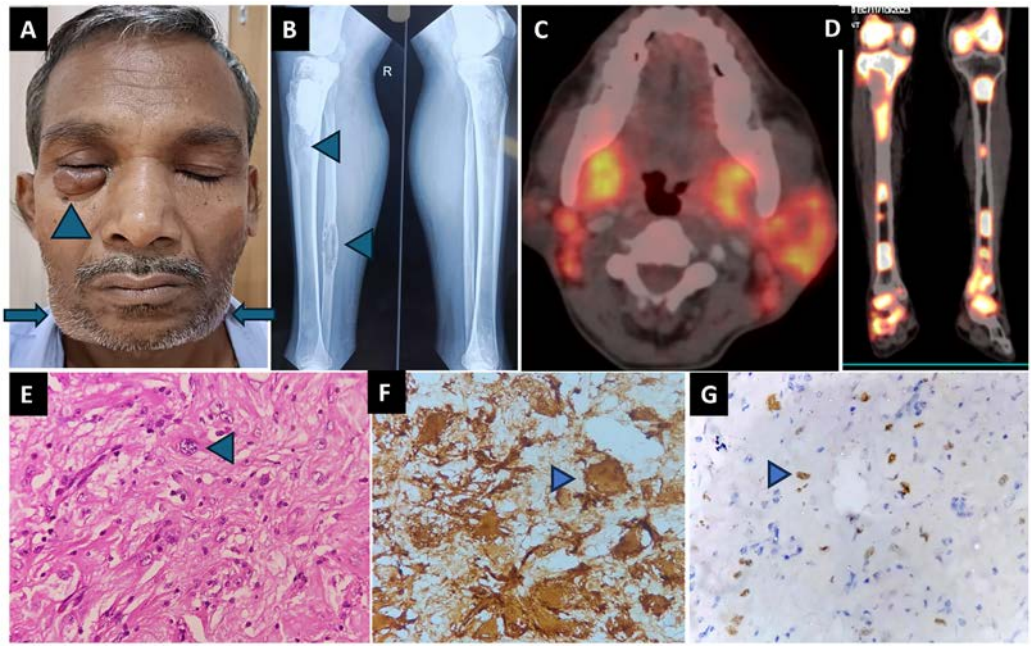

A 52-year-old man, presented with painless swelling of bilateral submandibular glands and multiple subcutaneous lumps for the last six years. Examination revealed (A, arrowhead) firm and nontender swellings over the right lower eyelid, left retroauricular area, and right calf; (A, arrows) enlarged bilateral submandibular glands; and ankle arthritis. Investigations showed raised markers of inflammation, leucocytosis, thrombocytosis, and normal liver and kidney function tests. Ultrasonography of the neck revealed bulky heterogeneous submandibular glands, an enlarged left parotid gland, and cervical lymphadenopathy. A radiograph of both legs (anteroposterior view) showed (B, arrowheads) expansile lytic lesions involving the right tibia and fibula. Whole body ^{18}F fluorodeoxyglucose–positron emission tomography showed (C) hypermetabolism in the bilateral submandibular glands and the left parotid gland, an exophytic soft tissue mass in the inferior aspect of the right eye, a right sinonasal mass, a left lung consolidatory mass, and (D) focal intense hypermetabolism in the marrow of the bilateral femora, tibiae, calcaneotalar, and tarsal bones. Histopathologic examination of the excised lesion from the right lower eyelid showed (E, arrowhead) clusters of histiocytes with emperipolesis on hematoxylin and eosin staining. On immunohistochemistry (IHC), the lesional histiocytes exhibited (F, arrowhead) strong S100 positivity and CD163 positivity. The coexpression of (G, arrowhead) OCT2 and cyclin-D1 was suggestive of extranodal Rosai-Dorfman disease (RDD).[1] He was prescribed prednisolone at 1 mg/kg body weight and oral methotrexate at 15 mg/wk, with gradual improvement of his symptoms over three months. The differentials for histiocytic neoplasms included Langerhans cell histiocytosis, Erdheim-Chester disease, and RDD. On IHC, positive CD163 and S100 and coexpression of OCT2 and cyclin-D1 on lesional histiocytes differentiate RDD from other histiocytic neoplasms. The treatment recommendations for RDD include glucocorticoids, cladribine, cytarabine, and oral methotrexate.[2]

Author disclosures are available at https://onlinelibrary.wiley.com/doi/10.1002/art.42970.

1. Abla O, Jacobsen E, Picarsic J, et al. Consensus recommendations for the diagnosis and clinical management of Rosai-Dorfman-Destombes disease. Blood 2018;131(26):2877–2890.
2. National Comprehensive Cancer Network. Histiocytic neoplasms (version 1.2024). 2024. Accessed July 14, 2024. http://www.nccn.org/professionals/physician_gls/pdf/histiocytic_neoplasms.pdf.

Alekhya Amudalapalli, MD
Rasmi Ranjan Sahoo, DM
Ashlesha Shukla, MD
Pradeepta Sekhar Patro, DM
drpradeepta07@gmail.com
Institute of Medical Sciences & SUM Hospital
Bhubaneswar, India

Arthritis & Rheumatology
Vol. 77, No. 1, January 2025, pp 119–120

American College of Rheumatology
Empowering Rheumatology Professionals

DOI 10.1002/art.42977

Clinical Images: A large disfiguring nasal mass and progressive dyspnea

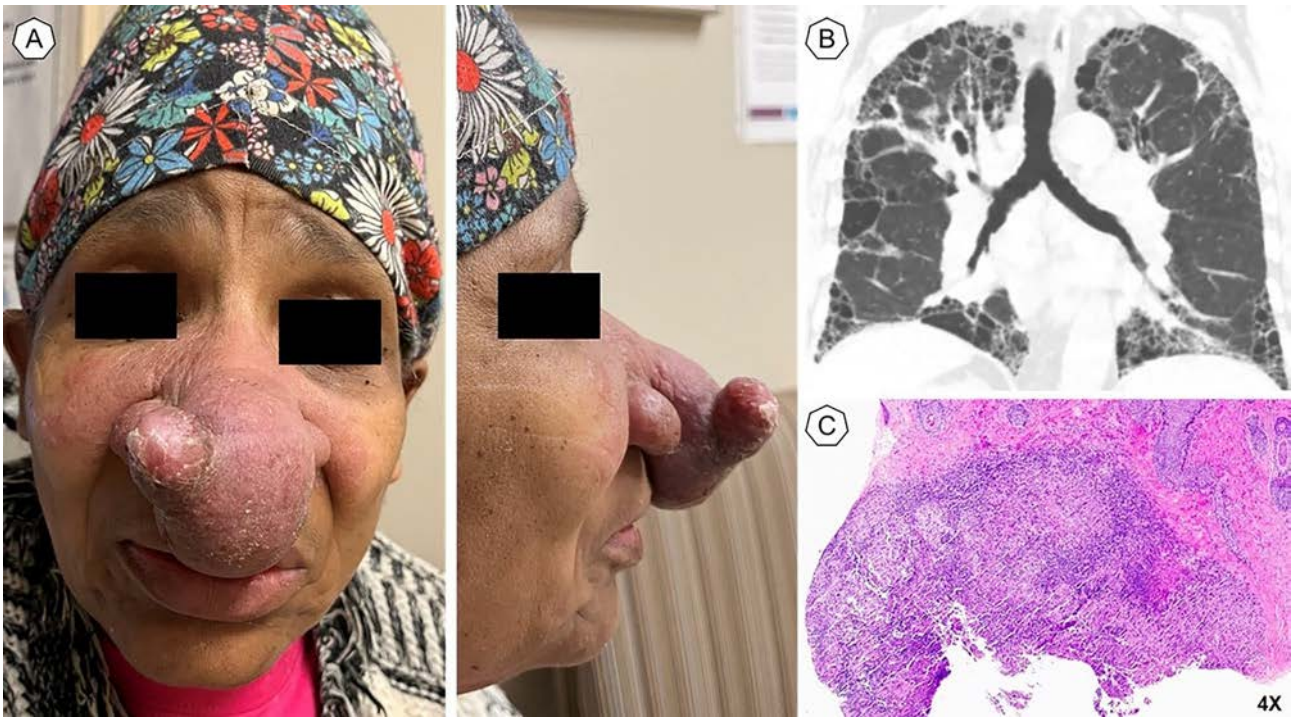

The patient, a 68-year-old woman, presented to the rheumatology clinic with a nasal mass and dyspnea. Two years ago, the patient developed (A) a nonpainful nasal mass that gradually increased in size, accompanied by worsening shortness of breath and cough. She showed no symptoms of arthralgias, palpitations, chest pain, sinus pain, or eye pain or redness, numbness, or weakness. Her laboratory testing results showed normal angiotensin converting enzyme, electrolyte, liver enzyme, and Ig levels; a normal urinalysis result; and negative QuantiFERON and HIV test results. Antinuclear antibody, rheumatoid factor, antineutrophil cytoplasmic antibody, and myositis-specific antibody panels were also negative. (B) Computerized tomography of her chest showed extensive honeycombing involving all lobes, nodular opacities in bilateral upper lobes, and mediastinal lymphadenopathy. (C) A biopsy of her nose lesion showed dermatitis with scattered well-formed nonnecrotizing granulomas in the mid and deep dermis composed of epithelioid histiocytes and multinucleated giant cells. Ten years earlier, she was diagnosed with suspected sarcoidosis following an evaluation for dyspnea and cough. Chest imaging at that time revealed mediastinal lymphadenopathy and bilateral interstitial nodular opacities. She underwent fine-needle aspiration of mediastinal lymphadenopathy, which showed benign respiratory cells and background lymphocytes with no evidence of granulomas or malignant cells, and subsequently underwent a transbronchial lung biopsy, which showed similar findings. Her symptoms improved with prednisone, but she was lost to follow-up. Based on her history and skin biopsy findings, a diagnosis of lupus pernio was made. She was prescribed 40 mg of prednisone daily and 20 mg of methotrexate weekly and received intralesional steroid injections, with improvement of her skin lesion (Supplementary Figure 1). Lupus pernio is a rare cutaneous manifestation of sarcoidosis that can present as a large exuberant disfiguring lesion.[1,2] Systemic glucocorticoids and immunomodulatory drugs are frequently preferred for these lesions, with up to 40% of patients having resolution of their lesions.[3]

Additional supplementary information cited in this article can be found online in the Supporting Information section (https://acrjournals.onlinelibrary.wiley.com/doi/10.1002/art.42977).

AUTHOR CONTRIBUTIONS

Renato Ferrandiz-Espadin: Writing – review and editing; writing – original draft; project administration; investigation. **Sonal Choudhary:** Investigation; writing – review and editing; supervision. **Didem Saygin:** Conceptualization; writing – review and editing; supervision.

DATA AVAILABILITY STATEMENT

Data sharing not applicable to this article as no datasets were generated or analysed during the current study.

Author disclosures are available at https://onlinelibrary.wiley.com/doi/10.1002/art.42977.

1. Abdelghaffar M, Hwang E, Damsky W. Cutaneous sarcoidosis. Clin Chest Med 2024;45(1):71–89.
2. Randhawa KS, Lee BW, Micali G, et al. Cutaneous sarcoidosis: lupus pernio and more. Ital J Dermatol Venerol 2022;157(3):220–227.
3. Stagaki E, Mountford WK, Lackland DT, et al. The treatment of lupus pernio: results of 116 treatment courses in 54 patients. Chest 2009; 135(2):468–476.

Renato Ferrandiz-Espadin, MD
renatoferrandiz@gmail.com
North Alabama Medical Center
Florence, AL
Sonal Choudhary, MD
University of Pittsburgh
Pittsburgh, PA
Didem Saygin, MD
Rush University Medical Center
Chicago, IL